Linear Time-History Analysis as EC8-compliant Design Method for Simplified Performance-Based Earthquake Engineering Assessment

Luca Lombardi

Department of Civil Engineering

University of Bristol

A dissertation submitted to the University of Bristol in accordance with the requirements for award of the degree of Doctor of Philosophy in the Faculty of Engineering

2019

Word Count: 78000

“The final challenge is not in predicting performance or estimating losses;

It is in contributing effectively to the reduction of losses and the improvement of safety.

We must never forget this.”

C. A. Cornell and H. Krawinkler,

Abstract

The routine analysis approach for seismic design of buildings is generally linear-elastic and carried out according to “force-based” approaches. These approaches are based on approximate evaluation of the dynamic structural response. Linear Time-History Analysis (LTHA) is not new in earthquake engineering but many codes, including Eurocode 8 (EC8), do not mention explicitly LTHA among the possible methods of analysis for design. LTHA can represent a simplified tool for engineers avoiding the complexity of nonlinear models for advanced analyses as well as approximate assumptions on the evaluation of the dynamic structural response. Eurocodes are currently under review for a second-generation release, for this reason, this research aims to deal with the gap in the code, related to the possibility of designing buildings through LTHA. A “force-based” EC8-compliant LTHA design framework is proposed and presented for the design of an archetype 12-storey Reinforced-Concrete (RC) Moment-Resisting-Frame (MRF) building located in medium-high seismicity area. Aspects such as: interaction between local force components, the estimation of P-Delta amplification factor, the damping modelling and, finally, the implementation of the behaviour factor are investigated. The novel aspect which characterises this research is the possibility to account for the seismic input variability, suiting design purposes, without losing the opportunity to capture specific response features such as pulse-like effects. The possibility to have a direct comparison between linear response at design stage and nonlinear response within a Performance-Based Earthquake Engineering (PBEE) assessment using the same suite of ground motions is herein investigated in order to propose a suitable approach for the derivation of fragility curves at design stage aimed at comparing and ranking different design solutions. The aim of this work is to open up new opportunities for designers towards a performance-based approach implemented at design stage avoiding the development of a nonlinear model to compare different design options.

Dedication and Acknowledgements

I would like to express the deepest gratitude to my advisor, Dr. Flavia De Luca, for the timeless support I have received from her since arriving to Bristol and throughout my PhD. Her patience, advice, encouragement, and enthusiasm guided me towards the conclusion of a unique experience at the University of Bristol, for which I feel privileged. Also, I would like to thank Dr. Raffaele De Risi, for his dedicated and countless support. I have had the opportunity with them to learn so many things, from personal to professional aspects, that I treasured up for ever. Our time together has always been an inspiration and I consider them both role model researchers.

I would like to thank Dr. Katsu Goda and Dr. John Macdonald for advising me throughout these years. Our meetings have always been helpful and I am grateful for their contribution to my thesis.

My special appreciations go to my former advisors, Prof. Federico Massimo Mazzolani and Dr. Antonio Formisano from the University of Naples "Federico II", since without them I would never have had the opportunity to start my PhD.

I would like to thank all of my friends in Bristol and Italy (one page would not be enough for mentioning them all!) for the best memories, my office mates (former and current) and the whole research group at the University of Bristol for being part of a large family, my students for their questions and enthusiasm, and the Alumni Foundation for my scholarship.

I truly thank my family for all their unconditional love and support.

Finally, I would like to thank Nikita, my favourite person, for our time together, in the past and in the future.

Bristol, 30/03/19

Author's Declaration

I declare that the work in this dissertation was carried out in accordance with the requirements of the University's Regulations and Code of Practice for Research Degree Programmes and that it has not been submitted for any other academic award. Except where indicated by specific reference in the text, the work is the candidate's own work. Work done in collaboration with, or with the assistance of, others, is indicated as such. Any views expressed in the dissertation are those of the author.

The following papers are based on the work described in this thesis:

1. De Luca F and **Lombardi L** (2017). EC8 Design through Linear Time-History Analysis versus Response Spectrum Analysis – is it an enhancement for PBEE?, 16th World Conference on Earthquake Engineering, Santiago, Chile, January 9-13.

   Author's contributions: The first author revised the manuscript; the second author provided the analyses, tables, figures, and first draft.

2. Di Cuia A, **Lombardi L**, De Luca F, De Risi R, Caprili S, and Salvatore W (2017). Linear Time History Analysis for EC8 Design of CBF Structures. X International Conference on Structural Dynamics, Rome, Italy, September 10-13.

   Author's contributions: The first author provided the analyses, figures, tables, and first draft; the second author supported the analyses; the other authors revised the manuscript.

3. **Lombardi L** and De Luca F (2018). Linear Time-History Analysis as EC8-compliant Design Method: What Seismic Input Selection?, 11th U.S. National Conference on Earthquake Engineering, Los Angeles, California, June 25-29.

   Author's contributions: The first author provided the analyses, tables, figures, and first draft; the second author revised the manuscript.

4. **Lombardi L**, De Luca F, and Macdonald J (2019). Design of Buildings through Linear Time-History Analysis Optimising Ground Motion Selection: A Case Study for RC-MRFs, Engineering Structures; 192:279-295.

   Author's contributions: The first author provided the analyses, tables, figures, and first draft; the other authors revised the manuscript.

5. **Lombardi L** and De Luca F (2019). Linear Time-History Analysis for Fragility Curves at Design Stage, Earthquake Engineering and Structural Dynamics (under review).

   Author's contributions: The first author provided the analyses, tables, figures, and first draft; the second author revised the manuscript.

The following papers are related to collaborations on other related topics not included in this thesis work:

6. Li Y, **Lombardi L**, De Luca F, Farbiarz Y, Blandon JJ, Lara LA, Rendon JF, Jiang JZ, and Neild SA (2019). Optimal Design of Inerter-Integrated Vibration Absorbers for Seismic

Retrofitting of a High-Rise Building in Colombia, XIIth International Conference on Recent Advances in Structural Dynamics, Lyon, France, April 15-17.

Author's contributions: The first author provided the analyses, tables, figures, and first draft; the second author supported the analyses and provided code scripts, some figures, and part of the draft; the other authors revised the manuscript.

7. Cross T, **Lombardi L**, De Luca F, De Risi R., Beardsley J, De Podesta M, Clark R, Rushton J, Alexander N, and Sextos A (2019). Performance comparison of lead rubber bearing and friction pendulum isolation systems on a school in Kathmandu. 2nd International Conference on Natural Hazards & Infrastructure, Chania, Greece, June 23-26.

   Author's contributions: The first author provided the analyses, tables, figures, and first draft; the second author supported the analyses and provided code scripts; the other authors revised the manuscript.

Signed: .....

Date .....

Contents

List of Figures

List of Tables

List of Symbols

Chapter 1	
q	Behaviour factor
R	Strength reduction factor
Chapter 2	
F	Force of a SDOF system
Δ	Displacement of a SDOF system
F_y	Yield force of a SDOF system
Δ_y	Yield displacement of a SDOF system
Δ_{max}	Maximum displacement of a SDOF system induced by an earthquake
F_{el}	Elastic force of a SDOF system induced by an earthquake
μ_Δ	Displacement ductility of a SDOF system induced by an earthquake
ζ	Damping ratio of a SDOF system
T	Period of vibration of a SDOF system
f	Frequency of a SDOF system
m	Mass of a SDOF system
K	Stiffness of a SDOF system
$S_{ae}(T)$	Elastic spectral pseudo-acceleration of a SDOF system at period T
T_C	Transition or corner period of the elastic spectrum of a SDOF system between the constant spectral pseudo-acceleration and the constant pseudo-velocity ranges
T_1	Fundamental period of vibration of a building
$S_{ae}(T_1)$	Elastic spectral pseudo-acceleration of a building at the fundamental period
F_b	Seismic base shear
z_i	Height of the i^{th} mass at the i^{th} storey of a building
z_j	Height of the j^{th} mass at the j^{th} storey of a building
m_i	Mass at the i^{th} storey of a building
m_j	Mass at the j^{th} storey of a building
λ	Correction factor for the effective modal mass attributed to the first mode of a building
C_t	Coefficient of building typology
ρ	Demand over capacity ratio of the ductile primary element of a building
ρ_{max}	Maximum demand over capacity building ratio of the ductile primary elements of a building

ρ_{min}	Minimum demand over capacity building ratio of the ductile primary elements of a building
$[M]$	Mass matrix of a MDOF system
$[K]$	Stiffness matrix of a MDOF system
$[C]$	Damping matrix of a MDOF system
$\{\ddot{u}(t)\}$	Relative acceleration vector of a MDOF system
$\{\dot{u}(t)\}$	Relative velocity vector of a MDOF system
$\{u(t)\}$	Relative displacement vector of a MDOF system
$\{\tau\}$	Influence coefficient vector of a MDOF system
$\{\ddot{u}_g(t)\}$	Earthquake GM acceleration vector
ζ_i	Damping ratio of the ith mode
α_M	Mass proportional coefficient in Rayleigh damping model
β_K	Stiffness proportional coefficient in Rayleigh damping model
$\{\phi\}_i$	Mode shape vector of the ith mode
M_i	Generalised modal mass of the ith mode
ω_i	Frequency of the ith mode
t	Time instant
$E(t)$	Structural response at time t
E_o	Peak of the structural response
E_{io}	Peak of the structural response of the ith mode contribution
T_i	Period of vibration of the ith mode
$S_a(T_i, \zeta_i)$	Pseudo acceleration at T_i for ζ_i
E_i^{st}	Modal static structural response of the ith mode contribution
E_{jo}	Peak of the structural response of the jth mode contribution
ρ_{ij}	Correlation coefficient between ith and jth mode
β_{ij}	Coefficient denoting the T_j over T_i ratio
ζ_j	Damping ratio of the jth mode
M	Bending moment of the structural member at the generic member's end
θ	Chord rotation of the structural member at the generic member's end
φ	Curvature of the structural member at the generic member's end
σ	Material stress
ε	Material strain
M_y	Bending moment at yielding stage at the generic member's end
M_u	Bending moment at ultimate stage at the generic member's end
M_{pc}	Bending moment at post-capping stage at the generic member's end

θ_y	Chord rotation at yielding stage at the generic member's end
θ_p	Chord rotation at capping stage at the generic member's end
θ_{pc}	Chord rotation at post-capping stage at the generic member's end
Δ_n	Displacement of a control point of a MDOF system
Γ	Participation factor of the translational mode of a MDOF system
F^*	Force of the equivalent SDOF system
Δ^*	Displacement of the equivalent SDOF system
K^*	Elastic stiffness of the equivalent SDOF system
F_y^*	Yielding force of the equivalent SDOF system
Δ_y^*	Yielding displacement of the equivalent SDOF system
Δ_u^*	Ultimate displacement of the equivalent SDOF system
T^*	Period of vibration of the equivalent SDOF system
m^*	Mass of the equivalent SDOF system
A^*	Area under the capacity curve of the equivalent SDOF system
Δ_t^*	Maximum displacement of the equivalent SDOF system induced by an earthquake
$S_{de}(T^*)$	Elastic spectral displacement of a SDOF system at T^*
q^*	Behaviour factor of the equivalent SDOF system
C_0	Coefficient of scaling
C_1	Coefficient of ductility
C_2	Coefficient of hysteresis shape
C_3	Coefficient of P-Δ effects
T_{eff}	Effective period of the building
T_{el}	Elastic fundamental period of the building
K_{el}	Elastic stiffness of the building
K_{eff}	Effective elastic stiffness of the building
$p[X\|Y]$	Conditional probability of X exceeding a specific threshold given Y
IM	Intensity measure
EDP	Engineering demand parameter
DM	Damage measure
DV	Decision variable
$\lambda[DV]$	Mean annual occurrence (or exceeding) rate of *DV*
$\lambda[IM]$	Mean annual occurrence (or exceeding) rate of *IM*
$p[IM]$	Mean annual probability of exceeding *IM*
$p[EDP\|IM]$	Conditional probability of *EDP* exceeding a specific threshold given *IM*
$\lambda[EDP]$	Mean annual occurrence (or exceeding) rate of *EDP*

$p[DM\|EDP]$	Conditional probability of *DM* exceeding a specific threshold given *EDP*
$p[EDP]$	Mean annual probability of exceeding *EDP*
$p[DM]$	Mean annual probability of exceeding *DM*
$p[DV\|DM]$	Conditional probability of *DV* exceeding a specific threshold given *DM*
S_{MS}	Spectral acceleration for short period
S_{M1}	Spectral acceleration at 1 second
a_{gR}	Reference peak ground acceleration
$S_{a,target}$	Spectral acceleration of the target spectrum
s_k	Scaling factor of the k^{th} GM spectrum
$S_{a,GM}$	Spectral acceleration of the GM spectrum
MSE_{GM}	Mean squared error value of the GM
$S_{a,\mu}$	Spectral acceleration of the average spectrum of the GM spectra
s_μ	Average scaling factor of the GM spectra
$RMSE$	Root mean square error value of the GM suite
m_μ	GM suite mean of the logarithmic spectral accelerations at T_i
m_{target}	Target mean of the logarithmic spectral accelerations at T_i
σ_μ	GM suite standard deviation of the logarithmic spectral accelerations at T_i
σ_{target}	Target standard deviation of the logarithmic spectral accelerations at T_i
w	Weighting factor
SSE_{GM}	Sum of the squared errors of the GM
Chapter 3	
Δ_{max}	Maximum roof displacement of the building
θ_{max}	Maximum chord rotation demand of the building
H_{tot}	Building total height
H_i	Building height of the i^{th} storey
I_g	Gross uncracked second moment of area of the member's cross-section
a_g	Peak ground acceleration
$v_{s,30}$	Shear-wave velocity in the top 30 m
T_R	Return period of the seismic action
EP	Exceedance probability
S	Soil factor
S_s	Stratigraphic amplification coefficient
S_T	Topographic amplification coefficient
η	Damping correction factor
F_o	Maximum amplification factor of the spectral acceleration

T_C	Period corresponding to the starting point of the constant velocity branch of the code spectrum
C_C	Coefficient of soil type
T_C^*	Period corresponding to the starting point of the constant spectral velocity branch of the spectrum for rigid and horizontal soil
T_B	Period corresponding to the starting point of the constant spectral acceleration branch of the code spectrum
T_D	Period corresponding to the starting point of the constant spectral displacement branch of the code spectrum
$a_{g,LS\text{-}LS}$	Peak ground acceleration for Life Safety-Limit State
$\overline{q_{sk}}$	Characteristic value of snow load on ground level
a_s	Site location above the level of the sea
q_{sk}	Characteristic value of snow load at roof level
μ_i	Snow load shape coefficient
C_e	Exposure coefficient
C_t	Thermal coefficient
b	Member width
h	Member depth
γ	Specific weight of material
G_k	Characteristic value of permanent load
Q_k	Characteristic value of variable load
γ_G	Partial factor for permanent load
γ_Q	Partial factor for variable load
Ψ_0	Factor of combination variable load for the fundamental combination
Ψ_2	Factor of combination variable load for the seismic combination
A_{Ed}	Design value of the Seismic load
G_{k1}	Characteristic value of permanent structural load
G_{k1}	Characteristic value of permanent non-structural load
Q_{k1}	Characteristic value of variable dominant load
Q_{k2}	Characteristic value of variable non-dominant load
IDR	Interstorey drift ratio
e_{ai}	Accidental eccentricity of the centre of mass for i direction
L_i	Dimension of the building in plan perpendicular to the seismic i direction
$\theta_{P\text{-}\Delta,i}$	Interstorey drift sensitivity coefficient at i^{th} storey
$N_{tot,i}$	Total gravity load at and above i^{th} storey
$d_{r,i}$	Inelastic interstorey drift at the centre of mass at i^{th} storey

$V_{tot,i}$	Total seismic shear at ith storey
h_i	Interstorey height at ith storey
f_{cd}	Design value of the compressive concrete strength
E_c	Young's modulus of concrete
v_d	Normalised axial force
f_{syd}	Design value of the tensile steel bar strength at yielding
E_s	Young's modulus of steel
γ_{Rd}	Overstrength factor
d_{bL}	Diameter of longitudinal bars
s	Stirrups spacing
MP_{UX}	Translational modal participating mass along X direction
MP_{UY}	Translational modal participating mass along Y direction
MP_{RZ}	Rotational modal participating mass about Z direction
$S_{ad}(T)$	Design spectral acceleration at T
Chapter 4	
α	Equivalent stiffness reduction factor
$S_{ad}(T_i)$	Design spectral acceleration at T_i of the benchmark building
$S_{ae}(T_i)$	Elastic spectral acceleration at T_i of the benchmark building
T_i	Period of vibration of ith mode of the benchmark building
$a_{g,LS\text{-}LS}$	Peak ground acceleration for Life Safety-Limit State
q_{LTHA}	Behaviour factor of the benchmark building for LTHA
q	Behaviour factor of the benchmark building for RSA
α_u/α_1	Overstrength ratio
I_e	Importance factor
R	Response modification factor
C_d	Deflection amplification factor
ζ_i	Damping ratio of the ith mode
α_M	Mass proportional coefficient in Rayleigh damping model
β_K	Stiffness proportional coefficient in Rayleigh damping model
ω_i	Frequency of the ith mode
$\theta_{P\text{-}\Delta}$	Interstorey drift sensitivity coefficient at ith storey
N_{tot}	Total gravity load at and above ith storey
$d_r(t^*)$	Inelastic interstorey drift at the centre of mass at time t^*
t^*	Time instant at which the maximum inelastic interstorey drift is achieved
$V_{tot}(t^*)$	Total seismic shear at time t^*
h	Interstorey height

e_a	Accidental eccentricity of the centre of mass
CX_{1or2}	GM acceleration time-history of the horizontal component 1 or 2 applied along X direction
CY_{1or2}	GM acceleration time-history of the horizontal component 1 or 2 applied along Y direction
$N_{Ed,c}(t)$	Design compressive axial force demand of the member's cross-section at time *t*
$N_{Rd,c}$	Design compressive axial force capacity of the member's cross-section
$N_{Ed,t}(t)$	Design tensile axial force demand of the member's cross-section at time *t*
$N_{Rd,t}$	Design tensile axial force capacity of the member's cross-section
f_{ck}	Characteristic value of the compressive concrete strength
γ_C	Partial factor for concrete
f_{syk}	Characteristic value of the tensile steel bar strength at yielding
γ_S	Partial factor for steel
$I_{eq,j}$	GM index of the GM spectrum horizontal component j
$S_{a,eq,j}(T_i)$	Spectral acceleration of the GM spectrum horizontal component j at T_i
$S_{a,target}(T_i)$	Spectral acceleration of the target spectrum
P_i	Weight of the period T_i
n_p	Number of relevant modes of vibration
$MP_{UX,i}$	Translational modal participating mass along X direction of ith mode
$MP_{UY,i}$	Translational modal participating mass along Y direction of ith mode
$MP_{RZ,i}$	Rotational modal participating mass about Z direction of ith mode
Chapter 5	
L_P	Plastic hinge length
ξ	Integration point in Two-Point Gauss-Radau integration rule
ω	Weight in Two-Point Gauss-Radau integration rule
$[\Phi]$	Modal matrix
$[M]$	Mass matrix of a MDOF system
$[K]$	Stiffness matrix of a MDOF system
G	Master node
$\{\phi_n\}$	Eigenvectors of the nth mode
$\{s_{n,k}\}$	Vector of distribution of forces of the nth mode along kth direction
$\Gamma_{n,k}$	Modal participation factor of the nth mode along kth direction
$\{\tau_k\}$	Influence coefficient vector along kth direction
$[I]$	Unity diagonal matrix
$\{f_{n,k}\}$	Vector of nodal forces of the nth mode along kth direction

$S_a(T_n)$	Spectral acceleration at period T_n
T_n	Period of vibration of the nth mode
q_{LTHA}	Behaviour factor of the benchmark building for LTHA
n_{pt}	Number of analysis time steps
dt	Time step increment
t	Time instant
$N_{Ed,c}(t)$	Design compressive axial force demand of the member's cross-section at time t
$N_{Rd,c}$	Design compressive axial force capacity of the member's cross-section
$N_{Ed,t}(t)$	Design tensile axial force demand of the member's cross-section at time t
$N_{Rd,t}$	Design tensile axial force capacity of the member's cross-section
DCR_t	Demand over capacity ratio in terms of tensile axial force
DCR_c	Demand over capacity ratio in terms of compressive axial force
f_{cd}	Design value of the compressive concrete strength
$v_{d,LIM}$	Normalised design axial force limit
f_{syd}	Design value of the tensile steel bar strength at yielding
$A_{s,tot}$	Total area of longitudinal bars of the member's cross-section
A_c	Concrete area of the member's cross-section
DCR	Demand over capacity ratio in terms of flexural behaviour
$M_{Ed}(t)$	Bending moment demand at time t
$N_{Ed}(t)$	Axial force demand at time t
$M_{Rd}(t)$	Bending moment capacity at time t
$N_{Rd}(t)$	Axial force capacity at time t
IDR	Interstorey drift ratio
θ	Chord rotation at the generic member's end
L_V	Shear span
θ_y	Chord rotation at yielding stage at the generic member's end
θ_u	Chord rotation at ultimate stage at the generic member's end
f_{cm}	Mean value of the compressive concrete strength
f_{sym}	Mean value of the tensile steel bar strength at yielding
f_{syk}	Characteristic value of the tensile steel bar strength at yielding
φ_y	Curvature at yielding stage at the generic member's end
E_s	Young's modulus of steel
h	Depth of the member's cross-section
d_{bl}	Diameter of the longitudinal bars
ω	Mechanical reinforcement ratio of the tension longitudinal reinforcement

ω'	Mechanical reinforcement ratio of the compression longitudinal reinforcement
ρ_{st}	Ratio of the transverse steel parallel to the direction of loading
ρ_{bd}	Ratio of the diagonal steel reinforcement in each diagonal direction
α	Confinement effectiveness factor
DCR_u	Demand over capacity ratio in terms of flexural behaviour at ultimate stage
DCR_y	Demand over capacity ratio in terms of flexural behaviour at yielding stage
$\theta_E(t)$	Chord rotation demand at time *t*
$\theta_{E,y}(t)$	Chord rotation demand about local axis y at time *t*
$\theta_{E,z}(t)$	Chord rotation demand about local axis z at time *t*
α_M	Mass proportional coefficient in Rayleigh damping model
β_K	Stiffness proportional coefficient in Rayleigh damping model
E_c	Young's modulus of concrete
f_{ctm}	Mean value of the tensile concrete strength
ρ_w	Ratio of the transverse steel
α_h	Horizontal confinement effectiveness factor
α_v	Vertical confinement effectiveness factor
h_o	Core concrete depth of the member's cross-section
b_o	Core concrete width of the member's cross-section
b_i	Distance between longitudinal bar laterally restrained by a stirrup corner or cross-tie along the perimeter of the member's cross section
ω_w	Mechanical reinforcement ratio of the transversal reinforcement
f_{symw}	Mean value of the transversal steel bar strength at yielding
r	Factor of steepness rate for the concrete softening behaviour
L	Length of the structural member
I_t	Second moment of area of the transformed cross-section
σ_x	Normal stress of the generic fibre
y	Distance of the generic fibre from the centroid of the cross-section
dA	Area of the fibre
ε_x	Axial strain of the generic fibre
y^*	Distance of the generic fibre from the neutral axis
ε_{sy}	Steel strain at the yielding stage
ε_{st}	Steel strain at the rupture stage
f_{stk}	Tensile steel bar strength at rupture
Chapter 6	
T_1	Fundamental period of the benchmark building

T_{10}	Period of vibration of the 10th mode of the benchmark building
T_P	Pulse period of the GM
q	Behaviour factor of the benchmark building for RSA
q_{LTHA}	Behaviour factor of the benchmark building for LTHA
$I_{eq,max}$	Maximum GM index between the two horizontal components
$RMSE_e$	Root mean square error value at the elastic level
$RMSE_d$	Root mean square error value at the design level
CoV	Coefficient of variation
e	Relative error
DCR	Demand over capacity ratio
R^2	Coefficient of determination for linear regression
a, b	Coefficient of linear regression
T_C	Upper limit of the period of the constant spectral acceleration branch of the code spectrum
IDR	Interstorey drift ratio
α	Equivalent stiffness reduction factor
I_g	Gross uncracked second moment of area of the member's cross-section
θ	Chord rotation at the generic member's end
S_a	Spectral acceleration
$\beta_{DCR\|Sa}$ or β	Logarithmic standard deviation of *DCR*
Φ	Standardised Gaussian Cumulative Distribution Function
$\eta_{DCR\|Sa}$	Median of *DCR*
μ_{DCR}	Average value of the *DCR*
$SaT1$	Spectral acceleration at the fundamental period of the benchmark building
μ_{SaT1}	Average value of the GM suite *SaT1* values
η_{SaT1}	Median of the *SaT1* values leading to the Limit State
n	GM suite size
$\mu_{\eta SaT1,n}$	Average value of bootstrapped η_{SaT1} values for GM suite size n
$\mu_{\beta,n}$	Average value of bootstrapped β values for GM suite size n
σ	Standard deviation

List of Abbreviations

PBEE	Performance-Based Earthquake Engineering
EC8	Eurocode 8
EC8-1	Eurocode 8 – Part 1
EC8-3	Eurocode 8 – Part 3
EC2	Eurocode 2
EC1-3	Eurocode 1 – Part 3
EC1-1	Eurocode 1 – Part 1
EC0	Eurocode 0
LFM	Lateral Force Method
RSA	Modal Response Spectrum Analysis
LTHA	Linear Time-History Analysis
NTHA	Nonlinear Time-History Analysis
NSA	Nonlinear Static Analysis
US	United States
CA	Cloud Analysis
IDA	Incremental Dynamic Analysis
MSA	Multiple Stripe Analysis
ABSSUM	Absolute Sum
MSE	Mean Squared Error
CQC	Combination Quadratic Complete
SRSS	Square Root of the Sum of Squares
RMSE	Root Mean Square Error
SSE	Sum of the Squared Errors
DCH	Ductility Class High
DCM	Ductility Class Medium
DCL	Ductility Class Low
IDR	Interstorey Drift Ratio
GM	Ground Motion
UHS	Uniform Hazard Spectrum
MCE	Maximum Considered Earthquake
CMS	Conditional Mean Spectrum
SDOF	Single-Degree Of Freedom
MDOF	Multi-Degree Of Freedom
DCR	Demand over Capacity Ratio

EDP	Engineering Demand Parameter
DV	Decision Variable
IM	Intensity Measure
DM	Damage Measure
RC	Reinforced-Concrete
MRF	Moment Resisting Frame
CBF	Concentrically Braced Frame
ADRS	Acceleration Displacement Response Spectrum
PEER	Pacific Earthquake Engineering Research centre
PSHA	Probabilistic Seismic Hazard Analysis
MCE	Maximum Considered Earthquake
UHS	Uniform Hazard Spectrum
CMS	Conditional Mean Spectrum
ESM	European Strong Motion database
EP	Exceedance Probability
PGA	Peak Ground Acceleration
FP	Fault Parallel
FN	Fault Normal
TCL	Tool Command Language
HPC	High Performance Computing
FEM	Finite Element Method
DOF	Degree Of Freedom
3D	Three-Dimensional
LS-LS	Life Safety-Limit State
DL-LS	Damage Limitation-Limit State
CoV	Coefficient of Variation
UC	Unacceptable Case

Chapter 1: Introduction

1.1. Background

In the past decades, several earthquakes have shown that economic losses (e.g., repair costs, downtime, casualties) occur for existing buildings designed according to obsolete prescriptions, but also for those designed according to modern seismic codes (e.g., Ramirez et al. 2012). A relevant part of such losses can be attributed to non-structural damage and minor structural damage for medium or severe earthquakes (Taghavi and Miranda 2003). Current seismic design codes for buildings are prescriptive in nature and they aim (i) to provide a life-safety level of protection under rare earthquakes through prevention of collapse and (ii) to mitigate property loss under frequent earthquakes through limitation of structural and non-structural damage (Fardis 2009). Performance-Based Earthquake Engineering (PBEE) is of high interest nowadays as it allows a transparent, scientific and more informative design, based on specific performance objectives and evaluating uncertainties related to them (e.g., Ghobarah 2001; Moehle and Deierlein 2004). There are several studies in literature applying the PBEE methodology to assess the risk of earthquake economic losses and the influence of structural design decisions on these losses for both new and existing buildings (e.g., Goulet et al. 2007; Ramirez and Miranda 2012; De Luca and Galasso 2015).

Nonlinear Time-History Analysis (NTHA) represents the most accurate method for assessing the structural fragility of buildings subjected to earthquake loadings but, notwithstanding the growth in computer processing power and software development, NTHA is generally time-consuming and it requires appropriate selection of ground motions (e.g., Haselton et al. 2017a; Zimmerman et al. 2017), numerical models (e.g., Jarrett et al. 2017; Deierlein et al. 2010) and acceptance criteria (e.g., Haselton et al. 2017b; Biskinis and Fardis 2010a; Biskinis and Fardis 2010b), which are aspects that often preclude its use for conventional design. NTHA is well suited to assess and retrofit existing buildings, but it can also be used to analyse new structures as long as their design is fully completed (NEHRP 2015; ASCE 2017). Contrarily, Nonlinear Static Analysis (NSA), is less demanding than NTHA and is widely implemented using various approaches in the majority of commercial software packages, mainly for the assessment and retrofitting of existing buildings. However, NSA requires a predefined lateral load distribution to be assigned and is not fully reliable in some cases, such us high-rise buildings, as shown in some studies (e.g., Fragiadakis et al. 2014). Furthermore, also in the case of NSA the design needs to be fully defined (e.g., full definition of reinforcement details for nonlinear modelling).

The routine analysis approach for code-based seismic design of buildings is generally linear and it accounts for ductility and nonlinear behaviour in an approximate way through the so-called "behaviour factor" (q) in Eurocode 8 (EC8, CEN 2004a) or "strength reduction factor" (R) in United States standards (e.g., ASCE/SEI 7-16, ASCE 2017). The q factor is used for design purposes to

reduce the elastic response spectrum for linear analyses. It accounts for the nonlinear response of a structure, associated with the material, the structural system and the design procedures (e.g., Mwafi and Elnashai 2002). All design approaches using *q* to reduce seismic forces are called "force-based" approaches. Among such methods, the Lateral Force Method (LFM) assumes a predefined force distribution and it is allowed for buildings which response is first-mode dominated, regular in plan and elevation, with a fundamental period within specific ranges defined by codes.

Many standards and codes, including EC8, assume Modal Response Spectrum Analysis (RSA) as the reference method for design. RSA is an approximate approach for the evaluation of linear dynamic response of buildings (e.g., Chopra 2012). Its approximation, well-known since the 1980s, lies in the combination step of the analysis for multiple modes. The Complete Quadratic Combination (CQC) is the most accurate combination rule for RSA (among the options suggested by codes) for its applicability to a wide class of structures, as suggested in many codes and standards such as EC8, New Zealand standards (SNZ 2004), the Italian building code (Italian Building Code 2018) and ASCE/SEI 7-16. However, the CQC presents some limitations for near-source impulsive earthquakes, unusually stiff buildings (such as dams or nuclear power plants) and buildings with relevant higher modes contribution, as discussed by many authors (e.g., Der Kiureghian 1981; Gupta 1992; Cacciola et al. 2004; De Luca and Verderame 2013; among others). Another weakness of RSA is that the combination of modal effects does not capture the sign and coupling of different components of member actions and system deformations. For example, it becomes an issue when the maximum Demand over Capacity Ratio (DCR) of a structural member subjected to the combined action of axial force and bending moment over time, for all load combinations, needs to be evaluated (e.g., Wilson 2015; Charney 2015). As a result of the widespread use of RSA, current professional practice in design still needs refinements; a balanced compromise between accuracy of structural response evaluation and simplicity of design procedure for all possible practical cases (i.e., high-rise, low-rise, regular and irregular structures) should be the target.

Recently, a new LTHA design procedure has been included in ASCE/SEI 7-16 and described in FEMA P-1050, suggesting response spectrum-matching of three wavelet adjusted ground motions as input, so that LTHA can be used as alternative to RSA (Charney 2015). However, this input selection not always allows matching an entire elastic code spectrum (Bommer and Acevedo 2004), it can modify important features of earthquakes such as pulse-like characteristics (BSSC 2015) and it can lead to bias when the inelastic response of structures is assessed (Bommer and Acevedo 2004; Iervolino et al. 2010b). Furthermore, this kind of selection exclude any opportunity to evaluate preliminarily the effect of record-to-record variability.

1.2.Aims and objectives

The aim of this thesis is to contribute to the development of design approaches towards a simplified EC8-compliant performance-based design framework using Linear Time-History Analysis (LTHA) as a novel seismic analysis method for buildings. The main aspects investigated in this thesis are:

- the possibility to enlarge analysis options in EC8 with LTHA as alternative to RSA for a larger applicability range of buildings. RSA is the reference seismic method of analysis in many design codes, including EC8, and it is conceived to be applied to any type of building, from low- to high-rise buildings either regular or irregular, despite its limits already found in literature. The CQC is the reference combination rule for RSA since 1980s and it assumes the white-noise approximation of correlation coefficient. It was found in literature that the CQC can lead to significant errors for unusually stiff buildings, near-field impulsive earthquakes, and building characterised by relevant higher modes contribution. Several attempts were made in the past in order to improve the CQC. However, either improved or not, the CQC leads to loss of both sign and coupling of local force components that can be an issue for verifications of structural members (e.g., coupling of axial force and biaxial bending moment in columns, axial force in braces, etc.). LTHA can overcome these limits providing a structural response that accounts for the interaction between natural frequencies of the building with those of earthquakes as well as actual coupling of local force components. The ASCE/SEI 7-16 allows using NTHA for design of buildings which features do not conform to code requirements. In this light, LTHA can represent a good compromise between the complexity of nonlinear modelling and the approximate assumptions of linear methods (i.e., preassigned distribution of lateral forces, loss of both sign and coupling of local force components when modal combination rules are used, etc.) and it can reliably evaluate the performance of structures in serviceability conditions. However, the challenge is how to use LTHA for design conditions at ultimate limit states. Moreover, LTHA allows to directly evaluate other response quantities such as storey velocities and storey accelerations which are currently investigated as Engineering Demand Parameters (EDPs) for verifications of non-structural elements;
- the possibility to account for the record-to-record variability in LTHA at design stage. This aspect can be used for characterising the uncertainty in Ground Motion (GM) selection for LTHA design towards a possible simplified approach for performance-based design of buildings. This design approach is significantly different from the deterministic or semi-probabilistic prescriptive approaches for design currently employed by design codes. Moreover, it would (i) allow using real (or simulated) ground motions for design, as per NTHA, instead of smoothed response spectra, and (ii) be much simpler than nonlinear analysis methods that require expertise in modelling choices, solution of complex numerical problems, high-performance computing, and interpretation of nonlinear dynamic responses. If the seismic input is the same, LTHA can

directly match NTHA, allowing the comparison of linear and nonlinear behaviours in a consistent way (contrarily to other linear analysis methods). It is evident that LTHA cannot replace nonlinear analyses for advanced studies but the proposal of an adequate design framework for buildings can make LTHA a useful and simple tool for engineers. Moreover, this approach would open up to a simplified PBEE methodology that allows deriving fragility curves at design stage that can be used to estimate economic losses due to earthquakes and compare design solutions. Therefore, an ideal "force-based" LTHA design framework should provide the opportunity to account for the seismic input variability, suiting design purposes without losing the possibility to capture specific response features such as pulse-like effects, contrarily to the procedure recommended by ASCE/SEI 7-16 and specified in FEMA P-1050.

The objectives of this thesis are:

- to review the methods of analysis suggested in current design codes, emphasising on EC8 recommendations but comparing the latter to the United States standards. Particular attention is given to (i) the description of the rationale behind the methods of analysis suggested by design codes for "force-based" and "displacement-based" design and assessment, (ii) the limits of applicability of such methods, (iii) main aspects related to the input selection (e.g., response spectrum, GMs), and (iv) differences between traditional seismic design philosophy and "performance-based" approach;
- to design an archetype Reinforced Concrete-Moment Resisting Frame (RC-MRF) building according to EC8 accounting for some critical aspects that are typical of professional practice and that can show limits of applicability of RSA. To do this, a detailed investigation of the benchmark RC-MRF buildings adopted in literature is firstly presented; then the archetype building considered in this work is designed according to EC8;
- to develop a Matlab/OpenSees code for design and assessment of buildings modelled both linearly and nonlinearly in order to come up with a robust modelling solution that can be used for analysing additional case study structures in future;
- to present the main LTHA design aspects and to propose a detailed EC8-compliant design framework for LTHA, showing results of different seismic input selections carried out according to EC8-recommendations for NTHA, and comparing results to those obtained by implementing spectral-matching of GMs (suggested by FEMA P-1050). This allows to assess the effect of record-to-record variability in LTHA and identify possible "unacceptable cases" due to the limits of the "force-based" capacity models developing a novel seismic input selection approach for LTHA with all the desirable characteristics for efficient design. The possibility to come up with a design tool which is simple and efficient for design purposes that can be used by engineers using LTHA design is herein targeted;

- to develop a procedure for deriving fragility curves based on LTHA results which can be directly compared to NTHA results for the same suite of GMs, with the aim of proposing LTHA as method within a simplified PBEE framework at design stage.

1.3.Structure of the thesis

Chapter 2 presents a literature review of the seismic analysis methodologies utilised for design and assessment of buildings according to codes and main theoretical/practical aspects and limits of applicability related to their use. Attention is given to the main difference between EC8 and United States standards and to the problem of GM selection for time-history analyses which represent the critical step for successful implementation of LTHA. Some GM selection procedures are presented and their limits for LTHA seismic input selection discussed.

Chapter 3 focuses on aspects related to the design of RC-MRF buildings which is the structural typology considered in this research. The definition of archetype structures is presented herein with the aim of justifying the choice of the benchmark building design aspects considered in this work. To do this, a literature review of the benchmark buildings analysed in literature is carried emphasising the added value of the case study structure considered in this work. Aspects related to the design of the benchmark building through RSA according to EC8 are examined.

Chapter 4 discusses the framework for LTHA as a "force-based" design approach for buildings and it presents the differences between the procedure recently suggested by FEMA P-1050 (NEHRP 2015) and the proposed EC8-compliant procedure investigated in this research. The proposed LTHA procedure is presented for the analysis of the benchmark building and it is discussed step-by-step for its potential implementation in commercial software packages. Comments related on how to implement the behaviour factor, to account in for P-Δ effects, to combine unidirectional responses, to verify acceptance criteria, to implement capacity design, and carry out other verifications are presented with the aim of providing a robust background for LTHA use. This chapter also presents a novel proposal for a GM index with the aim of identifying "unacceptable cases" in LTHA design due to the limitation of the capacity models.

Chapter 5 discusses the modelling problems of nonlinear analyses and it presents a Matlab/OpenSees code written in this research work for the design/assessment of buildings through linear and nonlinear analysis. The code is verified for the linear modelling aspects through a commercial software package (i.e., SAP2000) and for the nonlinear modelling part through both the results of an experimental test and a numerical example. The nonlinear modelling problem is investigated for the fibre-section plasticity models for which some useful modelling recommendations are also provided.

Chapter 6 summarises the results obtained from RSA and LTHA for the benchmark building, assuming for LTHA different GM suites. In this chapter, LTHA is investigated as EC8-compliant design method and results are compared to those obtained through NTHA assumed as benchmark for comparisons. Importance is given to the "unacceptable cases" in LTHA design and examples of using the proposed GM index for identifying them are presented.

Chapter 7 investigates LTHA as simplified method for deriving fragility curves at design stage within a performance-based seismic design approach. Fragility assessment of the benchmark building is carried out through Cloud Analysis (CA) and LTHA results are compared to those obtained through NTHA. In particular, the LTHA-based fragility assessment procedure is presented for two limit states (i.e., life-safety and damage-limitation limit state) and some aspects related to the uncertainty in ground motion selection, influence of the suite size, and influence of unacceptable cases in LTHA are investigated. Some recommendations for achieving reliable results with LTHA compared to NTHA are also presented.

Conclusions are drawn in Chapter 8, where future research directions are also presented.

This research work provides recommendations that could be implemented in future guidelines and/or design codes and it can open up to further studies on LTHA. The main aim of this work is contributing in refining the current seismic design practice, providing a useful tool for engineers and analysts that can be easily implemented by any commercial software package.

Chapter 2: Literature Review

Objectives of this chapter

Current seismic design practice for buildings is based on simple concepts that are well-understood by designers. However, these concepts are based on strong simplifications and approximations that are typically accepted for design. In this light, this chapter aims at the following objectives:

- to present a brief review of seismic analysis methods, showing their theoretical background, relevant aspects characterising their use, and their limits of applicability. Particular attention is given to the possibility of widening analysis options in Eurocode 8 (EC8) with Linear Time-History Analysis (LTHA);
- to discuss the nonlinear structural modelling options in order to investigate their reliability in simulating behaviour of structures under earthquake ground shaking. A thorough discussion on distributed plasticity models is included and comparison with concentrated plasticity models is provided;
- to introduce the Pacific Earthquake Engineering Research (PEER) centre Performance-based approach presenting its first version and the current one, and its main aspects that make it significantly different from the prescriptive code-based approaches;
- to present the current state-of-knowledge on Ground Motion (GM) selection, discussing latest research findings, algorithms, and limitations of current design codes GM selection.

2.1. Introduction

The methodologies of analysis allowed by current codes for the design and assessment of new and existing buildings differ from each other on the basis of the seismic action and structural response modelling. In this light, the structural response can be analysed by using as seismic input an equivalent distribution of lateral forces which is representative of the inertia forces acting on the structure and due to the earthquake or, alternatively, a more refined approach in which the seismic action is modelled as time-histories in terms of accelerations. These analyses can be performed as linear and nonlinear depending on how the structure is numerically modelled. In the first case, the nonlinear behaviour is not directly accounted in the structural response and equivalent approaches to capture inelasticity of materials and nonlinear geometry are typically adopted. In the second case, the structure is analysed considering inelasticity of materials and nonlinear geometry that can capture progressive levels of damage. Generally, there are four methods of analysis which are introduced in the following. In this chapter, the analysis methods are presented from the less accurate to the most accurate evaluating pros and cons of each method. The level of accuracy of simulating the structural behaviour tends to increase with the modelling complexity. With the increase of the accuracy there is an increasing computational effort.

In the following, a detailed discussion on the rationale behind the seismic analysis methods, structural modelling, and the main code-based aspects is presented. The seismic input selection is also presented being an important aspect which cannot be separated from the analysis problem. Particular attention is given to the procedures and provisions for buildings indicated in EC8 (CEN 2004a; CEN 2005) and ASCE/SEI 7-16 (ASCE 2017), the latter refers to the FEMA P-1050 (BSSC 2015) and includes, for the first time, detailed specifications for LTHA design and its practical application. It is highlighted that the current version of EC8, released in 2004, does not explicitly distinguish GM selection for LTHA and Nonlinear Time-History Analysis (NTHA). In fact, LTHA is not explicitly mentioned among the possible methods of seismic analysis. Therefore, the few available indications provided about the GM selection are generally referred to NTHA. Finally, a literature review on "performance-based" approach is presented, focusing on the new methodology suggested by FEMA P-58 for seismic performance-based assessment (FEMA 2018a; FEMA 2018b) and performance-based seismic design (FEMA 2018c), which represents a novelty not yet implemented in current design codes.

2.2.Linear analysis methods

Linear analysis methods in earthquake engineering represent an idealised concept typically accepted by current seismic design codes because of their simplicity and robust theoretical basis (Fardis 2009). Indeed, it is well-known that structures under seismic actions do not remain linear-elastic and exhibit nonlinearities of various type mainly due to deformations. From a practical point of view, it is intuitive that imposing elastic behaviour to structures in earthquake engineering is economically prohibitive (Paulay and Priestley 1992). For this reason, current codes for earthquake-resistant design allow structures to exhibit significant inelastic deformations under the design seismic actions, providing that integrity of the structural members and the structure itself are preserved (Paulay and Priestley 1992; Fardis 2009). In this light, design is conceptually based on forces, justifying the name "force-based" approaches, but it is structured in an equivalent way to account for adequate structural capacity in terms of energy dissipation and ductility (Fardis 2009).

The behaviour of structures designed according to "force-based" approaches for ductility can be idealised through an elastic-perfectly plastic force-displacement curve (F-Δ) in monotonic loading (see Fig. 2-1, Vidic et al. 1994). This behaviour is characterised by the stiffness (K), the yield force (F_y), and the maximum displacement (Δ_{max}). The ratio between the elastic force that the system would exhibit if it was linear-elastic (F_{el}) and the yield force is called behaviour factor ($q = F_{el} / F_y$) or strength reduction factor in the United States standards (R). The displacement ductility (μ_Δ) is defined as the ratio between the maximum displacement (Δ_{max}) and the yield displacement (Δ_y), i.e., $\mu_\Delta = \Delta_{max} / \Delta_y$. On the other hand, the seismic action is typically represented by the peak of the elastic response in terms of pseudo-acceleration (or velocity or displacement) of a Single-Degree Of Freedom (SDOF)

system for fixed value of the damping ratio ζ (the value commonly adopted is 5%) and varying value of period of vibration T or frequency $f = 1 / T$ (McGuire 2004; Chopra 2012).

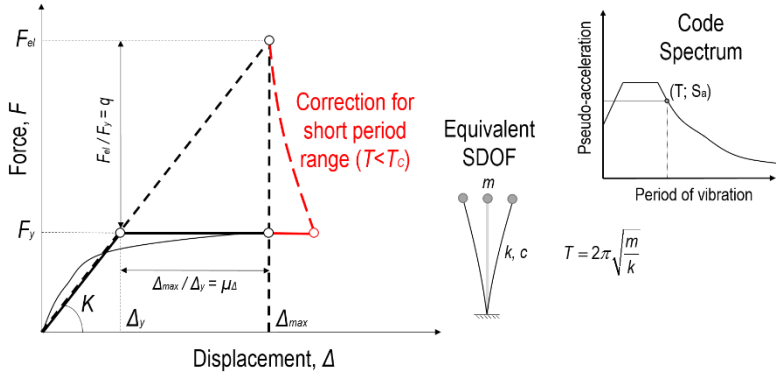

Fig. 2-1 Rationale behind the "force-based" approach for ductility (Vidic et al. 1994).

If m represents the mass of the SDOF, the elastic spectral pseudo-acceleration $S_{ae}(T)$ can be expressed as F_{el} / m and the period of vibration as $2\pi(m / K)^{0.5}$. The previous parameters can be related according to the empirical formulations in Eq. 2.1 (Vidic et al. 1994) where T_C is the "transition" or "corner" period of the elastic spectrum between the constant spectral pseudo-acceleration and the constant pseudo-velocity ranges.

$$\begin{aligned} &\mu_\Delta = q && \text{if } T \geq T_C \\ &\mu_\Delta = 1+(q-1)\frac{T_C}{T}, \quad q = 1+(\mu_\Delta - 1)\frac{T_C}{T} && \text{if } T < T_C \end{aligned} \tag{2.1}$$

In Eq. 2.1, the condition given by $T \geq T_C$ is typical of flexible SDOF systems and it is obtained by imposing the equality between the maximum displacement of the elastic and inelastic SDOF systems. It is known as "equal displacement rule" (Veletsos and Newmark 1960). The condition given by $T < T_C$ is typical of very stiff SDOF systems and it is obtained by imposing the equality between the areas under the elastic and inelastic SDOF systems' behaviour, from here the name "equal energy rule".

EC8, among many other design codes, utilises this theoretical principle for evaluation of the seismic design demand in structures designed according to "force-based" approach (e.g., values of the local forces used for verifications of structural elements). Design codes provide values of the behaviour factor (q) for ultimate limit states depending on the type, class of ductility, overstrength and regularity of the structure. These values are expected to be achieved in terms of "actual" hysteretic behaviour during earthquake events if prescriptive rules are satisfied in order to achieve adequate strength and ductility capacities (Fardis 2009). For structures which can be classified as irregular, the EC8 accounts for specific rules with the aim of penalising the ductility of the systems through smaller values of the behaviour factor.

Some researchers criticise this design approach pointing out that since the experimental evidence shows that the behaviour of structures, which are expected to exhibit damage due to earthquakes, is well described by deformations, design should be based on peak displacements rather than peak accelerations and forces (Priestley 2003). In this light, displacement capacity is meant to be more logical to damage control than strength, so the behaviour factor commonly used for design through linear analysis at ultimate limit states clearly assumes the meaning of "uncertainty factor", and its characterisation appears quite arbitrary because of the significant difference in terms of behaviour factor values between design codes (Calvi et al. 2008). Moreover, the residual displacements can be even more important than maximum displacements given the costs and difficulty of straightening a leaning building after an earthquake (Otani 1997). This problem is particularly relevant for those structures which should exhibit high hysteretic energy dissipation because they tend to have larger residual deformations than others. Lastly, the "force-based" design implies evaluating seismic demand on members that depends on their stiffness themselves. It was found that the member stiffness is essentially directly proportional to strength and rigorously seismic design should be an iterative process (Priestley 2003). All these aspects led to a new design philosophy called "displacement-based" (Calvi et al. 2008), even though the theoretical principle of the "force-based" design is considered adequate for design purposes and it still represents a simple and practical way for designers.

2.2.1. Linear static analysis

The linear static analysis, also known as Lateral Force Method (LFM) in the EC8, is the simplest analysis method, since it is based on the hypothesis that the first mode of vibration of regular buildings (i.e., translational) is representative of the whole structural behaviour. In light of this, a distribution of lateral forces proportional to the masses and their heights at each storey (pseudo inverted triangular) is applied along each main direction for three-dimensional buildings and then combined in order to take into account for both uncertainties in the location of masses and spatial variation of the seismic motion (CEN 2004a). The EC8 allows to perform such analysis only if the building is regular in elevation and the fundamental period of vibration T_1 is not too large in order to limit the contribution of the higher modes of vibration. Basically, the behaviour of these buildings which can be modelled as Multi-Degree Of Freedom (MDOF) systems is approximated to that of a SDOF system for which the maximum base shear can be evaluated as total mass of the system multiplied by the spectral pseudo-acceleration occurring at the top of the SDOF system (Fardis 2009).

Design codes provide smooth response spectra in terms of pseudo-acceleration (also known as Newmark-Hall functional spectral shape, McGuire 2004) representative of the seismic hazard at the site for specific probabilities of exceedance (or return period) in a certain time window (e.g., probability of exceedance of 10% in 50 years or return period of 475 years). A more detailed description on the seismic input selection is provided in Section 2.5. The equivalent lateral forces,

which are depicted in Fig. 2-2, are evaluated starting from the evaluation of the elastic spectral acceleration corresponding to the fundamental period of the building $S_{ae}(T_1)$. Thereafter, the static forces at each storey are evaluated as follows:

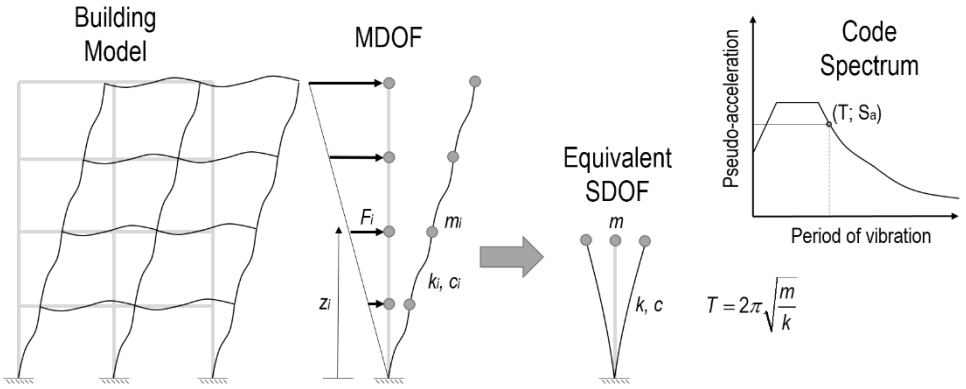

Fig. 2-2 Schematisation of the Lateral Force Method concept.

$$F_i = F_b \frac{m_i z_i}{\sum m_j z_j} \tag{2.2}$$

where F_b is the seismic base shear, z_i and z_j are the heights of the masses m_i and m_j above the level of application of the seismic action (i.e., foundation level or top of a rigid basement). The seismic base shear is determined using the following equation:

$$F_b = S_a(T_1) m \lambda \tag{2.3}$$

in which:

- $S_a(T_1)$ is the response spectral acceleration at the period T_1, evaluated from the code spectrum (either elastic and design depending on the limit state);
- T_1 is the fundamental period of vibration of the building, which can be approximately evaluated for buildings having heights up to 40 m as $T_1 = C_t H^{3/4}$ where C_t is a coefficient given in function of the type of structure and H is the height of the building;
- m is the total mass of the building, evaluated accounting for the gravity loads effectively acting with the seismic loads;
- λ is the correction factor for the effective modal mass attributed to the first mode (typically ranging between [0.85, 1.00] for regular buildings).

EC8 allows using this analysis method if T_1 is smaller than 4 times the corner period at the end of the constant branch of the code spectrum T_c and, anyway, smaller than 2 s. The evaluation of the fundamental period of vibration of buildings through empirical equations like the one suggested in EC8 (i.e., $T_1 = C_t H^{3/4}$) typically leads to smaller values compared to those obtained from modal analyses and it generally leads to conservative results being the spectral acceleration higher for

smaller values of periods (Chopra 2012). Empirical formulations are evaluated for limited building configurations and their use is becoming less popular because of the availability of commercial software packages that allow direct evaluation of the building properties through modal analysis (Chopra 2012).

A simplified "displacement-based" method included in EC8-3 (CEN2005) for the assessment and retrofitting of buildings, allows to use elastic spectra at ultimate limit states for deriving the design deformation values but very restrictive applicability criteria must be verified at an early stage. For instance, if ρ denotes the generic Demand over Capacity Ratio (DCR) of the ductile primary element of the building (expressed in terms of bending moment for frames and walls, and axial force for braces), it must result that the ratio ρ_{max} / ρ_{min} (among all the elements having $\rho > 1$) should be less than 2.5 and the DCR values of the brittle primary elements (evaluated in terms of shear) should be less than unity, with specific rules on how to calculate the demand values (CEN2005).

Due to its simplicity and conservativity, LFM is often used for preliminary analysis helping in dimensioning structures and roughly quantifying the seismic effects.

2.2.2. Linear dynamic analysis

The linear dynamic analysis or more commonly Linear Time-History Analysis (LTHA) is an analysis applied to a linear model of the structure in which the input is characterised by accelerometric waveforms resulting from an *ad hoc* seismic input selection. LTHA considers the interaction of the modes of vibration of structures with the typical frequencies of earthquakes for this reason is considered more accurate than LFM when higher modes' contribution must be considered (Chopra 2012). Differently from LFM, it consists in solving the dynamic problem as a succession of solutions corresponding to all times of interest *t*. From the mathematical point of view, the differential equations that govern the seismic response of a discrete linear MDOF system having [*M*], [*C*], and [*K*], mass, damping and stiffness matrices, can be expressed as shown in Eq. 2.4, where $\{\ddot{u}(t)\}$ is the relative acceleration vector, $\{\dot{u}(t)\}$ is the relative velocity vector, $\{u(t)\}$ is the relative displacement vector, $\{\tau\}$ is the influence coefficient vector, and $\{\ddot{u}_g(t)\}$ is the earthquake GM acceleration (Chopra 2012).

$$[M]\{\ddot{u}(t)\}+[C]\{\dot{u}(t)\}+[K]\{u(t)\}=-[M]\{\tau\}\{\ddot{u}_g(t)\} \tag{2.4}$$

The elastic stiffness matrix [*K*] is built up through the so-called stiffness influence coefficients associated to the degrees of freedom of the problem (Clough and Penzien 2003). They represent the internal forces developed in the system when a displacement equal to unity corresponding to a specific degree of freedom is applied while all the others are constrained. Displacements can be translations and rotations at the nodes of the system, and they depend on the boundary conditions (e.g., supports at the ground level) and constraint conditions (e.g., rigid diaphragm). The elastic stiffness matrix depends on both the geometric properties (e.g., second moment of area of the

element's cross-section) and the material properties of the elements within a structure (e.g., Young's modulus of the material). It is a symmetric matrix and is the same used by LFM for solving MDOF systems. The stiffness matrix can be built up to consider the contribution of static loads for solving problems affected by buckling of elements or second-order effects (BSSC 2015).

The mass matrix [*M*] is generally built up assuming lumped masses (which can be translational and rotational) at the nodes of the system which are related to the corresponding excited degrees of freedom ("lumped-mass matrix"). The off-diagonal terms of this matrix are null, being the acceleration of any mass-point able to produce an inertial force at that point only (Clough and Penzien 2003). This approach is particularly convenient for multi-storey buildings which floors can be assumed as rigid diaphragms because lumped masses would be defined only for the three rigid-body DOFs of the floor diaphragm in its own plane at each storey (Chopra 2012). Another approach is to evaluate the mass matrix in a consistent way as per the stiffness coefficients considering the mass influence coefficients ("consistent-mass matrix", Clough and Penzien 2003). In this way, the mass influence coefficients associated with a certain acceleration are defined as the nodal inertia forces which it produces (Clough and Penzien 2003). In the second case, the mass matrix is full and symmetric, and it requires a more computational effort for solving Eq. 2.4.

Regarding damping, it is impractical to calculate the coefficients of the damping matrix [*C*] from the characteristics of the structure because there are many other sources participating in energy dissipation (e.g., partitions, steel connections, mechanical equipment) which are typically not accounted for in the numerical model. Therefore, modal damping ratios (ζ_i, i = 1, …, n) based on experimental data are generally adopted in civil engineering practice (Chopra 2012). Some researchers recommended values of damping ratios for buildings based on the level of stress compared to yielding stage, type and condition of structures (Newmark and Hall 1982; Bachmann et al. 1995). For earthquake engineering and elastic problems (i.e., design), ζ is typically assumed equal to 5% in order to be consistent with the value adopted for constructing the response spectra (Chopra 2012). The most common model for the evaluation of the damping matrix is the Rayleigh damping (see Fig. 2-3) which assembles the damping matrix as a linear combination of the mass and stiffness matrices as per Eq. 2.5 where α_M and β_K are two coefficients which can be determined from the damping ratio and period of vibration (or frequency) of two modes of vibration, properly chosen to ensure that the computed damping ratios of the other (significant) modes are not too dissimilar (Chopra 2012). If more than two damping ratios need to be specified, the Caughey damping method allows to meet this requirement if specific checks are considered in order to avoid negative values of ζ computed for the other periods (Caughey 1960).

$$[C] = \alpha_M [M] + \beta_K [K] \tag{2.5}$$

Another alternative is represented by the so-called "superposition of modal damping matrices" method (Clough and Penzien 2003) which can be expressed as per Eq. 2.6, if [*M*] is a diagonal matrix, where $\{\Phi\}_i$ is the mode shape vector of the i^{th} mode of vibration, M_i is the generalised modal mass of the i^{th} mode of vibration (i.e., $\{\Phi\}_i^T [M] \{\Phi\}_i$), and ω_i is the frequency of the i^{th} mode of vibration (i.e., $\omega_i = 2\pi / T_i$).

$$[C] = [M]\left(\sum_i \frac{2\zeta_i \omega_i}{M_i} \{\phi\}_i \{\phi\}_i^T \right)[M] \tag{2.6}$$

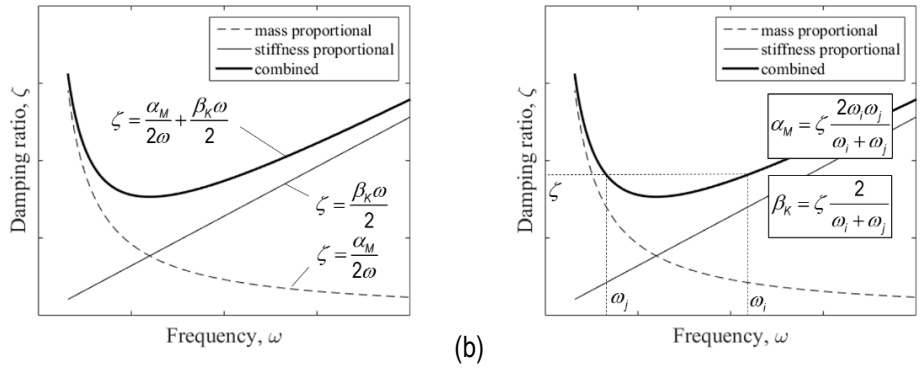

Fig. 2-3 Rayleigh damping: (a) variation of the damping ratio with frequency and (b) example of implementing Rayleigh damping by evaluating the mass-proportional coefficient (α_M) and the stiffness-proportional coefficient (β_K) from two fixed values of the frequency (ω_i and ω_j) and damping ratio (ζ) (adapted from Chopra 2012).

The vector $\{\Phi\}_i$ includes all the degrees of freedom of the structure unless the problem is based only on some of them (i.e., condensation of the matrix). The Rayleigh damping represents the most convenient method for practical analyses and many commercial software packages implement it, being computationally lighter than the others. It is worth mentioning that the approach presented above is consistent for "classical" damping matrices where it is assumed that similar damping is attributed throughout the structure (Chopra 2012). When different parts within the system are affected by significantly different levels of damping (e.g., soil-structure interaction, isolation, dampers), the "nonclassical" damping matrix of the system should be assembled considering the contribution given by the matrices of the different parts (Clough and Penzien 2003).

The dynamic equilibrium equations can be solved through different approaches such as direct integration and modal superposition (Chopra 2012). The modal superposition is based on the validity of uncoupled modal equations of motion and superposing their effects (typical for "classical" damping). Each equation is a SDOF equation of motion which can be solved either in the time-domain or in the frequency domain (Chopra 2012). Contrarily, for any other type of damping ("nonclassical") the modal equations of motion result to be coupled by modal damping coefficients and direct step-by-step integration is typically used (Chopra 2012). "Classical" damping systems can

be either analysed by modal superposition and direct integration. According to the direct integration approach, the time-history is divided into a certain number of equal-value time-steps in which the response is calculated. At the end of each time-step the response is updated for its use in the subsequent time-step (Chopra 2012).

The selection of GM acceleration time-histories (which can be real, artificial and simulated) must be carried out conforming to specific criteria for the specific site and limit state, and by considering a sufficient number of GM acceleration time-histories, as explained in Section 2.5.

LTHA represents a method of analysis that did not find consensus in the past at both research and codification level. Only recently some efforts have been made to investigate its capability for design purposes (Charney 2015). It is important to highlight that except for the recent FEMA P-1050, which recommendations are adopted by ASCE/SEI 7-16, none of the other current design codes, including EC8, include LTHA explicitly among the methods of seismic analysis. This research work aims at contributing on investigating LTHA as a "force-based" design method with the proposal of an EC8-compliant design framework presented in Chapter 4. Moreover, the possibility of using LTHA as method within a simplified PBEE framework for deriving fragility curves at design stage that can be used for comparative loss estimation of design solutions is investigated in Chapter 7.

2.2.2.1. Modal response spectrum analysis

Modal Response Spectrum Analysis (RSA) is often addressed as linear dynamic analysis and it represents the reference seismic design method according to many codes, including EC8. RSA is more accurate than LFM in evaluating the seismic response of buildings and it is conceived for design of buildings which do not meet the requirements for the applicability of LFM (i.e., irregular and tall buildings). The RSA is an approximate approach for the evaluation of linear dynamic response of structures where the seismic input is represented by a response spectrum instead of an acceleration time-history. It was conceived from the need to evaluate the peak response of structures from GMs without carrying out LTHA (Chopra 2012). It can directly determine the exact peak response of SDOF systems without carrying out LTHA but the results of the two analyses are different for MDOF systems (Chopra 2012). If $E(t)$ denotes the structural response over the time t, RSA employs results of static analysis (for each considered mode of vibration) combined on the basis of modal properties of structures, in order to calculate the peak value of the response E_o. The approximation lies in the assumption that the peak modal responses occur in the same time-instant (Chopra 2012). Specifically, the peak value of the i^{th}-mode contribution to the seismic response E_{io} is obtained from the response spectrum (e.g., code spectrum), which provides the pseudo-acceleration (either elastic or design depending on the limit state) at the modal period T_i for the assumed damping ratio of the i^{th}-mode ζ_i, denoted by $S_a(T_i, \zeta_i)$, and the modal static response E_i^{st}, as in Eq. 2.7.

$$E_{io} = E_i^{st} S_a(T_i, \zeta_i) \qquad i = 1,2,...,n \tag{2.7}$$

The pseudo-acceleration is positive, so the sign of the peak effect is the same of E_i^{st} which is calculated by static analysis of the structure subjected to the distribution of lateral forces proportional to the i^{th}-mode. All the vibration modes which relevantly contribute to the evaluation of the peak response should be accounted for (CEN 2004a). For instance, EC8, like many other design codes, requires that all the modes with more than 5% participating mass are considered in and the sum of their participating masses is greater than 90%. However, in some cases, 90% total participating mass cannot be necessarily enough to capture accurately the dynamic response of structures.

Response parameters obtained from each modal static analysis (e.g., element local forces, nodal displacements) are then combined according to the adopted combination rule (CEN 2004a). Several combination rules of modal response peak values have been proposed in the last century (e.g., Rosenblueth 1951; Wilson et al. 1981; Der Kiureghian 1981).

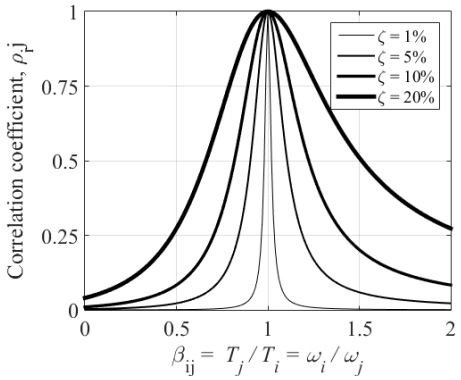

Fig. 2-4 Variation of the correlation coefficient with modal frequency (or period) ratio assuming constant modal damping ratio $\zeta_i = \zeta_j = \zeta$.

It was found that the sum of the absolute values (also known as Absolute Sum, ABSSUM) is usually too conservative and it can provide an upper bound value of the peak response (Chopra 2012). An alternative is the Square Root of the Sum of Squares (SRSS, Rosenblueth 1951) which can be expressed as per Eq. 2.8, but it provides excellent estimates of the peak response for structures having well-separated periods of vibration and subjected to wide-band ground motions (Cacciola et al. 2004).

$$E_o = \sqrt{\sum_{i=1}^{n} E_{io}^2} \tag{2.8}$$

The Complete Quadratic Combination (CQC, firstly used by Der Kiureghian 1981 and then proposed by Wilson et al. 1981) is a combination rule for RSA since 1980s and it was originally derived from the Random Vibration theory mainly for mechanical applications. If E_{io} and E_{jo} are respectively the values of the generic modal static analysis effects due to the vibration mode i and j, the peak value

can be obtained from Eq. 2.9, where ρ_{ij} is the correlation coefficient between i and j mode in which $\beta_{ij} = T_j / T_i$, being T_i and T_j the corresponding periods (see Fig. 2-4). The correlation coefficient ranges within [0, 1], and it is equal to unity for $i = j$ (i.e., $\beta_{ij} = 1$), decreasing rapidly as the periods are more distant, especially for small values of ζ.

$$E_o = \sqrt{\sum_{i=1}^{n}\sum_{j=1}^{n}\rho_{ij}E_{io}E_{jo}}$$
$$\rho_{ij} = \frac{8\sqrt{\zeta_i\zeta_j}(\beta_{ij}\zeta_i + \zeta_j)\beta_{ij}^{3/2}}{(1-\beta_{ij}^2)^2 + 4\zeta_i\zeta_j\beta_{ij}(1+\beta_{ij}^2) + 4(\zeta_i^2+\zeta_j^2)\beta_{ij}^2} \quad (2.9)$$

It was found that CQC presents some limitations for unusually stiff buildings such as nuclear power plants (Gupta 1992), near source impulsive earthquakes and structures having relevant higher modes contribution (De Luca and Verderame 2013). Gupta (1992) proposed a modification of ρ_{ij} which accounts for better estimates in case of low periods of vibration. Differently, Cacciola et al. (2004) proposed a simplified procedure for the evaluation of ρ_{ij} based on the power spectral density and duration of the GMs which is consistent with the adopted response spectra (which can be spectrum-compatible with the code-spectrum). Indeed, the traditional CQC rule assumes the white-noise approximation of correlation coefficients and it was found that it can lead to relevant errors when the response is influenced by modal responses having periods lower than the dominant period of the GM (Gupta 1992; Der Kiureghian and Nakamura 1993). De Luca and Verderame (2013) compared results of RSA, employing the traditional CQC and GM response spectra corresponding to different suites of real unscaled pulse-like/non pulse like GMs, against LTHA results, for the same GMs, and observed that the median maximum interstorey drift ratios and storey shears at upper storeys can be significantly underestimated with respect to LTHA for medium-high buildings, especially for pulse-like GMs having pulse period T_P lower than T_1.

Notwithstanding these studies, EC8 together with other design codes do not provide any specific indication and still recommend the traditional CQC rule as reference combination method. On the contrary, ASCE 7-16 recognises the limitations of RSA, allowing the use of other approved combination rules (e.g., CQC-4) and recommending to scale design forces obtained from RSA to be at least equal to the ones obtained from LFM. However, these procedures (whether optimised or not) do not solve another critical aspect related to loss of the sign and coupling of internal forces and displacements (Wilson 2015). Because of the combination rule, response parameters are given as absolute values (i.e., the double sum under the square root in Eq. 2.9 is always positive) as well as uncoupled values of the local force components (e.g., coupling of axial force and bending moments for three-dimensional problems). This is an issue for those cases where the sign of the internal force significantly changes the behaviour of the element (e.g., axial force in braces subjected to buckling) or when simultaneously-acting components lead to more accurate verifications (e.g., squat columns

subjected to axial force and biaxial bending moment). In some cases, it can be reasonable to assign the signs evaluated from the fundamental translational modes of vibration to the resulting response effects, but this cannot be adopted always in general (e.g., high-rise buildings).

2.3.Nonlinear analysis methods

Displacements are typically considered as a parameter better representative of structural damage rather than forces (Priestley 2003). For this reason, nonlinear analyses are preferred for the assessment of existing or retrofitted buildings for which these analyses are the reference methods (ASCE 2014; CEN 2005). However, they can be used for the evaluation of the seismic structural performance of new buildings, such as new buildings that do not conform to current codes requirements or, anyways, under specific request by owners and stakeholders (Deierlein et al. 2010; ASCE 2017). Their accuracy in results strictly depends on the adequacy of the seismic input as well as on sophisticated structural numerical models which must represent the behaviour of materials, sections and elements (Fardis 2009). Indeed, the nonlinear behaviour is generally due to the relationship between stress and strain from material behaviour such as ductile yielding, stiffness and strength degradation or brittle fracture, and the inclusion of large displacements in the compatibility and equilibrium relationships (Fardis 2009).

2.3.1. Nonlinear structural modelling

Nonlinear structural models can be classified depending on how the plasticity is modelled through the member cross-section and along its length (e.g., Deierlein et al. 2010; Haselton et al. 2017c). Beams, columns and braces can be modelled according to the plasticity models shown in Fig. 2-5. The simplest model consists in modelling the inelastic behaviour of structural members through a zero-length element such as the “plastic hinge” model with rigid-plastic behaviour (Fig. 2-5a) or “nonlinear spring hinge” model with a multilinear relation (i.e., backbone curve) characterised by change in stiffness at different stages as well as degradation in strength and deformation capacity under cyclic loading (Fig. 2-5b). These hinges only contribute to the rotation when the yielding capacity of the element at that section is achieved. For beams and columns, ductile behaviour is typically described in terms of bending moment versus chord rotation (M-θ) relations and the maximum seismic demand in these structural members generally occurs at their ends (Haselton et al. 2017c). These models are called “concentrated (or lumped) plasticity models” because they require the assignment of specific M-θ curves at the sections of the element where nonlinear behaviour is expected, while the element itself remains elastic (Ibarra et al. 2005; Haselton et al. 2008). Due to the simplicity of the formulation, the concentrated (or lumped) plasticity models are widely used by most of the commercial software packages and they result particularly convenient when the computational cost of the analysis is high such as for analysing very complex structures. More refined models are represented by the “distributed plasticity models” that allows capturing the plasticity spread throughout both the cross-section and the length of the element, and accounting for

the interaction between axial force and biaxial bending moment (Deierlein et al. 2010). The simplest distributed plasticity model consists in the "finite-length hinge" model with designed moment-curvature (M-φ) relation or cross-section discretised with fibre-type elements characterised by specific material stress-strain (σ-ε) relations (Fig. 2-5c). The plastic hinge length can be fixed or variable and the integration of the deformations along the plastic hinge length allows evaluating the hinge rotation and capturing the plasticity spread at the end of the member (Deierlein et al. 2010). Differently, the "fibre-section" model is not based on the definition of a plastic hinge length but it consists in integrating deformations at n discrete cross-sections along the element length which are in turn discretised through fibre elements (Fig. 2-5d). These two types of distributed plasticity models are based on the assumption that plane sections remain plane for increasing values of the curvature and the location of the sections (i.e., integration points) are typically determined by numerical integration rules (Scott 2011). The most complex distributed plasticity model is represented by the "finite element" model which discretised the continuum along the member length and through the cross-section through (micro) finite elements with specific behaviour (Fig. 2-5e). The latter is generally used for carrying out detailed studies at the local scale, such as stress distribution, propagation of cracks, effects of contact, because it requires a high computational cost (Deierlein et al. 2010).

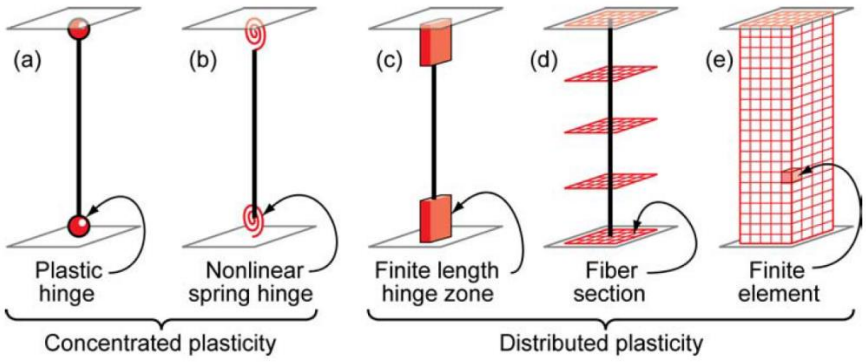

Fig. 2-5 Plasticity models of beam-column elements (after Deierlein et al. 2010).

2.3.1.1. Concentrated plasticity models

Concentrated (or lumped) plasticity models are widely used for evaluating the nonlinear response of buildings subjected to earthquake loading because of their required low computational cost compared to others. They are easy to implement, and they are nowadays used by engineers for design and assessment of new and existing buildings (e.g., Haselton and Deierlein 2008; De Luca et al. 2014; Fragiadakis et al. 2014). Historically, the concentrated plasticity models were introduced by Clough et al. (1965) who proposed the "two-component model" consisting of two beams, one with elastic behaviour and another one with elastic-perfectly plastic behaviour, working in parallel. Subsequently, Giberson (1967) proposed an enhanced version of the first model called the "one-

component model" which represents the ancestor of the current concentrated plasticity models. Nowadays, these models have achieved significant improvements in predicting nonlinear structural response thanks to experimentally calibrated backbone curves (M-θ) proposed in literature (Haselton et al. 2008; Biskinis and Fardis 2010a; Biskinis and Fardis 2010b). These curves are defined by critical points expressed in terms of bending moment and chord rotation at some stages, such as: yielding stage (M_y,θ_y), capping stage (M_u,θ_p), and post-capping stage (M_{pc},θ_{pc}) (see Fig. 2-6a). Such points are evaluated by means of empirical/mechanical equations that account for the hardening or softening behaviour of materials, the effects of transverse confinement in RC columns, the buckling of bars, the plastic hinge length, the bar slip, and the hysteretic degradation in strength and deformation capacities (e.g., Elwood et al. 2007; Kwon 2016; Haselton 2006; Biskinis and Fardis 2010a; Biskinis and Fardis 2010b). Concentrated plasticity models have limitations in representing accurately the interaction of axial force with biaxial bending moment. It is typically assumed by considering constant values of axial force even if sophisticated models have been developed which assume the yield surface and multiple backbone curves for varying levels of the axial force. However, this procedure generally leads to high computational cost and can generate numerical issues (Haselton et al. 2017c). Where the nonlinear shear behaviour and bond-slip deformation are of concern, additional zero-length elements having specific relations can be added at the ends of the structural member.

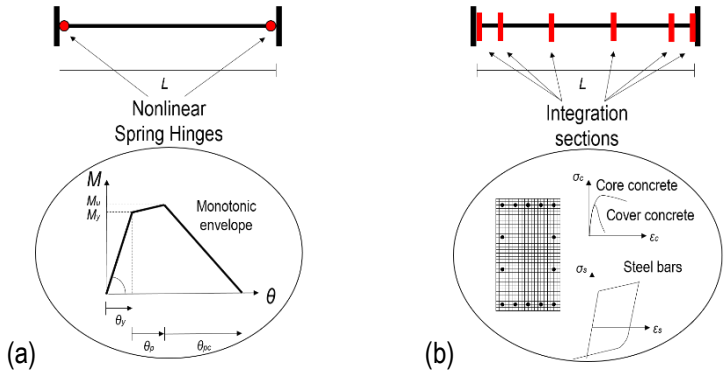

Fig. 2-6 Modelling of plasticity models of beam-column elements: (a) concentrated plasticity model with nonlinear spring hinges (adapted from Haselton et al. 2017c) and (b) distributed plasticity model with fiber-sections (adapted from Calabrese et al. 2010).

2.3.1.2. Fibre-based plasticity models

Fibre-based models, whether with plastic hinge length or not, are certainly the most used distributed plasticity models since they represent a good compromise in terms of accuracy and computational cost between concentrated plasticity models and finite-element models (Calabrese et al. 2010; Fragiadakis and Papadrakakis 2008). Contrarily to concentrated plasticity modes, fibre-based models allow plasticity to spread along the element length and do not require a preliminary evaluation of bending moment and chord rotation at different stages since the behaviour of the structural

member is directly described by the chosen section properties (i.e., geometry, material, and longitudinal steel reinforcement). The structural member (see Fig. 2-6b) is discretised in a certain number of cross-sections which position depends on the integration rule (e.g., Gauss-Lobatto, Newton-Cotes). The number of fibres, which are used for discretising the element cross-sections, impacts on the computational cost. For RC members, specific stress-strain (σ-ε) relations are assigned to the fibres in the cover region, core region, and longitudinal bar regions (Menegotto and Pinto 1973; Popovics 1973; Mander et al. 1988; Chang and Mander 1994). Transverse steel reinforcement is not explicitly considered in fibre-based models but its effects in terms of confinement are implicitly considering by modifying the σ-ε relation of the core region. In this way, concrete cracking, stress reversals, tension-stiffening, confinement effects, material hardening, and softening behaviour are described by the adopted material models. Early fibre-based models adopted the "stiffness" method (i.e., "displacement-based" formulation, Hellesland and Scordelis 1981; Mari and Scordelis 1984) where the displacement field is imposed though a linear variation of curvature along the element and the element forces are found by energy considerations (Calabrese et al. 2010). In contrast, the more recent "flexibility" method (i.e., "force-based" formulation, Neuenhofer and Filippou 1997; Spacone et al. 1996) strictly satisfies equilibrium without any restraints on the development of nonlinear curvature along the element (Calabrese et al. 2010). The two methods lead to same results for linear-elastic behaviour, but they can show significant differences in the nonlinear field when softening occurs. This aspect is well-known as "strain localisation" and it basically implies dependence on the discretisation and loss of objectivity in the softening stage (Zeris and Mahin 1988; Coleman and Spacone 2001). To overcome this issue, more displacement-based elements are typically used for each structural member so that the distance between the integration sections is somehow similar to the plastic hinge length (e.g., 10 elements per member as considered in Calabrese et al. 2010). For force-based elements, the newly introduced finite-length hinge model overcomes this issue by assuming a user-defined plastic hinge length that should be properly calibrated (Scott and Fenves 2006; Scott and Ryan 2013; Ribeiro et al. 2015; Ribeiro et al. 2017). Fiber-based models can consider the effects of the interaction between axial forces with biaxial bending moment on strength, stiffness and ductility of elements. Moreover, they can provide results in terms of curvature or stress and strains, and capture cracking effects and neutral axis shift (Haselton et al. 2017c). The effect of cracking and tension stiffening can be included in the material model (e.g., Belarbi and Hsu 1994). However, fibre-based models have some limitations such as cannot handle rebar bond-slip, capture rebar buckling and steel fracture, and account for complex pinching, unless sophisticated models are additionally considered making the computational cost high (Haselton et al. 2017c). Indeed, because of the basic assumption that plane sections remain plane for increasing values of the curvature, perfect-bond condition between concrete and steel reinforcement is implied. As per concentrated plasticity models, where the nonlinear shear behaviour

and bond-slip deformation are of concern, additional zero-length elements having specific relations can be added at the ends of the structural member.

2.3.2. Nonlinear static analysis

The Nonlinear Static Analysis (NSA) or pushover analysis was firstly introduced by FEMA 273 (FEMA 1997) and ATC-40 (ATC 1996) as a recommended procedure for the seismic evaluation and retrofit of concrete buildings. It nowadays represents the most used nonlinear method in professional practice for its availability in many commercial software packages which already implement code-conforming procedures. NSA is essentially an extension of the LFM within the nonlinear field. Basically, in such method the building is subjected to a lateral load distribution of forces which is proportionally scaled as the displacement of a control point (generally located at the roof level) increases up to the achievement of the ultimate condition (e.g., collapse mechanism or degradation level), while the gravity loads are constant (CEN 2004a). This distribution of forces is representative of the inertia forces of the seismic action and it should be assigned according to two distributions along both the main directions: (i) first translational mode-like distribution as per LFM or from modal analysis if LFM requirements are not met, and (ii) uniform distribution in order to simulate the inertia forces in a potential soft-storey mechanism at the bottom storey (CEN 2004a) The nonlinear behaviour of the building is conferred by means of plasticity models, which are assigned to the structural elements as explained in Chapter 5. The analysis result is represented by the "capacity curve" of the building which relates the base shear (F_b) to the displacement of a control point (Δ_n) at each increasing step of the analysis (CEN 2004a). Once the capacity curve is obtained, the building is transformed into an equivalent SDOF system in order to estimate the inelastic displacement demand in a consistent way with the response spectrum. The EC8 adopts the N2 procedure for the equivalent SDOF system definition (Fajfar 2000) which is based on the elastic-perfectly plastic idealisation of the capacity curve of the equivalent SDOF system (see Fig. 2-7). The capacity curve of the structure is firstly scaled by the participation factor of the translational mode denoted by Γ (i.e., $F^* = F_b / \Gamma$, $\Delta_n^* = \Delta_n / \Gamma$) and then bilinearised according to some rules (CEN 2004a). This bilinear curve is characterised by elastic stiffness K^*, yielding force F_y^*, yielding displacement Δ_y^*, and ultimate displacement Δ_u^* (see Fig. 2-7). The yielding force F_y^* and the ultimate displacement Δ_u^* are evaluated from the point at which the structure achieves the ultimate condition. The elastic stiffness, equal to F_y^* / Δ_y^*, can be evaluated from the period of the equivalent SDOF system:

$$T^* = 2\pi\sqrt{\frac{m^*\Delta_y^*}{F_y^*}} \tag{2.10}$$

where m^* is the mass of the equivalent SDOF system evaluated as $\Sigma_i m_i \Phi_i$, with Φ_i representing the horizontal displacement of the modal shape (normalised at the control node) of the lateral load distribution assigned to the structure at the i^{th} storey. The yielding displacement Δ_y^* is evaluated

through imposition of equal area (A^*) under the capacity curve (scaled by Γ) of the building and the bilinear one of the equivalent SDOF system, and it is calculated as follows:

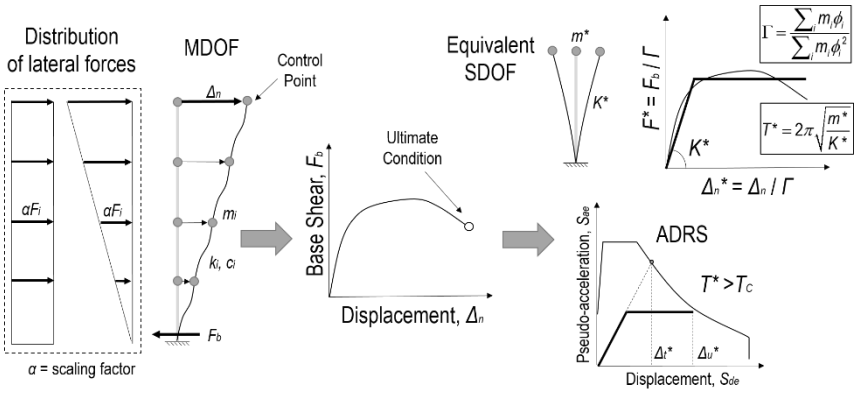

Fig. 2-7 Nonlinear Static Analysis with N2 procedure.

$$\Delta_y^* = 2\left(\Delta_u^* - \frac{A^*}{F_y^*}\right) \tag{2.11}$$

The verification according to the "displacement-based" approach is carried out on the Acceleration-Displacement-Response-Spectrum (ADRS, Mahaney et al. 1993) plane, checking that the ultimate displacement Δ_u^* is larger than the target displacement representative of the maximum displacement induced by the earthquake (Δ_t^*) which can be evaluated as per Eq. 2.12 (Vidic et al. 1994).

$$\begin{aligned} \Delta_t^* &= S_{de}(T^*) = \left(\frac{T^*}{2\pi}\right)^2 S_{ae}(T^*) \qquad \text{if } T^* \geq T_C \\ \Delta_t^* &= \frac{S_{de}(T^*)}{q^*}\left[1 + (q^* - 1)\frac{T_C}{T^*}\right] \geq S_{de}(T^*) \qquad \text{if } T^* < T_C \end{aligned} \tag{2.12}$$

In Eq. 2.12, $S_{de}(T^*)$ and $S_{ae}(T^*)$ represent the elastic spectral displacement and the elastic spectral pseudo-acceleration at T^*, respectively, both evaluated on the ADRS for the 5% damping ratio, while q^* is equal to $m^* S_{ae}(T^*) / F_y^*$. The N2 procedure was extended to account for the higher-modes effects by Kreslin and Fajfar (2011) but it is not included in any design code and commercial software package yet.

The ATC-40, proposed two procedures namely "capacity spectrum method" and "displacement coefficient method". The "displacement coefficient method" is based on the calculation of the target displacement as per Eq. 2.13 in which C_0, C_1, C_2, C_3 are some modification factors explained in the folowing, T_{eff} is the effective fundamental period, and $S_{ae}(T_{eff})$ the elastic response spectrum acceleration at the effective fundamental period of the building.

$$\Delta_t = C_0 C_1 C_2 C_3 S_{ae}(T_{eff})\left(\frac{T_{eff}}{2\pi}\right)^2 \tag{2.13}$$

Contrarily to the EC8, the ATC-40 basically modify the elastic spectral displacement at T_{eff} through a modification factor which accounts for scaling (C_0), ductility (C_1), hysteresis shape (C_2), and P-Δ effects (C_3). The effective period T_{eff} is evaluated as T_{el} (K_{el} / K_{eff})$^{0.5}$ where T_{el} and K_{el} are the elastic fundamental period and the elastic stiffness of the building along the direction in consideration, respectively, and K_{eff} is the effective elastic stiffness identified by constructing a secant line passing through the point on the capacity curve equal to 0.6 times F_y. Alternatively, the "capacity spectrum method", which is similar to the N2 method, is based on the reduction of the elastic spectrum, expressed in terms of effective damping, to intersect the capacity curve in the ADRS plane in order to find the performance point. Also in this case, the capacity curve of the structure obtained from NSA is scaled and bilinearised according to specific rules (ATC 1996). The main difference between the "capacity spectrum method" and the N2 method is the adoption for the latter of a ductility-strength-period relationship instead of highly-damped spectra in the ADRS plane but they are conceptually equivalent. Recently, a novel approach called FRACAS has been proposed which is based on the "capacity spectrum method" (Rossetto et al. 2016). This approach can overcome limits of the previous procedures that are not able of capturing the GM spectral shape and record-to-record variability (Minas and Galasso 2019). It consists in discretising the obtained equivalent SDOF capacity curve into a number of inelastic SDOF systems which are analysed under the considered GM to determine the inelastic part of the response spectrum that allows to identify the target displacement. This approach can be implemented for each GM of a selected suite.

For a SDOF system the difference in results between traditional NSA and the most rigorous Nonlinear Time-History Analysis (NTHA) is expected to be limited but it can be significant when the influence of the higher modes of vibration becomes relevant (Fragiadakis et al. 2014) and for the analysis of 3D realistic buildings, the majority of which are irregular in plan (Bhatt and Bento 2014). More specifically, it was found that traditional NSA can produce accurate estimations of peak floor displacements for low- and mid-rise buildings with symmetrical regular configurations (less than about five storeys, Deierlein et al. 2010) but it tends to overestimations for high-rise buildings (Onem 2008). Improvements of NSA including single-modal adaptive and multi-modal adaptive/non-adaptive methods were attempted in the past, but they substantially led to solving complex computations often requiring expert choices (e.g., Chopra and Goel 2002; Antoniou and Pinho 2004; Goel and Chopra 2005; Fragiadakis et al. 2007; Bhatt and Bento 2014;). However, these methods can show inconsistency in accuracy for other engineering parameters (e.g., peak plastic hinge rotation, storey shears, storey drifts and storey overturning moments), depending on the structural system, configuration, intensity of inelastic response, and development of soft-storeys (NIST 2010).

Notwithstanding NSA limits, it is still considered a useful tool to investigate general aspects of nonlinear behaviour of buildings such us checking issues in nonlinear modelling, investigating yielding mechanisms and alternative design parameters' choice (NIST 2010).

2.3.3. Nonlinear dynamic analysis

The nonlinear dynamic analysis or Nonlinear Time-History Analysis (NTHA) is undoubtedly the most complete and effective method of seismic analysis. The response of the structural system subjected to ground acceleration time-histories is obtained by solving Eq. 2.4, in which the stiffness matrix [*K*] is computed for each time step of the analysis on the basis of the hysteretic plasticity models assigned to the structural members (Chopra 2012). In this light, it explicitly simulates the cyclic energy dissipation of the structure in the nonlinear field.

Contrarily to LTHA which effects can be linearly added to those of gravity load analysis thanks to the validity of the superposition principle, expected gravity loads should be preliminarily included in NTHA so to account for their effects in terms of forces, deformations and P-Δ effects.

Rayleigh damping method was originally developed for LTHA, but it was extensively used in the past for NTHA as well. It was found that the Rayleigh damping model can lead to "spurious" damping forces and inaccurate results for NTHA (Chopra and McKenna 2016). Several procedures were proposed in order to eliminate or reduce the spurious damping forces (e.g., Bernal 1994; Hall 2006; Charney 2008; Chopra and McKenna 2016). One of these consisted in reducing their effect by using only the stiffness-proportional part of the Rayleigh model and eliminating the mass-proportional contribution (Hall 2006). Some other researchers proposed to use the tangent stiffness instead of the initial stiffness (i.e., elastic stiffness) in Rayleigh damping (Charney 2008; Jehel et al. 2014). This issue is mainly related to the identification of high damping forces when the structure passes the yielding stage which is against physics (from here the idea of avoiding the initial stiffness in computing damping forces and the use of the adjective "spurious"). However, this approach is an approximation and implies that the tangent stiffness matrix varies with time and shows increasing computational cost. Chopra and McKenna (2016) recommended using the superposition of modal damping matrices which eliminates the spurious damping forces. They also highlighted that this adoption is particularly recommended for structures which are modelled through lumped plasticity models rather than distributed ones. A recent work evaluated a new damping model where the damping forces are assumed being proportional to an estimate of the elastic component of velocity rather than the total velocity, which includes both elastic and plastic components (Luco and Lanzi 2017; Lanzi and Luco 2018). The damping ratio typically ranges between 1% and 5% for elastic periods in the range [$0.2T_1$, $1.5T_1$] (NIST 2010). It is generally recommended a value of 2.5% over the range of the dominant modes (PEER 2010) or between 1% and 2% (Willford et al. 2008).

Independently from the type of damping model, "classical" or "nonclassical", NTHA is based on direct step-by-step integration (Chopra 2012). The complexity of the algorithm and the choice of the analysis parameters are both aspects that limit the widespread use of such method of analysis in the

professional field. Moreover, the use of NTHA requires analysing the structure for a sufficient number of GMs selected to build up suites according to specific criteria (CEN 2004a).

2.4.Performance-Based Earthquake Engineering

Traditional seismic design philosophy mainly aims at preventing global or local collapse of structures from high-intensity earthquakes and is intended to control damage of structural and non-structural members of structures from minor to moderate-intensity earthquakes (e.g., Ghobarah 2001; Krawinkler and Miranda 2004). To achieve this target, design codes prescribe design and construction rules believing that structures can attain these desired performances. However, some past earthquakes (e.g., M6.7 1994 Northridge, M6.8 1995 Kobe) demonstrated that economic loss due to structural and non-structural damage (i.e., repair costs) as well as downtime (i.e., repair time) were unacceptably high, even for those structures that were designed according to modern codes (FEMA 1997). For instance, non-structural damage can be an important part of economic loss of buildings (e.g., damage of perimeter infill walls in RC buildings, Ricci et al. 2011; Barbosa et al. 2017). Therefore, research in the last decades pushed towards the development of methodologies which can both overcome the prescriptive nature of design codes and allow to control the economic losses and improve seismic risk decision-making when necessary.

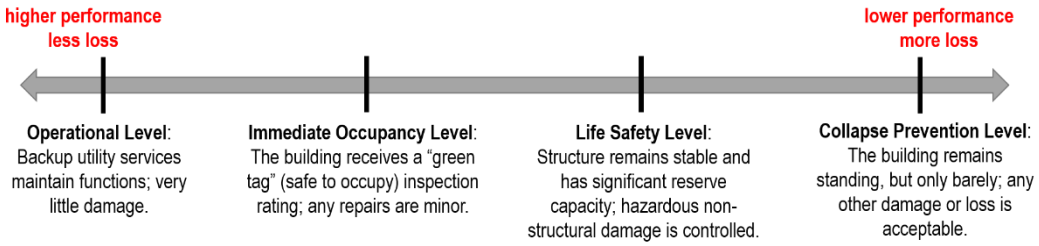

Fig. 2-8 Performance levels (adapted from FEMA 273).

Performance-Based Earthquake Engineering (PBEE) founds its origins in the Vision 2000 reports (SEAOC 1995) and ATC-40 (1996) where frameworks for designing new buildings and rehabilitating existing ones were respectively presented. These frameworks essentially assume NSA as reference method (the "capacity spectrum method" introduced in Section 2.2.1) and involve the selection of a desired performance level when the building is subjected to specified levels of seismic hazard. Similarly to ATC-40, FEMA 273 (FEMA 1997) provides a description of the "Performance Level" as the intended post-earthquake condition of a building to which corresponds a well-defined point on a scale measuring loss caused by earthquake damage (see Fig. 2-8); such loss can be expressed in terms of casualties (i.e., deaths and serious injuries), properties (i.e., building repair or replacement costs) and downtime (i.e., repair time and unsafe placarding). The combination of a structural performance level and a non-structural performance level, to form a complete description of an overall damage level, defines the "Building Performance Level" which is combined with the "Hazard

Level" to define the "Design/Rehabilitation Objective" (FEMA 1997). It is worth mentioning that seismic ground shaking is not the only hazard at the site but there could be multiple hazards such as fault rupture, liquefaction, landslides, inundation from offsite effects like dam failure or tsunami triggered by a catastrophic event (FEMA 1997). However, only recently multiple hazards are combined to represent holistic scenarios of catastrophic events.

The possible combinations of both performance and hazard levels conceptually defines a matrix (see Table 2-1) indicating the broad range of design/rehabilitation objectives (FEMA 1997). For instance, it may be chosen as goal for the rehabilitation of an existing RC building by the building owner the achievement of Life Safety Performance Level (both structural and non-structural) for the rare earthquake (having Exceedance Probability, EP, equal to 10% in 50 years), i.e. objective *k* in Table 2-1, For the objective *k*, it is expected that after the rare earthquake the rehabilitated structure presents some margin against partial or total structural collapse, with some structural members severely damaged and potentially significant non-structural components damage (repair costs may not be practical) and overall risk of life-threatening injury low with possible injuries due to failure of non-structural components (FEMA 1997). Subsequently, a specific numerical evaluation should be carried out to check that the building can meet each desired rehabilitation objective as a goal for the project (FEMA 1997). For instance, the structural performance goal in objective *k* can be achieved by verifying that the transient and permanent interstorey drifts ratios are lower than 2% and 1%, respectively. Equivalently for design of new building, the design process is adjusted until the performance assessment indicates that the risk of loss is considered acceptable by the building owner. To do this, FEMA 273 provides a qualitative description of the building performance levels in terms of both structural components for different typologies and several non-structural components. For structural components the verification is expressed in terms of interstorey drift ratios (e.g., 2% transient and 1% permanent for columns of reinforced-concrete frames at Life Safety level) while for non-structural components it is provided a general description about the damage level (e.g., width of cracks, overturning of items).

Table 2-1 Conceptual definition of the design/rehabilitation objectives (adapted from FEMA 273).

Earthquake Hazard Levels	***Building Performance Levels***			
	Operational	***Immediate Occupancy***	***Life Safety***	***Collapse Prevention***
EP = 50% in 50 years	a	b	c	d
EP = 20% in 50 years	e	f	g	h
EP = 10% in 50 years	i	j	k	l
EP = 2% in 50 years	m	n	o	p

Legend: EP = Exceedance Probability, a-p = objective (k+p defines the basic safety objective which represents a desirable goal to achieve for rehabilitation)

Table 2-2 reports the main differences between the traditional "force-based" prescriptive approach adopted by many design codes and the "performance-based" approach proposed by ATC-40 mainly for retrofit of existing buildings but applicable to new designed buildings as well. The main introduction in "performance-based" is the large participation of owners or stakeholders (e.g., privates, investors, public agencies, etc.) that together with designers are involved in the selection of the desired combination of performance and hazard levels that are used as design criteria (objective). This approach overcomes the traditional seismic design approach of using a single performance goal, i.e. Life Safety, allowing a better understanding of the probable performance of buildings for various events prior appropriate selection of hazard levels (FEMA 1996). Indeed, design codes rely on the concept that it is government's duty to protect the public safety and welfare but the reliability with which code procedures can attain the basic goal is not well-defined (FEMA 1996).

However, engineers at the time were not familiar with the tools employed within these performance-based approaches (i.e., nonlinear modelling), so peer review was an important part of the process (i.e., quality assurance program). Moreover, these frameworks were not detailed enough to provide well-defined acceptance criteria for all the major non-structural components at various earthquake severity levels but there were only qualitative descriptions of the damage levels related to them. Only recently research is pushing towards identification of limits mainly expressed in terms of storey velocity or acceleration for quantifying non-structural damage of different categories of non-structural components.

Table 2-2 Main differences between traditional seismic design and performance-based philosophy (adapted from ATC-40).

Aspect	***Prescriptive***	***Performance***
Basic format	Design codes; checklist	Safety/damage/downtime goals for specific seismic hazard levels
Owner's choice	Limited	Multiple
New buildings	Already applicable	Supplemental enhancement to prescriptive
Existing buildings	Partially applicable but limited	Fully applicable
Review requirements	Plan check normally sufficient	Peer review normally required
Design effort/cost	Traditional	Higher than for prescriptive only

The most recent performance-based methodology described in FEMA P-58 (FEMA 2018a; FEMA 2018b; FEMA 2018c) aims at specifying performance goals within a probabilistic framework so that inherent uncertainties in earthquake performance design and assessment can be accounted for in

the decision-making needs of owners and stakeholders. This approach is preferable because of the difficulty of predicting responses of structures, their damage, and consequences under earthquake shaking. Moreover, a probable performance expressed in terms of casualties, repair costs, repair time results being more meaningful to decision-makers (FEMA 2018a). In this way the definition of performance goals can be expressed in terms of annual probability of failure to attain the desired performance goal rather than using a standard approach based on discrete performance levels like the one presented earlier (FEMA 2018a). Furthermore, the methodology described in FEMA P-58 can be used to assess the performance of a building through different approaches: (i) intensity-based, where the performance is assessed for design earthquake shaking consistent with a code (or other) response spectrum, (ii) scenario-based, where the performance is assessed for an earthquake scenario consisting of a specific magnitude and fault-to-site distance (past or simulated), and (iii) time-based, where the performance is assessed considering all possible earthquakes that could occur in a specific time period and their probability of occurrence (FEMA 2018a).

The methodology described in FEMA P-58 is based on the framework for PBEE developed by the Pacific Earthquake Engineering Research (PEER) center (Moehle and Deierlein 2004) which assumes NTHA as reference method and can be applied to new and existing buildings as well as any other facility. According to this methodology, performance is measured in terms of probability of occurring casualties (i.e., deaths and serious injuries), properties (i.e., building repair or replacement costs) and downtime (i.e., repair time and unsafe placarding). This methodology is based on the evaluation of the conditional probabilities $P[X|Y]$ (cumulative distribution function of X conditioned on Y) of four steps of analysis called (i) hazard analysis, (ii) structural analysis, (iii) damage analysis, and (iv) loss analysis, to quantify the prediction of performance, as depicted in Fig. 2-9 (Porter 2003). The outcome of each step is characterised by one of the four generalised variables: Intensity Measure (*IM*, e.g. spectral acceleration at the fundamental period), Engineering Demand Parameter (*EDP*, e.g. interstorey drift ratio, plastic rotation), Damage Measure (*DM*, e.g. structural and non-structural damage description), and Decision Variable (*DV*, e.g. loss). According to the total probability theorem, the triple integral given by Eq. 2.14 allows to calculate the mean annual frequency of exceedance of a decision variable dv, $\lambda[DV > dv]$, that can be used to perform cost-benefit analysis for decision making problems (Porter 2003).

$$\lambda[DV > dv] = \int_{DM}\int_{EDP}\int_{IM} P[DV > dv \mid DM = dm]\, P[DM > dm \mid EDP = edp]\, P[EDP > edp \mid IM = im]\, \lambda[IM > im]\, dIM\, dEDP\, dDM \tag{2.14}$$

In the first step of the PEER's methodology, the hazard analysis at the site of interest allows to define the related mean annual frequency of exceedance of an intensity measure im, $\lambda[IM > im]$ as function of a particular ground shaking intensity measure which is called "hazard curve" (McGuire 2004). This step involves the characterisation of appropriate GM input for NTHA. From $\lambda[IM > im]$ it is possible to calculate the mean annual probability of exceeding im at a site, denoted by $P[IM > im]$ which is specific to the location (O) and design characteristics (D) of the facility. Current approach for

estimating $P[IM > im]$ at a given site is based on the data availability of past earthquakes and Probabilistic Seismic Hazard Analysis (PSHA). Databases in the last two decades have grown significantly so to cover a wide range of magnitudes, rupture mechanisms, site conditions, and distances. Such *IM* serves as a link between hazard curves provided by seismologists and structural analysis performed by engineers (Luco and Cornell 2007). An important aspect is related to the "efficiency" and "sufficiency" of the *IM* as predictor of *EDP*. These attributes can be quantified through (i) NTHA of a structure under a suite of ground motions and (ii) linear regression analysis (Luco and Cornell 2007). Specifically, a more efficient *IM* will result in a relatively small variability of *EDP* given *IM*, allowing a reduced number of analysis to estimate $P[EDP > edp \mid IM = im]$, introduced in the following step. On the other hand, a sufficient *IM* makes $P[EDP > edp \mid IM = im]$ statistically independent from other earthquake characteristics, such as magnitude and source-to-site distance (Shome and Cornell 1999). In this case, the estimation of $P[EDP > edp \mid IM = im]$ is accurate regardless of which GMs are used. The Peak Ground Acceleration (PGA) was used as *IM* in the past but it was found that the spectral acceleration at the fundamental period ($S_a(T_1)$) of the structure was a better *IM* than PGA for moment-resisting frames with first-mode periods lying within the moderate range (Luco and Cornell 2007; Shome and Cornell 1999). However, $S_a(T_1)$ may not be particularly efficient and sufficient for some cases, such as tall and long period buildings (affected by higher-modes and period elongation) and near-field ground motions (because of the limited spectral shape information) as found by Luco and Cornell (2007) and Shome and Cornell (1999). Moreover, $S_a(T_1)$ has been widely used as *IM* for two-dimensional models but it was found that it can be not efficient and sufficient for structures having significantly different periods in the two orthogonal directions (e.g., Barbosa 2011). Recent studies have proposed using vector-valued *IM* or average scalar-valued *IM* instead of traditional scalar-valued *IM* (Barbosa 2011; Kohrangi et al. 2016a; Kohrangi et al. 2016b).

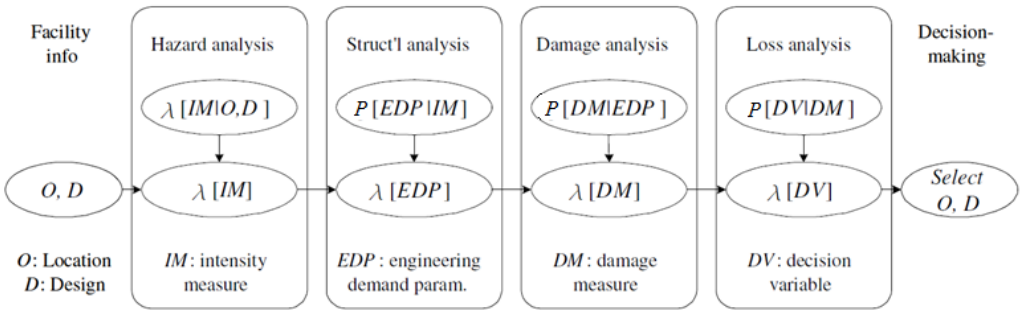

Fig. 2-9 Schematic of PBEE methodology (after Porter 2003).

The second step is to perform structural simulations to calculate the *EDPs* which characterise the response of the building for each GM selected. Typical *EDP*s are interstorey drift ratios, chord rotations, strains, and floor spectral acceleration. There are several procedures to define the correlation between *EDP* and *IM* needed in Eq. 2.14, such as the Incremental Dynamic Analysis

(IDA, Vamvatsikos and Cornell 2002; Vamvatsikos and Cornell 2004). In the IDA procedure, the building is analysed under a GM input having specific value of *IM* which corresponds an evaluated *EDP*. The analysis is repeated by scaling the same GM input and implementing the same operation for several other GMs which have characteristics consistent with the site condition (see Fig. 2-10a). From the discrete analysis points for each GM it is possible to evaluate the IDA curves (see Fig. 2-10b) which are then used to calculate relevant statistical relations between *IM* and *EDP* (Moehle and Deierlein 2004). A common tool typically employed in this step is the so-called "fragility curve" which represents the conditional probability that *EDP* exceeds a specific *edp* for a given *IM* = *im*, denoted by $P[EDP > edp \mid IM = im]$. Subsequently, it can be integrated with the $P[IM > im]$ to calculate the mean annual probability of exceeding *edp*, denoted by $P[EDP > edp]$, therefore the mean annual frequency of exceeding *edp*, denoted by $\lambda[EDP > edp]$ (Moehle and Deierlein 2004). Fragility curves are distinguished from "vulnerability curves" which, instead, show the development of damage as a function of the *IM*, and they are typically used in regional scale studies (D'Ayala et al. 2015). Vulnerability curves are not addressed in this thesis, but it is worth mentioning that fragility curves can be transformed into vulnerability curves through the evaluation of damage probabilities from fragility curves for a specific level of intensity and loss functions (D'Ayala et al. 2015).

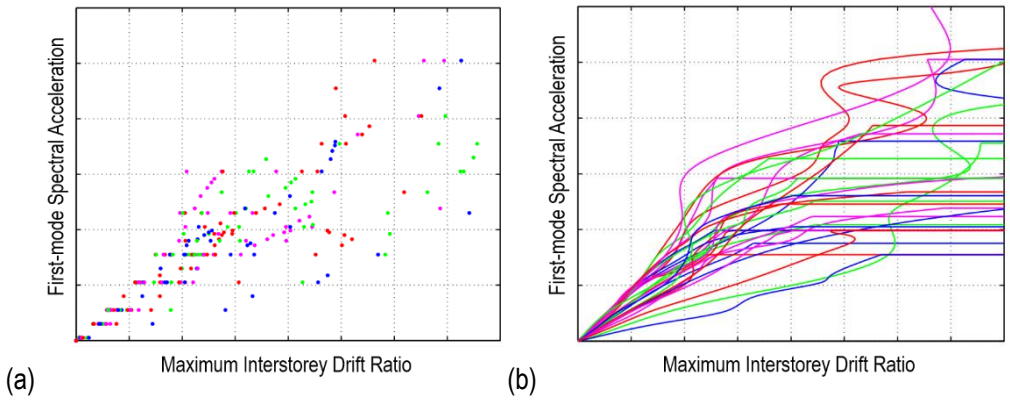

Fig. 2-10 Incremental Dynamic Analysis procedure: (a) the discrete analysis points and (b) the corresponding IDA curves (adapted from Vamvatsikos and Cornell 2002).

The next step is to perform damage analysis which relates the *EDP* to damage measures *DM* that, in turn, describe the physical damage of the building. In damage analysis, conditional damage probability relationships, $P[DM > dm \mid EDP = edp]$, are evaluated based on observational data from past earthquakes and test data from experimental tests in order to quantify damage for structural, non-structural and contents. The conditional damage probability relationship can be integrated with the $P[EDP > edp]$ to calculate the mean annual probability of exceeding *dm*, denoted by $P[DM > dm]$, therefore the mean annual frequency of exceeding *dm*, denoted by $\lambda[DM > dm]$ (Moehle and Deierlein 2004).

Finally, in the loss analysis step the decision variable *DV* is calculated in such a way that it is meaningful for decision makers. *DV* is typically expressed in terms of direct dollar losses, downtime, and casualties. Similarly to the previous steps, by integrating the conditional probability of *DV* given *DM*, denoted by $P[DV > dv \mid DM = dm]$ (representing "loss functions"), with $P[DM > dm]$ it is possible to calculate the mean annual probability of exceeding *dv*, denoted by $P[DV > dv]$, therefore the mean annual frequency of exceeding *dv*, denoted by $\lambda[DV > dv]$, that can be used to inform risk-management decisions (Moehle and Deierlein 2004).

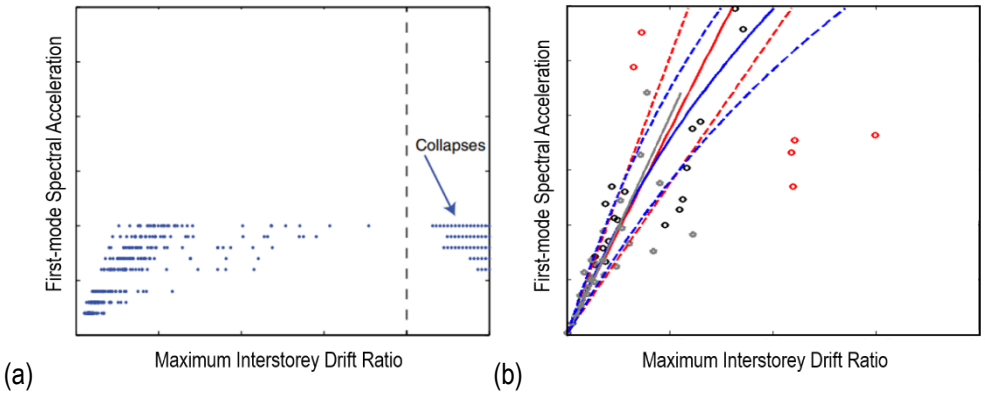

Fig. 2-11 Characterisation of the relationship between EDP and IM through (a) Multiple-Stripe Analysis (adapted from Bazzurro et al. 1998) and (b) Cloud Analysis (adapted from Jalayer and Cornell 2009).

Performance-Based Earthquake Engineering (PBEE) is of high interest nowadays and many research works contributed in spreading the PEER's methodology to assess the risk of economic losses and the influence of structural design and modelling decisions on these losses for both new and existing buildings (e.g., Porter et al. 2002; Goulet et al. 2007; Ramirez and Miranda 2012; Faggella et al. 2013; De Luca and Galasso 2015; Alam and Barbosa 2018).

There are alternative NTHA-based procedures to IDA available in the literature for characterising the relationship between *EDP* and *IM* and performing a probability-based seismic assessment, such as Multiple-Stripe Analysis (MSA, Bazzurro et al. 1998; Jalayer and Cornell 2009, see Fig. 2-11a) and the Cloud Analysis (CA, Bazzurro et al. 1998; Shome et al. 1998; Jalayer 2003, see Fig. 2-11b). In MSA, the building is analysed at discrete levels of *IM* for which different GM suites are used. This approach is common when the Conditional Spectrum or other approaches are used to select GMs that are representative of a specific site and *IM* level, since the GM target properties change at each *IM* level as well as the representative GMs (Iervolino et al. 2010c; Baker 2015). In this way, the procedure does not require to achieve the *IM* where all the GMs cause collapse (Baker 2015).

The application of MSA and IDA can be sometimes time-consuming as the NTHA are going to be repeated for increasing levels of *IM* by scaling the GMs (Jalayer et al. 2015). Moreover, excessive scaling of GMs within the IDA procedure may lead to bias when the scaling breaks the intrinsic relationship between intensity level and frequency content and duration of waveforms (Baker and

Cornell 2005; Lin and Baker 2013). In this light, the CA is particularly efficient since it involves the NTHA of the structure subjected to a set of scaled and/or unscaled GMs (Barbosa 2011; Jalayer et al. 2015). CA is based on the regression analysis to fit "cloud" data and was initially proposed to support a lognormal demand model with constant dispersion with the aim to allow a closed-form solution of the risk integral. The simplicity of its underlying formulation makes it a quick and efficient analysis procedure for fragility assessment or safety-checking (Cornell et al. 2002; Jalayer et al. 2015).

The CA has been used to model the record-to-record variability in GM selection as well as to propagate structural modelling uncertainties such as uncertainty in component capacity, mechanical material properties and constructional details (Jalayer et al. 2007; Jalayer et al. 2010). These uncertainties are also called "epistemic" uncertainties, and approximate ways to account for them were studied by many researchers (e.g., Cornell et al. 2002; Jalayer et al. 2007; Liel et al. 2009; Jalayer et al. 2010) in order to get a "robust" estimate of the structural reliability (Papadimitriou et al. 2001; Beck and Au 2002). An interesting approach is the Bayesian Cloud Method based on Monte Carlo simulations combined in a Bayesian framework in order provide a quantification of the uncertainty in the estimation of the fragility parameters due to the limited number of analyses performed in CA (Jalayer et al. 2015).

2.5.Seismic input selection

This section describes the main aspects related to the seismic input for the previous methodologies of analysis, whether static or dynamic. Earthquakes are recorded by accelerometric stations within a seismographic network which allow to collect GM acceleration time-histories. NTHA represents the seismic analysis method that more realistically allows to simulate the dynamic behaviour of buildings, therefore GM selection represents a critical step for its implementation. Given that NTHA is conceived as a method for structural performance assessment of existing buildings, it can be also used for design purposes as nowadays allowed by some design codes (e.g., ASCE 2017). In any case, GM selection should allow for an accurate estimation of the seismic performance based on the hazard at the site where the building is located (Iervolino et al. 2010a). Generally, the selection of GMs depends on the goals of the analysis, which can be different (Whittaker at al. 2011). Indeed, if the goal of the designer is, for example, the evaluation of the probability of collapse and related losses, then the record-to-record variability needs to be accounted for in the calculation of the structural response distribution (e.g., Whittaker at al. 2011). This is because for seismic performance assessment, probability of collapse and losses are explicitly computed in the seismic risk analysis. Contrarily, if the goal of the designer is designing a new building to achieve a specific level of performance then variability can be reduced in order to get stable estimates of mean (or median) response (e.g., Shome et al. 1998; Watson-Lamprey and Abrahamson 2006; Hancock et al. 2008). Depending on the type of performance evaluation, GM selection can be: (i) intensity-based which allows to evaluate the

structural performance of a building for a target response spectrum (e.g., code-spectrum), (ii) scenario-based which allows the evaluate the structural performance of a building for an earthquake scenario consisting of specific magnitude and source-to-site distance, and (iii) time-based which allows to evaluate the structural performance of a building over a time-window, considering all possible earthquakes and their probability of occurrence (FEMA 2012a; FEMA 2012b).

2.5.1. Code and guideline indications

Design codes suggest semi-deterministic procedures for design of buildings which basically represent temporary accepted solutions till when probabilistic seismic hazard data are fully available (McGuire 2004). They basically require as seismic input defining a Newmark-Hall functional shape response spectrum (e.g., McGuire 2004) representative of the hazard at the site for a specific probability of exceedance (i.e., 10% in 50 years) which can be built up according to specific rules (CEN 2004). Table 2-3 compares the instructions given by EC8 and FEMA P-1050, the latter adopted by ASCE/SEI 7-16. FEMA P-1050 considers the Maximum Considered Earthquake (MCE) which can be built up for specific Site Class and Seismic Design Category once obtained the spectral acceleration for short periods (S_{MS}) and at 1 second (S_{M1}) from the seismic map. The MCE accounts for adjustment when sites are not near an active fault (Luco et al. 2007). Differently, the EC8 allows to use two spectral shapes, namely Type 1 and Type 2 which depend on the magnitude of the earthquake that mostly contribute to the seismic hazard at the site. The elastic response spectra can be built up for specific Soil Type and Importance Class once obtained the reference peak ground acceleration (a_{gR}). In absence of specific geological information, the EC8 refers to the National Annex of the Country of interest (see Table 2-3). For example, EC8 points designers to the Italian Building Code (Italian Building Code 2018) for the Italian territory where the target spectrum is represented by a site-specific smoothed-elastic response spectrum based on the seismic hazard model developed by the Instituto Nazionale di Geofisica e Vulcanologia (INGV, Meletti et al. 2018). The shape of this spectrum practically coincides with the Uniform Hazard Spectrum (UHS) on rock for the site in question (Iervolino et al. 2010a). For the whole Italian territory, a seismic map provides the probabilistic seismic hazard parameters needed to build up the target spectrum for different probabilities of exceedance (or return periods). Recently, a new seismic hazard model for Europe has been developed which shows a generalised increase of the peak ground acceleration values with respect to the current Italian reference model (Woessner et al. 2015). The UHS has been the target spectrum in the design practice for the last two decades (Whittaker at al. 2011; Calvi 2018). It is obtained by averaging the results of probabilistic seismic hazard analysis at a uniform level of the annual rate (inverted value of the return period) for each period of vibration. Its limitation consists in the conservative implication that large-amplitude spectral accelerations will occur at all periods within a single GM (Bommer et al. 2000). Alternatively, FEMA P-1050 allows to use the Conditional Mean Spectrum (CMS) which provides the expected response spectrum conditioned on the occurrence of

a target spectral acceleration value at the period of interest and then computes the mean spectral acceleration at other periods (Baker 2011; Jayaram et al. 2011; Goda and Atkinson 2011). The CMS can be used as target spectrum in performance-based engineering and its spectral shape can be considered more consistent with the site of interest contrarily to the UHS (Baker 2011). However, the CMS may present some limits for nonlinear structures in which the higher-mode responses are important, since it may reduce drastically the contribution of those response.

Many codes and standards allow practitioners to define the seismic input by using real (or natural), artificial or simulated (or synthetic) GMs (Bommer and Acevedo 2004). Artificial GMs are not considered realistic and suitable for use in NTHA, and there can be difficulties in matching an entire elastic code spectrum (Bommer and Acevedo 2004). Real GMs are generally preferred by practitioners because of the high degree of expertise and uncertainty in determining the earthquake source parameters when simulated motions are considered (Bommer and Acevedo 2004). Also, real GMs are nowadays available from many databases, such as the PEER-NGA Ground Motion database (PEER 2014) and European Strong Motion database (ESM 2008); they have the benefit of accounting for the real frequency content, the correct time-correlation between the motion components and realistic energy content referred to seismological parameters. However, real GMs are still limited in number and current procedures of seismic input selection for NTHA generally require manipulations of them, as described in the following. The main issue with real GMs is that they can show a significant record-to-record variability for scenarios (i.e., a magnitude-distance pair).

In order to simplify the procedure of GM selection and accomplishment of spectrum-compatibility criteria, many tools have been developed and are freely available for practitioners (e.g., Iervolino et al. 2010a; Cimellaro and Marasco 2015; Jayamon and Charney 2015; among others). Some procedures achieve the spectrum-compatibility of real GMs through linear scaling of the spectral acceleration (i.e., so-called amplitude scaling). The GM is multiplied by a constant scaling factor so that the respective spectral acceleration and the target spectrum coincide at a specific period of vibration (generally the fundamental period of the structure, T_1), or alternatively in a way that the average of the scaled GM components of a suite of earthquakes closely matches the target spectrum in a specific range of periods of interest (see Table 2-3). It is preferable that the same scaling factor is applied to the two horizontal components and the vertical component to preserve the as-recorded relationship between them. Some studies assessed the limit of scaling factor values in order to avoid biased results (Shome et al. 1998; Luco and Bazzurro 2007; Iervolino and Cornell 2005). Experience has shown that not many GMs are necessary to get the spectrum-compatibility with the target spectrum, but a greater number of GMs could be necessary to reduce the record-to-record variability (e.g., Iervolino et al. 2008). As an alternative, some other procedures achieve matching with the target spectrum through artificial GMs obtained from real GMs and wavelet adjustment (i.e., so-called response-spectrum matching, Table 2-3) which, in principle, modifies the frequency content of a seed

motion (Hancock et al. 2006). Using spectral-matched GMs as an input helps to reduce the variability in the seismic demand, and therefore conceptually allows fewer GMs to be used to obtain stable estimates of the expected response (Hancock et al. 2006). This can be particularly useful for design purposes; however, some studies have shown that wavelet-adjustment procedures can lead to some bias in terms of cyclic responses (e.g., Iervolino et al. 2010b) and it may not be appropriate if pulse-like effects have to be captured (BSSC 2015). Another important aspect is that the selection of GM should be adequately qualified with regard to the seismogenetic feature of the sources and to the soil conditions appropriate to the site (CEN 2004a). This means that the selected GMs should ideally belong to the site of interest as well as be representative of the type of fault (e.g., strike slip, normal/oblique, reverse/oblique). Many areas in the world do not have enough recorded GMs to meet this requirement, for this reason, it is commonly accepted to select GMs from different sites. This can be justified by the fact that if the spectral shape is the parameter driving GM selection some hazard variables such as magnitude and distance may not be particularly relevant for an accurate estimation of the structural response (Iervolino and Cornell 2005). Alternatively, simulated (or synthetic) GMs can be used to achieve the required number of GMs at a site, and they are becoming of high interest thanks to the proposal of validated models against historical events (e.g., Galasso et al. 2013). These GMs are derived for example by physics-based methods or by stochastic GM models that can relate chosen seismicity features (e.g., moment magnitude and rupture-to-site distance) to properties of the GM models (e.g. Mavroeidis and Scotti 2013; Tsioulou et al. 2019).

Another important aspect is related to the representativity of T_1 as value employed for the evaluation of spectral acceleration in design or definition of period ranges within GM selection. For reinforced-concrete and masonry structures the estimation of this value, which depends on the stiffness of the structure itself, can be reasonable for low levels of seismic responses (far from yielding point). Experimental and numerical studies showed that the periods of vibration change due to the progressive damage occurring during an earthquake. This problem is called “period elongation” and it is shown that it can lead to periods of vibration of up to 1.8 to 2.5 times the initial period (e.g., Calvi et al. 2006). Katsanos and Sextos (2015) proposed simplified equations to evaluate period elongation based on the elastic fundamental period and strength reduction factor. Design codes account for period elongation of structures in GM selection by imposing spectrum-compatibility up to $1.5T_1$ (in the US, if properly justified through NTHA) and $2T_1$ (in Europe). GM selection is typically based on modal analysis results obtained from elastic models (i.e., the initial stiffness of numerical models is considered whether the model is linear or nonlinear). For design of buildings through linear analyses, it is generally suggested by design codes using equivalent reduction factors of the stiffness of the elements (Paulay and Priestley 1992).

Table 2-3 Comparison between EC8 and FEMA P1050 provisions on input selection for NTHA.

Condition	***EC8***	***FEMA P-1050***
Target Spectrum	National Annex otherwise Type 1 (M > 5.5) and Type 2 ($M \leq 5.5$) spectral shapes are defined.	Method 1 (MCE) or Method 2 (CMS). UHS is allowed as well.
Structural model	2D and/or 3D and swap of the two horizontal motion components.	3D and swap of the two horizontal motion components.
Matching procedure and number of ground motions	There is no explicit reference to the procedures allowed for ground motion manipulation. Minimum of 3 and: – if < 7 the envelope of the responses is the design value; – if ≥ 7 the average of the responses is the design value.	For LTHA: spectral-matching of 3 pairs only (from artificial or/and recorded) and the envelope of the responses is the design value. For NTHA: ≥ 11 ground motions, scaled or spectral-matched, and the average of the responses is the design value.
Matching tolerance	Average spectrum ≥ 90% of the target spectrum within [$0.2T_1 – 2T_1$] with S_{ae} (T = 0) ≥ a_g S.	For LTHA: average of the spectral-matched spectra ≥ 90% of the target spectrum within [$0.8T_{lower}$, $1.2T_1$]. For NTHA: – average spectrum of the maximum-direction spectra ≥ 90% of the target spectrum within [T_{lower} , $2T_1$]; – if spectral-matching is utilised, average spectrum of the spectral-matched components ≥ target spectrum within [$T_{lower,}$ $2T_1$].
Near-field conditions	No explicit mention of near-source conditions.	Spectral-matching shall not be utilized unless the pulse characteristics are retained after the matching. The rotation of the ground motion components to the fault-normal and fault-parallel directions is required, otherwise for all other sites they should be applied at arbitrary orientations

T_1 is the fundamental period and T_{lower} is the period necessary to achieve 90% participating mass in each orthogonal horizontal direction (it should not exceed 20% of the minimum translational period).

It is well-known that the reduction of stiffness of elements depends on the intensity and direction of axial load, magnitude and sign of bending moments, cross-section geometry, extension of cracks, amount of reinforcement, etc. (Paulay and Priestley 1992). Unless more accurate evaluations are performed, the EC8 suggests using the 50% of both the second moment of area and the shear area. This reduction is representative of the fact that the building might be subjected to initial stresses which lead to cracks during its life (e.g., due to the gravity loads or light earthquakes) and it approximately represents the secant stiffness at the yielding condition of elements based on experimental and numerical results (e.g., Biskinis and Fardis 2010). The ASCE/SEI 7-16 considers reductions of these quantities depending on the type of element and level of axial load (Paulay and Priestley 1992). In any case, adopting the uncracked cross-sections of elements is not recommended (Priestley 2003).

2.5.2. Algorithms for ground motion selection

Over the last ten years, several methods for checking the closeness to a target response spectrum were proposed. Youngs et al. (2007) proposed to evaluate the deviation of the response spectrum of the GM from the target one using the sum of squared differences between them through the measure of the Mean Squared Error (MSE) as per Eq. 2.15, where $S_{a,target}$ and $S_{a,GM}$ represent the spectral acceleration of the target spectrum and GM spectrum, respectively, T_i is the generic i^{th}-period within the period range [T_1, T_n] and n is the number of periods within the range. This was needed for quantifying differences in response spectral shapes of individual GMs to the target spectrum accounting for the natural variability of spectral shapes.

$$\varepsilon(T_i) = \ln\left[S_{a,\text{target}}(T_i)/S_{a,GM}(T_i)\right]$$

$$\text{Scale Factor} = \bar{\varepsilon} = \frac{1}{n}\sum_i \varepsilon(T_i) \qquad i = 1,...,n \tag{2.15}$$

$$\text{MSE}_{\text{GM}} = \frac{1}{n}\sum_i \left(\varepsilon(T_i) - \bar{\varepsilon}\right)^2$$

This measure determines the overall fit of the GM spectrum to the target one over the period range. Together with this formulation, Youngs et al. (2007) proposed a second measure for the spectral shape called “slope” of the GM spectrum to be compared to the slope of the target spectrum across the period range (Eq. 2.16).

$$\text{Slope} = \frac{\sum_i \left[\ln(T_i) - \overline{\ln(T)}\right]\cdot\left[\varepsilon(T_i) - \bar{\varepsilon}\right]}{\sum_i \left[\ln(T_i) - \overline{\ln(T)}\right]} \tag{2.16}$$

$$\overline{\ln(T)} = \frac{1}{n}\sum_i \ln(T_i)$$

Alternatively, the deviation from the target spectrum can be measured by the MSE between the Square Root of the Sum of the Squares (SRSS) of the average scaled spectrum of a suite made of N GMs and the target one. In this spirit, Naeim et al. (2004) proposed to minimise the distance between the mean spectrum of the GM suite from the target one, rather than each GM at a time. Naeim et al. (2004) proposed to minimise the error function Z within the range of periods [T_1, T_n] as per Eq. 2.17, where s_k is the scaling factor of the generic k^{th}-GM spectrum which is always > 0 and T_1 is the fundamental period of the structure.

$$Z = \min\left\{\sum_{T=T_0}^{T_n}\left(\sqrt{\frac{\sum_k\left[s_k S_{a,GM,k}(T_1)\right]^2}{\sum_k s_k^{\,2}}} - S_{a,\text{target}}(T_1)\right)^2\right\} \qquad k = 1,\ldots,N \tag{2.17}$$

This procedure does not guarantee that the final solution would not fall below the target spectrum within the period range of interest. To control this aspect, a second formulation is proposed to constraint the optimisation problem:

$$\sqrt{\frac{\sum_k\left[s_k S_{a,GM,k}(T)\right]^2}{\sum_k s_k^{\,2}}} - S_{a,\text{target}}(T) \geq 0 \qquad T_0 \leq T \leq T_n \tag{2.18}$$

Kottke and Rathje (2008) investigated an approach for GM selection which directly allows to consider the aleatory variability (standard deviation) of the suite. The success of the scaled fit can be quantified by the Root Mean Square Error (RMSE) as per Eq. 2.19, where $S_{a,\mu}$ is the spectral acceleration of the average spectrum for the suite of GMs.

$$RMSE = \sqrt{\frac{1}{n}\sum_i\left(\ln S_{a,\mu}(T_i) - \ln S_{a,\text{target}}(T_i)\right)^2} \tag{2.19}$$

For the RMSE calculation, Kottke and Rathje (2008) recommend using equally-spaced 100 periods at least so that short and long periods receive equal weight. Also, if equally-spaced periods in arithmetic space, shorter periods will be weighted less than longer periods. Two algorithms were proposed which are based on the application of individual scale factors for each GM to control the standard deviation of the suite. The "accordion method" is based on the evaluation of z_k for each GM as per Eq. 2.20, which provides positive or negative values.

$$z_k = \frac{1}{n}\sum_i \ln S_{a,GM,k}(T_i) - \frac{1}{n}\sum_i \ln S_{a,\mu}(T_i) \tag{2.20}$$

The distribution of z_k about its zero mean retains information regarding the position of the individual response spectrum relative to the median. In order to control the standard deviation of the suite, the scaling factors are evaluated according to Eq. 2.21, where α is a constant influence factor which is combined with the average scaling factor s_μ.

$$\ln s_k = \ln s_\mu + \alpha z_k \tag{2.21}$$

The α factor is iteratively modified to get the lowest standard deviation of the GM suite and the final value of the GMs scaling factors. An alternative algorithm is the "centroid method" which is proposed to have a better distribution of the GM spectra at some periods. This algorithm, which is only mentioned herein for the sake of simplicity, considers the probability density function defined by the target median response spectrum and the target standard deviation at each period and evaluates the centroid response spectra of the suite. Through an iterative process the individual scaling factors which fit the target standard deviation are obtained. However, this technique does not easily work with large GM suites and it cannot be used for the selection of unscaled GMs.

To overcome this problem, Jayaram et al. (2011) presented a different algorithm which select a suite of GMs whose spectra have a specified mean and variance. The measure of the dissimilarity can be carried out through the Sum of the Squared Errors (SSE) expressed in terms of differences between the logarithmic spectral acceleration of the (optionally scaled) GM and the target one as per Eq. 2.22.

$$SSE_{GM} = \sum_I \left(\ln S_{a,GM}(T_i) - \ln S_{a,\text{target}}(T_i)\right)^2 \tag{2.22}$$

The algorithm proposed by Jayaram et al. (2011) is based on the minimisation of the SSE of the suite, made of N GMs, which is evaluated according to Eq. 2.23, which form has been herein simplified in order to be consistent with the symbols and definitions adopted in this section. In Eq. 2.23, m_μ and m_{target} are the suite mean and target mean of the logarithmic spectral accelerations at period T_i, respectively, σ_μ and σ_{target} are the suite standard deviation and target standard deviation of the logarithmic spectral accelerations at period T_i, and finally w is a weighting factor indicating the relative importance of the errors in the standard deviation and the mean (it can be assumed equal to 1 but depends on the desired accuracy).

$$SSE = \sum_i \left[\left(m_\mu(T_i) - m_{\text{target}}(T_i)\right)^2 + w\left(\sigma_\mu(T_i) - \sigma_{\text{target}}(T_i)\right)^2 \right]$$

$$m_\mu(T_i) = \frac{1}{N}\sum_k \ln S_{a,GM,k}(T_i) \tag{2.23}$$

$$\sigma_\mu(T_i) = \sqrt{\frac{1}{N-1}\sum_k \left(\ln S_{a,GM,k}(T_i) - m_\mu(T_i)\right)^2}$$

Iervolino et al. (2010a) developed an algorithm for GM selection in which GMs are preliminarily ordered on the basis of the parameter in Eq. 2.24 which gives a measure of how much the GM spectrum deviates from the target one. Subsequently, the same equation, with $S_{a,GM}(T_i)$ replaced by $S_{a,\mu}(T_i)$, is used to select the best GM suite.

$$\delta_{GM} = \sqrt{\frac{1}{n}\sum_{i}\left(\frac{S_{a,GM}(T_i) - S_{a,\text{target}}(T_i)}{S_{a,\text{target}}(T_i)}\right)^2} \tag{2.22}$$

These algorithms for GM selection were conceived for NTHA and they are based on the evaluation of spectral acceleration differences between the target response spectrum and the individual/average response spectrum of the GM suite over a range of periods such as that imposed by codes for spectrum-compatibility requirements. Some of them utilise complex algorithms for solving an optimisation problem which aims at minimising the spectral difference between target and average spectra of the GM suite while some others allow minimising the standard deviation of the GM suite as well. The indexes considered by some of these algorithms (i.e., MSE, RMSE, SSE) are based on squared spectral differences which lead to absolute values. Moreover, some of them utilise factors which are defined at the discretion of users. These aspects motivated the proposal of a new index in Section 4.2.10, specifically addressed to LTHA design, which is based on the evaluation of the weighted average of the spectral differences at each relevant period of vibration of a building between target spectrum and GM spectrum of a suite. This index keeps the sign of the spectral differences and the weights are defined in terms of the participating masses of each mode of a building.

2.6.Conclusion

This chapter presents the main aspects related to the methods of seismic analysis suggested by current design codes. In particular, it is meant to highlight the limits of applicability and approximate assumptions typical of LFM and RSA that both make design process not always rational to designers. RSA is the reference method of analysis in many design codes, including EC8, and basically condenses the modal peak structural response contributions into one time-instant without accounting for the effective interaction between frequencies of the building and frequencies of GMs. It is indicated as method for designing irregular or tall buildings for which LFM is not applicable. However, while RSA can still lead to acceptable results for low/medium-rise buildings, it can lead to significant bias in structural response evaluation for unusually-stiff structures, structures with relevant higher modes contribution, and near-field pulse-like GMs. Several enhanced versions have been proposed for RSA in literature, but they did not find consensus among design codes. Notwithstanding these improvements, still, RSA does not capture the sign and coupling of local force components of members and system deformations making design often complicated from the practical point of view. As a result of the widespread use of RSA, current professional practice in design still needs refinements; a balanced compromise between accuracy of structural response evaluation and simplicity of design procedure for all possible cases (i.e., high-rise, low-rise, regular and irregular structures) should be targeted. LTHA represents an appealing alternative to overcome the approximate assumptions typical of linear analyses (i.e., preassigned distribution of lateral forces, loss of both sign and coupling of local force components, etc.), but also a simple tool for design of

buildings as addressed by FEMA P-1050 that implemented LTHA in a seismic code (ASCE/SEI 7-16) with detailed recommendations for design applications. Indeed, LTHA can predict in a reasonable way the behaviour of structures that show limited level of damage (i.e., serviceability conditions) and allows evaluating other response quantities such as peak accelerations and velocities that are typically used for loss estimation of non-structural elements that, as has been shown, represents an important part of the total loss for buildings designed according to modern seismic philosophy. It also accounts for a more realistic analysis approach that can be linked to physical characteristics of earthquakes (e.g., specific-field conditions, pulse-like earthquakes, statistical and probabilistic interpretation of results, etc.). However, the critical aspect for LTHA as well as NTHA is accounting for a proper GM selection. FEMA P-1050 suggests adopting the spectral-matching procedure based on wavelet adjusted GMs for LTHA input selection so that it can lead to results comparable to RSA but accounting for signs and coupling of local force components. However, FEMA P-1050 explicitly states that this procedure can be not consistent for near-field conditions (e.g., pulse-like GMs). All these aspects motivated this research work that aims at investigating a possible EC8-compliant framework for LTHA for its potential inclusion in the next generation of EC8. The scope is to open up to new opportunities for design of buildings within simplified performance-based methodologies, and LTHA is also proposed as method for derivation of simplified fragility curves at design stage.

Chapter 3: EC8-Design of RC-MRF Buildings

Part of this chapter is based on the following reference:

De Luca F and **Lombardi L** (2017). EC8 Design through Linear Time-History Analysis versus Response Spectrum Analysis – is it an enhancement for PBEE?, 16th World Conference on Earthquake Engineering, Santiago, Chile, January 9-13.

Objectives of this chapter

In the previous chapter, the methodologies suggested by current design codes for analysing buildings located in seismic areas were discussed. This chapter focuses on the linear analysis methods which are typically used by designers for dimensioning structural elements of buildings, and it is meant to show the structural design according to Eurocode 8 (EC8) of an archetype Reinforced Concrete (RC) building which can be considered as representative of a class of buildings in current design practice. This building is assumed as benchmark building for this research work. In this light, the following objectives are aimed in this chapter:

- to investigate the RC Moment-Resisting-Frame (MRF) buildings adopted in literature, in order to assess the design parameters typically assumed for research studies;
- to design the benchmark building considered in this research work accounting for real aspects that are typically encountered in the professional practice and that are not always be considered in research studies. This is an important aspect because the reliability of research results should be weighted on practical aspects rather than conceptualised ones;
- to present a brief but detailed review of EC8-design of RC-MRF buildings, considering (i) a practical example represented by the benchmark building assumed for this research work and (ii) identifying critical aspects that characterise design results.

3.1.Introduction

Among the many typologies of structures in civil engineering, buildings represent the primary source of economic and social losses due to earthquake-damage as shown by past events (Kircher et al. 1997). This is because buildings represent the predominant kind of facility in built environments providing residential, commercial, business, industrial, cultural, and healthcare activities.

Modern seismic codes and standards for buildings aim at designing buildings so to exhibit specific levels of performance under different intensity levels of expected earthquakes (CEN 2004a). These levels of damage are called “limit states” and are probabilistically related to different seismic design events. For example, EC8 (CEN 2004a) allows to design buildings for two limit states: (i) “No-

collapse", where protection of life under rare earthquakes is provided by preventing buildings collapse, (ii) "Damage Limitation", for which mitigation of property loss under frequent earthquakes is provided through limitation of structural and non-structural damage. "Damage Limitation" limit state aims at limiting the overall flexibility of buildings in order to show acceptable levels of integrity of all its parts under minor/moderate earthquakes. In this light, buildings can essentially show non-structural damage which is economically more convenient to repair (Fardis 2009). Contrarily, "No-collapse" limit state assumes that buildings subjected to strong earthquakes are expected to show significant levels of damage but in a such way that the corresponding incipient collapse mechanism can be consciously controlled. This feature can be conferred to buildings following specific design rules that aim at providing buildings with adequate strength and ductility (Fardis 2009).

For "No-collapse" limit state, design codes refer to specific areas within the structural types of system, which are entitled the role of "dissipative zones" because of their hysteretic energy dissipation capacity. For RC frame systems (the typology herein considered) it is expected that the dissipation of energy occurs by flexural behaviour of finite length regions at the ends of beams called "plastic hinges". Plastic hinges can be described by some phenomena that typically occur such as: cracking of concrete, yielding of the steel longitudinal rebars, spalling of concrete, and fracture/buckling of the steel longitudinal rebars at ultimate conditions (e.g., Tanaka and Park 1993). It was shown that because of the axial load acting in columns the dissipation of energy through plastic hinges at their ends can be strongly penalised compared to pure flexure, and it mainly depends on the level of axial force (e.g., Tanaka and Park 1993). Moreover, because of the spatial variability of earthquakes, columns are very likely subjected to biaxial flexure which is a more penalising condition than uniaxial flexure typical of beams (i.e., uniaxial flexural capacity is reduced, e.g., Bousias 1993; Biskinis 2007). In this light, current design codes prioritise the plasticisation of beams which can exhibit larger levels of energy dissipation than columns. Moreover, columns are responsible for the stability of other elements and for the integrity of the whole structural system due to vertical loads after an earthquake (and aftershocks) so they must clearly be stronger than beams. This aspect, that implies a certain hierarchy of resistances among elements of the same structure, is well-known as "capacity design" and it is applied between beams and columns from a flexural behaviour point of view but also between flexural and shear behaviour at element level (Park and Paulay 1975). In this light, the shear behaviour, which penalises the energy dissipation capacity of RC beam-column elements (from here called "brittle"), is typically governed through a series of rules aiming at oversizing members' shear capacities to allow large inelastic deformations due to flexure. All regions not designated as dissipative zones" are expected not to be damaged (i.e., zones outside the dissipative zones such as beam-to-column joints).

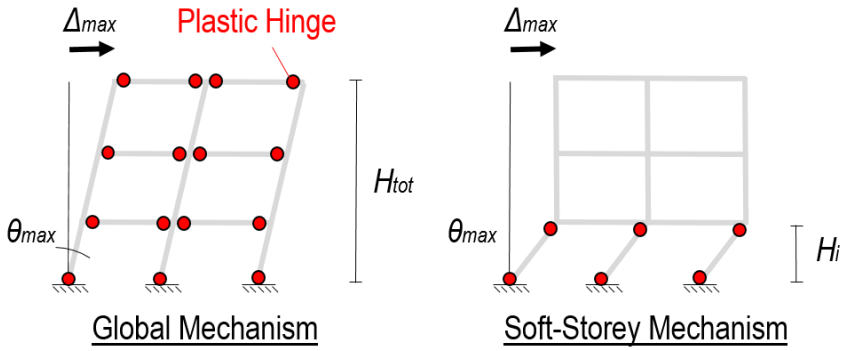

Fig. 3-1 Collapse mechanisms of MRF systems.

The mechanism resulting from this idealised concept is called "global mechanism" (see Fig. 3-1) and it is represented by the development of plastic hinges at beams' ends at different storeys as well as at the ground level column ends (i.e., above the connection to the foundation system or basement levels). This mechanism represents the best in terms of widest spread of the global displacement demand and energy dissipation throughout the entire structural system and it can be expressed as:

$$\Delta_{max} = \theta_{max} H_{tot} \tag{3.1}$$

where Δ_{max} is the maximum roof displacement demand, θ_{max} denotes the maximum chord rotation demand of the building and H_{tot} is the building height. The chord rotation demand of the building θ_{max} can be expressed as function of chord rotation demand of beams at every storey and columns at the ground level. The chord rotation of a member represents the angle between the normal to the element section at the ends and the chord connecting the two ends of the member. The definition of chord rotation demand and capacity of structural members is discussed in further detail in Chapter 5. However, it may happen that the mechanism is given by a concentration of inelastic demand in a specific storey rather than throughout the all storeys of the building (e.g., Lee 1996). If both the ends of the columns at that storey develop plastic hinges, the global displacement demand is just a portion of the one expressed by Eq. 3.1, being equal to:

$$\Delta_{max} = \theta_{max} H_i \qquad H_i < H_{tot} \tag{3.2}$$

where H_i is the height of the i^{th} storey where this mechanism called "soft-storey" takes place (see Fig. 3-1). If the building is designed to satisfy a certain seismic demand in terms of displacement, the "global mechanism" is preferable over the "soft-storey", being the inelastic contribution of the second mechanism mainly due to the "soft-storey" rather than "global" as per the first mechanism. For the example shown, it results that the second mechanism would need a larger source of ductility, i.e. H_{tot}/H_i times θ_{max} for a given Δ_{max}, that is generally not feasible to design and detail in practice. The impossibility to provide that amount of ductility by the columns of the "soft-storey" would very likely lead to collapse and loss of vertical stability. For this reason, the best way to spread the global

inelastic demand is preventing its concentration to a specific storey by oversizing columns so that they can mainly behave elastically, and the structural system tends to a behaviour similar to the "global mechanism". It was shown that in the reality the plastic hinge development never extends through the whole building and the upper storeys mainly behave elastically. Some researchers criticised this design concept because earthquakes in the past showed that even if building are designed according to the so-called "capacity design", the cost of repairing the many plastic hinges was often excessive compared to wall buildings (Otani 1997). This clearly emphasises the importance of residual deformations in defining damage control performance level. Paradoxically, the "soft-storey" mechanism can be economically more convenient than "global mechanism" if it is protected against shear failure and excessive local ductility demand (Otani 1997; Priestley 2000).

In seismic design, ductility or energy dissipation capacity are accounted for through the use of the behaviour factor (q). The theoretical principle behind q (explained in Chapter 2) assumes that if the building is designed in accordance with specific rules aiming at some corresponding detailing requirements, it is expected that the building would show a level of ductility at least equal to q. So, the behaviour factor is linked to the local ductility demands in members and hence to the corresponding detailing requirements (Fardis 2009). The EC8 allows designers to choose between three classes of ductility for MRF buildings: (i) Ductility Class Low (DCL), for which there is not any ductility associated to detailing and q must be assumed equal to 1.5 which represents the overstrength of the structural system due to redundancy; (ii) Ductility Class Medium (DCM), for which q can vary between [3.3, 3.9]; (iii) Ductility Class High (DCH), for which q can range between [4.95, 5.85]. Some researchers assessed the values of the behaviour factors and found out that design codes values are generally lower than those ones evaluated through nonlinear analyses (e.g., Kappos 1999; Elnashai and Mwafy 2002; Rodrigues et al. 2018). However, the EC8 allows using larger values if properly justified or even smaller values than those suggested if a more precautionary value is needed (Fardis 2009).

It is evident that if the structural system features of structural simplicity and uniformity, the "favourite" seismic performance of buildings described above can be more accurately predicted. Damage in strong earthquakes shown that irregular and geometrically complex structures perform on average worse than simple and regular ones (Fardis 2009). In this light, a simple and regular structural layout reduces the difference between the real response and the predicted one through analyses methods. If it is not, the real response may be completely different from the predicted one. For irregular buildings, the EC8 penalises the values of the behaviour factor with the intent of making design more conservative since the structural response may significantly differ from the real one.

3.2.Archetypical structures

The concept of archetypical (or prototypical) structures derives from the need to propose classes of structural systems within which similar structures statistically show the same performance. In this way, the archetypical buildings are representative of a group of buildings whose design performance can be systematically evaluated and quantified through appropriate design parameters (Haselton 2006). This problem arises because it is practically impossible to envision or attempt to quantify performance of all possible engineering applications (FEMA 2009). For this reason, if design parameters (e.g., beam bays, interstorey heights, fundamental period, etc.) are restrained within specific ranges, while still being reasonably representative of the variations that would be permitted in actual building designs, it is possible to generalise results by analysing only a limited number of archetype buildings (FEMA 2009). The FEMA P-695 (FEMA 2009) describes a recommended methodology for reliably quantifying building system performance and response parameters for use in seismic design. The purpose of the methodology provided by the FEMA P-695 is to provide a rational basis that when properly implemented in the seismic design process will result in equivalent safety against collapse due to earthquakes, comparable to that intended by current seismic codes, for buildings with different seismic-force-resisting systems (FEMA 2009). Indeed, configuration variables (e.g., occupancy and use, elevation and plan configuration, building height, structural system) and seismic behavioural effects (e.g., strength, stiffness, inelastic deformation capacity) play important roles for assessing collapse performance. More details about how structural models should be chosen can be found in FEMA P-695.

In the following, a brief review of some of the recent code-based seismic-force-resisting systems analysed in literature is presented (see Table 3-1, Table 3-2, and Table 3-3). Particular attention is shown on the adopted design parameters and systems attributes that were chosen in other studies for multi-storey RC-MRF regular buildings of ordinary class (i.e., residential or office areas). It is worth noting that this section is not meant to implement the methodology suggested by FEMA P-695 for assessing safety risk of these buildings because, in this case, more data from each work in literature would be needed to achieve this goal (especially regarding collapse mechanism, etc.). This review is presented to justify the adoption of the design aspects chosen for the benchmark building design presented in Section 3.3, such as geometry, material properties, ductility class, numerical model assumptions, soil type, and analysis method. This section is introduced in this thesis for its importance before commencing any study. The benchmark building considered in this research work is designed considering design parameters and systems attributes (both of impact to the system response) that are judged to be reasonable representations of the feasible design space (i.e., range of permissible configurations, structural design parameters, and other properties that define the application limits for a seismic-force-resisting system). This makes the benchmark building of this research work a potential archetype within its context of applicability.

Table 3-1 Summary of the design parameters and system attributes of recent code-based multi-storey RC-MRF regular buildings of ordinary class (part 1).

N	*Design Code*	*Ductility Class*	*Behaviour Factor*[4]	*No. of Storeys*	*Framing System*[3]	*Bay Length* (m)	*Interstorey Height* (m)	*Concrete Strength* (MPa)	*Steel Yield Strength* (MPa)
1	EC8	DCH	4.95, 5.85	[1, 10]	Space	5.00	3.00	25	450
2	Italian Building Code 2008/EC8	DCH, DCL[1]	3.90	[3, 9]	Space	[2.75, 5.70]	3.05, 3.40	28	450
3	Romanian Code 2006/EC8	DCH	-	9	Space	4.50, 5.50	3.15	25	300 (long.), 210 (trans.)
4	ASCE 7-02, ACI 318-02, IBC 2003	Special[2]	8 (*R*)	[1, 20]	Space/Perimeter	6.10, 9.10	4.60, 4.00	34, 48	460
5	EC8	DCM	3.90	[4, 16]	Space	7.50	3.50	35	440
6	EC8	DCM	3.90	3	Space	4.00	3.00	30	500
7	Italian Building Code 2008	DCH	-	4, 8	Space	4.50	3.00	25	450
8	ASCE 7-02, ACI 318-02, IBC 2003	Special[2]	8 (*R*)	4	Space/Perimeter	9.10	4.60, 4.00	34	460
9	Italian Building Code 2008/EC8	DCH, DCL[1]	3.90, 5.85	5	Space	[4.00, 7.00]	[2.50, 5.00]	25	450
10	EC8/Greek Code 2000	DCH, DCM, DCL[1]	[1.5, 5.85]	[4, 12]	Space	5.00		30	500
11	ASCE 7-05. ACI 318-05, IBC 2005	Special[2]	8 (*R*)	7	Perimeter	6.80, 7.30	4.20, 3.60	28	420
12	ASCE 7-10. ACI 318-11	Special[2]	8 (*R*)	20	Perimeter	6.40	3.66	52	414
13	EC8	DCH, DCM, DCL	[1.5, 5.85]	[2, 8]	Space	5.00	3.00	-	-
14	ASCE/SEI 7-05, ACI 318-08	-	-	6	Space	[3.60, 6.40]	3.70, 4.60	24	414

[1]Ductility Class Low (DCL) in Italian code corresponds to DCM in EC8
[2]Special Moment-Resisting Frame (SMRF) in US code corresponds to DCH in EC8
[3]In MRF systems, tributary gravity loads can be distinguished using perimeter frames versus frame configurations (description can be found in FEMA P-695)
[4]The indicated values consider the overstrength factor and (if applicable) reduction for irregularity

Table 3-2 Summary of the design parameters and system attributes of recent code-based multi-storey RC-MRF regular buildings of ordinary class (part 2).

N	Numerical Model	Cracked Flexural Stiffness	Foundation Fixity	Staircase Structural Modelling	Infills Structural Modelling	First-mode Period[1] (s)	Reference
1	2D	$0.50EI_g$	Y	N	N	[0.33, 1.39]	Petrone et al. 2014
2	3D	$0.50EI_g$ beams; $0.75EI_g$ columns	Y	Y	Y/N	[0.88, 1.66]	Ricci et al. 2018
3	3D	$0.50EI_g$ beams; $0.80EI_g$ columns	Y	N	N	0.784	Craifaleanu 2011
4	2D	-	Y/N	N	N	[0.42, 4.08]	Haselton et al. 2011, Haselton and Deierlein 2007
5	2D	$0.50EI_g$, $1.00EI_g$, $EI(M_y/\Phi_y)$	Y	N	N	[0.54, 2.86]	Rivera and Petrini 2011
6	2D	$0.50EI_g$	Y	N	N	-	Ulrich et al. 2014
7	3D	-	Y	N	Y/N	-	Ricci et al. 2013
8	2D	-	Y	N	N	[0.53, 1.25]	Goulet et al. 2007, Haselton and Deierlein 2007
9	3D/2D	$0.50EI_g$ beams; $0.70EI_g$ columns	Y	N	N	-	Braconi et al. 2013
10	2D	$0.50EI_g$	Y	N	N	[0.39, 1.23]	Panagiotakos and Fardis 2004
11	2D	-	Y	N	Y	[0.39, 0.72]	Wu et al. 2012
12	2D	$1.00EI_g$	Y	N	N	1.76	Visnjic et al. 2012
13	2D	$0.50EI_g$	Y	N	N	-	Papailia et al. 2012
14	2D	-	Y	N	Y	[0.50, 0.75]	Alam and Barbosa 2018

[1]*Period of vibration evaluated from numerical model.*

Table 3-3 Summary of the design parameters and system attributes of recent code-based multi-storey RC-MRF regular buildings of ordinary class (part 3).

N	Building Site	Target Spectrum	Soil Type	Analysis Method
1	-	a_g=0.25 g	B	RSA
2	Milan, Naples, L'Aquila (Italy)	a_g=[0.05, 0.26] g	C	RSA
3	Bucharest (Romania)	a_g=0.24 g	C	LFM
4	Los Angeles (California)	S_s=1.5 g, S_1=0.6 g	D[1]	RSA
5	-	a_g=0.35 g	A	RSA
6	-	a_g= [0.07, 0.31] g	B	LFM
7	Avellino (Italy)	a_g=0.19 g	B	-
8	Los Angeles (California)	-	D[1]	RSA
9	-	a_g=0.25 g	B	-
10	-	a_g=0.20, 0.40 g	C	LFM
11	Los Angeles (California)	S_s=1.5 g, S_1=0.5 g, Design Cat. E	D[1]	RSA
12	Los Angeles (California)	-	D[1]	RSA
13	-	a_g=[0.10, 0.35] g, Type 1	C	-
14	Salem (Oregon)	S_{Ds}=0.54 g, S_{D1}=0.32 g	D[1]	-

[1]*NEHRP soil category D.*

3.3.Case study: 12-storey RC-MRF regular building

In this section, the design of the benchmark building considered in this research work is presented. The main aspects related to its design for both seismic and non-seismic conditions are presented and discussed. The benchmark building is a 12-storey RC-MRF located in a medium-high seismicity area and designed according to EC8-1 (CEN 2004a) and EC2 (CEN2004b). In particular, design is performed for two ductility classes in order to study the differences in results due to the ductility class level. This building is representative of the majority of ordinary buildings in the Mediterranean region and it accounts for some aspects like the presence of a staircase, squat columns, maximum number of storeys resulting from ordinary concrete classes, relevant influence of higher-modes of vibration, and significant P-Δ effects. Typically, 12-storey RC buildings are designed with shear walls in order to control the deformability of medium-rise buildings. Therefore, the benchmark building represents a limit for RC-MRF building design.

3.3.1. General description

The benchmark building is located in L'Aquila (Italy), a seismic area that was significantly affected by the M6.3 2009 L'Aquila earthquake (Verderame et al. 2011). This building is designed twice for Ductility Class High (DCH) and Ductility Class Medium (DCM) according to EC8 and EC2, including specifications of the Italian National Annexes which refers to the Italian Building Code (Italian Building

Code 2018). The building has 25x15 m^2 floor area used for office activities. Interstorey heights are 3.6 m and 3.0 m at the first level and upper levels, respectively. Bay length is 5.0 m in both longitudinal (X) and transverse (Y) directions (see Fig. 3-2). The connection between floors is realised by means of staircase having inclined beams (supporting cantilever steps) connected by horizontal beams at landing and floor levels. Such beam configuration is also known as "knee beams" and it is commonly used in Italian building practice.

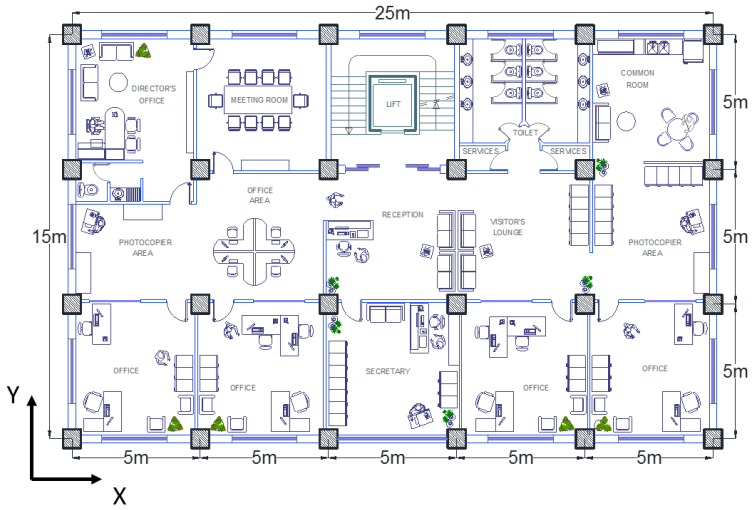

Fig. 3-2 Architectural drawing of the floor-type plan of the benchmark building.

3.3.2. Building site and site-dependent actions

The building is located in Pettino, a neighbourhood of L'Aquila (Italy), having longitude 13°34'38.90''E and latitude 42°37'72.20''N (see Fig. 3-3a). Soil class B (360 < $V_{s,30}$ < 800 m/s, EC8-1) is assumed for the seismic action characterization on the basis of information provided by the accelerometric stations located in the same area (see Fig. 3-3b, Luzi et al. 2017). According to the Italian national annex regarding EC8-1, seismic design loads are obtained from the definition of the reference Peak Ground Acceleration (PGA), a_{gR}, referred to rock and plane topographical surface conditions. Such parameter, together with others characterising the seismic hazard at the site, are estimated from probabilistic seismic hazard analysis carried out for the whole Italian territory (Meletti et al. 2007) and provided as site-dependent value for different values of the return period (T_R) of the seismic action, or equivalently of Exceedance Probability (*EP*) in 50 years. Subsequently, the horizontal elastic code response spectrum in terms of pseudo-acceleration for the specific site and building function can be obtained through Eq. 3.3 (Italian Building Code 2018):

(a) 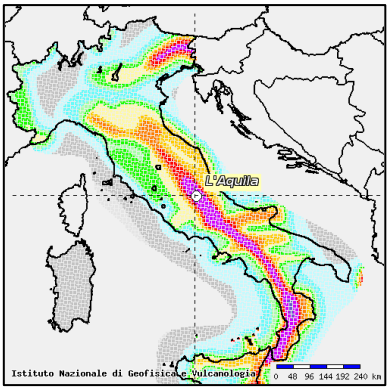

(b) 

Fig. 3-3 Identification of the building site: (a) Italian Seismic Hazard Map in terms of PGA (EP = 10%) (after Meletti and Martinelli 2008) and (b) accelerometric stations located nearby Pettino neighbourhood (identified by the red area).

$$
\begin{aligned}
&0 \le T \le T_B && S_{ae}(T) = a_g S \eta F_o \left[\frac{T}{T_B} + \frac{1}{\eta F_o} \left(1 - \frac{T}{T_B} \right) \right] \\
&T_B \le T \le T_C && S_{ae}(T) = a_g S \eta F_o \\
&T_C \le T \le T_D && S_{ae}(T) = a_g S \eta F_o \left(\frac{T_C}{T} \right) \\
&T_D \le T && S_{ae}(T) = a_g S \eta F_o \left(\frac{T_C T_D}{T^2} \right)
\end{aligned}
\qquad (3.3)
$$

where:

- T and $S_{ae}(T)$ are respectively the period of vibration and the corresponding elastic horizontal spectral acceleration of a linear single degree of freedom system;
- S is the soil factor, equal to $S = S_S S_T$, in which S_S is the stratigraphic amplification coefficient and S_T is the topographic amplification coefficient provided by the code depending on the soil type and the topographic condition at the site;
- η is the damping correction factor equal to 1.0 for reinforced-concrete structures having ζ = 5%, and it is assumed equal to $1 / q$ to determine the design spectrum for ultimate limit states, where q is the behaviour factor;
- F_o is the maximum amplification factor of the spectral acceleration;
- T_C is the period in correspondence to the starting point of the constant spectral velocity branch, provided by the relationship $T_C = C_C T_C^*$, in which T_C^*, is the period in correspondence to the starting point of the constant spectral velocity branch for rigid and horizontal soil, and C_C depends on the soil type;
- T_B is the period in correspondence to the starting point of the constant spectral acceleration branch, provided by the relationship $T_B = T_C / 3$;

– T_D is the period in correspondence to the starting point of the constant spectral displacement branch provided by the relationship $T_D = 4.0\, a_g / g + 1.6$.

For ordinary buildings of Importance Class II, the Italian National Annex prescribes using two limit states which correspond two different response spectra: (i) Damage Limitation-Limit State (DL-LS), i.e., the elastic spectrum with 63% probability of exceedance 50 years, corresponding to a return period (T_R) of 50 years; (ii) Life Safety-Limit State (LS-LS), assuming two behaviour factors (q) equal to 5.85 and 3.90 for DCH and DCM (EC8-1), respectively, and based on the elastic spectrum with 10% probability of exceedance of 50 years, corresponding to a return period of 475 years. Table 3-4 reports the values of the parameters which allow to plot the horizontal elastic code-spectra in terms of pseudo-acceleration for the benchmark building design (see Fig. 3-4a). The design spectra for DCH and DCM are obtained from Eq. 3.3 by replacing η with 1 / q and they are plotted in Fig. 3-4b. For T = 0 both the design spectra lead to $S_{ad} = a_g S$. It is worth noting that the design spectra corresponding for both DCH and DCM are modified from T > 1.10 s and T > 1.61 s, respectively, in order to consider the lower bound design value for the pseudo-acceleration imposed by EC8-1 (i.e., $S_{ad}(T) \geq 0.2\, a_{g,LS\text{-}LS}$) adopted by the Italian National Annex as well.

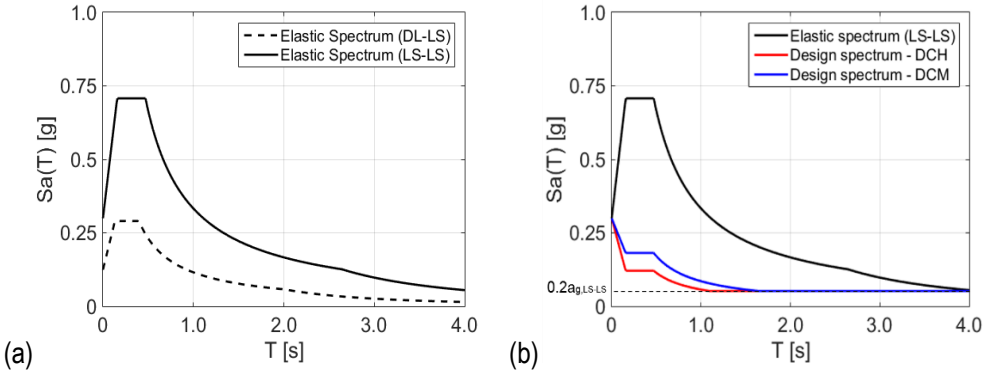

Fig. 3-4 Horizontal response spectra in terms of pseudo-acceleration for the benchmark building design: (a) elastic spectra at DL-LS and LS-LS, and (b) design spectra at LS-LS for DCH and DCM.

Table 3-4. Parameters for the characterising the elastic response spectra for the benchmark building design.

EP **(%)**	T_R **(y)**	a_g **(g)**	F_o **(-)**	T_C^* **(s)**	S_S **(-)**	C_C **(-)**	S_T **(-)**	T_B **(s)**	T_C **(s)**	T_D **(s)**
63	50	0.104	2.333	0.280	1.20	1.42	1.00	0.133	0.398	2.014
10	475	0.260	2.362	0.346	1.15	1.36	1.00	0.157	0.470	2.642

Possible snowfalls during the winter are taken into account in site-dependent loads definition, according to EC1-3 (CEN 2003) and the Italian National Annexes. L'Aquila is located at 750 m above the level of the sea (a_s) and it belongs to Zone III, for which the characteristic value of snow load on ground level is given by Eq. 3.4.

$$\overline{q_{sk}} = 0.51\left[1+\left(\frac{a_s}{481}\right)^2\right] \tag{3.4}$$

The value obtained from Eq. 3.4 is modified in order to account conditions at roof level, by applying the following expression:

$$q_{sk} = \mu_i C_e C_t \overline{q_{sk}} \tag{3.5}$$

where:

- μ_i is the snow load shape coefficient, assumed to be equal to 0.8 for angles of pitch of roof α included between 0° and 30°;
- C_e is the exposure coefficient, assumed to be equal to 1.0 for normal topography, where there is no significant removal of snow by wind on construction work, because of terrain, other construction works or trees;
- C_t is the thermal coefficient, which can be assumed equal to 1.0 for general cases.

From Eq. 3.5, the characteristic value of snow equal to 1.40 KN/m^2 is calculated and assumed in the following calculations for loads patterns definition.

3.3.3. Preliminary design

The benchmark building, in both ductility classes, is designed on the basis of structural simplicity, uniformity and symmetry criteria in order to obtain a clear and predictable transmission of the seismic forces (EC8-1). Section sizes of structural members are initially obtained by preliminary dimensioning on gravity loads and then modified on the basis of the design seismic demand.

One-way slabs are made of RC joists and hollow blocks having width respectively equal to 10 cm and 40 cm (see Fig. 3-5a). The direction of the joists is chosen in order to uniformly distribute floor loads to the beams. A concrete layer of 4 cm, which connects the RC joists at the top, is present at each floor (including roof level) in order to have sufficient in-plane stiffness for the distribution of horizontal inertia forces to the frames (i.e., rigid diaphragms). The slabs thickness is 20 cm which is equal to 1 / 25 of beam spans. The floor imposed load is 2.0 kN/m^2 (i.e., cat. B1, considering office destination, EC1-1, CEN 2001). The roof imposed load is 0.50 kN/m^2 (i.e., cat. H, considering normal maintenance and repair access, EC1-1). Moreover, due to the location of the building, a snow load equal to 1.40 KN/m^2 is considered on the roof surface (a_s = 750 metres above the sea level, m.a.s.l.).

Perimeter infills are constituted by double layer hollow clay bricks (see Fig. 3-5b). They are considered in the model as non-structural elements, realised in contact with the frame, without any structural connection with it. A reduction of 25% of the infill load is assumed in the following calculations in order to take into account the presence of openings. A 1.50 m high perimeter parapet is assumed on the roof.

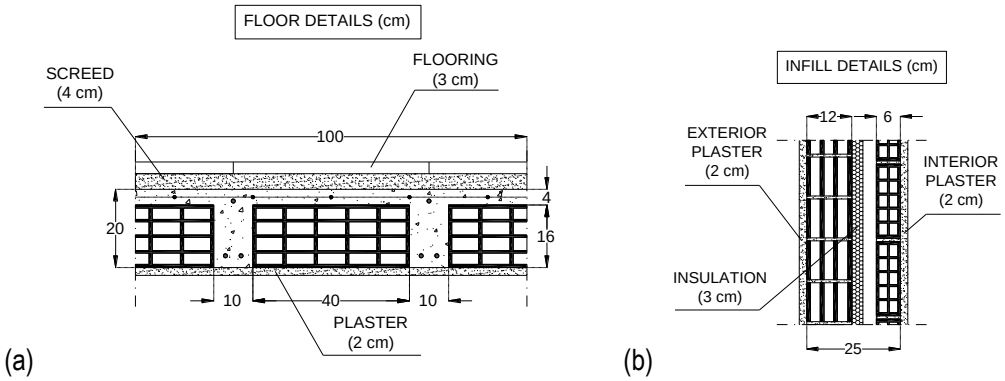

Fig. 3-5 Geometrical details of the benchmark building: (a) floor and (b) perimeter infill wall composition.

The staircase is arranged centrally and adjacent to the longitudinal building facade, in order to satisfy both architectural and structural symmetry requirements (see Fig. 3-2). It consists of inclined beams connected by horizontal beams in correspondence of landing and floor levels (also known as "knee beam"). Steps are considered to have a structural function and they are fixed to the inclined beams as cantilever beams (see Fig. 3-6). Staircases are areas susceptible to crowding; thus, an imposed load for cat. C2, equal to 4.0 KN/m^2, is assumed (EC1-1). The lift is placed in the space between the stairs and landing levels and it is considered disconnected from the main structure. Perimeter infills are constituted by double layer hollow clay bricks. They are considered in the model as non-structural elements, realised in contact with the frame, without any structural connection with it.

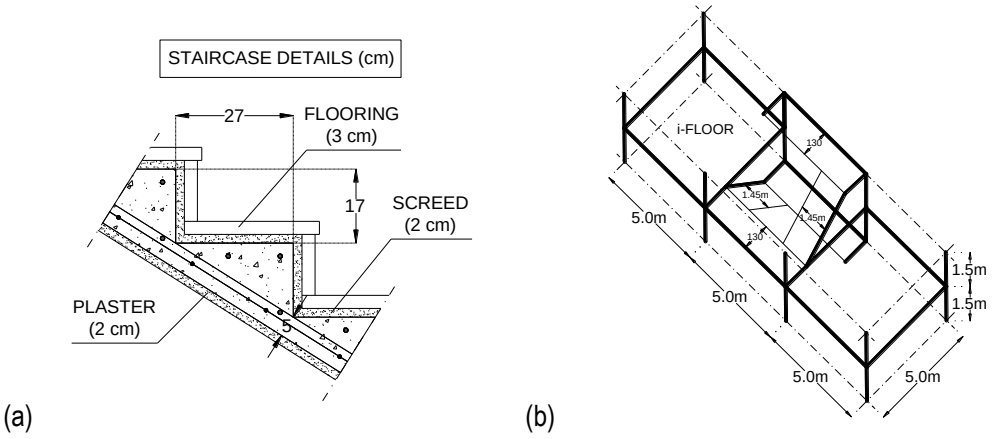

Fig. 3-6 Geometrical details of the benchmark buildings: (a) stair steps and (b) staircase composition.

Cross-sections of beams are assigned on the basis of values typically assumed in the constructional practice. Columns are designed in order to sustain an appropriate internal axial force both for seismic and non-seismic conditions, and they have to provide an adequate lateral stiffness to the structure. In addition, column cross-sections are assumed in order to satisfy smoothly the EC8-1 beam-to-column hierarchy of resistance condition (i.e., $\sum M_{Rc} \geq 1.3 \sum M_{Rb}$ where $\sum M_{Rc}$ and $\sum M_{Rb}$ are the sum of the bending moment capacities of the columns and beams framing the joint, respectively). Square cross-sections for all the columns are assumed allowing, approximately, an equal distribution of

lateral strength and stiffness in the two directions. Maximum columns' decrease at adjacent levels is 10 cm for reasons of regularity in elevation and constructional practice.

The evaluation of the gravity loads, considering the nominal density values of construction materials provided by EC1-1, is reported in Table 3-5 and it is characterised for floors, roof, staircase, and infills.

Table 3-5 Characterisation and evaluation of the area gravity loads on floors, roof, staircase and infills.

Floor loads per 1.0 m²						
Group	***Element***	***b* (m)**	***h* (m)**	***γ* (kN/m³)**	***G_k* (kN/m²)**	***Q_k* (kN/m²)**
Structural	Concrete slab	1.00	0.04	25.00	1.00	Imposed Load (cat. B1) 2.00 kN/m²
	RC joists (x2)	0.10	0.20	25.00	1.00	
	Hollow bricks (x2)	0.40	0.16	8.00	1.02	
				Total	3.02	
Non-structural	Mortar screed	1.00	0.04	20.00	0.80	
	Flooring	1.00	0.03	27.00	0.81	
	Plaster	1.00	0.02	15.00	0.30	
	Partitions	-	-	-	1.00	
				Total	2.91	
Roof loads per 1.0 m²						
Group	***Element***	***b* (m)**	***h* (m)**	***γ* (kN/m³)**	***G_k* (kN/m²)**	***Q_k* (kN/m²)**
Structural	Concrete slab	1.00	0.04	25.00	1.00	Imposed Load (cat. H) 0.50 kN/m² Snow Load 1.40 KN/m²
	RC joists (x2)	0.10	0.20	25.00	1.00	
	Hollow bricks (x2)	0.40	0.16	8.00	1.02	
				Total	3.02	
Non-structural	Mortar screed	1.00	0.04	20.00	0.80	
	Plaster	1.00	0.02	15.00	0.30	
	Coat	-	-	-	1.00	
				Total	2.10	
Staircase loads per 1.0 m²						
Group	***Element***	***b* (m)**	***h* (m)**	***γ* (kN/m³)**	***G_k* (kN/m²)**	***Q_k* (kN/m²)**
Structural	Tread	0.27	0.17	25.00	2.13	Imposed Load (cat. C2) 4.00 kN/m²
	Concrete slab	0.32	0.05	25.00	1.48	
				Total	3.61	
Non-structural	Mortar screed (going)	0.27	0.02	20.00	0.40	
	Mortar screed (riser)	0.02	0.17	20.00	0.25	
	Flooring (going)	0.31	0.03	27.00	0.93	
	Flooring (rise)	0.03	0.14	27.00	0.42	
	Plaster	0.32	0.02	15.00	0.36	
	Railing	-	-	-	0.69	
				Total	3.05	
Infill loads per 1.0 m²						
Group	***Element***	***b* (m)**	***h* (m)**	***γ* (kN/m³)**	***G_k* (kN/m²)**	***Q_k* (kN/m²)**
Non-structural	External brick	0.12	-	16.00	1.92	-
	Internal brick	0.08	-	16.00	1.28	
	External plaster	0.02	-	16.00	0.32	
	Internal plaster	0.02	-	16.00	0.32	
	Insulation	0.03	-	3.00	0.09	
				Total	3.93	

For the sake of simplicity, each member's ID derives from the intersection of the frames denoted as in Fig. 3-7. Frames in Y direction are denoted by a letter from A to F while frames in X direction are

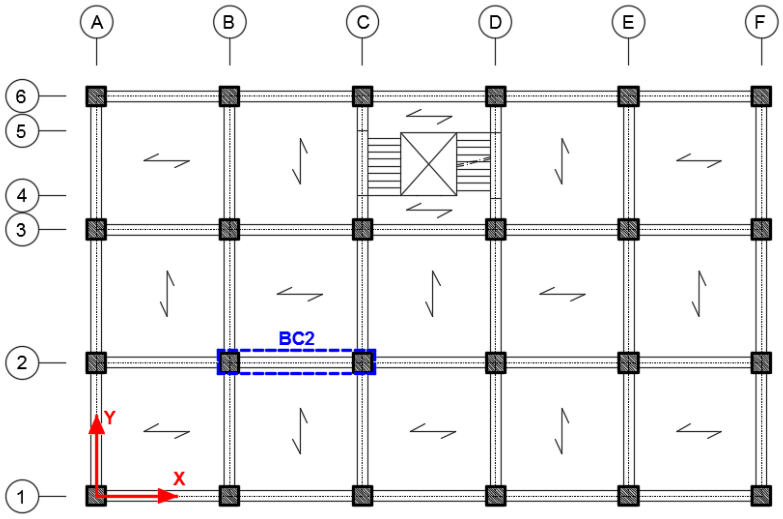

Fig. 3-7 Orientation of the one-way slab distribution and rule for denoting the ID of the elements.

denoted by a number from 1 to 6. Table 3-6 reports the load values acting on each beam, calculated on the basis of the area gravity loads described in Table 3-5. For example, beam BC2, shown in Fig. 3-7, is identified by frame 2 and frames B and C and its beam distributed load due to live loads (Q_k) is given by the area live load on floor (i.e., 2.00 kN/m^2) multiplied by half length of the beam C12 (i.e., 2.5 m) which is equal to 5.00 kN/m.

Finally, the characteristic values of loads are properly combined on the basis of the design situations, in order to derive their design values of them (EC0, CEN 2002). In non-seismic conditions of ultimate limit states, the structure must be able to resist to design loads obtained from the fundamental combination, as follows:

$$\sum_{j\geq 1}\gamma_{G,j}G_{k,j}\text{"+"}\gamma_{Q,1}Q_{k,1}\text{"+"}\sum_{i>1}\gamma_{Q,i}\psi_{0,i}Q_{k,i} \tag{3.6}$$

where

- " + " implies "to be combined with";
- $\sum$ implies "the combined effect of";
- $G_{k,j}$ is the characteristic value of a permanent action j;
- $\gamma_{G,j}$ is the partial factor for permanent action j;
- $Q_{k,1}$ and $Q_{k,i}$ are the characteristic value of the leading and accompanying i variable action, respectively;
- $\gamma_{Q,1}$ and $\gamma_{Q,i}$ are the partial factor for the leading and i variable action, respectively;
- $\psi_{0,i}$ is the factor for combination value of a variable action i.

In seismic design situation to ultimate and serviceability limit states, the following combination should be adopted (EC0):

$$\sum_{j\geq 1} G_{k,j} \text{ "+" } \sum_{i\geq 1} \psi_{2,i} Q_{k,i} \text{ "+" } A_{Ed} \tag{3.7}$$

where the previous definitions remain valid for the respective terms that appear in the above expression, while:

- $\psi_{2,i}$ is the factor for quasi-permanent value of a variable action *i*;
- A_{Ed} is the design value of seismic action.

Recommended values for both combinations and partial factors are adopted. The leading combination factor refers to imposed loads in building for Cat. B (offices areas), instead the secondary combination factor refers to snow loads for sites located at altitude $a_s \leq 1000$ m.a.s.l..

Table 3-6 Characterisation and evaluation of the distributed gravity loads on beams.

Floor and roof beam loads								
Group	***Beam***			***G_{k1}* (kN/m)**	***G_{k2}* (kN/m)**	***Q_{k1}* (kN/m)**	***Q_{k2}* (kN/m)**
Floor	AB1, AB6, CD1, CD6, EF1, EF6, A23, F23			-	7.37(1)	-	-
Floor	BC1, BC6, DE1, DE6, A12, A36, F12, F36			7.56(3)	14.64(1+ 3)	5.00(3)	-
Floor	AB2, AB3, BC2, BC3, CD2, DE2, DE3, EF2, EF3, B12, B23, B36, C12, C23, D12, D23, E12, E23, E36			7.56(3)	7.28(3)	5.00(3)	-
Roof	AB1, AB6, CD1, CD6, EF1, EF6, A23, F23			-	4.91(2)	-	-
Roof	BC1, BC6, DE1, DE6, A12, A36, F12, F36			7.56(4)	10.16(2+ 4)	1.25(4)	3.50(4)
Roof	AB2, AB3, BC2, BC3, CD2, DE2, DE3, EF2, EF3, B12, B23, B36, C12, C23, D12, D23, E12, E23, E36			7.56(4)	5.25(4)	1.25(4)	3.50(4)
Staircase beam loads								
Group	***Beam***	***G_{k1}* (kN/m)**	***M_{Gk1}* (kNm/m)**	***G_{k2}* (kN/m)**	***M_{Gk2}* (kNm/m)**	***Q_{k1}* (kN/m)**	***M_{Gk1}* (kNm/m)**	***Q_{k2}* (kN/m)**
Landing	CD6	-	-	7.37(1)	-	-	-	-
Landing (Knee)	C56, D56, C34, D34	7.56(5)	6.30(5)	7.28(5)	6.06(5)	10.00(5)	8.33(5)	-
Flight (Knee)	C45, D45	5.22(6)	3.79(6)	4.42(6)	3.93(6)	5.80(6)	4.21(6)	-
Floor	CD3	7.56(3)	-	7.28(3)	-	5.00(3)	-	-
Roof	CD3	7.56(4)	-	5.25(4)	-	1.25(4)	-	3.50(4)

The generic beam's ID derives from the rule explained in Fig. 3-7. Legend: 1 = infill load, 2 = parapet load, 3= floor load assuming an influence length of 2.5 m, 4 = roof load assuming an influence length of 2.5 m, 5 = landing load assuming a fixed-fixed beam scheme, 6 = flight load assuming a cantilever beam scheme. M = torsional distributed moment applied on knee beams.

3.3.4. Numerical model

The benchmark building is modelled in MIDAS Gen (SINCE 1989), a commercial software package typically used for professional applications. Infill, parapet and staircase loads are assigned to beams as distributed loads, while beams are loaded by means of area loads assigned to each floor field, according to Fig. 3-7. Loads are automatically converted to masses, according to the combination in Eq. 3.7. Beams and columns weights are automatically calculated by the software and converted to masses, once the material and its specific density are defined. Floor diaphragms at each level are automatically generated by MIDAS Gen. Diaphragms at intermediate landings of the staircase are not modelled, since the hypothesis of in-plane rigid body is not considered realistic due to the limited extension of landings compared to the floor area. Fig. 3-8 shows the structural model analysed in MIDAS Gen. The elastic flexural properties of the uncracked gross section stiffness of beams and columns are assumed in the model reduced by 50% for both ultimate and serviceability limit states (EC8-1). Shear deformability is neglected. The staircase considered in this study consists of inclined beams (flight beams) supporting the steps and supported, in turn, by elements of the frame system. Such beams work in the strong direction of their cross-section as elements subjected to the interaction of axial force and bending moment. For simplicity the multi-linear beams (also known as "knee beams") are modelled through a whole inclined beam connecting the beam-to-column joints at the floor and landing levels (Fardis 2009).

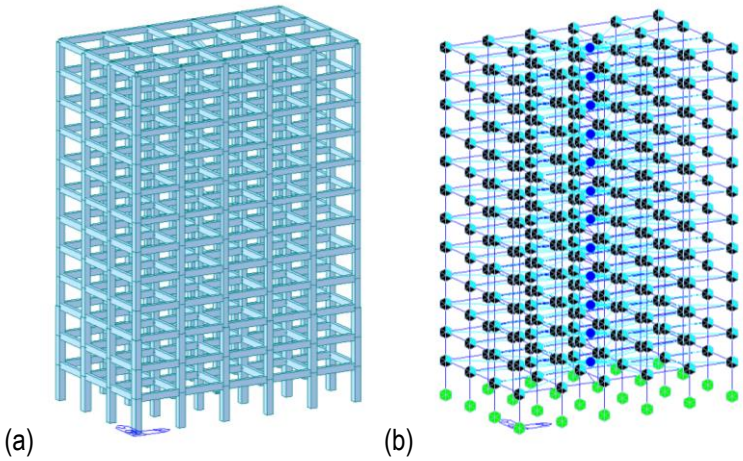

(a) (b)

Fig. 3-8 Numerical model of the benchmark building: (a) view of the structural model in MIDAS Gen and (b) boundary conditions, nodal masses and diaphragm constraint at each floor.

3.3.5. Seismic design

Seismic design of the benchmark building is performed by MIDAS Gen software. The seismic demand at LS-LS is obtained in a different way for the two design solutions based on different ductility class: (i) DCH, where the demand is evaluated by implementing the design spectrum for behaviour factor q equal to 5.85; (ii) DCM, where the demand is evaluated by implementing the design spectrum for q equal to 3.90 (see Fig. 3-4b). The capacity at LS-LS is carried out in terms of local forces and according to the capacity design rules (EC8-1). The demand at DL-LS is evaluated by implementing

the elastic spectrum as seismic input (see Fig. 3-4a). The capacity at DL-LS is based on the maximum Interstorey Drift Ratio (*IDR*) in compliance with damage limitation of non-structural elements which is assumed equal to 0.5% for buildings having non-structural elements of brittle material attached to the structure (EC8-1). The most unfavourable effects are obtained from the 100:30 combination rule of the lateral forces including effect of the accidental eccentricity of the centre of mass (e_{ai} = ± 0.05 L_i where L_i is the dimension of the building in plan perpendicular to the seismic action direction, EC8-1). The application of the two rules results in 32 combinations of the lateral forces along direction X and Y.

It is stated that, in this study, the effect of the accidental eccentricity is not investigated for LTHA therefore it is useful to comment herein, for the sake of comparison between RSA and LTHA, the results of the benchmark building designed without considering the accidental eccentricity (i.e., e_{ai} = ± 0.05 L_i rule) but with the spatial variation of the seismic motion (100:30 combination rule). Indeed, it is only mentioned here that the accidental eccentricity cannot be applied in LTHA in the same way as RSA, since it doesn't produce the same effect; in fact, the shift of the centre of mass changes the dynamic characteristics of the structure (De La Llera and Chopra 1994). However, several procedures have been proposed in literature to account for the effects of torsional GM in time history analyses (Basu et al. 2014), and they will be the object of further studies pointed out in Chapter 7. In this light, implementing accidental eccentricity it's beyond the scope of this study. The application of the 100:30 rules result in 8 combinations of the lateral forces in the main directions (i.e., swap between forces along X and Y including sign inversion) since the centre of mass is considered in its original position.

The benchmark building preliminarily designed for non-seismic conditions at ultimate limit state and serviceability limit state (EC2) is herein checked and modified in order to accomplish the requirements of EC8-1. Design is performed for DCH and DCM through RSA, starting from the same geometry of the elements. RSA is the reference design method of EC8-1 and it can be applied for any case where LFM applicability conditions are not satisfied. It is worth mentioning that LFM can be used for the design if the building is both regular in elevation and it presents fundamental period T_1 ≤ [4T_C, 2 s] (EC8-1). From a preliminary check it results that the benchmark building meets the requirements of regularity both in plan and in elevation (EC8-1) therefore the design through LFM is also allowed. However, RSA is adopted in the following implementing CQC rule and 5% damping ratios for all the modes in order to be consistent with the damping ratio used for the response spectrum. All the modes of vibration up to a cumulative effective modal mass of at least 90%, with an effective modal mass greater than 5% of the total mass must be considered in the CQC (EC8-1). For the verifications in terms of local forces, the signs of the translational modes' local forces are assigned to the combined results. Second-order effects (*P-Δ*) need to be taken into account for the entire structure by multiplying *a posteriori* all first-order action effects due to horizontal components

of the seismic action by 1 / (1 – $\theta_{P\text{-}\Delta}$) where $\theta_{P\text{-}\Delta}$ is the greatest of the values evaluated according to Eq. 3.8 for each direction (Fardis 2009).

$$\theta_{P\text{-}\Delta,i} = \frac{N_{tot,i}\, d_{r,i}}{V_{tot,i}\, h_i} \tag{3.8}$$

In Eq. 3.8, $\theta_{P\text{-}\Delta,i}$ is the interstorey drift sensitivity coefficient at i^{th}-storey; $N_{tot,i}$ is the total gravity load concurrent with the seismic action at and above i^{th}-storey; $d_{r,i}$ is the inelastic interstorey drift at the floor centre of mass, estimated via equal displacement rule (obtained multiplying the displacement by q); finally, $V_{tot,i}$ is the total seismic shear at i^{th}-storey, and h_i is the height of i^{th}-storey.

In the following the results obtained for DCH and DCM design are presented.

3.3.6. Design for Ductility Class High

Concrete C35/45 (f_{cd} = 19.83 MPa, E_c = 34077 MPa) is adopted for the whole building in order to control section dimensioning because of beam-to-column joint verifications. The minimum cross-section area is 70x70 cm^2 for all the columns at the lower storeys (from 1st to 3rd storey). It results from the limitation on the normalized axial force imposed by EC8-1 (i.e., $v_d \leq 0.55$ for DCH). Beam-to-column joint verifications for horizontal shear is the limiting design factor in DCH; it applies especially for the staircase joints and external joints at the upper storeys, the latter where the internal axial compressive force is smaller. The minimum column cross-section area is 60x60 cm^2, and it is adopted for all the columns at the upper storeys. Second-order effects (P-Δ) are taken into account by multiplying the effects of the seismic action by 1.14 since the greatest $\theta_{P\text{-}\Delta}$ is equal to 0.12 (evaluated from Eq. 3.8). The minimum number of the longitudinal bars into columns is imposed by the distance between consecutive bars restrained by horizontal hoops (≤ 150 mm) and unrestrained bar from nearest restrained bar (≤ 150 mm). The diameter of the longitudinal bars (B450C: f_{syd} = 391.30 MPa, E_s =200000 MPa) is increased to 22 mm only for staircase columns in order to satisfy the beam-to-column capacity design verification while for the rest of the elements it is assumed a diameter of 18 mm except for the staircase beams at the lower storeys. γ_{Rd} is 1.2 and 1.3 when calculating shear force demands for beams and columns, respectively. Stirrup spacing (s) in critical regions of beams is always limited by the longitudinal bars' diameter ($s \leq 6d_{bL}$). The only exceptions are the knee beams in the staircase, for which s results from the truss capacity model with the inclination of the compression strut at 45 degrees. Stirrup diameter is 10 mm in critical regions of all the columns in order to satisfy joint verification with feasible distances between hoops while it is 8 mm for all the beams except for the staircase beams. Stirrup spacing in the critical regions of columns is generally governed by the minimum value equal to $6d_{bL}$, except for columns in the staircase where the critical condition is that on confinement imposing the minimum value for ductility compliance. Stirrup spacing in beam-to-column joints is governed by the verification and it is often given by the minimum technological value (i.e., 6 cm is the minimum centreline distance between two stirrups of

10 mm diameter that allows cast concrete getting through). The maximum IDR attained in the building under the DL-LS elastic spectrum is about equal to 0.2%; well within the 0.5% limit.

3.3.7. Design for Ductility Class Medium

The seismic design of the building for DCM is based on the same concrete class (C35/45) and cross-sections dimensions as obtained for DCH design. Indeed, the same dimensioning is sufficient to satisfy the less restricting normalized axial force limit imposed by EC8-1 (i.e., $v_d \leq 0.65$ for DCM). No second-order effects amplification needs to be considered in this case since $\theta_{P\text{-}\Delta}$ is lower than 0.10. The minimum number of longitudinal bars in the columns results from the minimum distance between consecutive restrained bars (≤ 200 mm) and unrestrained bar from the nearest restrained bar (≤ 150 mm). The diameter of longitudinal bars is increased to 22 mm only for the staircase columns in order to satisfy the beam-to-column hierarchy of resistance condition for these elements while for the rest of the elements a diameter of 18 mm is assumed except for the staircase beams at the lower storeys. γ_{Rd} is 1.0 and 1.1 when calculating shear force demands for beams and columns, respectively. Stirrup spacing (s) in beams critical regions is governed by the minimum value equal to $8d_{bL}$, except for the staircase beams, for which the minimum distance between stirrups is that resulting from the truss capacity model. Stirrup diameter is 8 mm in all the beams and columns. The distance between stirrups in the critical regions of columns is governed by the confinement verification for ductility compliance at the lower storeys and the minimum value equal to $8d_{bL}$ at the upper storeys. Stirrup spacing in beam-to-column joints is assumed to be the same of the corresponding bottom columns, although for confined central joints this spacing can be doubled, being not greater than 150 mm. DL-LS verification is the same for DCH and DCM design since structure stiffness is the same for the two cases, being section dimensions the same.

3.3.8. Results discussion

Modal properties of the final benchmark building design are summarized in Table 3-7 where the periods of vibration (T), the translational modal participating mass along X and Y (MP_{UX} and MP_{UY}) and the rotational one about Z (MP_{RZ}) of the first ten modes are shown. These are the modes employed in the RSA and complying with the 90% rule on modal masses summation and 5% minimum on modes to be considered. The RSA is performed assuming conventional 5% damping ratio for all the modes resulting in the correlation coefficients ρ_{ij} matrix as shown in Fig. 3-9. It is relevant how T_i and T_j for the 5th and 6th modes are close, resulting in ρ_{56} equal to unity. The coupling behaviour between the second torsional mode (i.e., 6th mode) and the second translational mode in Y (5th mode) is due to the presence of the staircase that represents an irregular element within an overall regular building. The staircase identifies an area within the building that shows increase of mass (because it is susceptible to crowding and must be designed accounting for a larger imposed load, i.e. 4.0 KN/m^2 for cat. C2) and stiffness (because of squat columns and inclined connections

between consecutive storeys). Moreover, flight beams and squat columns can be subjected to high tensile axial forces that can significantly reduce flexural capacity of these elements (see Fig. 3-10).

Table 3-7 Summary of the modal properties of the benchmark building modelled in MIDAS Gen.

Mode number, i	***T_i* [s]**	***$MP_{UX,i}$* [%]**	***$MP_{UY,i}$* [%]**	***$MP_{RZ,i}$* [%]**
1	1.31	77.7	0.0	0.2
2	1.19	0.0	75.8	0.0
3	1.13	0.2	0.0	77.6
4	0.47	12.2	0.0	0.0
5	0.40	0.0	13.7	0.5
6	0.40	0.0	0.6	11.6
7	0.27	4.2	0.0	0.0
8	0.23	0.0	0.0	4.3
9	0.22	0.0	4.5	0.0
10	0.19	2.3	0.0	0.0
	Total	96.5	94.7	94.3

$$\left[\rho_{ij}\right] = \begin{bmatrix} 1.000 & 0.519 & 0.313 & 0.008 & 0.005 & 0.005 & 0.003 & 0.002 & 0.002 & 0.001 \\ & 1.000 & 0.789 & 0.010 & 0.007 & 0.007 & 0.003 & 0.002 & 0.002 & 0.002 \\ & & 1.000 & 0.011 & 0.007 & 0.007 & 0.003 & 0.002 & 0.002 & 0.002 \\ & & & 1.000 & 0.276 & 0.276 & 0.030 & 0.017 & 0.015 & 0.010 \\ & & & & 1.000 & 1.000 & 0.059 & 0.030 & 0.025 & 0.016 \\ & & & & & 1.000 & 0.059 & 0.030 & 0.025 & 0.016 \\ & & & & & & 1.000 & 0.279 & 0.191 & 0.073 \\ & & & sym & & & & 1.000 & 0.835 & 0.214 \\ & & & & & & & & 1.000 & 0.316 \\ & & & & & & & & & 1.000 \end{bmatrix}$$

Fig. 3-9 Correlation matrix for ρ_{ij} coefficient in CQC evaluated for the first ten modes of the benchmark building referred to periods T_i in Table 3-7 and relative damping ratio ζ_i assumed equal to 5% for all the modes.

Fig. 3-11 shows the intersection of the periods of vibration and the different code-response spectra together with the lower bound limit of $0.2a_{g,LS\text{-}LS}$ imposed by EC8-1, which affects design for DCH. The design spectral accelerations for DCH corresponding to the first three periods of vibration (i.e., $S_{ad}(T_1)$, $S_{ad}(T_2)$, and $S_{ad}(T_3)$) result equal to 0.052 g which are 25%, 39% and 46% smaller than the corresponding ones for DCM. However, the structural response of the structure designed for DCH is amplified by 14% due to the second-order effects (*P-Δ*) that are not needed to be accounted for in DCM design, being $\theta_{P\text{-}\Delta}$ lower than 0.10. For DL-LS the reference response spectrum is the same for both the design solutions. Fig. 3-12 shows the distribution of the seismic demand in terms of storey shear along direction X and Y of the building designed for LS-LS. For the sake of comparison, the storey shears for DCH are shown with and without the amplification for second-order effects. Results

show that the maximum base shear of the building designed for DCH with and without second-order effects is respectively 13% and 29% smaller than DCM in direction X while it is respectively 23% and 40% smaller in direction Y. These results allow to state that because of the relatively high deformability of the building, the lower bound limit of the DCH design spectrum and the P-Delta effects, the difference in design between DCH and DCM for the benchmark building is not particularly relevant. Basically, even if the building designed for DCH seems to be more appealing than DCM because of the possibility to rely more on ductility than strength (i.e., larger behaviour factor thus lower seismic forces than DCM), the large translational fundamental periods make design affected by both significant *P-Δ* effects and modification of the design response spectrum. The steel reinforcement details are mostly governed by verifications rather than minimum code requirements, except for the stirrups spacing and the distance between restrained longitudinal bars that are generally controlled by minimum requirements. In some cases, the stirrups spacing in members and beam-to-column joints is controlled by the minimum technological values (i.e., staircase).

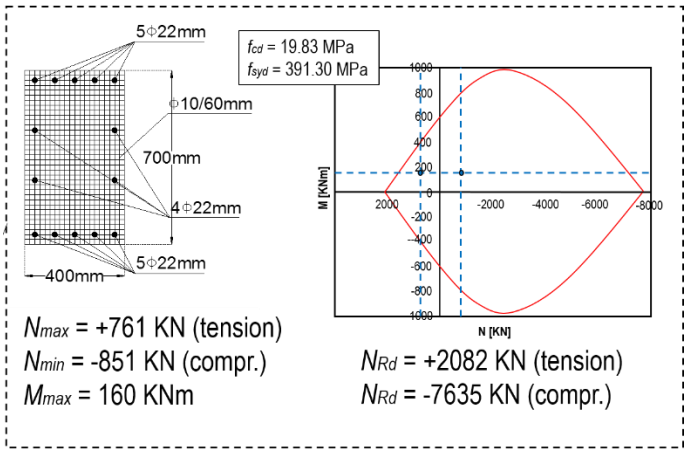

Fig. 3-10 Design check of the staircase: flight beam flexure verification.

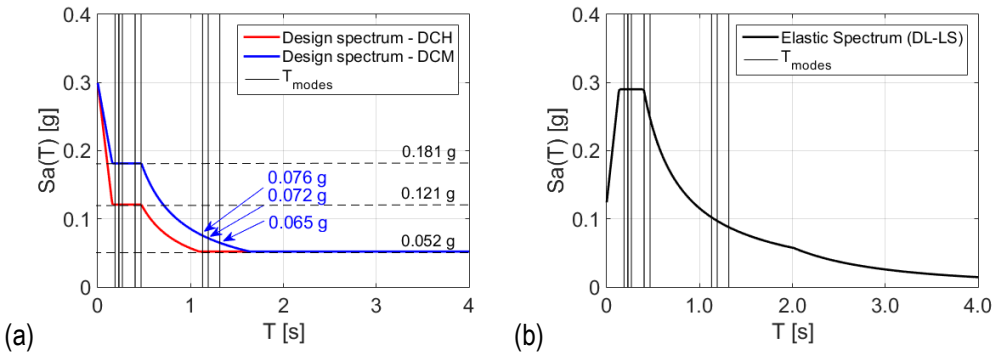

Fig. 3-11 Intersection of the periods of vibration and response spectra of the benchmark building at (a) LS-LS and (b) DL-LS.

Results in terms of deformability at DL-LS (see Fig. 3-13) confirm that design of the benchmark building, whether DCH or DCM, is essentially governed by strength rather than deformability. Indeed,

in order to satisfy the verifications of the beam-to-column joints and beam-column capacity design at LS-LS both higher concrete class and larger cross-sections of columns were needed, resulting in a building having reasonably higher lateral stiffness than other solutions tested in the preliminary stage. The largest IDR occurs between the 3rd and 4th storey where the cross-section of the columns is changed from 70x70 cm^2 to 60x60 cm^2.

Fig. 3-14 and Fig. 3-15 summarise the results of the design for both DCH and DCM, respectively, in terms of beam and columns geometrical and reinforcement details.

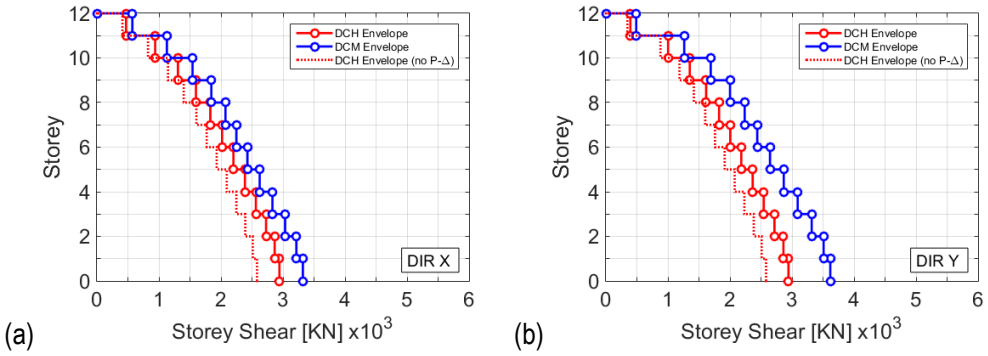

Fig. 3-12 Seismic demand on the benchmark building at LS-LS in terms of maximum storey shear: (a) direction X and (b) direction Y.

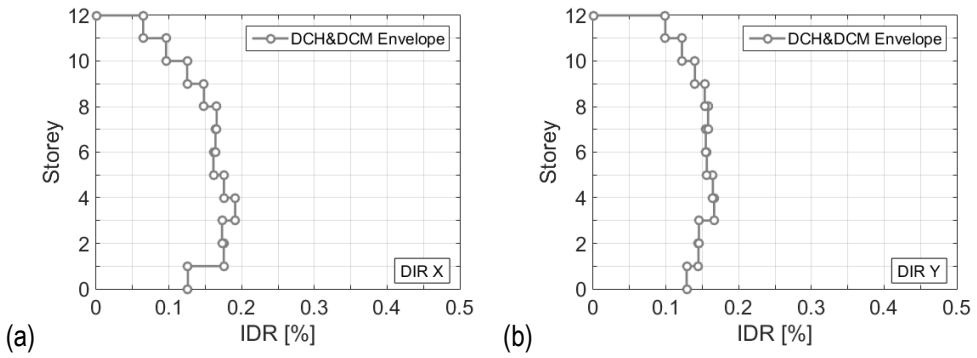

Fig. 3-13 Seismic demand on the benchmark building at DL-LS in terms of maximum Interstorey Drift Ratio (IDR): (a) direction X and (b) direction Y.

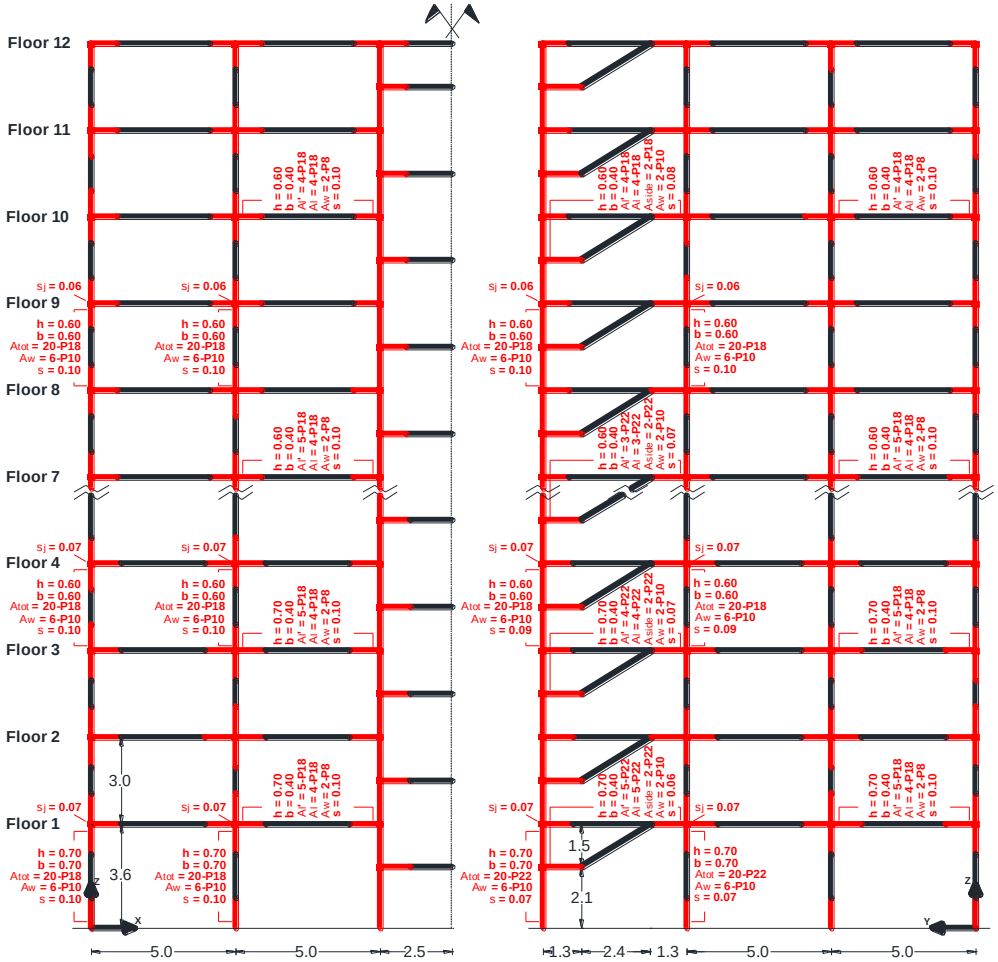

Fig. 3-14 Geometrical and reinforcement details for the benchmark building designed for DCH. Legend: h = section depth, b = section width, A_l = bottom longitudinal bars, A_l' = top longitudinal bars, A_{tot} = total longitudinal bars, A_{side} = total lateral longitudinal bars, A_w = stirrup bars, s = stirrups spacing in critical regions, and s_j = stirrups spacing in joints.

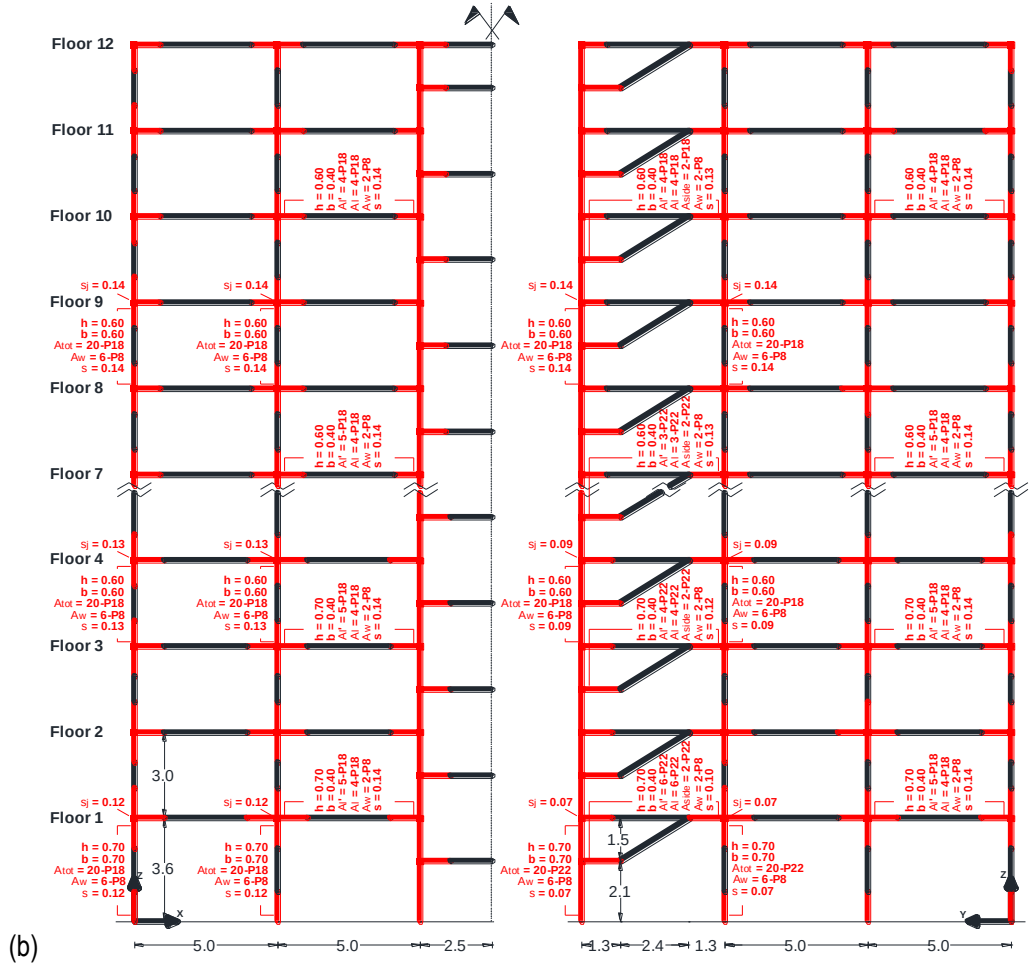

Fig. 3-15 Geometrical and reinforcement details for the benchmark building designed for DCM. Legend: h = section depth, b = section width, A_l = bottom longitudinal bars, A_l' = top longitudinal bars, A_{tot} = total longitudinal bars, A_{side} = total lateral longitudinal bars, A_w = stirrup bars, s = stirrups spacing in critical regions, and s_j = stirrups spacing in joints.

3.4.Conclusion

This chapter presents the main aspects related to the design of RC-MRF buildings according to EC8 showing a practical example which is represented by the benchmark building considered in this research work. Modern seismic design philosophy implemented by the design rules in current design codes is presented and the concept of archetypical structures is introduced, starting from the definition provided by FEMA P-695 which proposed a methodology to quantify safety risk and assess collapse of typical seismic-force-resisting systems. If design practice is guided by a series of rules on the choice of design parameters within the allowable design space, it is possible to study a limited number of models whose results can be generalised to the entire class representative of a specific model (i.e., archetype structure). While this aspect has been already pointed out by FEMA P-695 within the US context, Europe lacks a similar design practice. Moreover, many studies in literature (herein only some are presented) are still based on simplified numerical models which cannot reliably estimate the actual behaviour of buildings in Europe (e.g., 2D models, staircase neglected). All these aspects motivated the choice of the benchmark building presented in this research work that can be considered as representative of the majority of ordinary buildings in Italy and in general seismic prone areas in Europe. The main original features of the benchmark building are the assumption of a 3D model (avoiding the concept of representative 2D frames) and the presence of the staircase that even if it does not classify the building as irregular it introduces a realistic feature that can influence significantly the design choices in real practical applications.

This chapter presents a detailed description of the structural design of the benchmark building designed according to EC8 for DCH and DCM through RSA, showing a comparison between the two ductility classes and comments regarding some critical aspects found in the design. The benchmark building, which geometrical and reinforcement details are presented, is then assessed through LTHA and NTHA in Chapter 6. The choice of a 12-storey RC-MRF building is suitable to the scope of generalising the conclusions related to it in the next chapters to the class of RC-MRF buildings with a lower number of storeys.

Chapter 4: An EC8-compliant LTHA Design Framework

Part of this chapter is based on the following reference:

Lombardi L and De Luca F (2018). Linear Time-History Analysis as EC8-compliant Design Method: What Seismic Input Selection?, 11th U.S. National Conference on Earthquake Engineering, Los Angeles, California, June 25-29.

Lombardi L, De Luca F, and Macdonald J (2019). Design of Buildings through Linear Time-History Analysis Optimising Ground Motion Selection: A Case Study for RC-MRFs, Engineering Structures; 192:279-295.

Objectives of this chapter

This chapter introduces LTHA as a seismic analysis method for "force-based" design. In particular, a possible EC8-compliant LTHA design framework is presented herein and compared to the one recently proposed by FEMA P-1050 and included in ASCE/SEI 7-16. In order to provide a detailed description of the main steps characterising LTHA design implementation, a practical example is herein included which refers to the assessment of the 12-storey RC-MRF benchmark building designed through RSA described in the previous chapter. It is worth mentioning that this chapter does not provide a newly-designed benchmark building but it considers the one resulting from RSA design in order to show a direct comparison of the results of LTHA versus RSA that will be presented in Chapter 6. In this light, the following objectives are aimed in this chapter:

- to present a possible EC8-compliant LTHA design framework, describing the main steps for its implementation in commercial software packages in future (i.e., GM selection, modelling, behaviour factor, viscous damping model, second-order effects, load combinations, verification, and results interpretation). This framework is then implemented in an *in house* developed OpenSees/Matlab code which is described in the next chapter;
- to show the differences between the proposed EC8-compliant framework and the one recently described in FEMA P-1050;
- to propose a GM selection for LTHA analogous to NTHA and different from the procedure recommended by FEMA P-1050 for LTHA. A novel index is herein presented that is, in general, building dependent and can be used to control response variability in relation to the dynamic properties of the structure as well as to identify possible "unacceptable cases" due to limits of "force-based" capacity models for LTHA design.

4.1.Introduction

Linear Time-History Analysis (LTHA) is not new in earthquake engineering but many codes, including EC8 (CEN 2004a), do not mention explicitly LTHA among the possible methods of analysis for design. Indeed, LTHA has been used for *ad hoc* analyses in advanced applications, i.e., bridges, dams, or nuclear facilities (e.g., Yamaguchi et al. 2004; Nour et al. 2012) but only recently a "force-based" framework for LTHA-based design of structures was included in the ASCE/SEI 7-16, suggesting response spectrum matching of three pairs of GMs as input (e.g., through wavelet adjustment), so that LTHA can be used as alternative to the RSA (Charney 2015). In this way, LTHA can replicate as closely as possible the typical outcome of RSA with the benefit of accounting for coupling of the local force components (i.e., bending moment and axial force), typically lost within RSA procedure when the modal effects are combined through combination rules (BSSC 2015). For instance, this is a crucial aspect when the maximum Demand over Capacity Ratio (DCR) of a structural member subjected to the combined action of axial force and bending moment over time, for all load combinations, needs to be evaluated (Wilson 2015). LTHA simply solves the equation of motion for discrete linear Multi-Degree Of Freedom (MDOF) systems, considering the interaction of the modes of vibration with the typical frequencies of an earthquake defined by accelerometric waveforms (Chopra 2012). Its approximation falls in the fact that it cannot account for the the inelastic behaviour due to damage as Nonlinear Time-History Analysis (NTHA) does, but it can reliably estimate the behaviour of buildings in serviceability conditions (i.e., when behaviour is essentially elastic and limited structural damage is expected). This could be an important aspect for the possible use of LTHA, since experience has shown that a relevant part of economic losses due to medium and severe earthquakes is attributed to non-structural damage, especially for commercial, industrial and strategic buildings (e.g., Taghavi and Miranda 2003). LTHA, indeed, allows designers to determine other response quantities as well, such as absolute accelerations, relative accelerations and velocities, since some equipment can be sensitive to these response quantities. Having a reliable estimation of serviceability performance at the design stage can be very valuable for decision making. Therefore, the proposal of an EC8-compliant LTHA design framework for buildings, which can be implemented in commercial software packages and easily used by designers, represents an important aspect. An ideal "force-based" LTHA design framework should provide the opportunity to account for the seismic input variability, suiting design purposes without losing the possibility to capture specific response features such as pulse-like effects, contrarily to the procedure adopted by ASCE/SEI 7-16 (ASCE 2017) and recommended by FEMA P-1050 (BSSC 2015).

In the following, the proposed EC8-compliant LTHA design framework is presented and main steps for its possible implementation are discussed in detail. The proposed framework is compared to the one described by FEMA P-1050, implemented for a design example in FEMA P-1051 (BSSC 2016). Particular attention is given to the main aspects that basically prevented the widespread use of LTHA

in the past. A novel approach for optimising GM selection is presented herein and it is showed for different suites of GMs selected for the benchmark building in Chapter 6.

4.2.The proposed EC8-compliant LTHA design framework

In this chapter, a new procedure for EC8-compliant "force-based" design is proposed and differences with respect to FEMA P-1050 are presented. The proposed procedure is presented for the assessment of the benchmark building designed for DCH and described in Section 3.3, but general discussions are also provided for its applicability to different cases study structures (e.g., irregular buildings). The proposed design procedure encompasses the relevant aspects already discussed in EC8 and it provides recommendations on how to verify the structural compliance of members using the output of an LTHA. Aspects such as: accounting for the interaction between bending moments and axial force in the design of elements, the estimation of P-Delta amplification factors, the implementation of the behaviour factor, and the selection of GMs are discussed in detail, providing a procedure for LTHA, analogous to the consolidated practice pursued in the case of RSA. In addition to the aspects already known in the literature and stated in design codes, this chapter includes an approach to how identify possible "unacceptable cases" for LTHA due to the limitations of the "force-based" capacity models, as will be explained more in detail later.

The proposed procedure can be split in three stages, namely Pre-Processing, Processing and Post-Processing for its implementation in software or routines. In the Pre-Processing, the numerical model, in terms of geometry, gravity loads, GM time-histories, and analysis settings are defined. The pre-dimensioning of the structure can be performed through RSA and subsequently assessed through LTHA. In the Processing stage, the gravity load and time-history analyses are performed. In the Post-Processing stage, the results are analysed to evaluate P-delta effects, combinations of effects, and acceptance criteria. In order to make clear the explanation of the procedure, the Post-Processing is split in two parts depicted in Fig. 4-1 and Fig. 4-2.

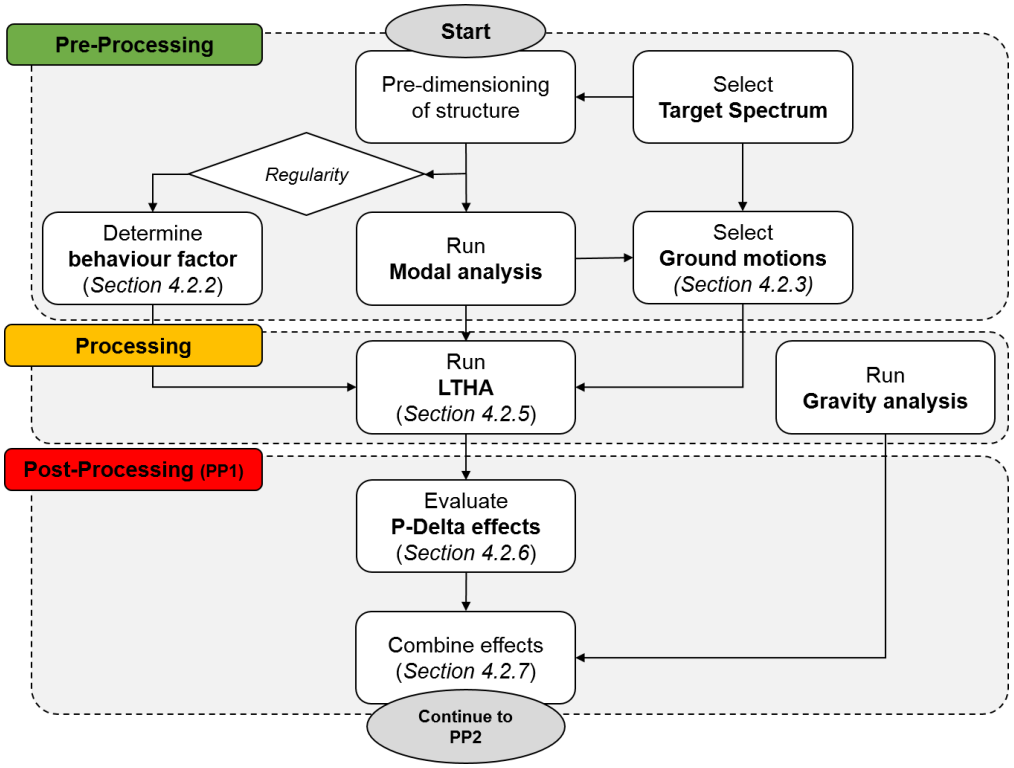

Fig. 4-1 Flowchart of the proposed LTHA design framework: pre-processing, processing and post-processing stage.

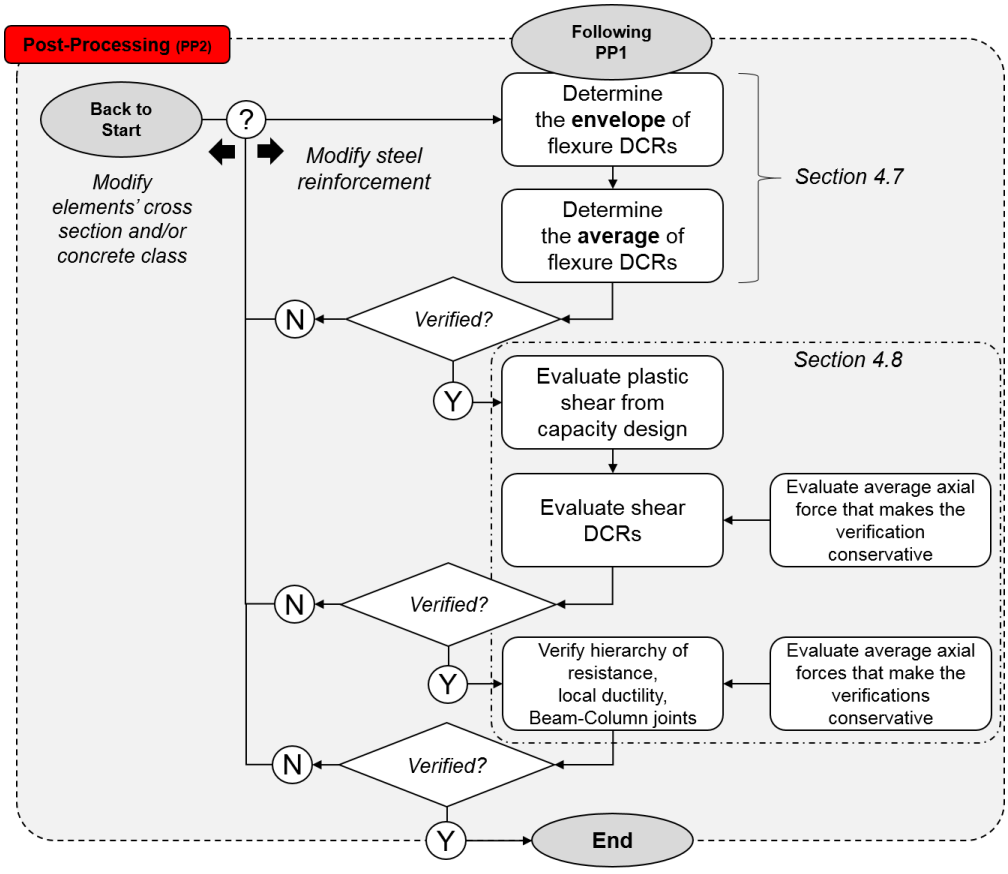

Fig. 4-2 Flowchart of the proposed LTHA design framework: verifications within the post-processing stage.

4.2.1. Linear modelling

The linear model of the building to be analysed should be built up in the same way as adopted by LFM and RSA. Two-dimensional models have been widely used in the past for simplified calculations but nowadays, thanks to the progress in computer-based computations, three-dimensional models can be easily built up without much effort. FEMA P-1050 indicates that three-dimensional analysis is required for all the systems analysed through LTHA, for this reason herein the same recommendation is made. The benchmark building is modelled in OpenSees (OpenSees 2006) by means of "elasticBeamColumn" elements (see Fig. 4-3), but any finite element analysis commercial software which adopts linear-elastic beam elements could be used in general. Concrete C35/45 is adopted for the whole building, resulting in a Young's Modulus E_c equal to 34.08 GPa calculated as per EC2 (CEN 2004b). For concrete structures, cross-section flexural stiffness of members should account for an equivalent reduction of stiffness (e.g., from cracking). According to EC8-1, this can be obtained by reducing the flexural second moment of area and shear area each by 50% (i.e., $I = \alpha I_g$ where I_g is the gross uncracked second moment of area and α is the equivalent stiffness reduction factor). This reduction depends on many aspects such as extension of cracks, magnitude and sign of bending moment, amount of reinforcement, intensity and sign of axial load, cross-section geometry, etc. (Priestley 2003). This stiffness reduction is representative of the fact that the building might be subjected to initial stresses which lead to cracks during its life (e.g., due to the gravity loads or minor earthquakes) and it represents the secant stiffness at the yielding condition of elements based on experimental and numerical results (e.g., Biskinis and Fardis 2010a). Some other design codes indicate α equal to 40% and 70% for beams and columns, respectively (SNZ 2004; ACI 2008). The equivalent stiffness reduction factor can be also assumed equal to 40% for columns subjected to tensile axial forces and high ductility frames in serviceability limit state conditions (Priestley 2003). Contrarily, for steel buildings the gross second moment of area and shear area are considered as they are. Torsional stiffness should be accounted for by adopting a proper torsional constant value. Some commercial software use the formulation reported in Young and Budynas (2002). Staircases or other elements which affect the structural response should be accounted for in the model (Fardis 2009). The staircase should be modelled since it can characterise the inherent torsional features of buildings, both in terms of mass and stiffness. For simplicity the staircase beams (also known as "knee beams") are modelled as in the detail of Fig. 4-3 through a whole inclined beam connecting the beam-to-column joints at the floor and landing levels (Fardis 2009). Storey diaphragms are assigned to each floor, except for the staircase landings for which the hypothesis is not applied. Floor loads, external infills and members self-weight are assigned through distributed loads; members self-weight masses are assigned to the ends of each member while floor and infill masses are lumped at the centre of mass of each storey, both evaluated according to the "half-and-half" seismic weights distribution criterion.

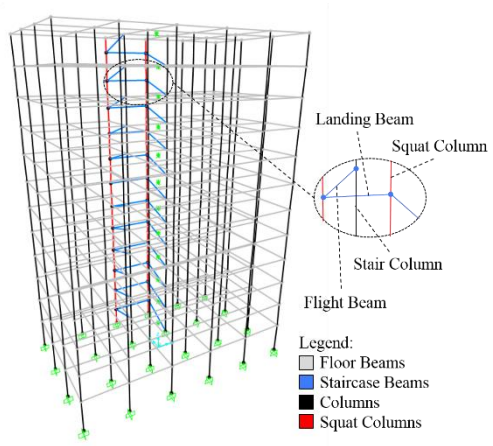

Fig. 4-3 Numerical model of the benchmark building and identification of structural element groups: floor beams, staircase beams, columns, and squat columns.

4.2.2. Behaviour factor

For typical "force-based" design approaches the elastic code-spectrum for ultimate limit states is divided by the behaviour factor q in order to obtain the corresponding design demand on elements. In the following, the benchmark building designed for DCH is considered and its q is equal to 5.85 (CEN 2004a). However, for LTHA the spectrum-compatibility in GM selection is evaluated on the elastic code-spectrum. For this reason, the time-histories could be in principle divided by q. However, the lower bound limit of the pseudo-acceleration (i.e., $S_{ad}(T_i) \geq 0.2a_{g,LS\text{-}LS}$, where for the example presented here $a_{g,LS\text{-}LS}$ is equal to 0.2604 g) imposed by EC8-1 modifies the shape of the design spectrum where the pseudo-acceleration results to be lower than such limit (see Fig. 4-4a). Herein, it is suggested to conservatively evaluate the behaviour factor for LTHA (q_{LTHA}) as follows:

$$q_{LTHA} = \min\left[S_{ae}(T_i)/S_{ad}(T_i)\right]_i \qquad \forall T_B \leq T_i \leq T_1 \tag{4.1}$$

where T_i is the period of vibration of the mode ith, $S_{ae}(T_i)$ is the value of the spectral acceleration corresponding to T_i evaluated on the elastic code-spectrum (for the example presented here T_B is equal to 0.1568 s) and $S_{ad}(T_i)$ is the ordinate corresponding to the design spectrum (see Table 4-1 for their values). Eq. 4.1 identifies the minimum value of the behaviour factor all over the different spectral ordinates of the structure and then this value is applied to each one of the GM components, resulting in spectra scaled by $1/q_{LTHA}$. It is worth noting that the proposed approach keeps the validity of the spectrum-compatibility within the range of the relevant periods of vibration (see Fig. 4-4b) and it makes sure that the minimum allowed behaviour factor over the periods is used, as in LTHA only one value can be applied and not a different one per each spectral ordinate as in RSA. If the benchmark building was designed for DCM (see Fig. 3-11), q_{LTHA} would have been equal to q (i.e., 3.90) because the lower bound limit of the pseudo-acceleration does not affect the periods of the building.

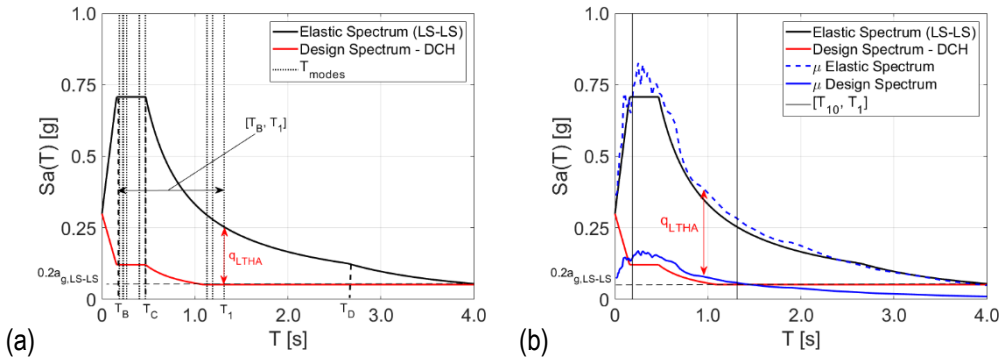

Fig. 4-4 Behaviour factor for LTHA: (a) evaluation of q_{LTHA} and (b) its application to the spectra of a suite of GM where μ denotes the mean spectrum of the suite.

If the building is irregular in elevation, EC8-1 suggests reducing the value of the behaviour factor by 20% in order to get a higher seismic demand. Similarly, for buildings which are irregular in plan, the overstrength coefficient, denoted by α_u/α_1, is replaced by the average of its value and 1.0 (EC8-1). This approach can be applied also within the proposed procedure through Eq. 4.1 because $S_{ad}(T)$ is evaluated from $S_{ae}(T)$ by means of q. It is worth mentioning that EC8-1 provides the upper limits of the behaviour factor that designers can use. In some cases, it may be useful to choose a more conservative value of the behaviour factor in order to increase the safety margins of the design (Fardis 2009). On the other hand, for conforming situations (i.e., reflecting the case of regular buildings), the values suggested by EC8-1 are generally lower than those evaluated through nonlinear analyses (e.g., Kappos 1999, Elnashai and Mwafy 2002). The assumption in Eq. 4.1 is consistent with the maximum value of q usable for RSA as the GM can be scaled by only one value while the response spectrum can be scaled by different q-values at different spectral ordinates. This is the case for the design of the benchmark building regardless of the assumption of q as the design spectrum cannot go lower than $0.2a_{g,LS\text{-}LS}$ and this limit affects the design. The behaviour factor proposed for LTHA is valid regardless of the discretionary assumption made for q by the designer to determine the design spectrum.

For the example presented here, q_{LTHA} is equal to 4.86 and it is applied to reduce the GM accelerations of the suite presented in Chapter 6. This procedure allows the use of a behaviour factor that does not depend on the GM selection as it is evaluated with respect to the design code spectrum. The procedure according to FEMA P-1050 considers the modification of the response for inelastic behaviour *a posteriori*, by evaluating the maximum elastic base shear along each main direction and multiplying it by I_e/R, where I_e is the importance factor and R the response modification factor (see FEMA P-1050 for how these parameters are evaluated). Then the base shear scale factor along each main direction is evaluated as the minimum between unity and the ratio between the base shears given by the static analysis and the one described above. This factor is subsequently utilised to amplify LTHA results in order to determine the combined responses and to lead to probabilities of

collapse which are consistent with RSA and LFM. In contrast, this procedure is not required for displacements that are taken as those computed from the elastic response multiplied only by C_d/R where C_d is the deflection amplification factor.

Table 4-1 Periods of vibration (Ti), modal participating masses ($M_{PUX,i}$, $M_{PUY,I}$, and $M_{PRZ,i}$), and elastic and design spectral accelerations (S_{ae} and S_{ad}) corresponding to each period of vibration of the benchmark building.

Mode number, i	T_i [s]	$MP_{UX,i}$ [%]	$MP_{UY,i}$ [%]	$MP_{RZ,i}$ [%]	$S_{ae}(T_i)$ [g]	$S_{ad}(T_i)$ [g]
1	1.31	77.7	0.0	0.2	0.2532	0.0521
2	1.19	0.0	75.8	0.0	0.2796	0.0521
3	1.13	0.2	0.0	77.6	0.2945	0.0521
4	0.47	12.2	0.0	0.0	0.7074	0.1209
5	0.40	0.0	13.7	0.5	0.7074	0.1209
6	0.40	0.0	0.6	11.6	0.7074	0.1209
7	0.27	4.2	0.0	0.0	0.7074	0.1209
8	0.23	0.0	0.0	4.3	0.7074	0.1209
9	0.22	0.0	4.5	0.0	0.7074	0.1209
10	0.19	2.3	0.0	0.0	0.7074	0.1209
	Total	96.5	94.7	94.3		

4.2.3. Ground motion selection

GM selection procedures require preliminary knowledge of the site and the periods of vibration of the building of interest. The first step for the input selection is to determine the target spectrum for the considered limit state at the site. According to EC8-1, the elastic spectrum should be obtained from the country's National Annex specifications (see Table 2-3). As shown in Section 3.3.2, the benchmark building is located in L'Aquila, Italy. The Italian National Annex specifications for EC8 design allow the definition of a site-dependent elastic response spectrum for the whole territory (Italian Building Code 2018; Meletti et al. 2007) depending on the considered limit state. Subsequently, the fundamental period of vibration of the building is needed in order to define the lower and upper tolerances for spectrum-compatibility. The fundamental period of the structure can be roughly obtained from empirical formulae, but only modal analysis can reveal which modes of vibration significantly contribute to the structural response. Therefore, in order to have results that are consistent with the structural members' capacities, pre-dimensioning of the structure is needed (for example, performed through LFM or even RSA).

Real GMs are available from the most common GM databases such as the European Strong Motion database (ESM 2008), the PEER NGA Ground Motion database (PEER 2014), etc. There are many tools online that allow to perform GM selection. It is worth mentioning that, GM selection should be carried out to account for the seismogenetic features of the source, as also stated in EC8-1. However,

the lack of sufficient recorded earthquakes for many sites makes it challenging, especially for medium-high seismic regions like the one herein considered. For this reason, the current practice for design (i.e., intensity-based approach according to FEMA P-58) allows the selection of earthquakes from different sites as long as it satisfies the code-requirements in terms of spectrum-compatibility, even if the selection does not meet the regional characteristics (Iervolino et al. 2010b). Another important aspect herein pointed out is related to the shape of target spectra for sites nearby faults (e.g., Chioccarelli and Iervolino 2013, Almufti et al. 2015, Kohrangi et al. 2018). Most of the seismic design codes, including the Italian code, provide generic target spectra regardless of the closeness to the fault or directivity effects, etc. The selection of GMs based on spectral shape is problematic for near-field regions and is still debated.

For the near-field conditions GMs should be rotated to the fault-normal (FN) and fault-parallel (FP) directions given the strike angle, according to FEMA P-1050. This is proposed because for sites located within 5 km of an active fault there is a tendency for response spectra to be larger in the FN direction than in the FP direction (Campbell and Bozorgnia 2007; Watson-Lamprey and Boore 2007). However, in some cases it is not true that the maximum amplitude of the acceleration is obtained along the FN direction. For these GMs which exhibit directionality, the direction of maximum motion is generally aligned at varying azimuths. A more detailed discussion can be found in Stewart et al. (2011) and Giannopoulos et al. (2018). EC8 does not provide any recommendations about this topic, so the approach suggested in FEMA P-1050 is recommended here. It is important to note that when performing analyses of buildings, swapping of the GMs must be applied in order to adversely load both the main directions of the buildings. Fig. 4-5 shows the rule for rotating horizontal GM components 1 and 2 give their orientation (e.g., 90-0°, E-N, 47-317°) and the strike angle which denotes the FP direction. For the example in Fig. 4-5, GM components 1 has orientation equal to 250° while the strike angle is equal to +40°. The rotation of GM components 1 to FP is equal to the difference between the strike angle and the record angle, i.e. 210°.

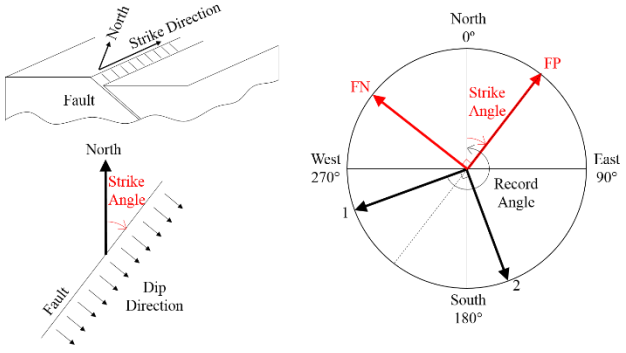

Fig. 4-5 Rotation of the GM components to the Fault-Normal (FN) and Fault-Parallel (FP) given the strike angle (adapted from USGS, https://earthquake.usgs.gov/).

Herein the possibility of using the spectrum-compatibility procedure provided for NTHA is considered. Indeed, if LTHA GM selection procedure is perfectly compatible with the selection for NTHA, it allows a direct comparison between linear and nonlinear results using the same suite of GMs. This comparison is not achievable if conventional RSA design is performed or the spectral-matching procedure suggested by FEMA P-1050 for LTHA is considered. In order to evaluate the influence of the EC8-compliant GM selection on LTHA design, both in terms of demand and capacity, different suites of earthquakes are herein considered in this research work, including spectral-matching, and they are discussed in Chapter 6.

4.2.4. Damping models

Many commercial software packages for structural analysis used by designers employ the Rayleigh damping model to evaluate damping forces in time-history analyses (Chopra and McKenna 2016). This model is based on the user-definition of the damping ratios for only two periods of vibration while the damping ratios at other periods depend on the mass α_M and stiffness β_K proportional constants (Chopra 2012), as explained in Section 2.2.2. Fig. 4-6 shows a comparison between the two damping models in terms of seismic response of the benchmark building analysed for two GMs. According to Rayleigh damping model, the damping ratio ζ_i for the i^{th}-mode having frequency ω_i can be expressed as per Eq. 4.2 (Chopra 2012).

$$\zeta_i = \frac{\alpha_M}{2\omega_i} + \frac{\beta_K \omega_i}{2} \tag{4.2}$$

For the benchmark building, the solution of Eq. 2.5 results in the mass and stiffness proportional constants being equal to α_M = 0.2571 rad/s and β_K = 0.0097 s/rad, respectively, when the damping ratios of the 1st and 3rd mode of vibration are each set to 5%. In this way, it would result from Eq. 4.2 in the damping ratio for the 10th mode being equal to 15% as shown in Fig. 4-6a. It is possible to observe in Fig. 4-6b that if the damping ratios at higher modes of vibration are not properly controlled when using Rayleigh damping model, like in this example, the maximum storey shears can be underestimated up to 16%. ASCE/SEI 7-16 allows using Rayleigh damping model for LTHA as long as the damping ratios associated with the higher modes are not excessive. To control this effect, ASCE/SEI 7-16 requires that the damping in all included modes are less than or equal to 5%. FEMA P-1050 recommends using superposition of modal damping matrices for time-history analyses which is herein adopted for the benchmark building with a damping ratio equal to 5% for each mode in accordance with the damping used for the RSA (BSSC 2015). Recently, the use of the Rayleigh damping model has not been suggested for NTHA since it can lead to “spurious” damping forces as shown in Chopra and McKenna (2016). Herein, superposition of modal damping matrices is adopted for LTHA by using the “modalDamping” command in OpenSees. This assumption is consistent with that made for NTHA as explained in Chapter 5 for comparing directly LTHA to NTHA in Chapter 6.

The comparison between an optimised use of Rayleigh damping model and superposition of damping matrices is not investigated in this research work.

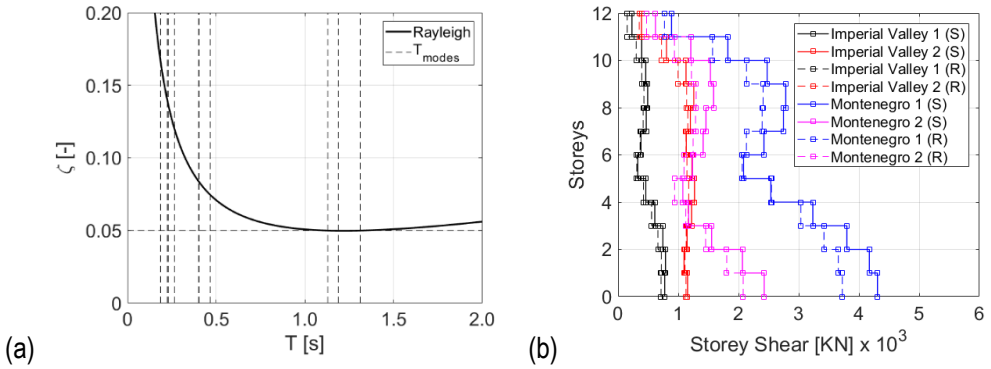

Fig. 4-6 Example of comparison between Rayleigh (R) and Superposition of modal damping matrices (S) damping models for the benchmark building analysed along X direction: (a) Rayleigh damping ratios at different periods and (b) seismic demand in terms of maximum storey shear for M5 1979 Imperial Valley and M6.9 1979 Montenegro ground motion components 1 and 2.

4.2.5. Time-history analyses

Thanks to the linearity of the analysis, each GM horizontal component can be applied independently along each of the main horizontal directions and subsequently combined with the gravity loads analysis according to the superposition principle. A direct-integration transient analysis method is used in OpenSees to solve the equations of motion of the benchmark building subjected to dynamic loading (Eq. 2.4). The Newmark method is used in OpenSees to numerically integrate the equations. The default parameters γ = 0.50 and β = 0.25 are assumed for the analyses. It is worth mentioning here that even if GMs are applied independently along each direction, some torsional effects due to irregularity in plan are accounted for. For the example, the staircase clearly represents an irregular aspect within the behaviour of the building both in terms of mass and stiffness. However, these torsional effects are not that relevant to make the overall behaviour of the benchmark building irregular according to EC8 regularity requirements. FEMA P-1050 allows including P-Delta effects in the analysis as explained Section 4.2.6. In this case, time-history analyses should be performed considering directly the contribution of the gravity loads which are used to build up a constant geometrix stiffness matrix. However, this approach is not recommended as also explained in Section 4.2.6.

4.2.6. P-Delta effects

P-Delta effects for linear analyses are typically quantified through the evaluation of the interstorey drift sensitivity coefficient $\theta_{P\text{-}\Delta}$ (EC8-1). FEMA P-1050 allows using a methodology in which P-Delta effects are directly included in the model by forming a constant geometric stiffness matrix created from gravity loads analysis (Wilson and Habibullah 1987; Wilson 2004). This approach is already implemented in commercial software packages (e.g. MIDAS Gen). However, it was observed that

because of the period elongation of buildings it can lead to unconservative responses compared to the case without P-Delta effects (Aswegan and Charney 2014). Otherwise, a static analysis is required by FEMA P-1050 to determine the interstorey drift sensitivity coefficient $\theta_{P\text{-}\Delta}$. Herein, it is proposed to evaluate the P-Delta effects according to EC8-1 in the same way as considered for linear static analyses identifying the time step in LTHA for which the maximum interstorey drift ($d_r(t^*) = d_{r,max}$) is achieved, as follows:

$$\theta_{P-\Delta} = P_{tot} d_r(t^*) / \left(V_{tot}(t^*) h\right) \qquad d_r(t^*) = d_{r,\max} \tag{4.3}$$

where P_{tot} is the total gravity load at and above the storey considered in the seismic design situations, h is the interstorey height, and V_{tot} (t^*) is the storey shear corresponding to the maximum interstorey drift achieved over time (amplified by q for ultimate limit states according to the displacement rule when $T_1 \geq T_C$). The interstorey drift sensitivity coefficient $\theta_{P\text{-}\Delta}$ can be evaluated for each horizontal GM component, in the two main directions. The amplification factor value, defined as $1/(1-\theta_{P\text{-}\Delta})$, equal to the maximum one evaluated between the two main directions among the storeys can be considered for each earthquake so that the equilibrium and coupling of GM components is preserved (Fardis 2009). The amplification factor can be applied *a posteriori* when performing the combinations of the unidirectional responses for each earthquake within the GM suite. In this way, the amplification of the effects is applied excluding the contribution of the gravity loads. The proposed approach provides a P-Δ amplification consistent with LTHA avoiding performing a supplementary linear static analysis as suggested by FEMA P-1050.

4.2.7. Load combinations and accidental eccentricity

Once the unidirectional responses from each GM have been obtained and the amplification factor to account for the P-Delta effects has been evaluated from them, the seismic combinations, with gravity loads included, can be performed to evaluate the most unfavourable effects (e.g., maximum/minimum local forces, displacements, reactions, etc.). For each earthquake (i.e., pair of horizontal components 1 and 2), this procedure results in eight possible combinations of the horizontal components with swap of the GM components ($\pm CX_{1or2} \pm CY_{2or1}$), if accidental eccentricity e_a is neglected. If accidental eccentricity is accounted for through a shift of the centre of mass (see Fig. 4-7), as also described in FEMA P-1050, it results in 8 x 5=40 (4 cases with the centre of mass shifted by 5% and one without shift) possible combinations. It is worth noting that the shift of the centre of mass changes the modal characteristics of the structure (De La Llera and Chopra 1994), and it inevitably leads to greater number of analyses to perform. Aswegan and Charney (2014) observed that by shifting the centre of mass the periods of vibration do not change much while the modal participating masses can change significantly, and it leads to coupling the torsional and translational modes. Several procedures have been recently proposed to account for the effects of torsional GM in time-history analyses (e.g., Basu et al. 2014) but the current design codes do not

include any of them. One aspect to note is that the GM components are combined by applying simultaneously 100% of their effects along the two orthogonal directions as per NTHA; so that occurrence of more than one component can be handled rigorously avoiding the application of the 100:30 combination rule employed for RSA (Fardis 2009).

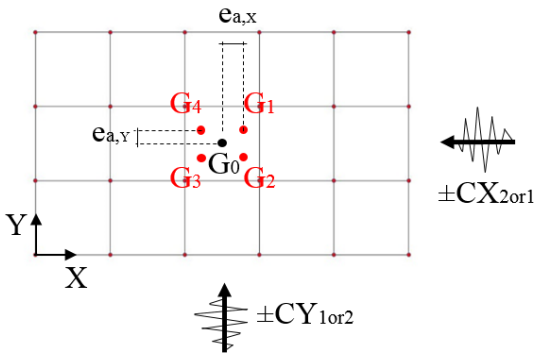

Fig. 4-7 Load combinations and accidental eccentricity rule.

4.2.8. Acceptance criteria

One of the benefits of performing LTHA is the possibility of calculating the DCR of effects (e.g., bending moments, interstorey drift ratios, etc.) step by step in the time domain for each seismic combination, by accounting for the actual interaction between bending moments and axial forces, if, obviously, the coupling between the as-recorded GM components is preserved (as recommended herein). Even though this operation can be time consuming, this is an important aspect when capacities depend on demand such as the case of members subjected to axial force and bending moment (see Fig. 4-8). Design of buildings according to capacity design typically starts by considering in the first place the behaviour of the dissipative members such as flexural behaviour of beams and columns for MRF systems. The proposed procedure is summarised in Fig. 4-2 and it is based on the following steps:

– the maximum flexural DCR value of each element, among the seismic combinations, should be evaluated for each earthquake so that the envelope accounts for the actual interaction between bending moments and axial force. For columns, the flexural DCR is evaluated separately in each direction with the uniaxial bending moment capacity reduced by 30% (as suggested by EC8-1) to account for the biaxial bending, even though EC2 provides an expression for biaxial verifications. Herein, the rigorous biaxial flexural verification recommended by EC2 is not considered for the sake of consistency with NTHA. For NTHA, indeed, EC8-3 (CEN 2005) does not provide any recommendation for verifying structural members under biaxial bending in terms of chord rotations. Moreover, the proposed biaxial capacity models in the literature are not calibrated on a sufficiently large number of experimental tests (e.g., Bousias et al. 2002). Strictly speaking, the flexural DCRs should

be evaluated step-by-step for each combination of the components of GM, then assuming the envelope for each earthquake for the average evaluation. It is suggested herein that the maximum value of flexural DCR over the earthquake duration should be considered. Also, because the single earthquakes are not spectrum-compatible when independently analysed, it might result that members fail under compression or tension. In these cases, the acceptance criteria can be changed in terms of axial DCR. For pure compression the DCR can be evaluated as $N_{Ed}(t)$ / 0.55 $N_{Rd,c}$ (for DCH), where $N_{Rd,c}$ is the compressive axial capacity given by the concrete contribution only. For pure tension the DCR can be evaluated as $N_{Ed}(t)$ / $N_{Rd,t}$, where $N_{Rd,t}$ is the tensile axial capacity given by the yielding of the reinforcement. More details about these verifications can be found in Chapter 5;

- the average flexural DCR value, for the GM suite, of each member should be obtained and judged by the designer. It is suggested to avoid calculating "decoupled" flexural DCRs by calculating the average values of maximum/minimum axial loads and bending moments (which very likely are not coupled) since this operation generally leads to overconservative designs.

For the example presented here, the flexural capacity of members is evaluated through fibre-based section analysis in order to have a more accurate evaluation of the cross section flexural capacity than analytical formulations. The axial force acting on the cross-section is accounted for in the flexural capacity evaluation. The concrete cross-section is discretised in a sufficient number of longitudinal fibres, having the Mander monotonic stress-strain relation (Mander et al. 1988). Confined concrete behaviour is assigned to the fibres within the area defined by the transversal steel reinforcement. Fibres, having the Menegotto-Pinto monotonic stress-strain relation (Menegotto and Pinto 1972), account for the longitudinal steel reinforcement, including side bars. Concrete and steel strengths refer to the corresponding design values. For unconfined concrete, the design strength is evaluated as 0.85 f_{ck}/ γ_C, where f_{ck} is the characteristic compressive cylinder strength (equal to 35 MPa) and γ_C is the partial factor for concrete (equal to 1.50). For confined concrete, the design strength is evaluated according to EC8-3 (CEN 2005) specifications. For steel reinforcement, the design strength is evaluated as f_{syk}/ γ_S, where f_{syk} is the characteristic yield strength (equal to 450 MPa) and γ_S is the partial factor for reinforcing steel (equal to 1.15). It is worth mentioning here that the capacity of structural members could be evaluated assuming as material strength the mean value in lieu of the design one. This assumption, more suitable for assessment rather than design, is discussed in Chapter 6.

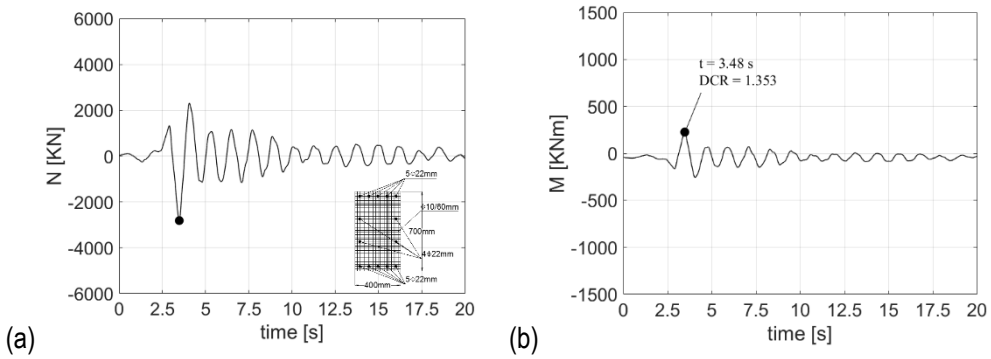

Fig. 4-8 Evaluation of the maximum DCR through LTHA of a staircase beam subjected to (a) axial force (N) and (b) bending moment (M) as function of time.

4.2.9. Capacity design, hierarchy of resistance and other verifications

Once the flexural design is performed and cross-sections of elements are defined in terms of longitudinal reinforcement, the design shear forces (also known as plastic shears) can be determined in accordance with capacity design rules. The capacity models for shear currently available in the literature do not account for biaxial loading conditions. For this reason, the shear DCRs are separately referred to each local axis of the cross-section. For simplicity, the design shear forces of elements subjected to axial force can be calculated from the average value of the axial force (from the GMs of the suite) acting at each end of the element that maximises the shear demand evaluated through capacity design rule (i.e., from the maximum bending moment capacity at each end of the element). The shear capacity can be simply calculated from the average value of the axial force acting at each end of the element that minimises the shear capacity. The shear capacity can be calculated according to the truss model with variable inclination (EC2). For the benchmark building, the strut angle is assumed equal to 45 degrees for beams while it can change for columns, according to EC8 prescriptions for DCH. Capacity design can be checked considering the average axial force that minimises the values of the resisting bending moments in columns at the considered end. For beam-to-column joint verifications, the joint capacity can be calculated from the average axial force that makes the verification conservative.

4.2.10. Unacceptable cases

Because of the use of a linear-elastic model, it may result that the average DCRs for the selected suite of GMs are very large. This aspect mainly depends on the earthquake spectra that show significant differences with respect to the design response spectrum. Specifically, the average DCRs can be significantly dependent on the largest DCRs related to the GMs, applied along a certain direction, that significantly amplify the structural response, leading to over-dimensioning of elements and, hence, expensive design solutions. Similarly to the index proposed by Jayaram et al. (2011) to quantify the similarity between a GM response spectrum and the target one, a new index is herein

proposed to control the effects on the structure of each earthquake GM horizontal component in the selected suite. This approach is based on the evaluation of the weighted average of the differences (or errors) of the spectral accelerations corresponding to each relevant period of vibration of the structure through the GM index:

$$I_{eq,j} = \sum_{i=1}^{n_p}\left[P_i\left(S_{ae,eq,j}(T_i) - S_{\text{a,target}}(T_i)\right)\right] \Big/ \sum_{i=1}^{n_p} P_i \qquad j = 1,2$$
$$P_i = \sqrt{MP_{UX,i}^2 + MP_{UY,i}^2 + MP_{RZ,i}^2} \tag{4.4}$$

where P_i is the weight of the i^{th} period of vibration (T_i), which is defined in terms of the participating masses of the mode, $S_{ae,eq,j}(T_i)$ and $S_{a,target}(T_i)$ are the GM and target (design for ultimate limit states) spectral accelerations corresponding to the mode, and n_p the number of relevant modes of vibration. Using the rigid diaphragm assumption, the weight of each mode can be expressed as the square root of the sum of the squares of the two translational ($MP_{UX,i}$ and $MP_{UY,i}$) and one rotational ($MP_{RZ,i}$) participating mass related to the in-plane displacements *UX*, *UY* and rotation *RZ*, respectively.

Fig. 4-9 shows an example of evaluation for I_{eq} according to Eq. 4.4 for the benchmark building and three GM spectra depicted in Fig. 4-9a. Modal analysis properties of the first ten modes are those reported in Table 4-1 while other parameters are reported in Table 4-2. Fig. 4-9b shows the differences in terms of spectral acceleration between GM and target spectra for simplicity denoted by $Diff(T_i)$ and such differences multiplied by the modal weight P_i. Results show that earthquake #1 (grey line and dots), which response spectrum is significantly below the target one and spectral differences at the relevant periods are always negative, presents I_{eq} equal to -0.0402 g and it is expected that it would lead to low values of DCRs for a building initially designed through RSA and that target spectrum. Differently, earthquake #3 (blue line and dots), which response spectrum is closer to the target one, presents positive spectral differences which are larger at the first three periods, and I_{eq} equal to +0.0339 g; it is expected that this earthquake would lead to DCRs larger than earthquake #1 but similar to RSA design. Finally, earthquake #2 (red line and dots) presents response spectrum higher than the target one and larger positive spectral differences at the first three periods than earthquake #3; this earthquake shows the largest I_{eq}, being equal to +0.0976 g and it is expected that it would lead to the largest DCRs compared the previous earthquakes. For the sake of GM selection optimisation, earthquake #2 could be erased from the suite and replaced with another one showing lower index value or scaled down. Fig. 4-9b shows the small "correction" of the differences in terms of spectral acceleration at the periods which show larger modal participating masses (i.e., predominant modes), and the large "correction" of such differences at the periods which show smaller modal participating masses (i.e., higher modes). For earthquake #3 such "correction" shows that higher modes contribution is still relevant compared to the other ones, as confirmed by the blue dots at the 4th to 6th periods of vibration.

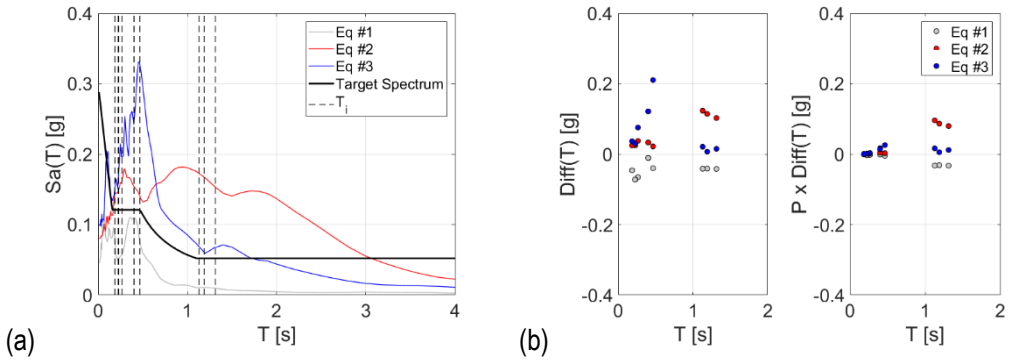

Fig. 4-9 Example of evaluation for I_{eq}: (a) ground motion spectra of three earthquakes compared to the target spectrum and (b) non-weighted and weighted differences at different periods T_i in terms of spectral accelerations for simplicity denoted by Diff(T_i) and Pi x Diff(T_i).

Eq. 4.4 assumes that the same GM component is applied along both the main directions of the building since the spectral acceleration differences at different periods are evaluated from the same GM spectrum. However, swapping of the GM components is always required when analyses are performed, therefore, this can be assumed if the maximum I_{eq} between the two components (i.e., j = 1,2) is considered for a generic earthquake.

Contrarily to Jayaram et al. (2011), the index in Eq. 4.4 avoids using the sum of the squared differences in order to keep the sign (+/-) of the differences at multiple spectral ordinates and it is inspired by the approach of weighting the spectral acceleration values used in Shome and Cornell (1999) and Luco and Cornell (2007) where the modal participation factors of the building are used as weights. Shome and Cornell (1999) introduced the concept of using the weighted average of the spectral accelerations at the first three modes as intensity measure to get a substantial reduction in dispersion with respect to the normalisation at the first-mode spectral acceleration when higher modes are important. Subsequently, Luco and Cornell (2007) refined this concept in order to reflect both the contribution of higher modes and inelasticity on structural demands.

The following aspects should be considered when using Eq. 4.4:

- for some conditions the evaluation of I_{eq} can lead to cancelation of the differences at different periods for "as-recorded" GMs. The condition $I_{eq} \approx 0$ is not therefore equivalent to the "ideal" condition of matching the target spectrum through a spectral-matching procedure;
- I_{eq} is proposed for three-dimensional buildings where more than two periods of vibration and swapping of the horizontal GM components are both considered;
- there is not a unique relationship between I_{eq} and the effects of GMs (i.e., two earthquakes can certainly show similar values of I_{eq} but different effects on structures).

In Chapter 6, the proposed index is compared to a different one which implements the well-known Square Root of the Sum of Squares (SRSS) of the spectral differences, widely applied for NTHA ground motion selection.

Table 4-2 Example of evaluating I_{eq} for the benchmark building and three ground motions depicted in Fig. 4-9: P_i is the modal weight expressed in terms of modal participating masses (see Table 4-1), and $S_{ad,target}(T_i)$ and $S_{ad,eqj}(T_i)$ are the design spectral accelerations corresponding to each period of vibration of the building (T_i) evaluated on the target spectrum and the ground motion spectrum j, respectively.

Mode number, i	P_i [-]	$S_{ad,target}(T_i)$ [g]	$S_{ad,eq1}(T_i)$ [g]	$S_{ad,eq2}(T_i)$ [g]	$S_{ad,eq3}(T_i)$ [g]
1	77.65	0.0521	0.0099	0.1546	0.0670
2	75.84	0.0521	0.0108	0.1661	0.0591
3	77.62	0.0521	0.0104	0.1754	0.0730
4	12.20	0.1209	0.0808	0.1427	0.3311
5	13.71	0.1209	0.1100	0.1540	0.2421
6	11.62	0.1209	0.1100	0.1540	0.2421
7	4.21	0.1209	0.0556	0.1582	0.1963
8	4.31	0.1209	0.0485	0.1458	0.1511
9	4.49	0.1209	0.0485	0.1458	0.1511
10	2.25	0.1209	0.0747	0.1453	0.1574

4.3.Conclusion

This chapter aims to contribute to developing and investigating a potential EC8-compliant design framework using LTHA for its possible inclusion in the second-generation release of Eurocodes. It describes the proposed framework in detail, step-by-step, showing a comparison with the one already proposed by FEMA P-1050 and adopted by ASCE/SEI 7-16. The proposed framework is presented for the assessment of the 12-storey RC-MRF benchmark building designed through RSA for DCH and described in Section 3.3. Such example is meant to enlarge the practical examples of LTHA design available in literature. Indeed, FEMA P-1051 (2016) shows as example a 12-storey steel MRF building designed through LTHA. The main difference between the two LTHA design frameworks, apart from their implemented procedures which are consistent with the corresponding design code prescriptions, consists in the GM selection procedure. While FEMA P-1050 suggests the non-uniform wavelet-based spectral-matching of three pairs of GMs in order to use LTHA as alternative to RSA, in the proposed EC8-compliant framework the GM selection is carried out in the same way as NTHA so to allow a direct comparison between linear and nonlinear results using the same suite of GMs. This comparison is not achievable if conventional RSA design is performed or the spectral-matching suggested by FEMA P-1050 is considered, especially in seismic areas prone to near-field conditions (e.g., pulse like GMs) as also highlighted in FEMA P-1050. EC8 does not provide any recommendations regarding near-field conditions therefore this aspect is herein discussed. The

critical aspect for a suitable GM selection procedure is to find a balanced compromise between control of the variability in the suite of GMs, better suiting design purposes, without losing the opportunity to capture, at design stage, part of the record-to-record variability in different field-conditions. However, when spectrum-compatibility is used for LTHA input, it is shown that unacceptable cases may occur due to strong earthquakes and limits of the "force-based" capacity models at ultimate limit states. These unacceptable cases can make LTHA design particularly problematic when evaluating capacities of RC elements according to the "force-based" approach, resulting in disproportionately high DCR values and therefore expensive solutions in order to accomplish such verifications. For this reason, a novel index (I_{eq}) is proposed to control record-to-record variability in a way that the same GM selection is also usable in NTHA. Moreover, this index, used together with specific criteria that are explained in this chapter, allows to identify possible unacceptable cases in LTHA design as shown in Chapter 6 where different GM suites are selected. The proposed design framework is also recommended for designing irregular buildings, but further investigations are needed.

Chapter 5: Linear and Nonlinear Modelling in OpenSees

Part of this chapter is based on the following reference:

Lombardi L, De Luca F, and Macdonald J (2019). Design of Buildings through Linear Time-History Analysis Optimising Ground Motion Selection: A Case Study for RC-MRFs, Engineering Structures; 192:279-295.

Lombardi L and De Luca F (2019). Linear Time-History Analysis for Fragility Curves at Design Stage, Earthquake Engineering and Structural Dynamics (under review).

Objectives of this chapter

In the previous chapter, the proposed EC8-compliant design framework based on Linear Time-History Analysis (LTHA) is presented in detail. This chapter presents the implementation of such framework in an *in house* developed OpenSees/Matlab code which can be used, in general, to design and assess the performance of buildings through linear and nonlinear analyses. In this light, the objectives of this chapter are:

- to deaggregate, conceptually, the proposed design framework in multiple coding tasks (e.g., definition of nodes, definition of elements, definition of vertical loads, running time-history analyses, performing seismic combinations, etc.) that allow to gather the aspects related to each of them in a transparent and flexible way in Matlab and OpenSees;
- to provide a reliable code framework and useful modelling recommendations for performing LTHA, comparing results of the benchmark building with those obtained from a commercial software package such as SAP2000;
- to provide a reliable code framework and useful modelling recommendations for modelling Reinforced-Concrete Moment-Resisting-Frame (RC-MRF) buildings through fibre-section nonlinear models and analysing them through Nonlinear Time-History Analysis (NTHA). Results of an experimental test available in literature are used to verify the numerical modelling assumptions which are used to analyse a simple case study represented by a three-dimensional portal frame through NTHA and pushover analysis.

5.1. Introduction

The progress in computer science and information technology in the last decades has led to developing many software packages with the aim of helping engineers in solving typical problems within the structural and geotechnical field. The Finite Element Method (FEM) is nowadays implemented in many software packages and it is used to evaluate the numerical response of structures under static and dynamic loadings (e.g., ABAQUS, Börgesson 1996; MSC/NASTRAN,

Rodden and Johnson 1994, among many). The calibration of numerical models represents an important step in order to get an accurate matching of the predicted numerical response to the physical experimental one (e.g., Haukass and Scott 2006). Many software packages adopt validated numerical models at the material and element scale thanks to numerous experimental and numerical studies carried out in literature. However, the accuracy in prediction of behaviour of real-scale buildings subjected to earthquakes represents something that is not always possible to validate against large scale experimental tests in laboratory due to modelling uncertainties related to pre-processing decisions. As result of the current practice, numerical models to analyse buildings' behaviour subjected to earthquakes are strongly empirically driven and they should require reliability analyses to characterise related uncertainties (e.g., Liu and Kiureghian 1991). FE reliability methods to characterise uncertainty represent a novel aspect that has been adopted by the current PBEE methodology (Moehle and Deierlein 2004), as described in Section 2.4, and it is based on the definition of input parameters as random variables to represent the uncertainties and evaluate response variance, covariance, sensitivities, and probabilities (McKenna 2011).

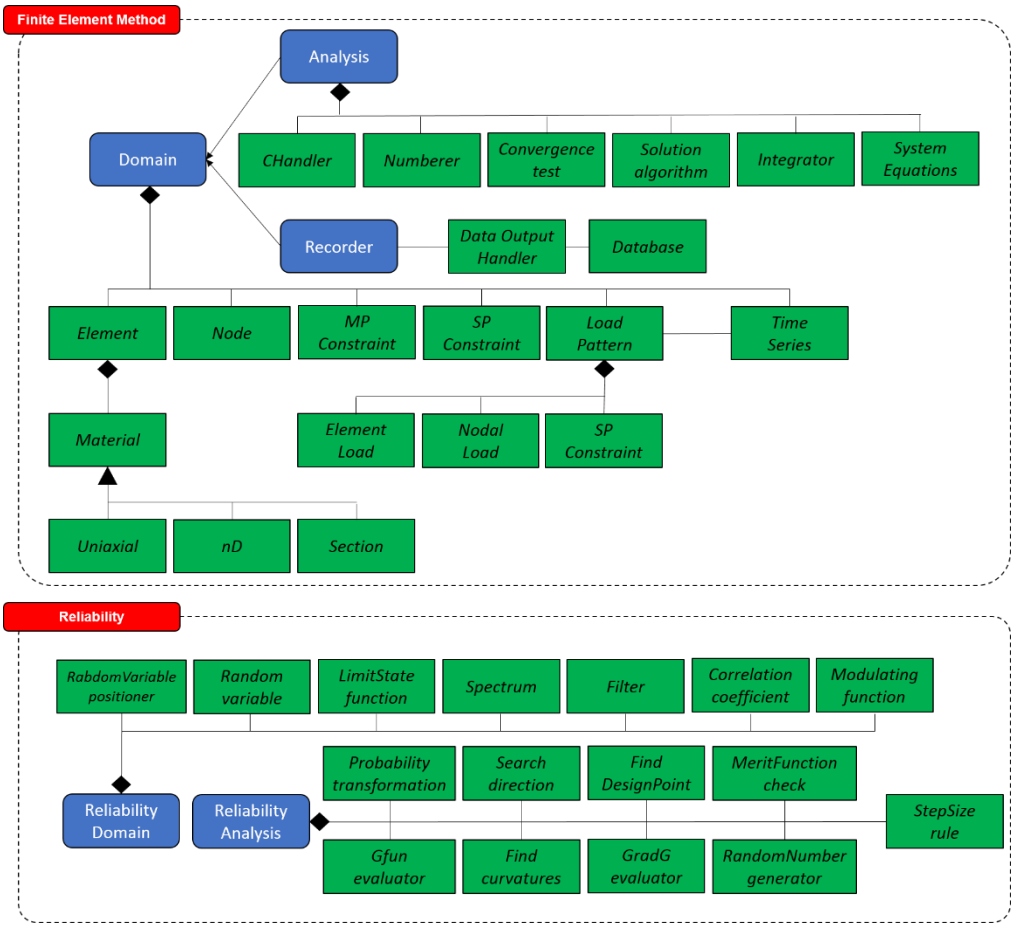

Fig. 5-1 The OpenSees software framework for FEM and FE reliability analysis and their classes (after McKenna 2011).

The Pacific Earthquake Engineering Research (PEER) centre developed an open source software mainly for scientific applications, the Open System for Earthquake Engineering Simulation (OpenSees 2006), which performs nonlinear analysis of structural and soil systems using either a standard FEM or an FE reliability analysis (see Fig. 5-1, McKenna 2011). This software, addressed more specifically to scientific applications, allows to analyse problems in a more flexible way than many available commercial software packages. Indeed, OpenSees allows adding new material and element models which can be easily compiled in the source code (e.g., Li et al. 2019), experimenting the effect on the numerical response of using different solvers, integration schemes, solution algorithms, and convergence parameters, as well as using parallel processing for High Performance Computing (HPC) problems (McKenna 2011). In this way, researchers can use a common open source framework which allows to share always new commands and updated libraries made by a community of developers worldwide. Fig. 5-1 shows the modularity of OpenSees framework and some of its customisable classes. The inputs which describe elements, nodes, constraints, and loads are provided in Tool Command Language (TCL) scripts (recently the OpenSeesPY version is available, in which the inputs are developed in Python), and the outputs are chosen by users through specific recorders. Recently, several supplementary tools for OpenSees have been proposed to provide a user-friendly visual interface with continuous guidance for pre- and post-processing stage, such as STKO (ASDEA 2019) and Build-X (Psyrras and Sextos 2018).

In the following, the design framework described in Section 4.2 is implemented in a code developed in this research work, which performs Lateral Force Method (LFM), modal Response Spectrum Analysis (RSA), Linear Time-History Analysis (LTHA), single-modal non-adaptive Nonlinear Static Analysis (NSA), and Nonlinear Time-History Analysis (NTHA) through OpenSees and uses Matlab scripts (MathWorks 2015) to accelerate the pre- and post-processing stage. This code can run multiple analyses in series and in parallel. Post-process evaluates Demand Over Capacity (DCR) values in terms of flexural, shear behaviour and interstorey drift ratios. An additional part for post-process is developed to evaluate results in a probabilistic approach consistent with PBEE methodology, as explained in Chapter 6.

5.2.Developed code framework structure

The code herein described is tested on Microsoft Windows and Linux operating system (MACOSX is not tested yet), with some changes for the second regarding the post-processing stage. It has been tested to analyse three-dimensional RC and steel MRF systems as well as X-cross Concentrically Braced Frame (CBF) systems (e.g., Di Cuia et al. 2017). The framework structure of the code follows the one of commercial structural software packages, being split in three stages: Pre-Processing, Processing and Post-Processing. Fig. 5-2 and Fig. 5-5 show the code framework structure related to the Pre-Processing and Processing stage, respectively. The code framework is structured by means of Matlab scripts which in turn are made of functions tackling minor tasks within the scripts.

In the Pre-Processing stage (see Fig. 5-2), users start with defining the building details in terms of linear and nonlinear material properties, geometry, longitudinal and transversal reinforcement details, nodes of the model, connectivity and orientation of the elements, and beam loads. Herein, an Excel worksheet, namely "structure_details.xlsx", is considered as input but any table exported from a commercial software can be used if users feel more confident with a Graphic User Interface (GUI). Indeed, the flexibility of this code relies in the possibility to work with ordered arrays and matrices which can be used to create lists of nodes, elements, loads and so on. Such Excel worksheet consists of three sheets: (1) "Building_Properties", in which the number of bays along X and Y direction, their lengths, the interstorey height, and the total height of the building are defined; (2) "Member_Properties", in which the ID of the elements, their connectivity (i.e., ID of the nodes at their ends), spatial orientation, cross-section properties (depth, width, area, second moments of area, torsional moment of area), length, shear length, material properties (elastic moduli, Poisson ratio, and specific weight), steel reinforcement details (cover, bars diameter, number of bars per layer, number of transversal legs, and stirrups spacing), and beam loads (dead and live loads) are defined; (3) "Nonlinear_Member_Properties", in which for each element described in the previous sheet, the mechanical properties related to fibre-based section modelling are defined (mean values of material strength, strain values at different behavioural stages, cyclic behaviour parameters, plastic hinge length and confined concrete properties); (4) "Masses", in which nodal masses related to elements and floors are automatically evaluated. More details about nonlinear modelling parameters are described in the following.

Subsequently, the numerical model in OpenSees is built up through the Matlab script named "BUILD_MODEL.m" which consists of the following functions (see Fig. 5-2):

- "define_data.m", this function creates the "data.tcl" script in which the parameters in "Building_Properties" are set as values in OpenSees. The generated script contains the ID of the elements (e.g., beams, columns, braces) and the ID of the nodes, gathered for each storey. These groups are then used to define the recorders of the analyses (i.e., elemen localforces, node displacements, reactions);
- "define_nodes.m", this function creates the "nodes_location.tcl" script in which the nodes of the numerical model are set as command in OpenSees. OpenSees allows defining only numerical values for the ID of the nodes. The ID numbering order suggested herein starts from 1 at the ground level and it continues along the X direction firstly, along the Y direction secondly, and along the Z direction at each storey level. Nodes related to the presence of landings in the staircase can be numbered by following the last storey node so that they can be gathered separately from the storey nodes. In addition, the location of the centre of mass at each storey is calculated in the Excel sheet "Masses" but, without losing any generality, it can be easily provided by any commercial software. For the latter, numbering starts from

a higher ID (i.e., 100000) so that there is no conflict between elements nodes' ID and master nodes' ID. The rule herein adopted is 100000 x *i* where i represents the generic storey;

- "assign_diaphragms.m", this function creates the "storey_diaphragms.tcl" script in which such condition is set as command in OpenSees. Such condition is assigned considering the ID of the storey nodes (called slave) and the ID of the centre of mass (called master) at each storey;
- "assign_boundary_constraints.m", this function creates the "boundary_constraints.tcl" script in which the boundary condition is set as command in OpenSees. It takes the ID of the nodes at the ground floor and it fixes all the degrees of freedom of such nodes. Moreover, it fixes the out-of-plane degrees of freedom of the centre of mass at each storey according to the diaphragm condition;

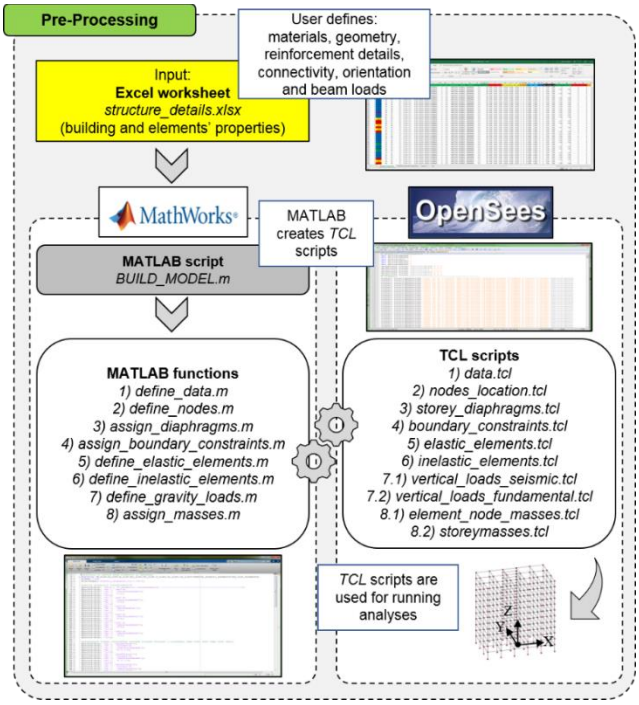

Fig. 5-2 Flowchart of the developed MATLAB/OpenSees code: pre-processing stage.

- "defines_elastic_elements.m", this function creates the "elastic_elements.tcl" script in which the linear-elastic behaviour of the elements is set as command in OpenSees. In particular, herein is implemented the "elasticBeamColumn" element which requires the element's ID, joint connectivity (i.e., ID of the nodes at the ends), cross-section area, Young and shear moduli, moments of area about z and y local axes, torsional moment of area and geometric transformation. The benchmark building is build up with 793 elements of which 481 are beams and 312 are columns. Herein, the geometric transformation which transforms member's stiffness and local forces from the local coordinate system to the global one (see Fig. 5-3) is set in a such way that local axis z is oriented according to global axis +Z for

beams and –X for columns (therefore y for columns is oriented according to +Y). It's worth mentioning that "elasticBeamColumn" element command in OpenSees does not account for the shear deformability. Possible solutions which allow to account for the shear deformability are by means of "forceBeamColumn" element command with "Elastic section" command, or through "ElasticTimoshenkoBeam" element command. In both cases, a proper value of the shear factors along cross-section local axes must be considered. However, the "ElasticTimoshenkoBeam" element command does not seem always convenient (e.g., three-dimensional multi-storey buildings or complex structures) as the signs of the element local force components are referred to the global coordinate system instead of the local one;

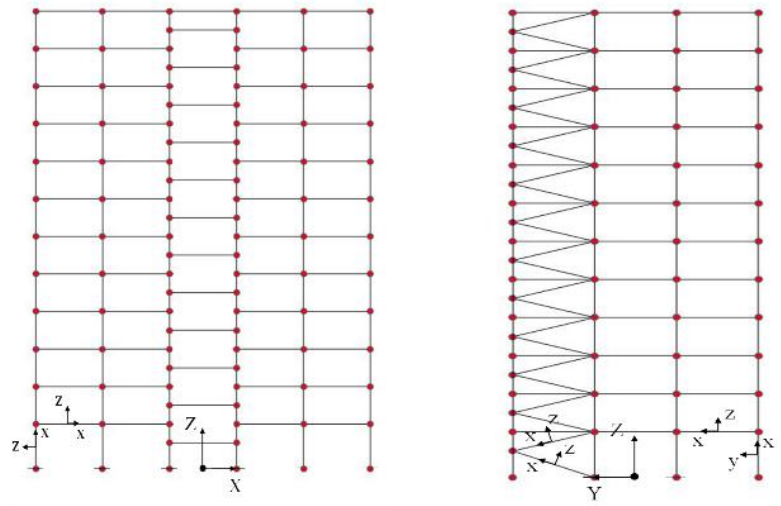

Fig. 5-3 Orientation of the local axes with respect to the global axes for the geometric transformation of the elements of the benchmark building.

– "defines_inelastic_elements.m", this function creates the "inelastic_elements.tcl" script in which the nonlinear behaviour of the elements modelled through cross-sections with fibre elements is set as command in OpenSees. For RC beam and columns, it is suggested using "forceBeamColumn" element with plastic hinges and modified two-point Gauss Radau integration rule ("HingeRadau", Scott and Fenves 2006). The user can specify the plastic hinge lengths L_p at the element ends. In particular, the modified two-point Gauss-Radau integration rule applies integration points ξ and weights ω at {0, 8/3 L_p, L - 8/3 L_p, L} and {L_p, 3 L_p, L - 4 L_p, L - L_p}, respectively (see Fig. 5-4). In this way, the Gauss-Radau integration rule allows the representation of linear curvature distribution exactly and the characteristic length will be equal to the value L_p specified by the user when deformations due to strain-softening behaviour localise at the element ends (Scott and Fenves 2006). The plastic hinge lengths are calculated according to the formulation reported in EC8-3. The shear span is assumed equal to half-element length for beams and columns (e.g., Mpampatsikos et al. 2008; De Luca et al. 2014), but users can modify this value in the "structure_details.xlsx"

Excel worksheet for individual members if a more accurate value is considered. At each integration point, the element section is discretized into three regions: (i) cover region with unconfined concrete properties and "Concrete02" material model (Yassin 1994), (ii) core region with confined concrete properties and "Concrete02" material model (Yassin 1994), and (iii) longitudinal reinforcement with steel properties and "SteelMPF" material model (Kolozvari et al. 2015) (see Fig. 5-4). Materials properties are assumed according to EC2 and EC8-3. Concrete fibres are assumed to be equal to 2x2 cm^2, small enough to evaluate reliably concrete cover damage but not too small to increase computational cost. The Young's Modulus of unconfined and confined concrete is assumed to be the same. Firstly, the script calls the material (or materials) constitutive behaviour and then it defines the torsional stiffness through "section Aggregator" as *GJ* where *G* and *J* are the shear modulus and the torsional constant of the cross-section, respectively. It is worth mentioning that for nonlinear beam-column elements with RC fibre section the storey diaphragm generates spurious axial forces in floor beams and it changes the response of the building. In order to avoid such effect, a negligible axial stiffness is proposed herein to every floor beam (excepted for staircase beams) through "section Aggregator". Subsequently, the described behaviourally-assembled cross-sections are assigned to each element of the building. It is herein suggested to use a similar approach for modelling steel beams which are pinned at their ends. Indeed, through "section Aggregator" and "forceBeamColumn" element with plastic hinges at the ends, it is possible to confer the beam end-release condition by assigning a negligible flexural stiffness without the need of using "TwoNodeLink" elements as typically adopted, which can be challenging to use for modelling very complex structures. It is worth mentioning that bond-slip and nonlinear shear behaviour are not herein modelled because they are not expected to be relevant for buildings designed according to the EC8-1 which accomplish modern seismic criteria (as it is the case for the benchmark building considered);

- "defines_gravity_loads.m", this function creates the "vertical_loads_seismic.tcl" and "vertical_loads_fundamental.tcl" scripts in which the distributed loads transferred from floors according to the considered load combination (e.g., seismic and fundamental) are set as command in OpenSees. This is carried out thanks to the one-to-one correspondence between the ID of beams and the load value assigned to each of them in the Excel worksheet;
- "assign_masses.m", this function creates the "element_node_masses.tcl" and the "storeymasses.tcl" scripts in which masses due to elements' self-weight and floor loads are are set as command in OpenSees. The first is assigned as in-plane translational mass to the nodes of the building frame. The second is assigned as in-plane translational and rotational nodal masses. This is carried out thanks to the one-to-one correspondence

between the ID of nodes and the mass value evaluated for each of them in the Excel worksheet.

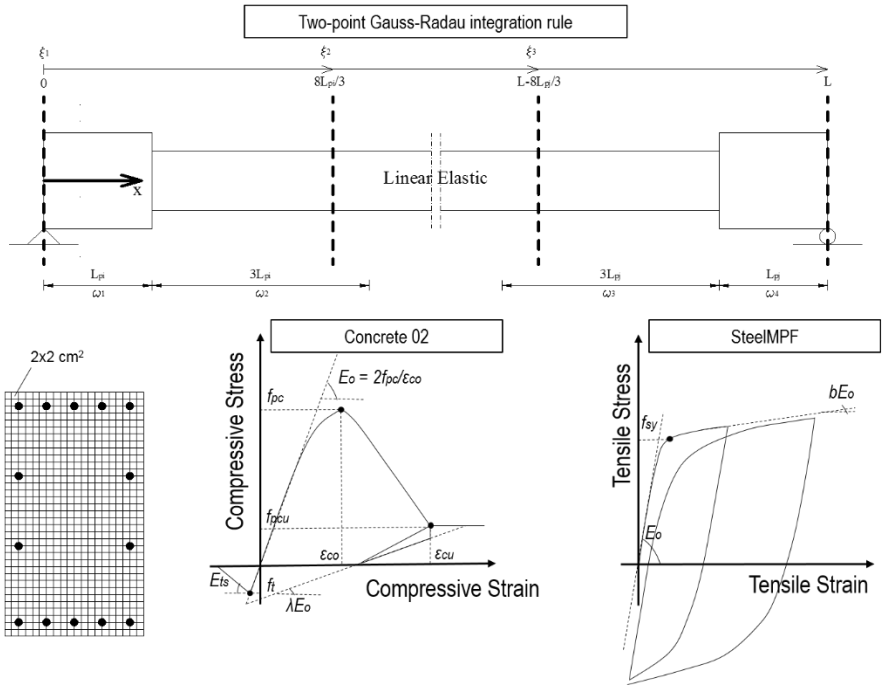

Fig. 5-4 Nonlinear beam-column model adopted in OpenSees for analysing the benchmark building through NTHA: the modified Two-point Gauss-Radau plastic hinge integration method (adapted from Scott and Fenves 2012), and discretisation of the member's cross section through fibre elements together with the implemented Concrete 02 (adapted from Yassin 1994) and SteelMPF material models (adapted from Kolozvari et al. 2015).

The numerical model in OpenSees is assembled in the Processing stage by means of the Matlab-generated TCL files described above. In the following the structure of the code for linear and nonlinear analyses that is depicted in Fig. 5-5 is described. For each of these analyses, a Matlab script launches OpenSees that, in turn, finds its analysis settings in specific TCL scripts (recorders, constraint handler, numberer, construction of the system of equations, algorithm type, integrator type, etc.) as described in the following:

- "RUN_GRAVITY_ANALYSIS.m", this script simply runs the gravity loads analysis through OpenSees that finds the analysis settings in "GRAVITY_ANALYSIS.tcl";
- "RUN_MODAL_ANALYSIS.m", this script runs the modal analysis through OpenSees and it extracts the modal matrix, mass matrix and stiffness matrix of the numerical model which are used subsequently for running the RSA. OpenSees finds the command for solving the eigenvalue problem in "MODAL_ANALYSIS.tcl" where the eigenvector output is organised to build up the modal matrix in accordance with the extracted mass and stiffness matrices. The mass matrix and stiffness matrix are obtained from a procedure defined in "UTIL.tcl";
- "RUN_RSA.m", this script includes a built-in procedure (explained in Section 5.2.1) for running the RSA since there are no specific commands in OpenSees for running this method

of analysis. This procedure is explained in Section 5.2.1 and it is based on the definition of a response-spectrum in terms of pseudo-acceleration and results of modal analysis. Subsequently, "CHECK_RSA.m" script runs the post-processing stage where results of the processing stage are elaborated;

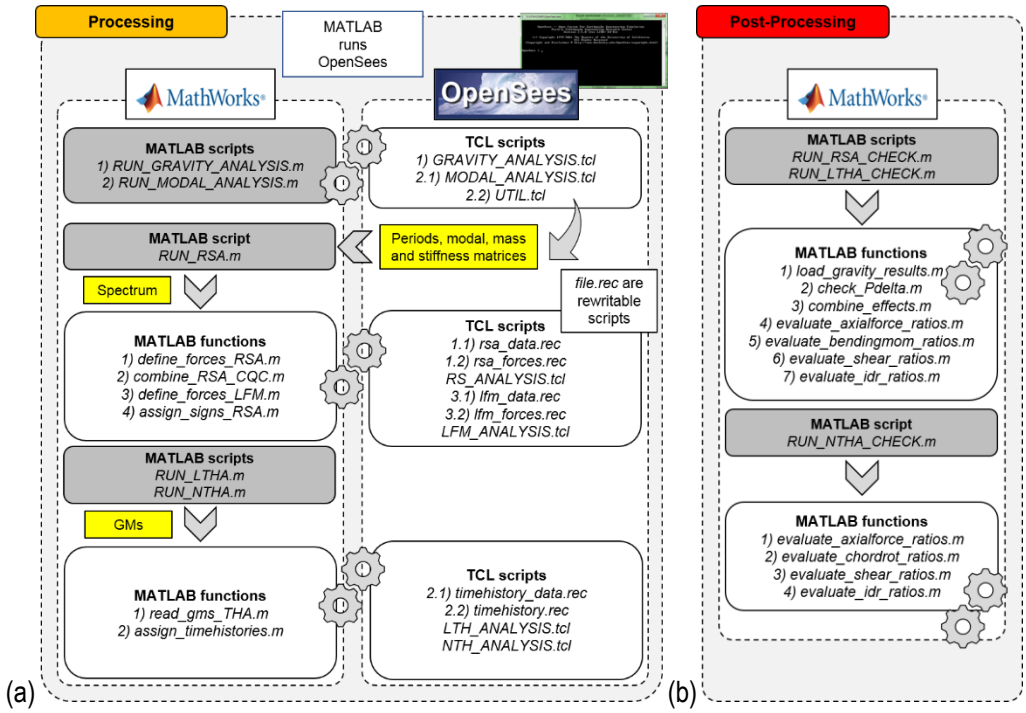

Fig. 5-5 Flowchart of the developed MATLAB/OpenSees code: (a) processing stage and (b) post-processing.

– "RUN_LTHA.m" and "RUN_NTHA.m", these scripts run respectively the LTHA and the NTHA through OpenSees which analysis settings are found in "LTH_ANALYSIS.tcl" and "NTH_ANALYSIS.tcl", respectively. The superposition of modal damping matrices for evaluating the damping forces is implemented in these files with a damping ratio set equal to 5% and 1% for LTHA and NTHA, respectively (Chopra 2012; De Luca et al. 2014). It is worth noting that no details are provided in the EC8 on the value of the damping ratio for NTHA. However, it is commonly assumed for NTHA a smaller value than 5% since most of the structural damping is assumed to be dissipated through nonlinear behaviour of the structural members. The sensitivity of results to different damping ratio values for NTHA is not investigated herein. These Matlab scripts include a built-in procedure for reading the GM name, the time-histories in terms of acceleration as well as the number and the value of the analysis time-steps for each GM. For LTHA, the evaluation of the behaviour factor for ultimate limit states is implemented according to Section 4.2.2 once the code spectrum is defined by users and results of the modal analysis are available. Subsequently, "CHECK_LTHA.m" script runs the post-processing stage where results of the processing stage are elaborated.

5.2.1. Linear analyses: processing stage

In this section, aspects of the Matlab/OpenSees code addressed to the gravity loads analysis, modal analysis, RSA and LTHA are described showing as example the benchmark building described in Section 3.3. For the linear static analyses, the same settings are adopted. For RSA, the way how the modal matrix [Φ] is built up from the modal analysis depends, for the sake of consistency, on the structure of the mass [M] and stiffness [K] matrices extracted from OpenSees. These matrices depend on the constraints (e.g., rigid diaphragm), the numberer and the constraint handler assumed for the analyses (Mazzoni et al. 2007). The numberer assigns Degrees-Of-Freedom (DOF) to the nodes of the numerical model based on a certain criterion chosen by the user. For example, the numberer "Plain", which is used herein, assumes as numbering criterion the way how nodes are stored in the domain. Herein, nodes (i.e., IDs) are defined from the smallest to the biggest where the biggest are represented by the master nodes at each storey (see Section 5.2). The constraint handler determines how the constraint equations are enforced in the analysis (Mazzoni et al. 2007). Herein the constraint handler "Transformation" is adopted, which transforms the stiffness matrix by condensing out the constrained DOFs (Mazzoni et al. 2007). The stiffness and mass matrices of the benchmark building have both size 1044 x 1044 being the number N of the active DOFs equal to 1044 (see Table 5-1). Indeed, the storey diaphragm constraints all the DOFs of the nodes belonging to the same storey to have in-plane behaviour mastered by the centre of mass of that storey (X-Y plane, being Z the vertical global axis) while the DOFs of the nodes belonging to the landing levels of the staircase preserves their freedom. Fig. 5-6 shows the structure of the stiffness matrix and an example of evaluating an element of the matrix at $i = j = 1010$; the order of the active DOFs starts with UZ of the node 25 (being the first 24 nodes at the ground level fixed) and it ends with RZ of the master node at the 12th storey (G_{12}). The stiffness and mass matrices are extracted from OpenSees in "UTIL.tcl" by means of "PrintA" command. The stiffness matrix is extracted from OpenSees by perfoming a one-step static analysis with linear algorithm and load control integrator. The mass matrix is extracted by performing a one-step transient analysis with time increment equal to unity, Newton algorithm and Central Difference integrator.

Table 5-1 Number of Degrees-Of-Freedom of the 12-storey benchmark building.

Node group	***N nodes***	***Boundary condition/ constraint***	***Active DOF***	***N Active DOFs***
Ground	24	Base fixity	-	-
Storeys	12 x 24 = 288	Rigid diaphragms	UZ, RX, RY	864
Staircase landing	2 x 12 = 24	-	UX, UY, UZ, RX, RY, RZ	144
Master	12	Out-of-plane fixity	UX, UY, RZ	36
			Total	1044

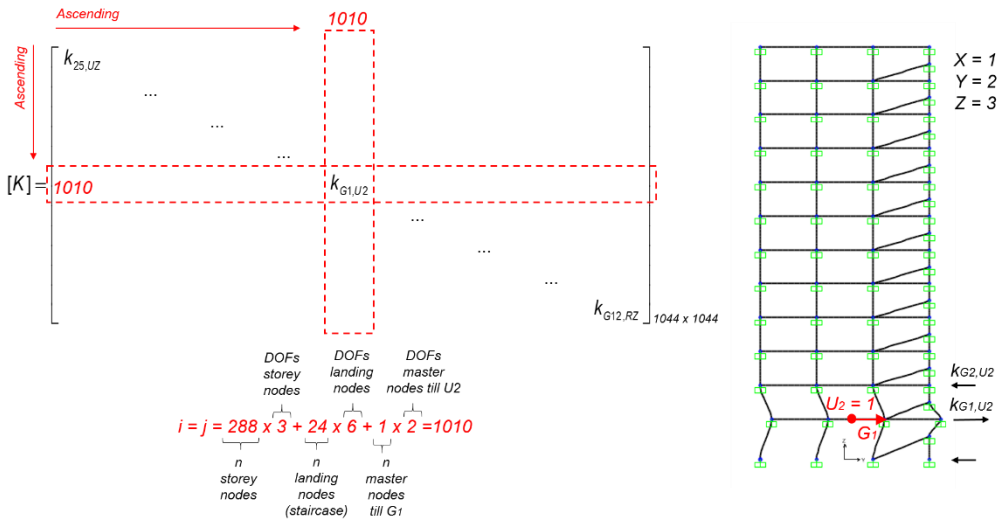

Fig. 5-6 Structure of the stiffness matrix [K]: evaluation of the element $k_{G1,U2}$ due to the activation of the translational DOF along direction Y (=2), U2, of the master node G1.

The modal matrix [Φ] is built-up in "MODAL_ANALYSIS.tcl" in such a way that its eigenvectors $\{\varphi_n\}$ are consistent with the DOFs of the mass and stiffness matrices for each mode of vibration *n* defined by the user. Therefore, its size is equal to the number of modes multiplied by *N* (i.e., *n* x 1044). RSA is implemented in OpenSees as described in Section 2.2.2.1. When the RSA is launched through the "RUN_RSA.m" script (see Fig. 5-5a), the code runs four consecutive functions which are:

– "define_forces_RSA.m", this function evaluates the nodal forces related to the responses along direction X and Y for each mode of vibration. Firstly, the distributions of the forces proportional to each period of vibration along both the directions $\{s_{n,k}\}$ are obtained as per Eq. 5.1 (Chopra 2012).

$$L_{n,k} = \{\varphi_n\}[M]\{\iota_k\} \qquad M_{n,k} = \{\varphi_n\}[M]\{\varphi_n\}^T \qquad k = X,Y$$
$$\Gamma_{n,k} = \frac{L_{n,k}}{M_{n,k}} \qquad \{s_{n,k}\} = \{\Gamma_{n,k}\}[M]\{\varphi_n\}^T \tag{5.1}$$

The eigenvectors obtained from "MODAL_ANALYSIS.tcl" are normalised with respect to the largest displacement along both X and Y directions and this is checked by ensuring that condition in Eq. 5.2 is verified (Chopra 2012).

$$[I] = [\Phi][M][\Phi]^T \tag{5.2}$$

Subsequently, the nodal forces related to the responses along direction X and Y for each mode of vibration $\{f_{n,k}\}$ are evaluated as per Eq. 5.3 where $S_a(T_n)$ denotes the spectral acceleration corresponding to the period of vibration T_n evaluated from the response spectrum defined by the user. Such nodal forces are assigned to the numerical model in the "rsa_forces.rec" script which is called in "RS_ANALYSIS.tcl" when the analysis is ran.

Another script called "rsa_data.rec" keeps record of which mode and direction is used during the processing stage;

$$\{f_{n,k}\} = \{s_{n,k}\} S_a(T_n) \qquad k = X,Y \qquad (5.3)$$

- "combine_RSA_CQC.m", this function is working when all the analyses have successfully finished and it reads the outputs of each modal analysis in terms of local forces, displacements, and reactions, and combined them according to the CQC rule;
- "define_forces_LFM.m", this function evaluates the lateral forces according to the LFM described in Section 2.2.1. Info related to the storey masses and total mass of the building are read from the "structure_details.xlsx" Excel worksheet. Such lateral forces are assigned to the numerical model in the "lfm_forces.rec" script which is called in "LFM_ANALYSIS.tcl" when the analysis is ran. Another script called "lfm_data.rec" keeps record of which direction is used during the processing stage;
- "assign_signs_RSA.m", this function reads the sign of the outputs of LFM analysis in terms of local forces, displacements, and reactions, and it assigns such sign to the corresponding values obtained after combining the modal analyses of RSA according to the CQC rule.

The LTHA is performed in OpenSees through the "RUN_LTHA.m" script (see Fig. 5-5a) where two functions are implemented:

- "read_gms_THA.m", this function reads the GM time-histories in terms of acceleration that the user wants to analyse under the numerical model. This function reads the GM name, the time-step, the number of steps, and the acceleration at each time-step. Herein GM are downloaded from the ESM database (ESM 2008) and the PEER-NGA Ground Motion database (PEER NGA 2014) where different file formats are employed. The format recognised in this code is simply a text file where columns refer to [time-step; acceleration]. The acceleration can be either expressed in m/s^2 and *g* but user needs to specify this in "LTH_ANALYSIS.tcl". A Matlab-based tool is herein developed which converts PEER format in a compatible way. This function is the same used for NTHA;
- "assign_timehistories.m", this function evaluates the behaviour factor for LTHA (q_{LTHA}) according to the procedure described in Section 4.2.2, and it applies the same to the GM time-histories. This function writes some files which are then used in "LTH_ANALYSIS.tcl", such as: (i) "timehistory_data.rec" where number of GMs, ID of the GM, time-step (*dt*), and number of steps (*npt*) are written, and (ii) "timehistory.rec" where the time-history acceleration of each horizontal GM component is written to be read by "LTH_ANALYSIS.tcl". Subsequently, the function runs OpenSees and it perform the analysis by applying each time-history (scaled by q_{LTHA}) along X and Y directions. This function is the same used for NTHA (without scaling by q_{LTHA} for NTHA) where both the

horizontal GM components are applied together with the gravity loads and then swapped along X and Y. The analysis time-step (*dt*) is assumed equal to the time-step of the GM time-histories and it can be reduced for NTHA, if needed, as explained in Section 5.2.3.

The described analyses are performed considering the analysis settings reported in Table 5-2. It is worth mentioning that the developed code utilises the same analysis settings of LFM for running the static analyses for each modal contribution needed to perform RSA, as described in Section 2.2.2.1.

Table 5-2 Analysis settings for linear analyses in OpenSees.

Setting	***LFM***	***LTHA***
Constraints	Transformation	Transformation
Numberer	Plain	Plain
System	FullGeneral	FullGeneral
Test	NormDispIncr	NormDispIncr
Test tolerance	1.0e-8	1.0e-8
Iterations	6	6
Algorithm	Linear	Linear
Integrator	LoadControl (λ = 0.1)	Newmark (γ = 0.50, β = 0.25)
Analysis	Static	Transient
Analyse (n increments)	10	npt
Analyse (time-steps)	-	dt

5.2.2. Linear analyses: post-processing stage

Results of RSA and LTHA are then elaborated in the post-processing stage through the "RUN_RSA_CHECK.m" and "RUN_LTHA_CHECK.m" scripts, respectively, in order to perform the verifications in terms of strength and deformability according to the selected limit state (i.e., ultimate or serviceability limit states). For LTHA, the procedure implemented in the code is described in Section 4.2. The structure of the code related to the post-processing is depicted in Fig. 5-5b and it is basically the same for RSA and LTHA with the difference that the post-processing of LTHA is analysed for each time-step. These scripts are constructed by the following functions:

- "load_gravity_results.m", this function reads the results of the gravity loads analysis in terms of local forces, displacements and reactions which are then used for combining these effects with those evaluated from RSA and LTHA;
- "check_Pdelta.m", this function reads the results of the RSA and the LTHA and it evaluates the interstorey drift sensitivity coefficient $\theta_{P\text{-}\Delta}$ according to the EC8-1, for ultimate limit states, for direction X and Y. For LTHA, this is done by implementing the rule in Eq. 4.3 which consists in identifying the time-step where the corresponding maximum (in absolute)

interstorey drift occur and evaluating the storey shear at the same time-step. Subsequently, the maximum amplification factor between the two main directions among the storeys is considered for amplifying the local forces when the seismic combinations are employed;

- "combine_effects.m", this function reads the results of the RSA and the LTHA and it combines their seismic effects with the gravity loads effects. For RSA, this is implemented by combining the 100:30 combination rule of the lateral forces effects along ±X and ±Y and by neglecting the accidental eccentricity. For LTHA, this is implemented by combining the 100% of the GMs effects along ±X and ±Y for each time-step. For ultimate limit states, the effects in terms of forces are amplified by the P-Delta amplification factor while displacements are amplified by the behaviour factor;
- "evaluate_axialforce_ratios.m", this function reads the properties of the elements in the "structure_details.xlsx" Excel worksheet (i.e., geometry, steel reinforcement and material properties) and it evaluates the axial capacity in tension and compression of such elements. Subsequently, this function evaluates the DCR in terms of axial behaviour for each time-step (for LTHA) and combination, as per Eq. 5.4, in the case of RC elements, where $N_{E,t}$ and $N_{E,c}$ respectively denotes the demand tensile and compressive axial force while $N_{Rd,t}$ and $N_{Rd,c}$ the corresponding capacities evaluated from the design values of the concrete strength f_{cd}, the steel yield strength f_{syd}, the normalised axial force limit v (equal to 0.55 and 0.65 for DCH and DCM, respectively), the concrete area of the cross-section A_c, and the total steel area of the longitudinal reinforcement $A_{s,tot}$;

$$\begin{aligned} DCR_t(t) &= N_{E,t}(t) / N_{Rd,t} \qquad & N_{Rd,t} &= f_{syd} A_{s,tot} \\ DCR_c(t) &= N_{E,c}(t) / N_{Rd,c} \qquad & N_{Rd,c} &= \nu f_{cd} A_c \end{aligned} \tag{5.4}$$

- "evaluate_bendingmom_ratios.m", this function reads the properties of the elements in the "structure_details.xlsx" Excel worksheet (i.e., geometry, steel reinforcement and material properties) and it evaluates the flexural capacity of such elements through fiber-based section analysis implemented in a uniaxial monotonic moment-curvature routine used for the purpose (see Fig. 5-7). The concrete cross-section of the element is discretised in a sufficient number of longitudinal fibres, having the Mander monotonic stress-strain relation (Mander et al. 1988). Confined concrete behaviour is assigned to the fibres within the area defined by the transversal steel reinforcement. Fibres, having the Menegotto-Pinto monotonic stress-strain relation (Menegotto and Pinto 1972), account for the longitudinal steel reinforcement, including side bars. Concrete and steel strengths refer to the corresponding design values. For confined concrete, the design strength is evaluated according to EC8-3 specifications. The axial force acting on the cross-section is accounted for in the flexural capacity evaluation. For the columns, the rigorous approach of accounting for the biaxial bending moment capacity model, as indicated in EC2, is not considered

herein. However, the simplified approach consisting in reducing by 30% the uniaxial bending moment capacities, as indicated in EC8-1, is implemented. This function evaluates the DCR in terms of flexural behaviour for each time-step (for LTHA) and combination as per Eq. 5.5. If the DCR in terms of axial behaviour is greater than unity, the corresponding DCR value is saved for the outputs;

$$\begin{aligned}
&DCR(t) = \frac{M_E(t)}{M_{Rd}(N_E(t))} && if \quad N_E(t) < N_{Rd}(t) && \\
& && && \text{beams} \\
&DCR(t) = \frac{N_E(t)}{N_{Rd}} && if \quad N_E(t) \geq N_{Rd}(t) && \\
&DCR(t) = \max\left[\frac{M_{E,y}(t)}{0.7M_{Rd,y}(N_{Ed}(t))}, \frac{M_{E,z}(t)}{0.7M_{Rd,z}(N_E(t))}\right] && if \quad N_E(t) < N_{Rd}(t) && \\
& && && \text{columns} \\
&DCR(t) = \frac{N_E(t)}{N_{Rd}} && if \quad N_E(t) \geq N_{Rd}(t) &&
\end{aligned} \tag{5.5}$$

- “evaluate_shear_ratios.m”, this function reads the properties of the elements in the “structure_details.xlsx” Excel worksheet (i.e., geometry, steel reinforcement and material properties) and it evaluates the shear capacity of RC elements according to the truss capacity model described in EC2. The evaluation of the shear demand is performed according to the capacity design by calculating the plastic shears from the flexural capacities at the ends of the elements, considering the contribution of the axial forces that maximise the plastic shears and minimise the shear capacities. For LTHA, the evaluation of the capacities is performed considering the average axial forces of a suite of GMs that minimise the shear capacities;
- “evaluate_idr_ratios.m”, this function evaluates the DCR in terms of IDR for each time-step (for LTHA) and combination, assuming 0.5% as capacity values for DL-LS (CEN 2004a) and 2% as capacity values for LS-LS (ATC 1996; FEMA 1997; FEMA 2000). The limit of transient IDR equal to 2% is indicated for concrete frames buildings at Life-Safety Building Performance Level (see Table 2-1) which combines structural and non-structural Life-safety levels described in FEMA 273 (FEMA 1997) and ATC-40 (ATC 1996). FEMA-356 (FEMA 2000) However, the user can modify the IDR limits anytime accordingly to the desired Building Performance Levels.

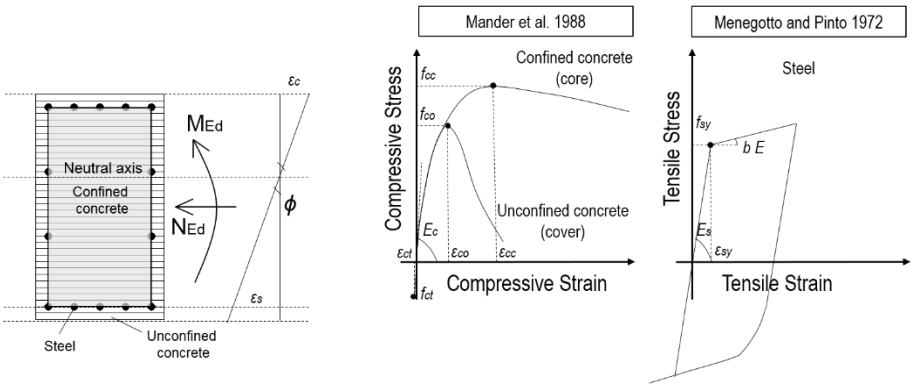

Fig. 5-7 Fibre-based section analysis of a RC element with unconfined and confined concrete modelled with Mander et al. 1988.

5.2.3. Nonlinear Modelling: processing stage

In this section, aspects of the Matlab/OpenSees code addressed to the NTHA are described showing as example the benchmark building described in Section 3.3. The NTHA is performed in OpenSees through the "RUN_NTHA.m" script (see Fig. 5 4a) which runs the same functions described in Section 5.2.1 for LTHA. The only difference consists in applying simultaneously the GM time-history components 1 and 2 which are written in two files named "timehistory1.rec" and "timehistory2.rec". These files are subsequently read by "NTH_ANALYSIS.tcl" in which the seismic combinations are performed. The numerical model of the building is firstly analysed under the gravity loads using a load-controlled static analysis with 10 steps. Then "loadConst" command in OpenSees is used to reset the time to zero so that the time-history starts from time-step equal to zero. In this script, the damping forces are evaluated according to the superposition of modal matrices (with damping ratios set equal to 1%) through the "modalDamping" command in OpenSees. P-delta effects are accounted for in the analysis through the geometric transformation command in OpenSees.

NTHA is performed considering various settings that are changed on the basis of the numerical convergence (see Table 5-3). In particular, the code starts by applying Krylov-Newton and by varying the time-step increment and/or tolerance if numerical issues occur, and subsequently the code changes the algorithm if Krylov-Newton does not find a solution. This procedure is implemented in "NTH_ANALYSIS.tcl" by means of additional scripts called "TransientConverge.tcl" and "SolutionAlgorithm.tcl".

Table 5-3 Analysis settings for NTHA in OpenSees.

Setting	***NTHA basic settings***	***NTHA iterative settings***
Constraints	Transformation	-
Numberer	Plain	-
System	FullGeneral	-
Test	NormDispIncr	-
Test tolerance	10^{-8}	$Tol_1 = 10^{-7}$, $Tol_2 = 10^{-6}$, $Tol_3 = 10^{-5}$, $Tol_4 = 10^{-4}$
Iterations	500	-
Algorithm	KrylovNewton	Alg_1 = NewtonLineSearch (Initial Interpoled, Tol. = 0.6), Alg_2 = … (Secant, Tol. 0.8), Alg_3 = … (Secant, Tol. 0.2), Alg_4 = Newton (Initial), Alg_5 = ModifiedNewton (initial), Alg_6 = Broyden
Integrator	Newmark (γ = 0.50, β = 0.25)	-
Analysis	Transient	-
Analyse (n increments)	npt	-
Analyse (time-steps)	dt ($dt_{Min} = dt/10^6$, $dt_{Max} = dt$)	$dt_1 = dt/10$, $dt_2 = dt/10^2$, $dt_3 = dt/10^3$, $dt_4 = dt/10^4$, $dt_5 = dt/10^5$

It is worth mentioning that for the benchmark building considered in this work and the GMs suites analysed in Chapter 6 and Chapter 7, NTHA did not encounter serious convergence issues (e.g., no collapse cases or instability are found). Some of the analysis settings in Table 5-3 were not necessary, such as the maximum number of iterations is considerably large (i.e., 500) as well as the iterative test tolerance values (10^{-6} to 10^{-4}) and time-step reduction ($dt/10^2$ to $dt/10^5$).

In addition to element local forces, global displacements and reactions, chord rotations are provided by the nonlinear analysis through the "recorder Element chordRotation" command in OpenSees. Fig. 5-8 shows the evaluation of the chord rotation θ of a beam and a column at one end, defined as the angle between the chord connecting the element end to the point of contraflexure (where the bending moment is zero) and the tangent to the element longitudinal axis at that end (e.g., Mpampatsikos et al. 2008). If the node rotates of $+\theta_1$ and the chord connecting the end to the zero-moment point (identified by the shear span L_V) rotates of $+\theta_2$, the chord rotation is evaluated as $\theta_2 - \theta_1$.

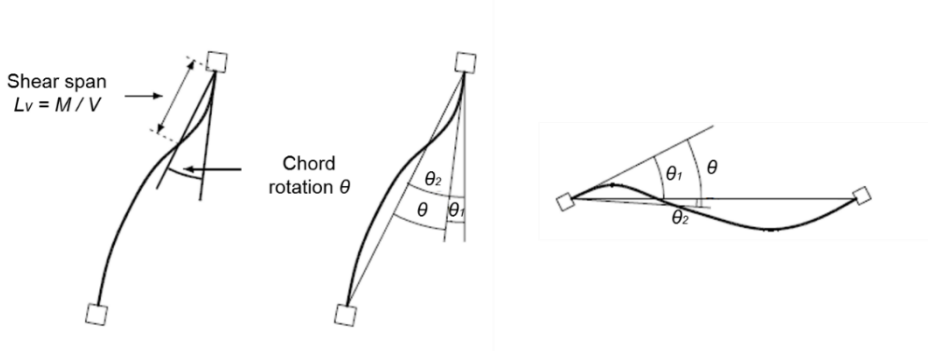

Fig. 5-8 Definition of beam and column chord rotations at one end (source Mpampatsikos et al. 2008).

5.2.4. Nonlinear analyses: post-processing stage

Results of NTHA are then elaborated in the post-processing stage through the "RUN_NTHA_CHECK.m" script, in order to perform the verifications in terms of strength and deformability according to the failure mechanism (i.e., shear or flexure). The structure of the code related to the post-processing is depicted in Fig. 5-5b and it is similar to LTHA with the difference that the post-processing of NTHA is based on the evaluation of DCR according to EC8-3. The different functions are:

– "evaluate_chordrot_ratios.m", this function reads the properties of the elements in the "structure_details.xlsx" Excel worksheet (i.e., geometry, steel reinforcement and material properties) and it evaluates the flexural capacity of RC elements in terms of chord rotation at the yielding θ_y and ultimate θ_u stages (Biskinis and Fardis 2010a; Biskinis and Fardis 2010b). Concrete and steel strengths refer to the corresponding mean values. For concrete, the mean compressive strength f_{cm} is obtained according to the EC2. For steel, the mean yielding strength f_{sym} is evaluated as 1.15 f_{syk} (Fardis 2009). The chord rotation at yielding stage is shown by Eq. 5.6, where the evaluation of the yielding curvature φ_y is carried out in a simplified way by implementing the formulation suggested by Biskinis and Fardis (2010a), i.e. 1.75 f_{sym} / (E_s h) where E_s and h are the Young's modulus of steel (i.e., 200000 MPa) and the cross-section depth, respectively.

$$\theta_y = \varphi_y \frac{L_V}{3} + 0.0013\left(1+1.5\frac{h}{L_V}\right) + 0.13\varphi_y \frac{d_{bl} f_{sym,bl}}{\sqrt{f_{cm}}} \tag{5.6}$$

Other parameters in Eq. 5.6 are L_v which denotes the shear span (assumed equal to half length of the element) and d_{bl} which denotes the diameter of the longitudinal reinforcement. For ultimate limit states, the chord rotation capacity is evaluated as per Eq. 5.7 where γ_{el} is assumed equal to 1.5 for primary element, v is the adimensional axial load, ω and ω' are the mechanical reinforcement ratios of the tension (including the web reinforcement) and compression longitudinal reinforcement, respectively, ρ_{st} is the ratio of the transverse steel parallel to the direction of loading, ρ_{bd} is the steel ratio of diagonal reinforcement in each

diagonal direction (assumed to be zero), and α is the confinement effectiveness factor. These values are evaluated according to the EC8-3.

$$\theta_u = \frac{1}{\gamma_{el}} 0.016 \cdot 0.3^{\nu} \left[\frac{\max(0.01;\omega')}{\max(0.01;\omega)} f_{cm} \right]^{0.225} \left(\frac{L_V}{h} \right)^{0.35} 25^{\left(\alpha \rho_{st} \frac{f_{sym,bt}}{f_{cm}} \right)} 1.25^{100\rho_{bd}} \tag{5.7}$$

For Life-Safety Limit State (LS-LS) the chord rotation capacity is imposed to be equal to 0.75 of the ultimate chord rotation value. Biaxial behaviour of the columns is accounted in the verification multiplying the uniaxial chord rotation capacity by 0.7 as indicated in the EC8-1 for verifications in terms of bending moment. Herein, this assumption is made so that there is direct correspondence with the linear-elastic procedure described in the previous section. The biaxial capacity model is not herein investigated but some researchers proposed methods validated on experimental tests (e.g., Bousias et al. 2002). Subsequently, this function evaluates the DCR in terms of chord rotation for each time-step and combination;

$$DCR_u(t) = \frac{\theta_E(t)}{3/4\theta_u(t)}; \qquad DCR_y(t) = \frac{\theta_E(t)}{\theta_y(t)} \qquad \text{beams}$$

$$DCR_u(t) = \max\left(\frac{\theta_{E,x}(t)}{0.7\theta_{u,x}(t)}, \frac{\theta_{E,y}(t)}{0.7\theta_{u,y}(t)} \right); \; DCR_y(t) = \max\left(\frac{\theta_{E,x}(t)}{0.7\theta_{y,x}(t)}, \frac{\theta_{E,y}(t)}{0.7\theta_{y,y}(t)} \right) \qquad \text{columns} \tag{5.8}$$

– "evaluate_shear_ratios.m", this function reads the properties of the elements in the "structure_details.xlsx" Excel worksheet (i.e., geometry, steel reinforcement and material properties) and it evaluates the shear capacity of RC elements according to EC8-3.

5.3.Verification of the OpenSees modelling framework

The modelling framework described in the previous section is herein verified to proof its adequacy for analysing the benchmark building considered in this research work. This verification is carried out for both the linear and the nonlinear modelling procedures presented in Section 5.2. For the linear modelling procedure, the benchmark building is modelled in SAP2000 (Computer and Structures, Inc. 1976), a commercial software package typically used for professional applications but that has been used in the research field in the past. Compared to MIDAS Gen (SINCE 1989), SAP2000 allows obtaining the stiffness and mass matrices that have been discussed in Section 5.2.1. The linear modelling procedure is verified considering the modal analysis, the gravity loads analysis, the RSA, and the LTHA in both OpenSees and SAP2000. In contrast, the nonlinear modelling procedure is verified considering an RC column which was experimentally tested in the past under quasi-static lateral loading. Moreover, the nonlinear modelling procedure for NTHA and pushover analysis are compared in the following for a simple 3D application. The comparison between nonlinear modelling approaches in OpenSees and commercial software packages is not herein investigated. For the purposes of this research work, the goal is to show that the nonlinear modelling procedure used herein is capable of predicting the response of RC-MRF buildings accurately.

5.3.1. Linear modelling framework verification

The numerical model is built-up in SAP2000 according to Section 4.2.1, considering flexural stiffness of the elements reduced by 50%. Fig. 5-9 shows the results of the modal analysis for the first six modes of vibration. The results of the modal analysis performed in OpenSees are reported in Table 4-1, and they result in perfect agreement until to the 5th decimal digit, confirming that mass and stiffness matrixes are assembled in the same way as SAP2000.

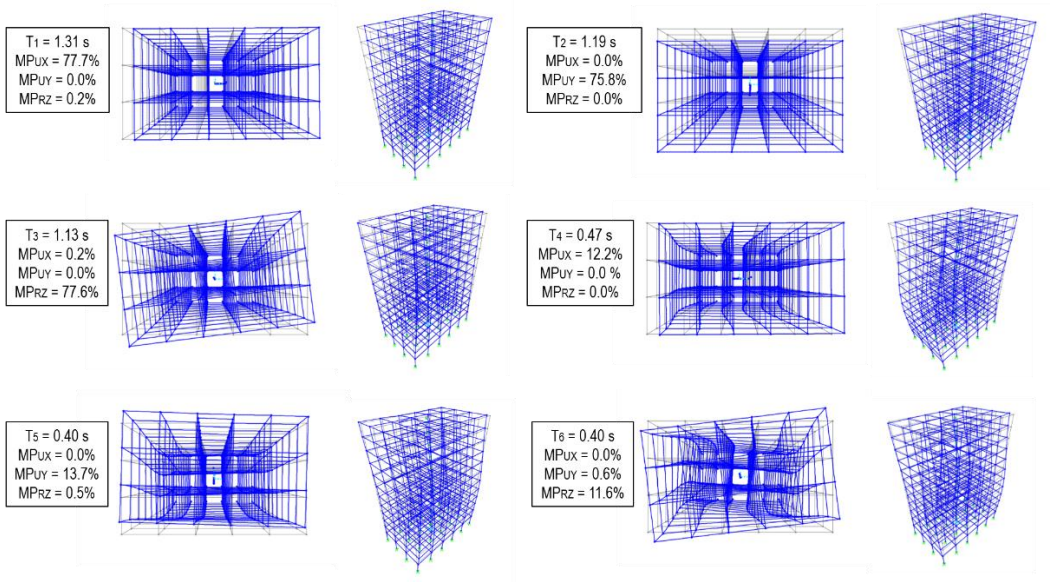

Fig. 5-9 Modal analysis results of the benchmark building modelled in SAP2000.

In the following, the OpenSees modelling framework is verified with regard to the gravity loads analysis in order to show the accuracy related to the assignment of the beam elements. The results comparison between OpenSees and SAP2000 is shown in terms of storey vertical forces in Fig. 5-10a. These storey vertical forces represent the vertical resultant force given by the horizontal cutting-line at the bottom of the columns at each storey. In this evaluation, the contribution of the inclined beams (i.e., flight beams) is also considered by evaluating the vertical components of both the axial force and the shear force of these beams at each storey. Fig. 5-10b shows the comparison in terms of storey shear between RSA results of OpenSees and SAP2000. The accuracy of the implemented RSA procedure in the code allows to confirm its validity. Finally, the linear modelling framework is verified for LTHA considering the M6.9 1979 Montenegro earthquake. GM horizontal components are applied along +X and +Y directions together with gravity loads from the seismic combination (i.e., G_k + 0.3 Q_k). LTHA is performed considering Rayleigh damping method because SAP2000 does not allow to set superposition of damping matrices. This verification is carried out to check that the linear combination is correctly implemented in the code developed herein. For Rayleigh damping method, the mass and stiffness proportional constants (see Section 4.2.4) are equal to α_M = 0.2571 rad/s and β_K = 0.0097 s/rad, respectively, when the damping ratios of the 1st and 3rd mode of vibration are each set to 5%. A total of 4823 time-steps having time interval of 0.01

s and Newmark integration method with parameters γ = 0.50 and β = 0.25 are assumed for the analysis in SAP2000 as per OpenSees. Fig. 5-11 shows the results in terms of base shear along X and Y which allows to observe the perfect matching of results.

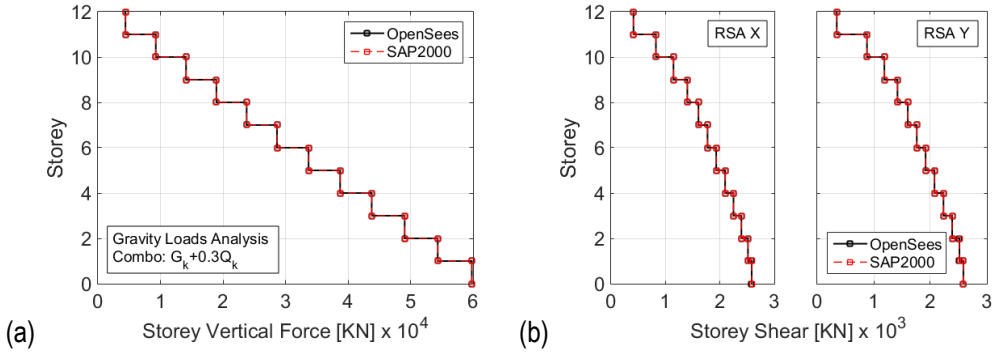

Fig. 5-10 Verification of the OpenSees framework for (a) gravity loads analysis and (b) RSA along direction X and Y.

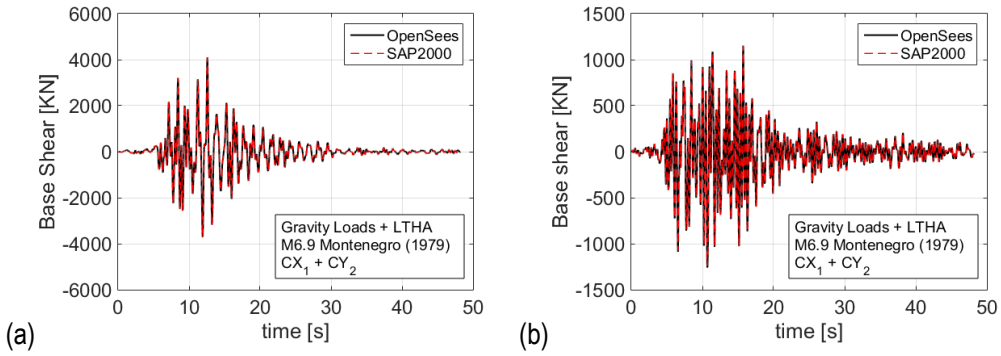

Fig. 5-11 Verification of the OpenSees framework for LTHA: (a) direction X and (b) direction Y.

5.3.2. Nonlinear modelling framework verification

The nonlinear modelling procedure adopted herein, based on force-based elements with fibre-section hinges as described in Section 5.2, accounts for several aspects that were investigated by researchers in the past and that led to developing nonlinear model for accounting of inelastic behaviour. Distributed plasticity models are well-known to overcome some critical modelling aspects related to concentrated plasticity models, such as: (i) evaluating locations and moment-rotation relations to assign to members in the pre-processing stage, (ii) adopting sophisticated and approximate methods to account directly for the interaction of axial force with biaxial bending moment, and (iii) the elastic stiffness adjustment of members (Deierlein et al. 2010; Haselton et al. 2017c). From the physical point of view, distributed plasticity models can directly capture (i) the hardening or softening of materials, (ii) the effect of transverse confinement, (iii) the effects of crack opening (i.e., neutral axis shift), (iii) the axial force influence on the stiffness, strength and ductility, and (iv) the spread of plasticity along the member length (Haselton et al. 2017c). Moreover, the force-based flexibility method, which formulation problem is governed by equilibrium conditions without restrictions to the displacement-field, allows to simulate accurately the nonlinear response of MDOF

systems considering a single beam-column element per structural member, contrarily to the displacement-based stiffness method (Fragiadakis and Papadrakakis 2008; Calabrese et al. 2010). In this way, the number of DOFs, and therefore the stiffness matrix, remains the same as concentrated plasticity models (Haselton et al. 2017c). It is certainly more convenient than the displacement-based where more beam-column elements are generally needed per structural member in order to accurately evaluate the nonlinear curvature by means of linear segments (Fragiadakis and Papadrakakis 2008; Calabrese et al. 2010). OpenSees allows using different numerical integration options such as Gauss-Lobatto, Gauss-Legendre, Radau, Newton-Cotes, among many (Scott and Fenves 2012). The modified two-point Gauss-Radau integration rule for force-based flexibility elements with specified plastic hinge lengths, which is implemented herein, allows an accurate evaluation of the softening behaviour due to the localisation of deformations in the element (Fig. 5-4, Scott and Fenves 2006). This is achieved by considering a characteristic length for softening plastic hinges equal to the user-defined plastic hinge length which is not directly assumed by other integration rules (Scott and Fenves 2006). However, a proper calibration of the plastic hinge length and moment-curvature hardening is generally required (Scott and Ryan 2013; Ribeiro et al. 2015; Ribeiro et al. 2017).

5.3.2.1. Case study 1: Analysis of an RC column

In order to show the accuracy of the nonlinear modelling procedure in OpenSees adopted in this research work for RC members, the experimental results of the specimen N7 tested by Tanaka and Park (1990) are considered. Experiment data are available in the PEER database developed by Berry et al. (2004). This database reports geometry, material properties, reinforcement details, failure mode, test configuration (including P-Delta configuration), axial load, lateral force-displacement history, and other relevant information for many RC column tests carried out in literature. The specimen N7 tested by Tanaka and Park is a cantilever rectangular RC column with rigid base and constant axial load equal to 2913 KN (normalised axial force = 0.30) applied at the top of the column (see Fig. 5-12). The test configuration was designed so that no modification of the results needed to be accounted because of the axial load components during the test (i.e., P-Delta). The reinforcement details were designed so that the failure mode can be classified as flexure-critical. Indeed, the nonlinear modelling procedure described in Section 5.2 is not meant to simulate the nonlinear behaviour of structural members characterised by the shear-critical failure mode. Therefore, this aspect allows to compare the numerical and experimental results. Table 5-4 reports the evaluation of other properties needed to characterise the material models used in the following. It is worth noting that these properties are evaluated according to formula indicated by the Eurocodes because this section is meant to validate the nonlinear modelling procedure used for the assessment of the benchmark building considered in this research work. The differences between formula adopted by the American standards and the Eurocodes is not herein investigated.

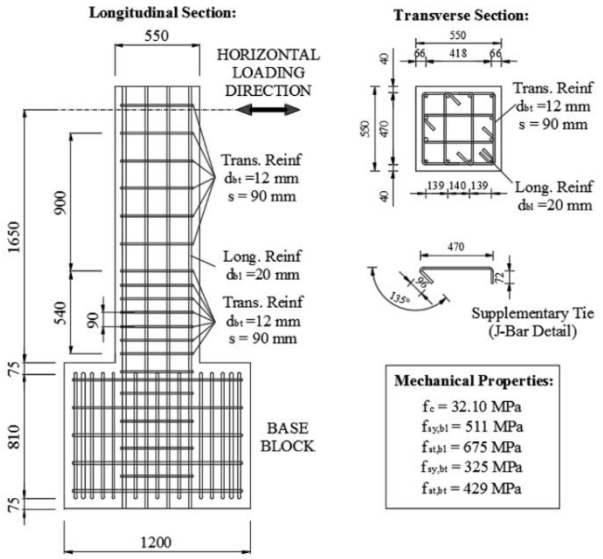

Fig. 5-12 Geometrical, material and reinforcement details of specimen N7 tested by Tanaka and Park (1990).

Table 5-4 Evaluation of other properties referred to the specimen N7 tested by Tanaka and Park (1990).

Parameter	***Formulae***	***Reference***	***Value***
Concrete Young's modulus	$E_c = 22000\left(f_{cm}/10\right)^{0.3}$	EC2	31216 MPa
Concrete nominal compressive strength	$f_{ck} = f_{cm} - 8$	EC2	24.10 MPa
Concrete mean tensile strength	$f_{ctm} = 0.3 f_{ck}^{2/3}$	EC2	2.53 MPa
Transversal steel volumetric ratio	$\rho_w = 2\min\left(\rho_{wz}, \rho_{wy}\right)$	Fardis 2009	0.023
Confinement effectiveness factor	$\alpha = \alpha_h \alpha_v$ $\alpha_h = (1-0.5s/b_o)(1-0.5s/h_o)$ $\alpha_v = \left[1-\sum b_i^2/(6b_o h_o)\right]$	EC8-3	0.624
Transversal steel Mechanical volumetric ratio	$\omega_w = \rho_w f_{symw}/f_{cm}$	Fardis 2009	0.237
Confined concrete Mean compressive strength	$f_{ccm} = f_{cm}\left[1+3.7\left(\alpha 0.5\omega_w\right)^{0.86}\right]$	EC8-3 (Fardis 2009)	44.72 MPa

In the following, different constitutive relations for concrete (confined and unconfined) are implemented, here referred as Case 1, Case 2 and Case 3, in order to show which one allows to simulate the behaviour of the RC column more accurately. Steel reinforcement behaviour is modelled through "SteelMPF" (Kolozvari et al. 2015) which implements an enhanced version of the Menegotto-Pinto extended by Filippou et al. (1983) to include isotropic strain hardening effects. Compared to "Steel02" which uses the model developed by Filippou et al. (1983), "SteelMPF" allows the definition of different yield stress values and strain hardening ratios for tension and compression, and it

considers degradation of cyclic curvature parameter for strain reversals in both pre- and post- yielding regions (Kolozvari et al. 2015). A strain hardening ratio for tension and compression equal to 0.01 and the default parameters values to describe the curvature of the cyclic behaviour, i.e. R_0, c_{R1}, c_{R2}, a_1, a_2, a_3, and a_4 (equal to 20, 0.925, 0.15, 0.0, 1.0, 0.0, and 1.0, respectively), are assumed. The Young's modulus of steel is assumed equal to 200000 MPa (CEN 2004b). The fibre-section is then assembled by combining elastic shear and torsional behaviour through "section Aggregator" command in OpenSees. Fibres of 1x1 cm^2 are considered for this example. The torsional stiffness is evaluated considering the torsional constant for rectangular cross-sections according to Young and Budynas (2002). Finally, the column is modelled through "element forceBeamColumn" command with "HingeRadau" plastic hinge at the fixed end. The plastic hinge length is assumed equal to 0.50 m as observed from the experimental test (see Tanaka and Park 1990). P-Delta effects are accounted for through the geometric transformation. The cyclic lateral load is applied according to the loading protocol adopted for the experimental test. The analysis is performed as static-cyclic analysis with varying algorithm depending on the occurrence of convergence issues (see Table 5-3) and displacement control at the level of application of the cyclic lateral force (i.e., 1.65 m). In addition, the self-weight of the column is added at the top (=14 KN).

The effects of using the different concrete models are shown in Fig. 5-13, where the following cases are analysed: (i) Case 1 which implements the "Concrete01 based on the Kent-Scott-Park model (Scott 1980) with degraded linear unloading/reloading stiffness according to Karsan and Jirsa (1969) and no tensile strength; (ii) Case 2 which implements the "Concrete02", similar to the previous one but with tensile strength and improvements in the unloading/reloading stiffness (Yassin 1994), and (iii) Case 3 which implements the "Concrete07" based on the Chang-Mander model (Chang and Mander 1994). Concrete01 and Concrete02 do not allow to set the initial stiffness of concrete equal to the Young's modulus evaluated in Table 5-4 but this is imposed through the compressive strain corresponding to the peak stress as reported in Table 5-5. In contrast, Concrete07 allows to set a value for the initial stiffness but, for the sake of consistency with the previous models, the same criterion is adopted herein. Case 1 and Case 2 allows to perform the analysis with displacement increment of 0.001 m without any numerical issue while Concrete07 required a smaller displacement increment, equal to 0.0001 m, to make the analysis achieve the convergence. This is due to the unloading/reloading paths used by Concrete07 that show higher nonlinear trends compared to Concrete01 and Concrete02. Moreover, Concrete07 uses a factor to control the steepness rate for the softening behaviour denoted by r (Tsai 1988) always larger than unity and that should be properly calibrated (see Table 5-5). For values of r larger than unity, the softening behaviour results to be steeper (see Fig. 5-13b-c). For Concrete01 and Concrete02, the softening behaviour can be controlled by defining the post-peak residual point (see Table 5-5) that if set different from zero is beneficial for the analysis convergence since it provides a stable solutions when concrete shows

high deformations. Results in Fig. 5-13a show that Case 3 would need a better calibration of the softening behaviour compared to Case 1 and Case 2. The difference between Case 1 and Case 2 does not appear relevant in this example. However, it can be relevant for RC beams where the compressive axial force is null in buildings and neglecting tensile strength can lead to the shift of the neutral axis due to the presence of cracks already for vertical loads in serviceability conditions.

Table 5-5 Concrete stress-strain relations implemented for simulating the response of specimen N7 tested by Tanaka and Park (1990).

Case	Type	Concrete model	Compressive peak strain	Compressive post-peak behaviour	Tensile post-peak behaviour
1	Concrete01	Unconfined	$\varepsilon_{co} = 2f_{co} / E_c$	$f_{cu} = 0.2f_{co}$, $\varepsilon_{cu} = 0.015$	$E_{ts} = f_{ct} / 0.002$ *
		Confined	$\varepsilon_{cc} = 2f_{cc} / E_c$	$f_{cu} = 0.8f_{cc}$, $\varepsilon_{cu} = 0.03$	$E_{ts} = f_{ct} / 0.002$ *
2	Concrete02	Unconfined	$\varepsilon_{co} = 2f_{co} / E_c$	$f_{cu} = 0.2f_{co}$, $\varepsilon_{cu} = 0.015$	$E_{ts} = f_{ct} / 0.002$ *
		Confined	$\varepsilon_{cc} = 2f_{cc} / E_c$	$f_{cu} = 0.8f_{cc}$, $\varepsilon_{cu} = 0.03$	$E_{ts} = f_{ct} / 0.002$ *
3	Concrete07	Unconfined	$\varepsilon_{co} = 2f_{co} / E_c$	$r = 2$	
		Confined	$\varepsilon_{cc} = 2f_{cc} / E_c$	$r = 1.1$	

**E_{ts} represents the inclination of the tensile post-peak softening as shown in Fig. 5-4 and that value is typically adopted in literature for controlling numerical instability.*

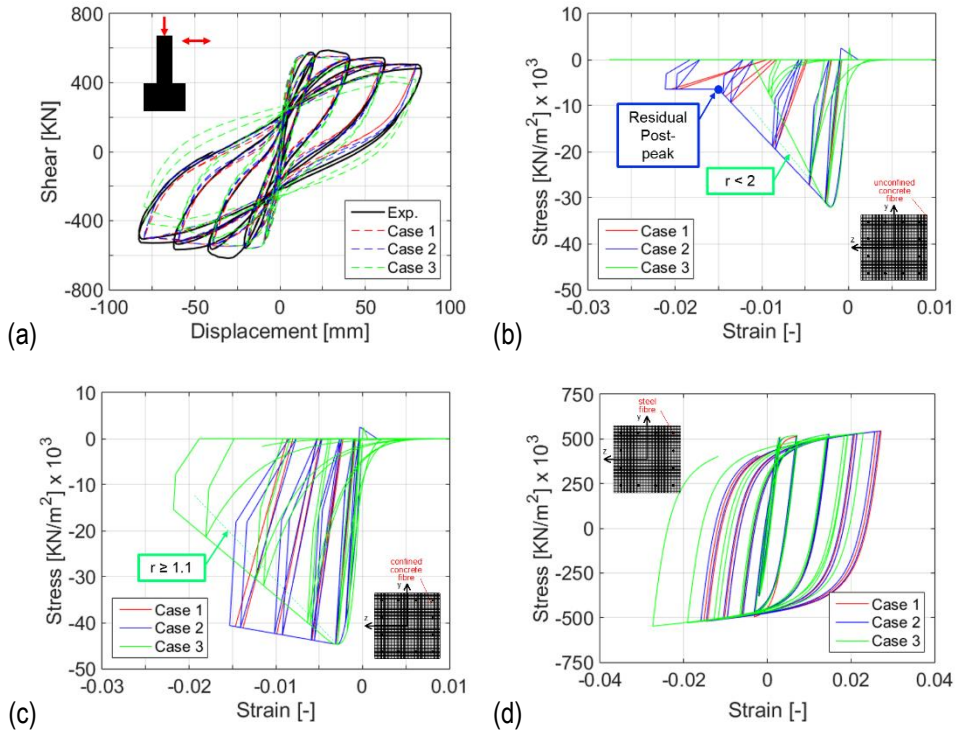

Fig. 5-13 Prediction of the cyclic response of the specimen N7 tested by Tanaka and Park (1990) for Case 1 (concrete01), Case 2 (concrete02), and Case 3 (concrete07): (a) shear versus displacement response, (b) unconfined concrete response of a fibre in the cover region, (c) confined concrete response of a fibre in the core region, and (d) steel response of a fibre-bar in the corner.

This example shows that Case 2 represents a convenient model since it does not lead to convergence issues due to significant nonlinearities in the unloading/reloading paths, it is easy to calibrate compared to other models, and it results to be efficient in simulating the nonlinear response of RC elements with flexural-type failure such that of the considered column. The goodness of the prediction capability can be observed in terms of stiffness, strength, and hysteretic loops. The investigation of other modelling procedures does not fall within the purposes of this research work, therefore this model is considered accurate enough for analysing the benchmark building through NTHA.

It is worth mentioning that even if fibre-based modelling can provide measure of the curvature, the latter loses its physical meaning when the behaviour of the RC cross-section goes beyond the cracking stage due to cover spalling, bar buckling, concrete crushing, etc. (Fardis 2009). For this reason, the chord rotation is a better measure for acceptance criteria of RC members. For increasing values of the lateral force, the chord rotation of a cantilever column is evaluated as ratio between the top drift Δ and the column length L which coincides with the shear span L_V (i.e., $\theta = \Delta / L$). The RC cross-section at the bottom of the column, where the maximum bending moment occurs, initially behaves linearly-elastic, with slope M / φ (where φ denotes the curvature in that section) which represents the elastic flexural stiffness $E_c I_t$ of the uncracked section where I_t is the second moment of area of the transformed cross-section (i.e., which considers the contribution of stiffness of the steel bar areas as well). The bending moment is evaluated as $\int \sigma_x y \, dA$ where σ_x is the normal stress of the generic fibre, y represents the distance of that fibre from the centroid of the cross-section, and dA the area of the fibre. The normal stress is related to the axial strain ε_x by means of the σ-ε constitutive relation of the material, σ_s-ε_s for steel and σ_c-ε_c for concrete. Because of the plane-section assumption of fibre-based models, the axial strain ε_x to the distance y^* from the neutral axis is related to the curvature by means of the relation $\varepsilon_x = \varphi \, y^*$.

In the following, the flexural behaviour of the RC column at the fixed-end section is described in terms of uniaxial bending moment and chord rotation (M-θ) and, for the sake of comparison, a monotonic backbone is built-up by evaluating the points (M_i,θ_i) at different stages i, such as (1) cracking, (2) yielding, (3) maximum, and (4) ultimate condition (Fig. 5-14a).

The cracking stage (stage 1 in Fig. 5-14a, M_{cr},θ_{cr}) is achieved when the cover concrete stress in the tensile region is equal to the tensile concrete strength (i.e., $\sigma_c = f_{ctm}$). The chord rotation at the cracking stage can be easily calculated from the elastic theory of beams as per Eq. 5.9 where L denotes the length of the cantilever for which the shear span L_v coincides with L. The values of the bending moment and chord rotation at the cracking stage are equal to 357 KNm and 8.2×10^{-4} rad, respectively. The curvature at cracking is equal to 1.6×10^{-3} 1/m. The elastic flexural stiffness $E_c I_t$ for evaluating the chord rotation at cracking is typically assumed equal to $E_c I_c$ (=238037 kNm^2) where

I_c is the second moment of area of the only concrete area (i.e., $bh^3/12$). However, this stage can be reasonably neglected for the analysis of buildings since it is generally accepted that RC members are already cracked when a strong earthquake occurs (Fardis 2009). For this reason, the M-θ relation is generally assumed linear up to yielding (Fig. 5-14b).

$$\theta_{cr} = \frac{M_{cr} L}{3 E_c I_t} \tag{5.9}$$

The yielding stage (stage 2 in Fig. 5-14a, M_y,θ_y) typically corresponds to the yielding of the longitudinal steel reinforcement (i.e., $\varepsilon_s = \varepsilon_{sy}$ where ε_{sy} is the steel strain corresponding to the mean yielding strength of steel f_{sym}), assuming that the concrete cover has not achieved yet the peak stress value (i.e., $\sigma_c < f_{cmo}$, if tension is positive). However, it may happen in general that if the axial load is high, the moment-curvature diagram shows a relevant nonlinear behaviour of the concrete cover in the compressive before the steel yields in tension (Fardis 2009). In this case, it is suggested to assume as limit for concrete "yielding" the value $\varepsilon_{c,max} = 1.8\, f_{cm} / E_c$ (Panagiotakos and Fardis 2001). The chord rotation at yielding can be evaluated as per Eq. 5.6 (Biskinis and Fardis 2010a) which considers contributions of the flexural and shear behaviour as well as the anchorage slip of bars. Anchorage slip of bars is not considered in the evaluation of the response through fibre-based model because of the perfect-bond condition assumed by the plane-section hypothesis. The curvature at yielding stage can be accurately evaluated by means of empirical formula, such as $\varphi_y = 1.75\, f_{sym} / (E_s\, h)$ where E_s and h are the Young's modulus of steel and the cross-section depth, respectively (Biskinis 2007). The curvature at yielding stage evaluated from the fibre-based model is equal to 7.6×10^{-3} 1/m which is very similar to the one evaluated from the empirical formulae (= 8.1×10^{-3} 1/m). The values of the bending moment and chord rotation at the yielding stage are equal to 729 kNm and 7.9×10^{-3} rad, respectively.

The maximum stage (stage 3 in Fig. 5-14a, M_{max},θ_{max}) is typically assumed as the point where spalling of concrete cover in the compressive region occurs (i.e., crushing of unconfined concrete) and it is conventionally identified by the condition $\varepsilon_c = \varepsilon_{cu}$ where ε_{cu} is equal to 0.35% (CEN 2004b) while steel bars in the tensile region show strain hardening (i.e., $\varepsilon_{sy} < \varepsilon_s < \varepsilon_{st}$ where ε_{st} denotes the tensile strain of steel at rupture typically ≥ 5%, CEN 2004b). For DCH, steel Class C should provide enough ductility with controlled strain hardening (i.e., $1.15 \le f_{stk} / f_{syk} < 1.35$, where f_{stk} is the tensile characteristic strength at rupture of the steel bar, CEN 2004a). The fibre model for steel bar does not consider the rupture phenomenon but check of the maximum achieved strain in tension should always be done in order to evaluate the failure type (i.e., concrete crushing or steel rupture). The ratio between the steel strength at rupture and yielding is equal to 1.32 for the case analysed being compatible with steel Class C. The evaluated bending moment at the maximum stage is equal to 865 kNm and it results being 18% larger than M_y. The EC8 does not provide any formulae for evaluating the chord rotation corresponding to this stage. Indeed, in the European practice, it is common to

assume a tri-linear (or bi-linear, neglecting the cracking stage) backbone with perfectly-plastic branch after the yielding stage, neglecting the stage at concrete cover spalling (see Fig. 5-14b). However, since the fibre-based model provides the curvature at this stage (φ_{max} =2.0x10^{-2} 1/m), the corresponding chord rotation can be evaluated by means of the mechanical formulae in Eq. 5.10 (Fardis 2009), suggested by the EC8-3 as alternative to Eq. 5.7, where L_{pl} denotes the plastic hinge length. The plastic hinge length evaluated from Eq. 5.10b is equal to 0.69 m against 0.50 m from the experimental evidence (25% larger). The chord rotation at the maximum stage evaluated employing the corresponding curvature is equal to 1.4x10^{-2} rad.

$$\theta_{\max} = \theta_y + \left(\varphi_{\max} - \varphi_y\right) L_{pl}\left(1 - \frac{0.5L_{pl}}{L_V}\right)$$
$$L_{pl} = 0.1L_V + 0.17h + 0.24\frac{d_{bl}f_{sym,bl}}{\sqrt{f_{cm}}} \quad (5.10)$$

The ultimate stage (stage 4 in Fig. 5-14a, M_u,θ_u) is identified as that point where the cross-section has shown significant plastic deformations in the region defined by the plastic hinge length L_{pl}. The chord rotation ad this stage according to EC8-3 is evaluated as per Eq. 5.7 which nature is purely empirical (Biskinis and Fardis 2010b). The bending moment corresponding to this stage is difficult to be identified since the post-peak behaviour for large plastic deformations can depend on concrete crushing of the core-concrete region, and steel bar rupture and buckling. It is conventionally assumed as that value to which corresponds a bending moment capacity drop of 20% of its peak value (i.e., 0.8 M_{max}, De Luca et al. 2014). The bending moment and the chord rotation at this stage are equal to 692 kNm and 3.8x10^{-2} rad, respectively.

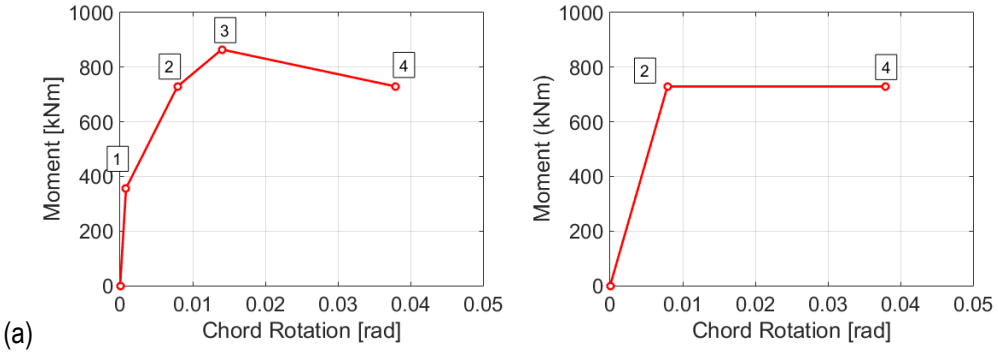

Fig. 5-14 Fibre-based numerical response of the specimen N7 tested by Tanaka and Park (1990) in terms of chord rotation versus bending moment and backbone curve: (a) cracking, yielding, max, and ultimate stages and (b) simplified curve with yielding and ultimate stages.

5.3.2.2. Case study 2: Analysis of a 3D RC-MRF portal

In order to perform the analysis of the benchmark building through NTHA in OpenSees, the nonlinear modelling framework for RC buildings is herein verified showing the study of a 3D one-bay and one-

storey (i.e., portal) building (Fig. 5-15). The portal is characterised by 5 m bay width along X and Y directions and 3.6 m storey height and is modelled as described in Section 5.2.3. Concrete class C25/30 (E_c = 31476 MPa, f_{cm} = 33 MPa) and steel 450C (f_{sym}= 518 MPa) are adopted. No equivalent stiffness reduction due to cracks is herein applied in order to keep consistent the comparison between linear and nonlinear models in terms of initial stiffness. Nodes at the ground floor are assumed to be fixed to all the degrees of freedom. Floor diaphragm constraint is assigned through "rigidDiaphragm" in OpenSees assuming that the master node coincides with the centre of the floor. The structure is symmetric both in terms of geometry and loads therefore both the centre of stiffness and the centre of mass coincide with the centre of the floor. The member mass is calculated assuming a specific weight of concrete equal to 25 kN/m^3 and is assigned to each end of the members according to the half-and-half criterion. Translational floor masses of 32 t are assigned along X and Y at the master node together with a rotational mass of 132 t m^2. Columns are orientated so that the local axis z is parallel to global axis -X while beams are orientated so that the local axis z is parallel to global axis +Z (see Fig. 5-15). In this way, the lateral stiffness of the portal results being larger along X direction.

The rigid diaphragm condition, when nonlinear beam-column elements with fibre-sections (whether force-based or displacement-based) are used, enforces a condition of zero axial strain at the beam centreline. For cross-sections where the neutral axis does not shift as consequence of bending in the beam, the axial strains at the centreline are zero and the rigid diaphragm does not create any problem. This could be the case of elastic materials or steel sections because no shift of the neutral axis occurs. However, for RC cross-sections the increase of bending in beams can lead to the neutral axis shift when the concrete strain in the tensile region is larger than the strain value corresponding to the tensile strength. In this case the rigid diaphragm changes the response of the whole structure. This is due to some spurious axial forces in beams that change both the bending moment demand and capacity at the beam ends and, in turn, the shear forces in columns. This issue is well-known in literature and its effect for the example in this section is shown in Table 5-6 where results of gravity analysis for the linear model (as benchmark) and for nonlinear model are shown for the case of a beam. In Table 5-6 it is possible to observe that because of the rigid diaphragm the beam is subjected to axial force and bending moment. To fix this issue, here is proposed to use axial force release for beams through "section Aggregator" command in OpenSees. This command is basically used to assemble a negligible axial stiffness of an end-beam section with the flexural stiffness of that section already characterised by the assigned fibre-section. In this way, the connectivity of the beam and its flexural behaviour are unchanged while the negligible axial stiffness avoids generating axial forces into beams. This is done for the beams while for columns this approach is not applied. Table 5-6 also shows the importance of considering the concrete tensile strength that if it is neglected can increase the bending moments at the ends of beams.

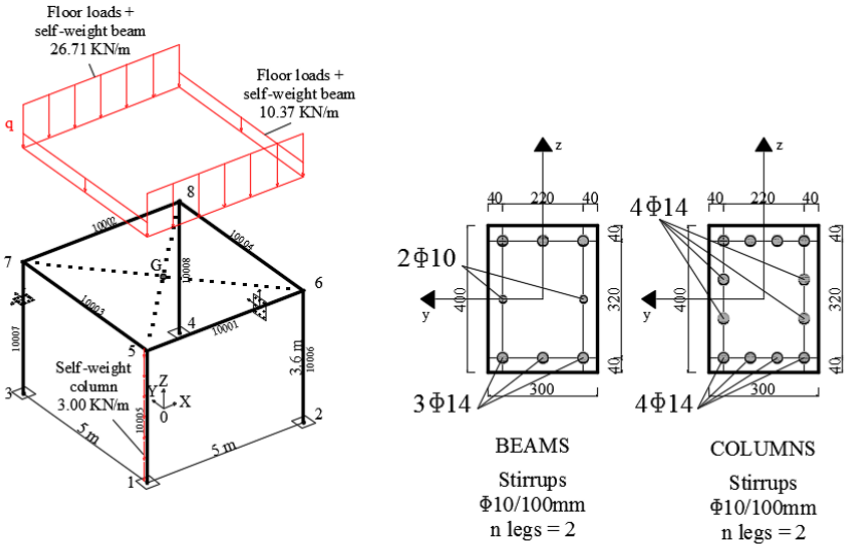

Fig. 5-15 Schematisation of the 3D RC-MRF portal modelled in OpenSees.

Table 5-6 Rigid diaphragm and concrete tensile strength effects on beam 10001 of the 3D RC-MRF portal for gravity loads

Case	Rigid diaphragm	Axial release	Concrete tensile strength	N_5 (KN)	V_5 (KN)	M_5 (KNm)
Linear	yes	-	-	0	66.78	40.91
Nonlinear	yes	yes	yes	0	66.78	40.26
Nonlinear	yes	yes	no	0	66.78	47.23
Nonlinear	yes	no	yes	29.74	66.78	40.11

The RC portal is analysed through NTHA considering as seismic input the M6.4 2000 South Iceland earthquake (aftershock) horizontal GM components 1 and 2 applied along X and Y directions, respectively, and then swapped (see Fig. 5-16). The portal is first analysed under gravity loads and subsequently through NTHA as explained in Section 5.2.3. GM time-histories in terms of acceleration are amplified by a factor equal to 4 in order to lead the structure to significant nonlinear behaviour. This is done because the aim of this section is to assess the capability of the nonlinear modelling framework. Fig. 5-17 shows the base shear versus storey drift curves obtained through NTHA together with pushover curves obtained by analysing the portal along +X, -X, +Y, and -Y directions. These pushover curves are plotted in order to have a benchmark that shows the monotonic unidirectional behaviour of the portal without the effects of the cyclic and biaxial response. Results show that the pushover analysis curves well envelope the hysteretic response of the portal subjected to the earthquake. The nonlinear response of the RC portal is dominated by the GM horizontal component 2 (see Fig. 5-16b) that achieves a maximum acceleration of about 3 g and pushes the portal until to about 1.5 m along both the directions. Indeed, the most critical seismic combination for the response along X is given by CX_2 + CY_1 that is when the GM component 2 is applied along X,

while the most critical combination for the response along Y is given by $CX_1 + CY_2$ that is when the GM component 2 is applied along Y. Typical limits in terms of IDR for RC-MRF buildings are 2% for Life-Safety and 4% for Collapse Prevention (FEMA 1997) indicating that this structure very likely achieved the collapse. It is worth mentioning that collapse is not herein investigated, and the implemented nonlinear modelling framework is not capable of predicting it. If collapse is targeted, the nonlinear model should include some behavioural aspects that are not implemented herein, such as nonlinear shear behaviour, bond-slip of bars, pinching, buckling of bars in compression and rupture of bars in tension. This is more conveniently achieved by implementing concentrated plasticity models (e.g., Haselton and Deierlein 2008).

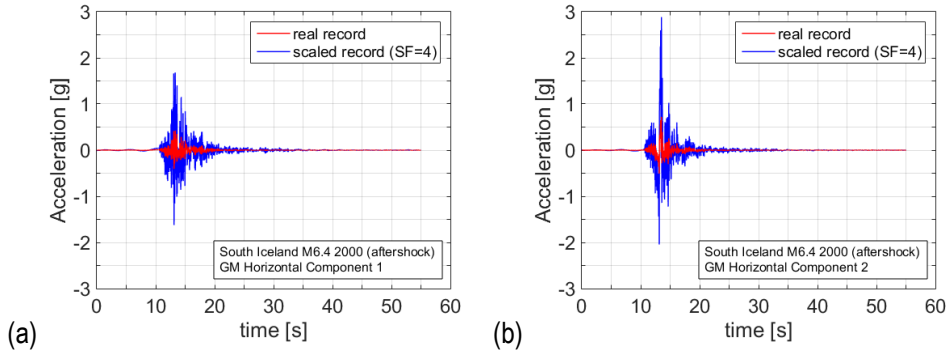

Fig. 5-16 Ground motion horizontal components utilised for analysing the 3D RC-MRF portal through NTHA: (a) component 1 and (b) component 2 of the South Iceland M6.4 2000 earthquake (aftershock) scaled by 4.

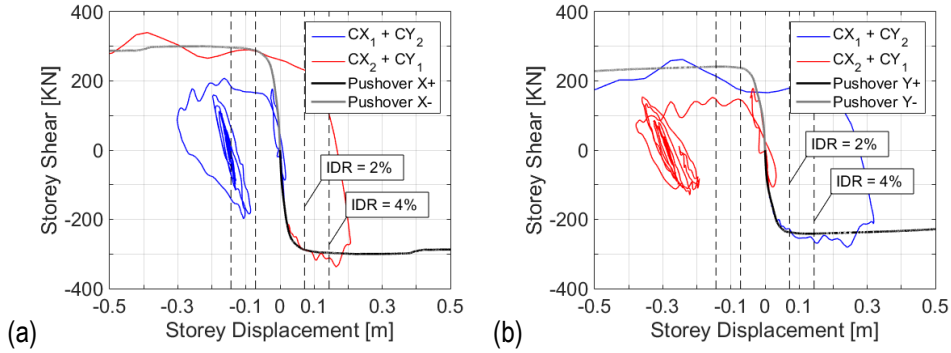

Fig. 5-17 Storey Shear versus storey displacement curve obtained from NTHA (considering swap of the GM horizontal components) benchmarked to the same curve obtained from unidirectional pushover analysis: (a) direction X and (b) direction Y.

The seismic response of beams and columns is shown in Fig. 5-18 where it is possible to observe the progressive achievement of different stages identified in terms of chord rotation, such as damage limitation (θ_y), Life Safety (3/4 θ_u) and Near Collapse (θ_u). Results of pushover analysis are also shown in Fig. 5-18 in order to present a benchmark for the hysteretic response evaluated through NTHA. From Fig. 5-18b-c it is possible to observe the influence of the biaxial flexural behaviour on the seismic response of columns and the comparison with the uniaxial flexural behaviour evaluated

from unidirectional pushover analyses. While the biaxial seismic demand of the columns is accurately evaluated through the fibre-section model, the biaxial capacity that in a more rigorous way could be evaluated as per Eq. 5.11 (Fardis 2009) is herein evaluated in a simplified way which is consistent with the simplified procedure allowed by the EC8-1 for linear analyses (see Eq. 5.8). This assumption is made so that there is direct correspondence with the linear-elastic procedure for LTHA described in Section 4.2.8. Biaxial behaviour of the columns is accounted in the evaluation of DCR multiplying the uniaxial chord rotation capacity by 0.7 as indicated in the EC8-1 for verifications in terms of bending moment (i.e., M_{Ed} / (0.7 M_{Rd}) where M_{Ed} is the demand and M_{Rd} is the capacity). The biaxial capacity model is not investigated in this research work, but some researchers proposed methods validated on experimental tests (e.g., Bousias et al. 2002).

$$DCR(t) = \left(\frac{\theta_y(t)}{\theta_{\text{Limit-State,y}}(t)} \right)^2 + \left(\frac{\theta_z(t)}{\theta_{\text{Limit-State,z}}(t)} \right)^2 \qquad 5.11$$

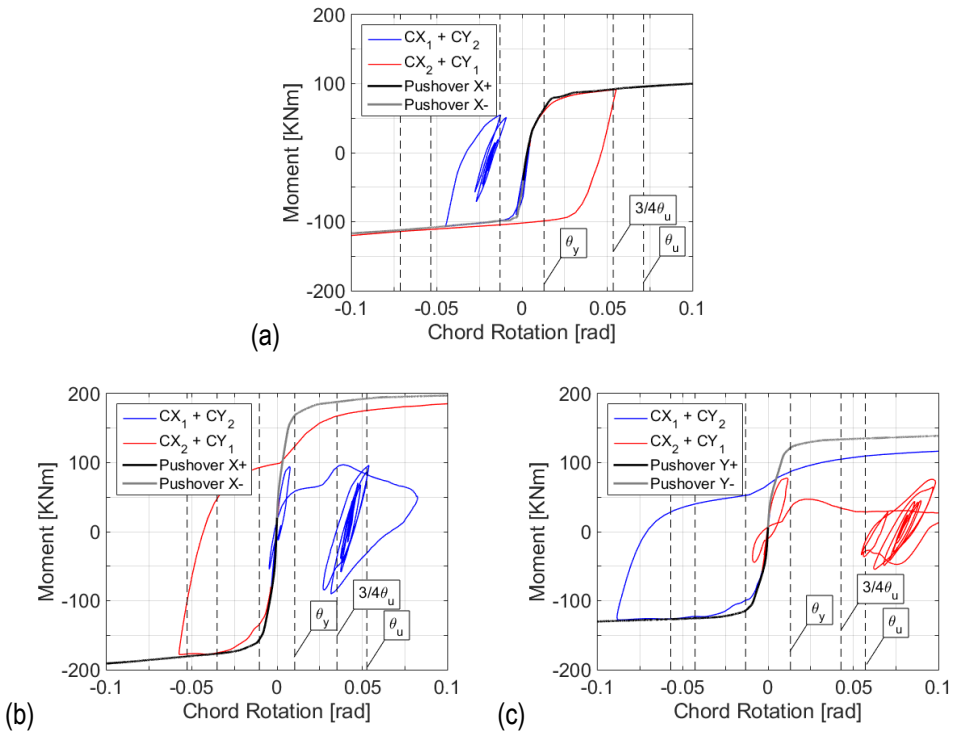

Fig. 5-18 Flexural response evaluated through NTHA (considering swap of the GM horizontal components) benchmarked to the one obtained from unidirectional pushover analysis: (a) beam 10001, (b) column 10005 bending about y (X-Z plane), and (c) column 10005 bending about z (Y-Z plane)..

5.4.Conclusion

In this chapter the linear and nonlinear modelling in OpenSees is presented by describing the code framework developed in this research work for analysing buildings. The code is presented for RC-

MRF buildings, in particular showing as example the numerical model of the benchmark building presented in Chapter 3, but it can be extended to steel MRF buildings and braced frame buildings (e.g., X-CBF buildings) even if this is not directly presented herein (see Di Cuia et al. 2017). This code works by means of implemented Matlab routines that allow creating and analysing the numerical model in the OpenSees framework. A post-processing module allows to elaborate the results obtained from OpenSees and to carry out the verifications of structural members according to the acceptance criteria consistent with the analysis method. The linear modelling framework of the developed code is verified against results of a commercial structural software package such as SAP2000 that allows to output the mass and stiffness matrices that are used for LTHA. The nonlinear modelling framework of the developed code, based on "forceBeamColumn" element with fibre-sections and "HingeRadau" plastic hinges at the ends of the structural member, is validated against results of an RC column experimentally tested in the past and it shows to be reliable in estimating the nonlinear response of RC members which behaviour is flexural-dominated. "Concrete02" uniaxial material model for concrete-fibres results to be particularly easy to calibrate and it avoids numerical issues for numerical models characterised by elevated number of degrees of freedom, such as the benchmark building.

Moreover, because this research work aims to assess the behaviour of EC8-designed buildings which are meant to show a flexural-dominated behaviour of structural members as they are capacity-designed, other types of failures are not investigated herein (e.g., nonlinear shear behaviour, bond-slip, etc.). Results of the experimental and numerical results are also used to describe the local acceptance criteria typically employed for concentrated plasticity models and recommended by EC8-3 to assess the nonlinear structural response of beams and columns, such as the chord rotation at different stages. In the following chapter, the seismic response of the benchmark building analysed through NTHA is assessed in terms of chord rotation capacity. This is crucial for this research work because if design, in the first place, is based on local verifications expressed in terms of bending moments, its counterpart for assessment through nonlinear analyses is based on chord rotations. Finally, the nonlinear modelling framework for NTHA is tested for the analysis of a 3D one-storey one-bay RC-MRF building. Pushover analyses results are also used to represent a benchmark for the interpretation of NTHA results. NTHA results show consistency with pushover results and this allows to promote the nonlinear framework for the next step described in the next chapter. An important aspect mentioned in this chapter is the capability of fibre-section models in predicting biaxial response in columns. This topic is not herein further investigated, and the biaxial capacity is evaluated in a simplified way that is consistent with design through linear analyses, as explained in Section 4.2.8.

Chapter 6: LTHA Design and Assessment

Part of this chapter is based on the following reference:

Lombardi L, De Luca F, and Macdonald J (2019). Design of Buildings through Linear Time-History Analysis Optimising Ground Motion Selection: A Case Study for RC-MRFs, Engineering Structures; 192:279-295.

Lombardi L and De Luca F (2019). Linear Time-History Analysis for Fragility Curves at Design Stage, Earthquake Engineering and Structural Dynamics (under review).

Objectives of this chapter

The OpenSees/Matlab code framework described in the previous chapter is herein used to analyse the 12-storey RC-MRF benchmark building designed through RSA. The objectives of this chapter are:

- to compare RSA and LTHA results in order to show main differences when designing for two limit states: (i) Life Safety-Limit State (LS-LS) and (ii) Damage Limitation-Limit State (DL-LS). For LTHA, results are presented for (i) different suites of Ground Motions (GMs) selected to be spectrum-compatible with the target spectrum, and (ii) a suite of spectral-matched GMs through wavelet adjustment according to the procedure indicated in FEMA P1050. Particular attention is given to the variability of LTHA results and its correlation with outliers of the GM suites that can lead to "unacceptable cases";
- to present with a practical example how the I_{eq} index proposed in this research work can be used for selecting GMs to reduce both variability and effects of "unacceptable cases" in results. An optimal value of the I_{eq} index obtained from fitting LTHA results of a sufficient number of GMs considering different field-conditions (i.e., far-field and near-field) is found;
- to assess RSA design through NTHA considering the same GMs suites adopted for LTHA design, in order to show the goodness of LTHA results and shortcomings of RSA.

6.1.Introduction

LTHA is becoming of interest nowadays as confirmed by its recent inclusion in ASCE/SEI 7-16 (ASCE 2017) and described in FEMA P-1050 (BSSC 2015). RSA is the reference design method but the accuracy of the CQC rule can lead to differences with respect to LTHA. De Luca and Verderame (2013) investigated the accuracy of CQC in RSA comparing results of LTHA for different GM suites to those obtained through RSA employing corresponding jagged GM spectra. They showed that RSA can underestimate the median maximum IDR at the upper storeys of a two-dimensional 6- and a 12-

storey RC-MRFs and such underestimation can achieve about 20%. For pulse-like GMs having pulse period T_P lower than the fundamental period T_1, this underestimation can increase up to 40% for the 12-storey building. RSA generally underestimate the median maximum storey shears and this underestimation is generally higher at the upper storeys, increasing up to 20% for the 12-storey building but being generally neglectable at the base. Aswegan and Charney (2014) proposed a design framework for buildings based on LTHA. However, prior LTHA inclusion in the US code, there was a considerable amount of debate because of the proposal of a new and not-fully investigated procedure (Charney 2015). Therefore, the best compromise was achieved by developing an LTHA-based design procedure as much consistent as possible with the RSA procedure that has been used by designers since the 80's (Charney 2015). The seismic input selection was simplified with the assumption of the spectral-matching procedure consisting of wavelet adjusted GMs that basically eliminates issues related to selecting and scaling of GMs. To simplify the process of spectral-matching for designers, Jayamon and Charney (2015) developed a free-available interactive computational tool called the "Spectrum Match Toolkit" that uses the time-domain spectral matching approach by adding wavelets to the original accelerogram. Aswegan and Charney (2014) presented the procedure implemented by FEMA P-1050 with an example consisting of a regular 4-storey steel building with two special MRFs along each direction and compared LTHA to RSA, the latter employing the code spectrum. They showed that the enveloped base shear of LTHA employing three pairs of spectral-matched GMs is basically the same of RSA while the enveloped IDR at the upper storeys can be about 25% larger than RSA. They also showed a comparison with LTHA employing the three pairs of real (scaled) GMs and showed that the enveloped base shear can be up to 51% higher than RSA while the enveloped IDR can be 60% higher than RSA. They also investigated accidental eccentricity by shifting the centre of mass and observed that the periods of vibration do not change much while the modal participating masses can change significantly, and it leads to coupling the torsional and lateral modes. In the presented procedure Aswegan and Charney proposed to evaluate the P-Delta effects from a static analysis instead of directly including them in the mathematical model. Indeed, for the latter it is possible that the effects could be less than the model without P-Delta effects because of the associated period elongation (Aswegan and Charney 2014). In the linear analysis context, this period elongation is exclusively given by the addition of the constant geometric stiffness matrix created from gravity loads analysis (Wilson and Habibullah 1987; Wilson 2004).

In order to help designers with a practical example of design according to FEMA P-1050, FEMA P-1051 (BSSC 2016) presented an irregular 12-storey steel building with five special MRFs. The irregularity is due to the presence of re-entrant frames and distribution of mass in elevation. Contrarily to the procedure proposed in Aswegan and Charney (2014), the example in FEMA P-1051 uses the P-Delta effects directly included in the analysis through the geometric stiffness matrix. The geometric

matrix is evaluated from the gravity loads applied to the buildings and it is maintained as constant during LTHA. In this case, the modal properties of the building slightly changed (i.e., the periods elongation was less than 6%). It is also noticed that results including P-Delta effects can be unconservative with respect to those without P-Delta effects.

This chapter shows the results obtained for the regular 12-storey RC-MRF benchmark building presented in Section 3.3, which is meant to contribute in investigating on LTHA as design method of analysis with a different case study compared to the ones available in literature. The EC8-compliant design procedure proposed in Section 4.2 is considered to compare LTHA results to RSA and, for the first time in literature, LTHA results of a realistic building are compared to those of NTHA. The comparison between LTHA and NTHA is achieved thanks to the assumption for LTHA of the same GM selection utilised for NTHA. This aspect characterises one of the novelties of this research and it allows for a better understanding of the behaviour of the building.

6.2.LTHA as design method: comparison with RSA

In this section, results obtained from LTHA are compared to those obtained from RSA for the 12-storey RC-MRF benchmark building described in Section 3.3. The procedure for implementing LTHA is described in Section 4.2. The code framework for the linear modelling of the benchmark building, analysis settings, and post-processing of the outputs is described in Section 5.2. For the sake of comparison, the benchmark building, which is designed through RSA, is assessed through LTHA and comments on possible re-design solutions are presented. This is assumed because RSA is the reference design method according to the EC8-1 and design of buildings typically involves choices made by designers that are not necessary univocal (i.e., given a DCR higher than unity a designer can update the design in different ways such as increasing or changing the reinforcement, changing the class of concrete, re-dimensioning members, etc.). Herein the optimal design of buildings is not investigated, therefore if LTHA results are presented assuming as benchmark the design solution obtained through RSA it is possible to benefit of a direct comparison between LTHA and RSA design. In the following, the comparison is presented for two limit states: (i) Life Safety-Limit State (LS-LS) and (ii) Damage Limitation-Limit State (DL-LS). The variability of LTHA results is quantified through the Coefficient of Variation (CoV) defined as ratio between the standard deviation and the average values. The difference between LTHA and RSA is expressed in terms of relative error (denoted by e = (LTHA-RSA)/RSA)).

6.2.1. Design comparison at Life Safety-Limit State:

For LS-LS, it is expected that the benchmark building under strong earthquakes presents significant level of damage, but it still retains sufficient residual lateral strength and stiffness to protect life during subsequent events (Italian Building Code 2018). The reference seismic action for the benchmark building is expressed in terms of elastic target spectrum with 10% probability of exceedance in 50

years (return period of 475 years) (Italian Building Code 2018). EC8-1-based design at LS-LS adopts the "force-based" design approach which relies on the use of the behaviour factor q in order to account for the ductility of the building. At design level, the reference elastic response spectrum is reduced by means of the behaviour factor (q) of the building in order to obtain the design target spectrum. As described in Section 3.3, the behaviour factor according to EC8-1 for a regular multi-storey RC-MRF building designed for Ductility Class High (DCH) is equal to 5.85. However, the proposed LTHA design procedure is based on the evaluation of a specific behaviour factor for LTHA (denoted by q_{LTHA}) that is evaluated being equal 4.86 (see Section 4.2.2). This value is smaller than q adopted for RSA because of the lower bound limit of the design spectral acceleration at LS-LS imposed by the EC8-1 and it complies with the condition that in LTHA only one behaviour factor can be used as the different modes are not decoupled as in RSA. In order to investigate an optimal design for LTHA at LS-LS, different suites of GMs are considered in the following, and results are commented in terms of global seismic demand (i.e., storey shears and interstorey drift ratios) and subsequently in terms of DCR values from flexural verifications for different groups of structural members, as indicated in Fig. 4-3 (i.e., floor beams, staircase beams, columns, and squat columns). An important aspect herein investigated is the use of the proposed I_{eq} index for selecting GMs and identifying possible "unacceptable cases".

The definition of "unacceptable case" in the LTHA context when using "force-based" design is related to the situation in which a building designed as EC8 compliant through RSA (as in this case) shows disproportionate and unrealistic high values of DCR especially in the case of combined axial force and bending moment due to the high variation of axial force in LTHA and the recurring case of tension and bending in the structural members leading to DCRs that are significantly high (e.g., from 10 up to 1000). This is a limitation of the "force-based" capacity model assumed by EC2 and in general by codes when verifying an element under tension and bending in dynamic condition. Significant variations of axial load in RC elements are not really investigated in literature through numerical and experimental results.

To show this explicitly, an example of time-history in terms of axial load and bending moment obtained from LTHA employing a generic real GM is provided in Fig. 6-1 where results of LTHA, RSA, gravity analysis, NTHA, and LTHA employing the same GM but spectrally-matched to the target spectrum through wavelet adjustment (referred to as LTHA SM) are showed. It is possible to observe that when the building is analysed through LTHA, because of the large seismic demand imposed by the GM, the squat column is subjected to an elevated bending moment about local axis z and tensile axial force (see Fig. 6-1a) equal to 1011 kNm and 2911 kN, respectively. Fig. 6-1b shows the N-M_z interaction plane where it is possible to observe the point at t = 3.48 s when the maximum DCR equal to 75 occurs. This condition does not seem to be such dramatic for RSA and LTHA SM that show similar DCR values, equal to 0.39 and 0.34. In the same way, NTHA results confirm that the condition

of the squat column is not that dramatic, being the maximum DCR value in terms of chord rotation equal to 0.10. The use of the lexical expression "unacceptable case" recalls the meaning of this expression in the context of NTHA and its discussion in the recent version of ASCE 7-16 (Haselton et al. 2017a; 2017b) and FEMA P1050 (BSSC 2015). In the following is showed that it is possible to control the "unacceptable cases" through the proposed I_{eq} index.

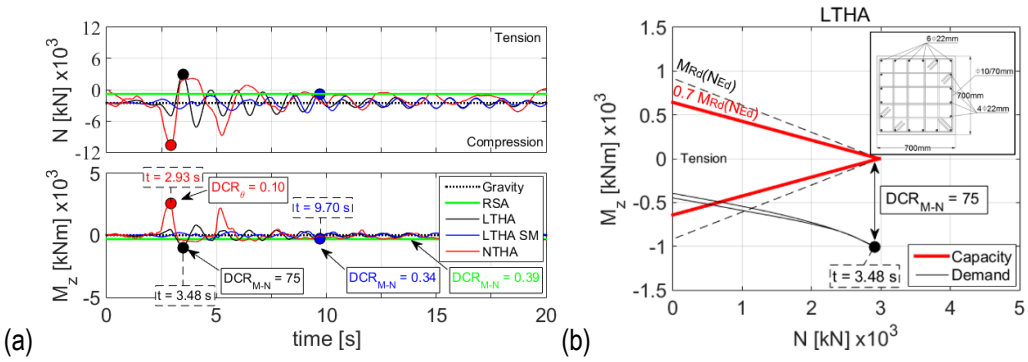

Fig. 6-1 Example of "unacceptable case" for a squat column at the first storey of the benchmark building analysed through RSA, LTHA, LTHA SM, and NTHA: (a) axial force and bending moment about local axis z over time, and (b) axial force versus bending moment interaction plane for LTHA verification.

Another comparison herein investigated is between LTHA and RSA in terms of displacements at LS-LS. According to the EC8-1, displacements at ultimate limit states can be evaluated from the results of the linear analysis employing the design seismic action (i.e., design spectrum obtained from the behaviour factor) multiplied by the behaviour factor, typically valid for buildings having $T_1 > T_C$, where T_C is the upper limit of the period of the constant spectral acceleration branch of the smoothed (code) spectrum (Vidic et al. 1994). For LTHA, the behaviour factor is assumed to be q_{LTHA} proposed in this research work (i.e., 4.86) while for RSA it is equal to 5.85. Moreover, because of the susceptibility of the benchmark building to the second-order effects, displacements are amplified by the P-Delta amplification factor evaluated from the interstorey drift sensitivity coefficient (CEN 2004a). It is worth mentioning that with this approach, more consistent with a "displacement-based" design approach, "unacceptable cases" do not occur.

6.2.1.1. Suite of Unspecified-Field Unscaled (UF-U) GMs

A suite of seven pairs of unscaled real GMs is selected from the European Strong Motion database (ESM 2008) to be spectrum-compatible with the target spectrum for the LS-LS. Such suites are meant to be selected without any distinction in terms of field conditions (i.e., "Unspecified-Field" condition). The selection of UF-U suite is performed through the Matlab-based software REXEL (Iervolino et al. 2010a). REXEL allows to obtain the disaggregation of the seismic hazard at the site of interest in this thesis (i.e., Pettino, a neighborhood of L'Aquila, Italy). It results that deaggregating the hazard for spectral acceleration corresponding to one second (denoted by $S_a(T_1)$), the earthquakes contributing to the hazard at the site are in the intervals of moment magnitude and source-to-site distance equal to [4.5, 8] M and [0, 60] km, respectively. These intervals are assumed in the following for selecting

other possible GM suites. The spectrum-compatibility is performed so that the average of the selected GMs (μ) matches the target spectrum between 10% lower and 30% upper tolerances over the period range [0, 4] s, even though the EC8-1 requires compatibility within the period range of [$0.2T_1$, $2T_1$] which is included in [0, 4] s. It is worth mentioning that the 30% upper tolerance is not indicated by EC8, but it is suggested in Iervolino et al. (2010a) where a lower value can also be used at the discretion of the user. The goodness of the spectrum-compatibility can be observed in Fig. 6-2a.

Notwithstanding the good matching of the average spectrum to the target spectrum, the variability of the selected spectra is high, indicated in Fig. 6-2a by the average ± one standard deviation (i.e., $\mu \pm \sigma$). The Coefficients of Variation (CoVs) evaluated at the periods of vibration of the benchmark building range between [0.36, 0.89] with largest values at the first three periods. However, standards and codes do not impose any restriction on the variability therefore this GM suite is still code-compatible. Fig. 6-2b shows the comparison between code-design spectrum and GM design spectra obtained reducing the elastic spectra by q_{LTHA}. The Root Mean Square Error (RMSE) is typically used to quantify the difference of the selected suite with respect to the target spectrum (Kottke and Rathje 2008). In the following, the RMSE index, evaluated as per Eq. 2.19 within the period range of [T_{10}, T_1], is calculated at the elastic level (denoted by $RMSE_e$) and at the design level (denoted by $RMSE_d$), the latter being more consistent with design purposes. The evaluated $RMSE_e$ and $RMSE_d$ are equal to 0.0602 g and 0.0321 g, respectively, and they are used in the following to compare UF-U suite to other suites (i.e., UF-SM, UF-S1, and UF-S2).

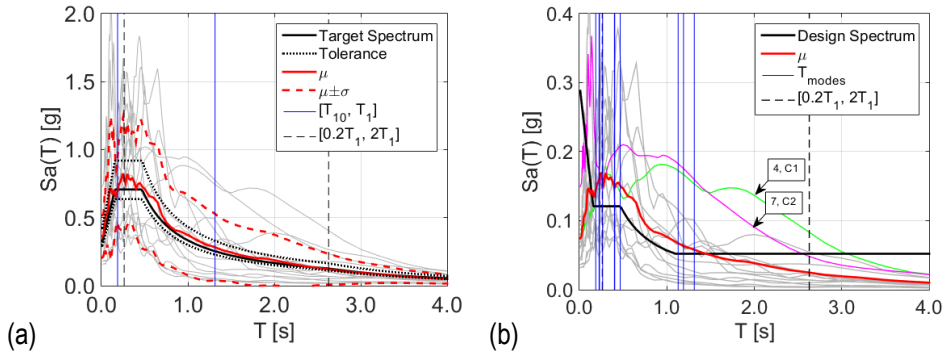

Fig. 6-2 GM selection at LS-LS for the suite of UF-U: (a) spectrum-compatibility with the elastic code spectrum of seven pairs of real (unscaled) ground motions and (b) comparison between design code-spectrum and design ground motion spectra. In the figure μ denotes the average spectrum and ±σ its one standard deviation.

The comparison between RSA and LTHA for this suite of GMs is shown in Fig. 6-3 in terms of maximum storey shears along X and Y directions over time and combinations. It is worth mentioning that according to the EC8, the average of the results obtained from the seven pairs of GMs should be used for design purposes. The P-Delta amplification factor for LTHA ranges between [1, 1.11] while it is equal to 1.14 for RSA. The CoV evaluated at each storey ranges between [0.37, 0.66] (see

Fig. 6-4) which is mainly due to the high CoV values of the GM spectra at the first periods of vibration of the benchmark building. The relative error of LTHA respect to RSA ranges between [0.57, 1.10] with highest values at the upper storeys (see Fig. 6-5). Table 6-1 reports the I_{eq} values of the selected GMs where the largest values are found for earthquake #4 and #7 which represent the strongest earthquakes within the UF-U suite. The comparison LTHA versus RSA for this suite of GMs in terms of maximum IDR at LS-LS along X and Y directions over time and combinations is shown in Fig. 6-6. While the CoV values are slightly larger than the CoV values in terms of maximum storey shears (see Fig. 6-7), the relative error of LTHA respect to RSA tends reduce when the comparison is in terms of deformability (see Fig. 6-8).

Table 6-1 GM index I_{eq} [g] evaluated for the UF-U suite selected for LS-LS.

Suite	**GM component**	**Earthquake number**						
		1	***2***	***3***	***4***	***5***	***6***	***7***
UF-U	1	0.0491	-0.0402	0.0302	0.0976	-0.0390	-0.0210	-0.0107
	2	-0.0142	-0.0415	0.0017	0.0527	0.0339	-0.0011	0.1124

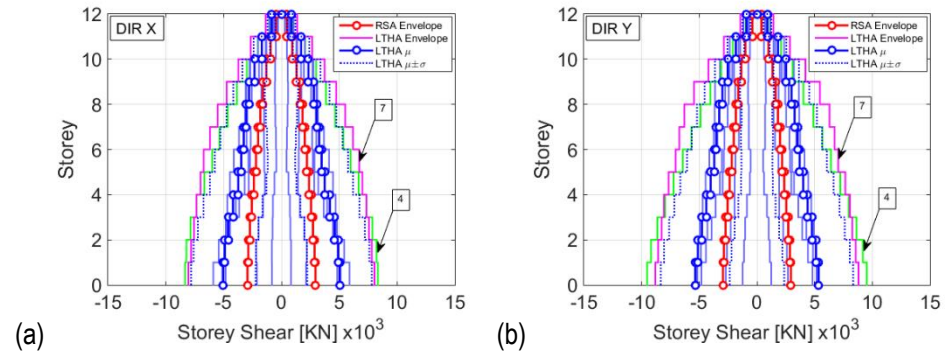

Fig. 6-3 Comparison of the seismic demand between LTHA and RSA in terms of maximum storey shear along (a) X and (b) Y directions at LS-LS for the suite of UF-U. In the figure μ denotes the average, ±σ its one standard deviation and "envelope" the envelope of the seismic combinations. Plots indicated by the text boxes represent the most critical earthquakes for LTHA design as shown by the corresponding I_{eq} values in Table 6-1.

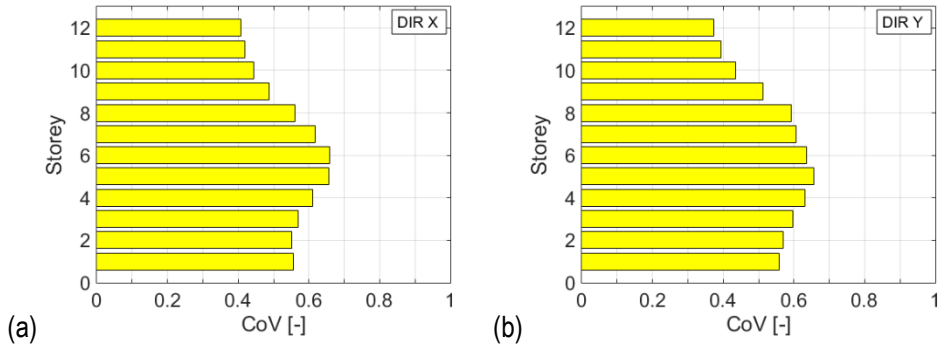

Fig. 6-4 Coefficients of Variation (CoVs) expressed as ratio of the first standard deviation (σ) and average (μ) of the maximum storey shears along (a) X and (b) Y direction at LS-LS for the suites of UF-U.

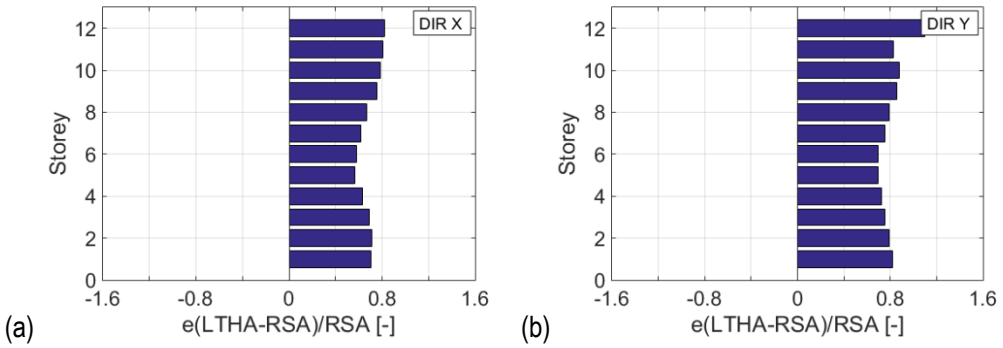

Fig. 6-5 Relative errors between LTHA and RSA in terms of storey shear along (a) X and (b) Y direction at LS-LS for the suites of UF-U.

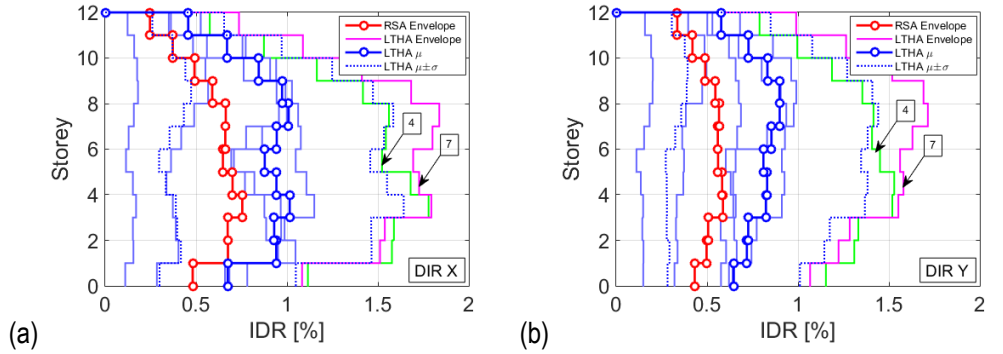

Fig. 6-6 Comparison of the seismic demand between LTHA and RSA in terms of maximum Interstorey Drift Ratio (IDR) along (a) X and (b) Y directions at LS-LS for the suites of UF-U. In the figure μ denotes the average, ±σ its one standard deviation and "envelope" the envelope of the seismic combinations. Plots indicated by the text boxes represent the most critical earthquakes for LTHA design as shown by the corresponding I_{eq} values in Table 6-1.

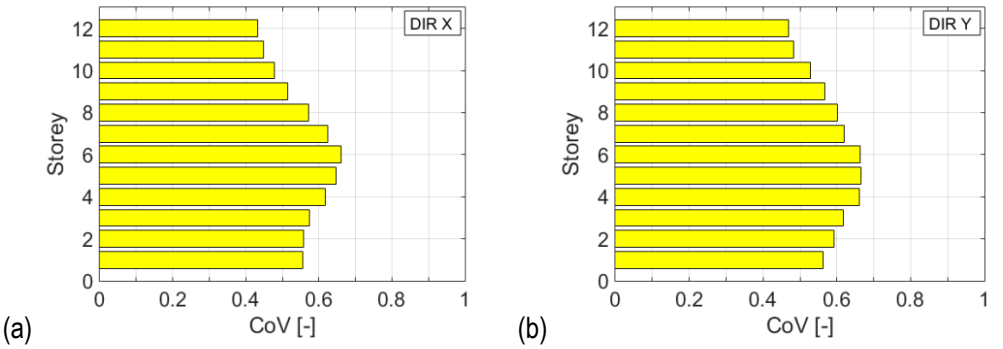

Fig. 6-7 Coefficients of Variation (CoVs) expressed as ratio of the first standard deviation (σ) and average (μ) of the maximum Interstorey Drift Ratio (IDR) along (a) X and (b) Y direction at LS-LS for the LTHA suites of UF-U.

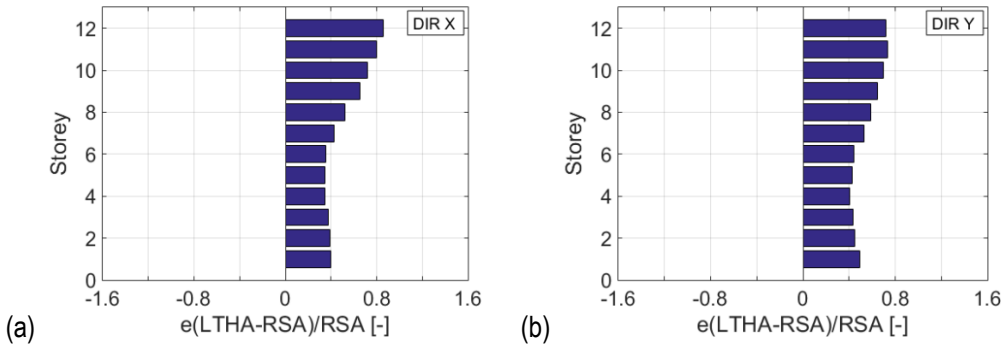

Fig. 6-8 Relative errors between LTHA and RSA in terms of maximum Interstorey Drift Ratio (IDR) along (a) X and (b) Y direction at LS-LS for the suites of UF-U.

6.2.1.2. Suite of Spectral-Matched (SM) GMs

A sub-suite made of three pairs of spectral-matched GMs is obtained through wavelet adjusted GMs from the UF-U suite, selected to be compliant with the FEMA P-1050 provisions for LTHA. In the following it is called UF-SM (i.e., "Unspecified-Field-Spectral-Matched"). The spectral-matching is performed through the Spectrum Match Toolkit (Jayamon and Charney 2015). The first ten modes of vibration are considered adequate for the benchmark building to cover higher-mode effects and to impose the period range for the matching (i.e., $[T_{10}, T_1]$). Fig. 6-9a shows the goodness of the match according to FEMA P-1050 specifications. As expected, the variability is considerably reduced with respect to UF-U. The Coefficients of Variation (CoVs) evaluated at the periods of vibration of the benchmark building range between [0.01, 0.05]. Fig. 6-9b shows the comparison between code-design spectrum and GM design spectra obtained by reducing the elastic spectra by q_{LTHA}. The evaluated $RMSE_e$ and $RMSE_d$ are equal to 0.0086 g and 0.0212 g, respectively, which are smaller than UF-U.

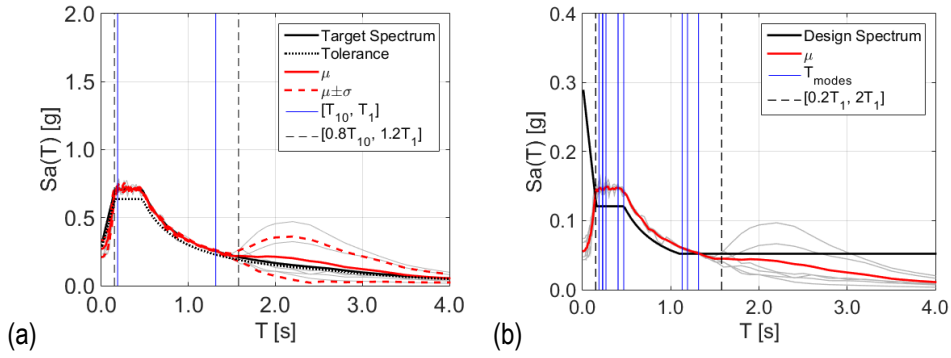

Fig. 6-9 GM selection at LS-LS for the suite of UF-SM: (a) spectral-matching with the elastic code spectrum of three pairs of ground motions through wavelet adjustment and (b) comparison between design code-spectrum and design ground motion spectra. In the figure μ denotes the average spectrum and ±σ its one standard deviation.

The comparison between RSA and LTHA for UF-SM suite is shown in Fig. 6-10 in terms of maximum storey shears along X and Y directions over time and combinations. It is worth mentioning that according to the LTHA design procedure described in FEMA P-1050, the envelope (not the average) of the results obtained from the three pairs of GMs should be used for design purposes. The P-Delta

amplification factor for LTHA is equal about 1.11 for the three earthquakes, while it is equal to 1.14 for RSA. The CoV at each storey is much lower than UF-U ranging between [0.02, 0.20] (see Fig. 6-11) but it tends to increase compared to the CoV values of the GM spectra at the periods of vibration of the benchmark building. The relative error of LTHA respect to RSA ranges between [0.13, 0.79] with highest values at the upper storeys (see Fig. 6-12). The comparison LTHA versus RSA for this suite of GMs in terms of maximum IDR at LS-LS along X and Y directions over time and combinations is shown in Fig. 6-13. While the CoV values are pretty much the same of those in terms of maximum storey shears (see Fig. 6-14), the relative error of LTHA respect to RSA tends reduce when the comparison is in terms of deformability (see Fig. 6-15).

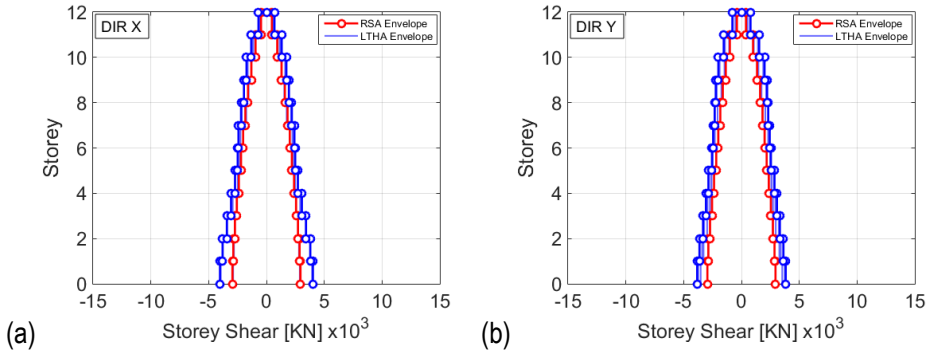

Fig. 6-10 Comparison of the seismic demand between LTHA and RSA in terms of maximum storey shear along (a) X and (b) Y directions at LS-LS for the suite of UF-SM. In the figure "envelope" denotes the envelope of the seismic combinations.

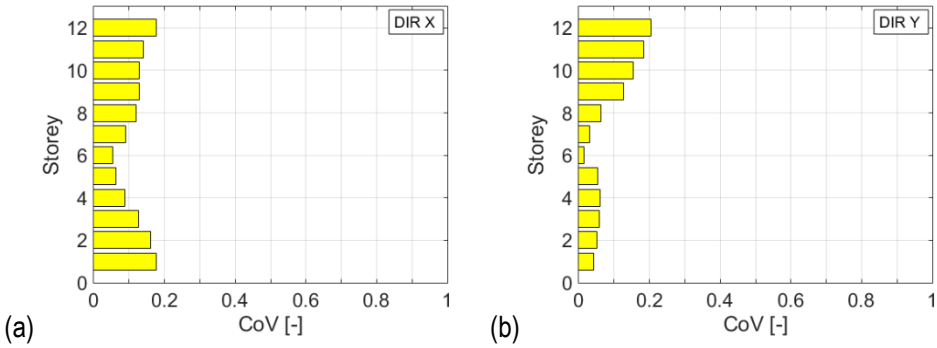

Fig. 6-11 Coefficients of Variation (CoVs) expressed as ratio of the first standard deviation (σ) and average (μ) of the maximum storey shears along (a) X and (b) Y direction at LS-LS for the suites of UF-SM.

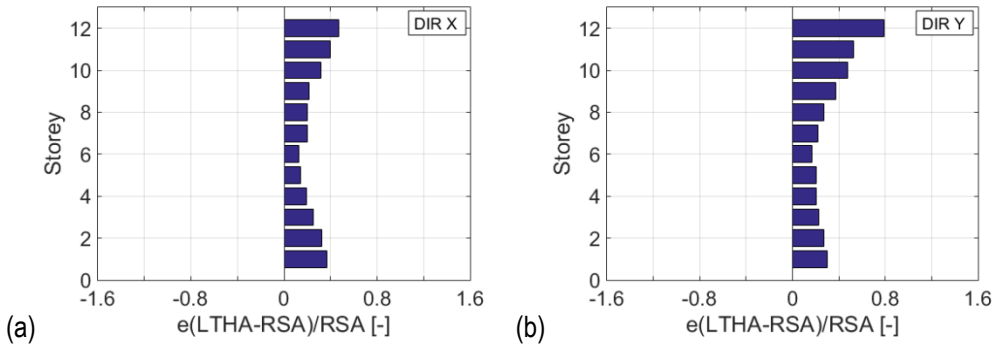

Fig. 6-12 Relative errors between LTHA and RSA in terms of storey shear along (a) X and (b) Y direction at LS-LS for the suites of UF-SM.

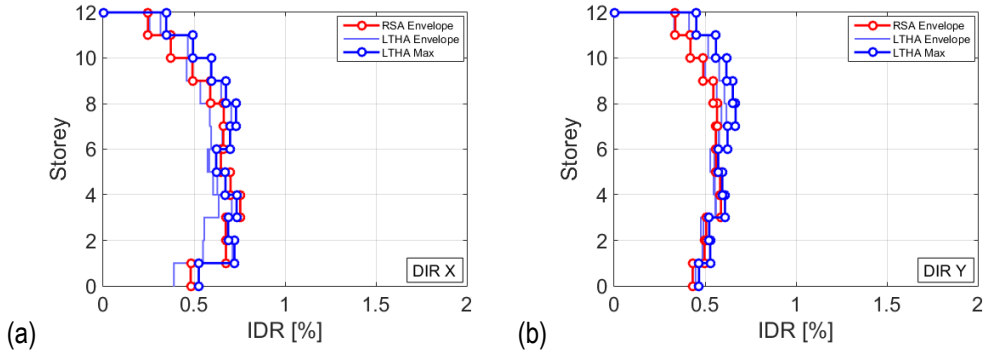

Fig. 6-13 Comparison of the seismic demand between LTHA and RSA in terms of maximum Interstorey Drift Ratio (IDR) along (a) X and (b) Y directions at LS-LS for the suites of UF-SM. In the figure "envelope" denotes the envelope of the seismic combinations.

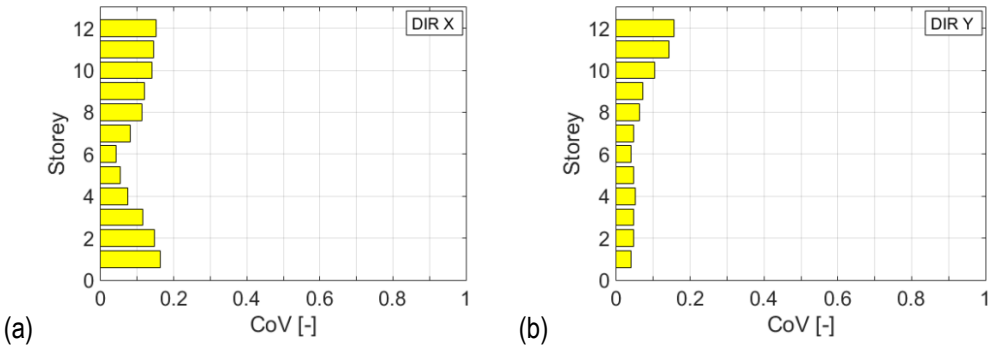

Fig. 6-14 Coefficients of Variation (CoVs) expressed as ratio of the first standard deviation (σ) and average (μ) of the maximum Interstorey Drift Ratio (IDR) along (a) X and (b) Y direction at LS-LS for the LTHA suites of UF-SM.

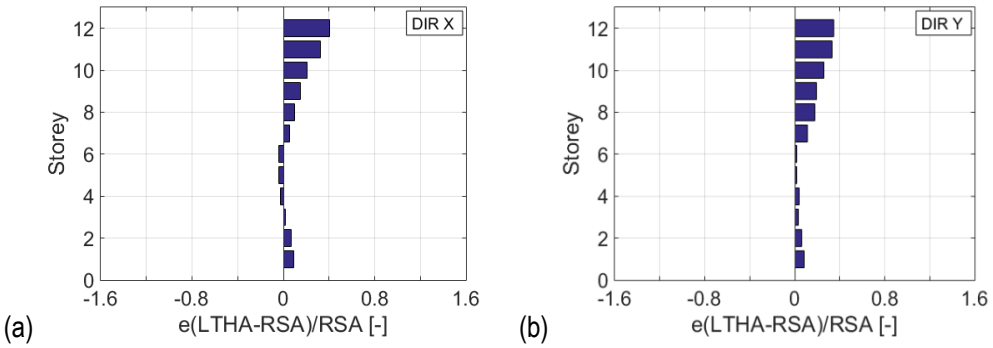

Fig. 6-15 Relative errors between LTHA and RSA in terms of maximum Interstorey Drift Ratio (IDR) along (a) X and (b) Y direction at LS-LS for the suites of UF-SM.

6.2.1.3. Suites of Unspecified-Field Scaled (UF-S) GMs

In order to investigate an optimal LTHA input selection and its effects on the results, two suites of seven pairs of scaled real GMs are considered herein. The first suite is based on the UF-U suite, scaled in order to reduce the effect of the strongest GMs (i.e., earthquakes #4 and #7) and to still accomplish the spectrum-compatibility requirements (see Fig. 6-16a). This suite is referred in the following as UF-S1 and its design spectra are shown in Fig. 6-16b. The scaling factors used for each pair of GMs range between [0.60, 4.50] and they are consistent with the maximum allowable scaling values recommended in literature in order to avoid biased results (Bommer and Acevedo 2004; Luco and Bazzurro 2007). These GMs are scaled by using the I_{eq} index so that each pair of GMs presents $I_{eq,max}$ lower than 0.05 g in order to limit the unacceptable cases found in UF-U, as described in the following. The Coefficients of Variation (CoVs) evaluated at the periods of vibration of the benchmark building range between [0.53, 0.77] with largest values at the last three periods. The evaluated $RMSE_e$ and $RMSE_d$ are equal to 0.2497 g and 0.0716 g, respectively, which are larger than UF-U. These differences are mainly due to the dissimilarities between the average spectrum and the target one in the lower period range where the GM spectra present higher spectral acceleration values.

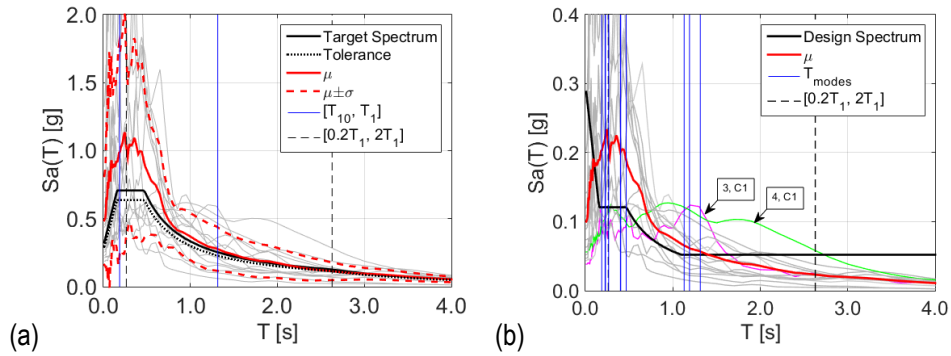

Fig. 6-16 GM selection at LS-LS for the suite of UF-S1: (a) spectrum-compatibility with the elastic code spectrum of seven pairs of real (scaled) ground motions and (b) comparison between design code-spectrum and design ground motion spectra. In the figure μ denotes the average spectrum and ±σ its one standard deviation.

The comparison between RSA and LTHA for UF-S1 is shown Fig. 6-17 in terms of maximum storey shears along X and Y directions over time and combinations. It is worth mentioning that according to the EC8, the average of the results obtained from the seven pairs of GMs should be used for design purposes. The P-Delta amplification factor for LTHA ranges between [1, 1.11] while it is equal to 1.14 for RSA. The CoV for UF-S1 ranges between [0.09, 0.33] (see Fig. 6-18) and it is mainly due to the high CoV values of the GM spectra at the lower periods of vibration of the benchmark building. The relative error of LTHA respect to RSA ranges between [0.53, 1.36] with highest values at the upper storeys (see Fig. 6-19). Table 6-2 reports the I_{eq} values of the selected GMs where the largest values are found for earthquake #1, #3 and #4 which represent the strongest earthquakes within the UF-S1 suite. The comparison LTHA versus RSA for this suite of GMs in terms of maximum IDR at LS-LS along X and Y directions over time and combinations is shown in Fig. 6-20. The CoV values are similar to those in terms of maximum storey shears at the lower storeys (see Fig. 6-21), the relative error of LTHA respect to RSA tends reduce when the comparison is in terms of deformability (see Fig. 6-22).

Table 6-2 GM index I_{eq} [g] evaluated for the UF-S1 suite selected for LS-LS.

Suite	**GM component**	**Earthquake number**						
		1	***2***	***3***	***4***	***5***	***6***	***7***
UF-S1	1	0.0491	0.0461	0.0492	0.0489	-0.0364	0.0119	-0.0324
	2	-0.0142	0.0402	0.0151	0.0174	0.0437	0.0468	0.0415

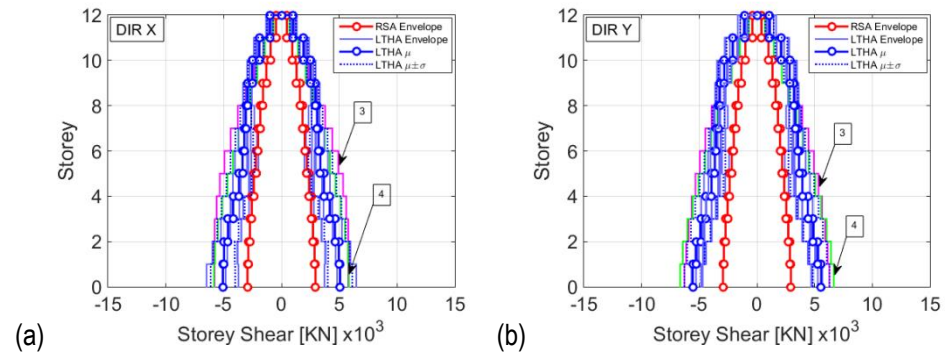

Fig. 6-17 Comparison of the seismic demand between LTHA and RSA in terms of maximum storey shear along (a) X and (b) Y directions at LS-LS for the suite of UF-S1. In the figure μ denotes the average, ±σ its one standard deviation and "envelope" the envelope of the seismic combinations. Plots indicated by the text boxes represent the most critical earthquakes for LTHA design as shown by the corresponding I_{eq} values in Table 6-2.

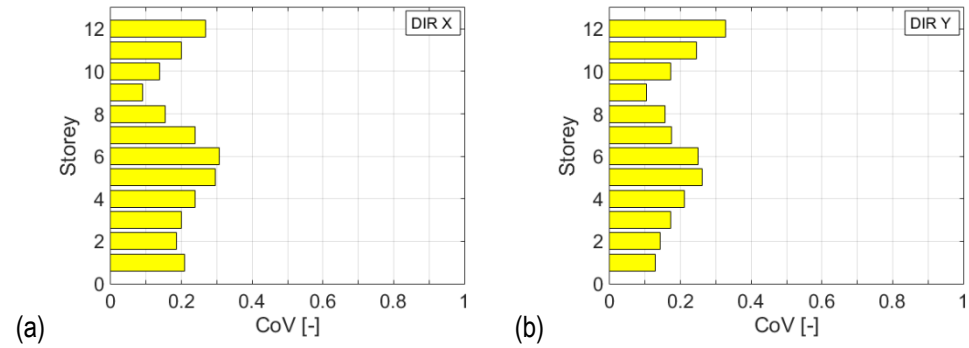

Fig. 6-18 Coefficients of Variation (CoVs) expressed as ratio of the first standard deviation (σ) and average (μ) of the maximum storey shears along (a) X and (b) Y direction at LS-LS for the suites of UF-S1.

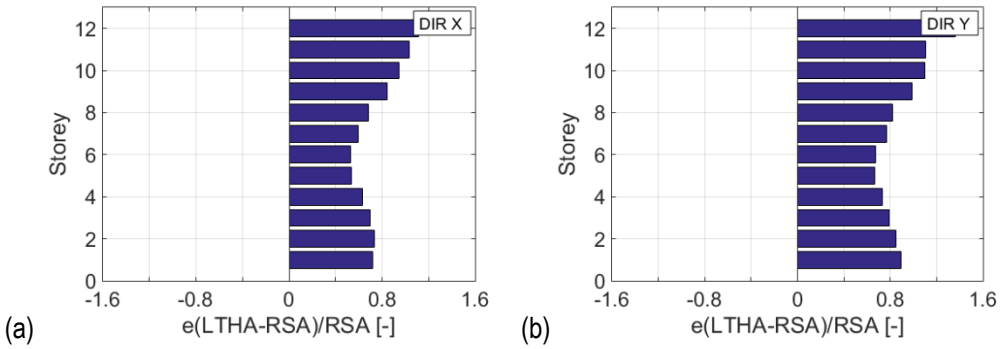

Fig. 6-19 Relative errors between LTHA and RSA in terms of storey shear along (a) X and (b) Y direction at LS-LS for the suites of UF-S1.

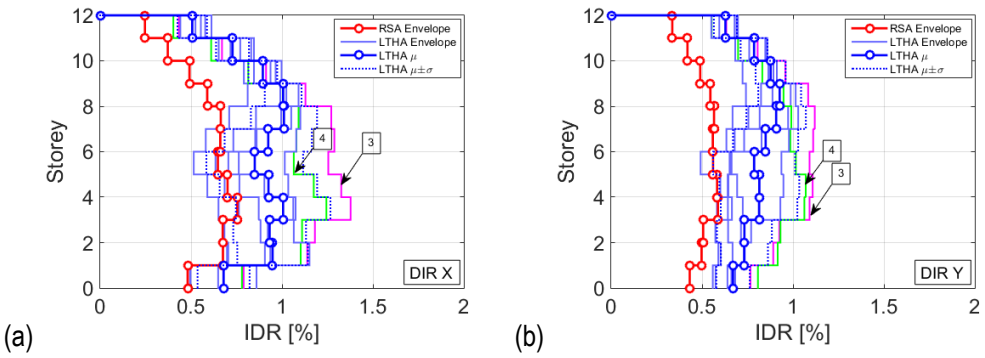

Fig. 6-20 Comparison of the seismic demand between LTHA and RSA in terms of maximum Interstorey Drift Ratio (IDR) along (a) X and (b) Y directions at LS-LS for the suites of UF-S1. In the figure μ denotes the average, ±σ its one standard deviation and "envelope" the envelope of the seismic combinations. Plots indicated by the text boxes represent the most critical earthquakes for LTHA design as shown by the corresponding I_{eq} values in Table 6-2.

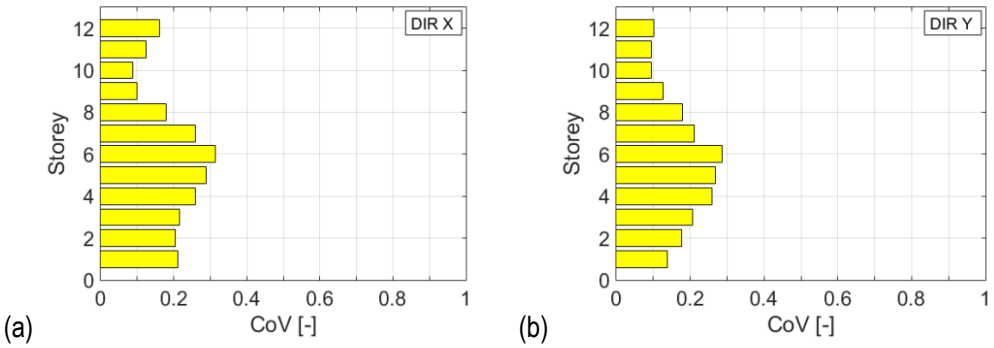

Fig. 6-21 Coefficients of Variation (CoVs) expressed as ratio of the first standard deviation (σ) and average (μ) of the maximum Interstorey Drift Ratio (IDR) along (a) X and (b) Y direction at LS-LS for the LTHA suites of UF-S1.

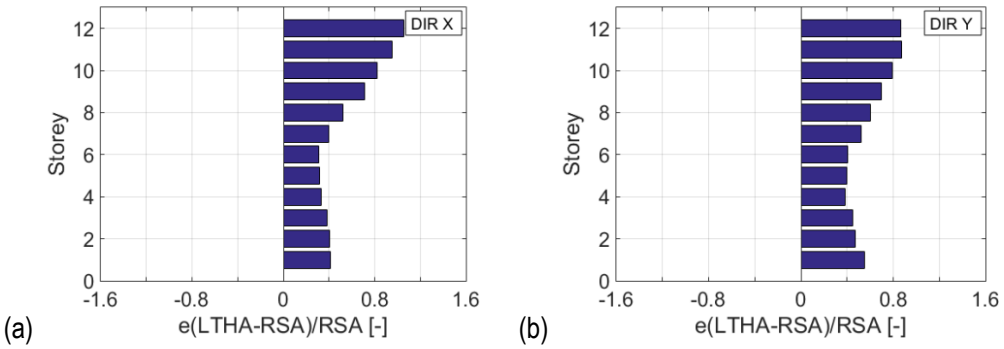

Fig. 6-22 Relative errors between LTHA and RSA in terms of maximum Interstorey Drift Ratio (IDR) along (a) X and (b) Y direction at LS-LS for the suites of UF-S1.

The second suite of scaled GMs, selected from the latest version of the PEER NGA West2 ground motion database (PEER 2014), presents a reduced record-to-record variability (see Fig. 6-23a). It is called in the following UF-S2 and it is selected, based on the results of the disaggregation of the seismic hazard at the site of interest, to have compatible moment magnitude and source-to-site distance values, as shown later. These GMs are selected by using the I_{eq} index, so that their $I_{eq,max}$ is lower than 0.04 g, as described in the following. The scaling factors for UF-S2 range between [1.18, 2.50]. Fig. 6-23b shows the comparison between code-design spectrum and GM design spectra obtained by reducing the elastic spectra by q_{LTHA}. It is worth noting that the 30% upper tolerance considered for UF-U is not applied for these cases. Indeed, regarding this aspect, these selections are chosen with the intent of controlling the individual GM spectra instead of their average spectrum. The Coefficients of Variation (CoVs) evaluated at the periods of vibration of the benchmark building range between [0.25, 0.40] with largest values at the first period. The evaluated $RMSE_e$ and $RMSE_d$ are equal to 0.2061 g and 0.0625 g, respectively, which are slightly lower than to those of UF-S1 and larger than UF-U. Similarly to UF-S1 suite, the differences are mainly due to the high spectral acceleration values of the GM spectra in the lower period range.

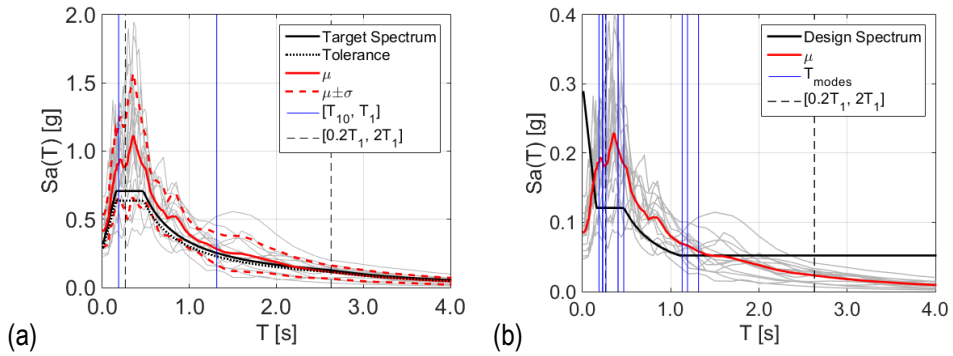

Fig. 6-23 GM selection at LS-LS for the suite of UF-S2: (a) spectrum-compatibility with the elastic code spectrum of seven pairs of real (scaled) ground motions and (b) comparison between design code-spectrum and design ground motion spectra. In the figure μ denotes the average spectrum and ±σ its one standard deviation.

The comparison between RSA and LTHA for UF-S2 is shown Fig. 6-24 in terms of maximum storey shears along X and Y directions over time and combinations. It is worth mentioning that according to the EC8, the average of the results obtained from the seven pairs of GMs should be used for design purposes. The P-Delta amplification factor for LTHA ranges between [1, 1.11] while it is equal to 1.14 for RSA. The CoV for UF-S2 ranges between [0.07, 0.32] (see Fig. 6-25) and it is mainly due to the CoV value of the GM spectra at the first period of vibration of the benchmark building. The relative error of LTHA respect to RSA is lower than UF-S1 and it ranges between [0.26, 1.19] with highest values at the upper storeys (see Fig. 6-26). From the results it appears that UF-S2 is better than UF-S1 as confirmed by the lower values of CoV and relative error. Table 6-3 reports the I_{eq} values of the selected GMs where the largest value is equal to +0.0334 g. The comparison LTHA versus RSA for UF-S2 suite in terms of maximum IDR at LS-LS along X and Y directions over time and combinations is shown in Fig. 6-27. The CoV values are similar to those in terms of maximum storey shears at the lower storeys (see Fig. 6-28), the relative error of LTHA respect to RSA tends reduce when the comparison is in terms of deformability (see Fig. 6-29).

Table 6-3 GM index I_{eq} [g] evaluated for the UF-S2 suite selected for LS-LS.

Suite	***GM component***	***Earthquake number***						
		1	***2***	***3***	***4***	***5***	***6***	***7***
UF-S2	1	0.0333	0.0333	0.0334	0.0078	0.0307	0.0171	0.0315
	2	0.0331	0.0313	0.0015	0.0326	0.0192	0.0328	0.0099

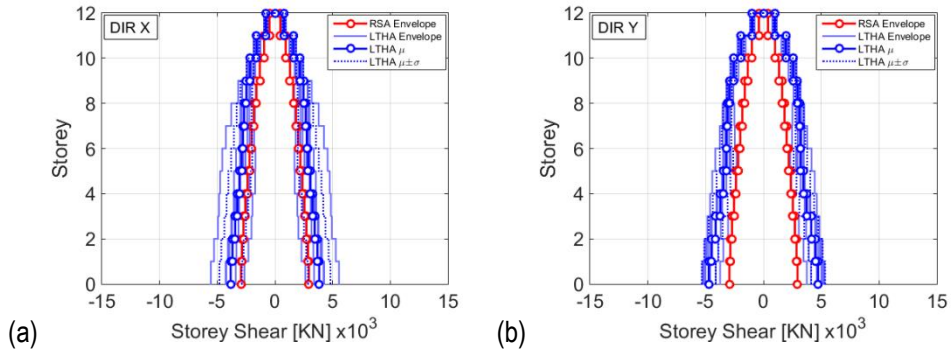

Fig. 6-24 Comparison of the seismic demand between LTHA and RSA in terms of maximum storey shear along (a) X and (b) Y directions at LS-LS for the suite of UF-S2. In the figure μ denotes the average, ±σ its one standard deviation and "envelope" the envelope of the seismic combinations.

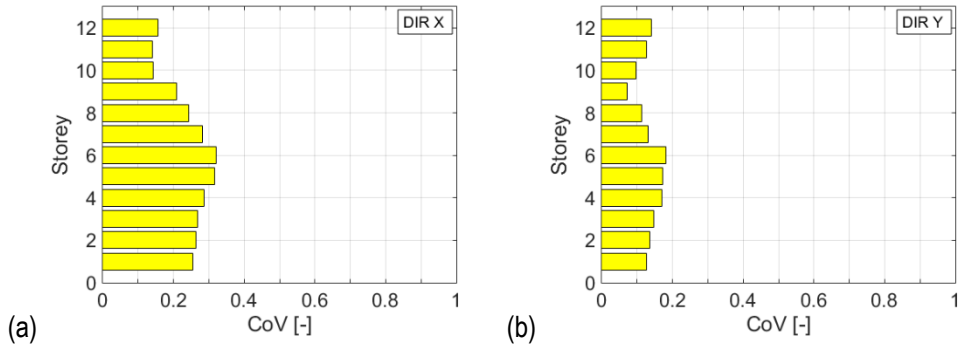

Fig. 6-25 Coefficients of Variation (CoVs) expressed as ratio of the first standard deviation (σ) and average (μ) of the maximum storey shears along (a) X and (b) Y direction at LS-LS for the suites of UF-S2.

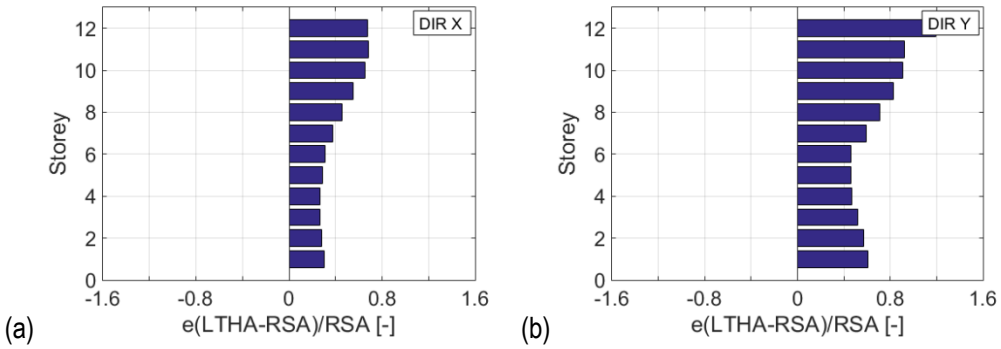

Fig. 6-26 Relative errors between LTHA and RSA in terms of storey shear along (a) X and (b) Y direction at LS-LS for the suites of UF-S2.

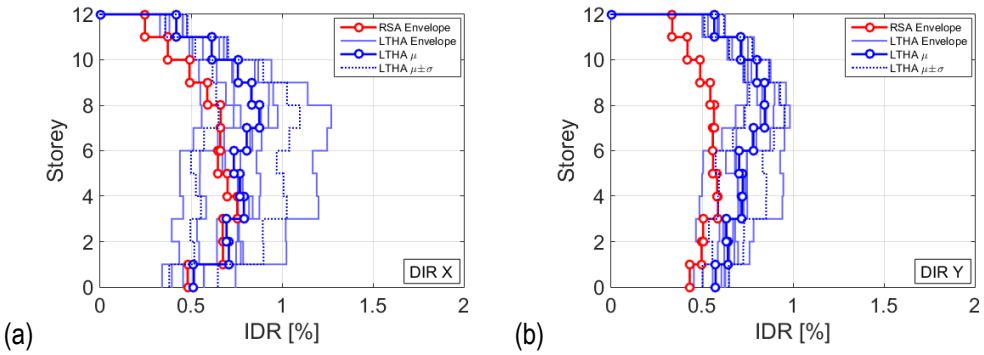

Fig. 6-27 Comparison of the seismic demand between LTHA and RSA in terms of maximum Interstorey Drift Ratio (IDR) along (a) X and (b) Y directions at LS-LS for the suites of UF-S2. In the figure μ denotes the average, ±σ its one standard deviation and "envelope" the envelope of the seismic combinations.

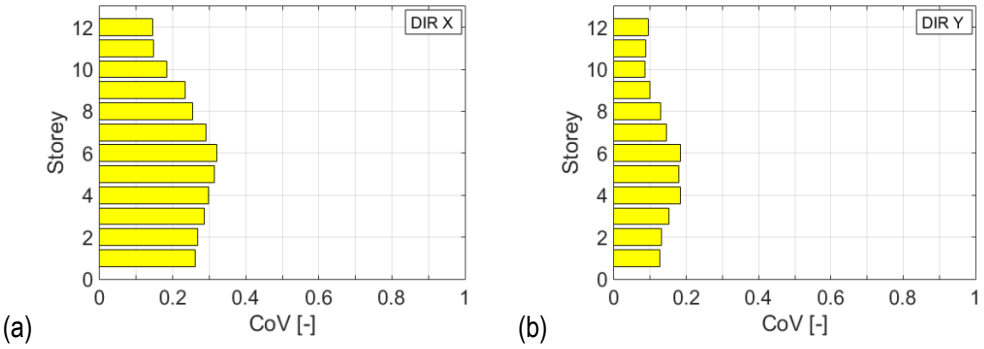

Fig. 6-28 Coefficients of Variation (CoVs) expressed as ratio of the first standard deviation (σ) and average (μ) of the maximum Interstorey Drift Ratio (IDR) along (a) X and (b) Y direction at LS-LS for the LTHA suites of UF-S2.

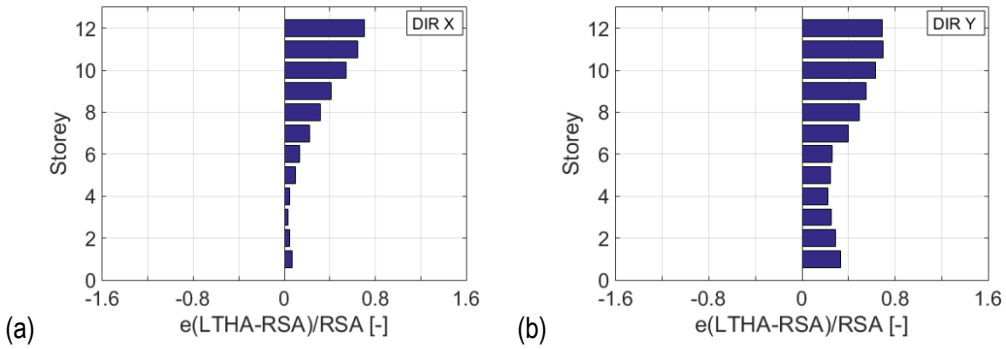

Fig. 6-29 Relative errors between LTHA and RSA in terms of maximum Interstorey Drift Ratio (IDR) along (a) X and (b) Y direction at LS-LS for the suites of UF-S2.

6.2.1.4. Results comparison

Results for "force-based" design are showed in Fig. 6-30 where the maximum flexural DCR value is evaluated at each storey for the different selected GM suites. Results for UF-U (Section 6.2.1.1) show that the benchmark building designed through RSA, presents insufficient longitudinal reinforcement in most beams and columns when it is checked through LTHA. Failures seem to be

particularly critical for beams and columns of the staircase. These elements are subjected to high axial forces (both of tension and compression) and bending moments. In fact, the average values of the DCR in terms of flexure for these elements are highly dependent on the DCR values of the strongest earthquakes within the GM suite, such as earthquake #4 and #7 (see Fig. 6-2b) that have the largest values of $I_{eq,max}$ (i.e., the maximum value of I_{eq} between the two horizontal GM components for each earthquake, as explained in Section 4.2.10), equal to +0.0976 g and +0.1124 g respectively (see Table 6-1). Re-design of the elements showing DCR values greater than unity leads to increasing longitudinal steel reinforcement in beams and, in turn, increasing longitudinal and transversal steel reinforcement in columns, especially those of the staircase. However, it results problematic with this assumption satisfying the capacity design check and the verification of beam-to-column joints. This solution would rigorously suggest changing structural system of the staircase to reinforced-concrete shear walls as typically adopted in practice for medium-high rise buildings.

Results in Fig. 6-30 for UF-SM (Section 6.2.1.2) show that the maximum flexural DCR values are largely lower than UF-U, even if they are still larger than unity for the floor beams and landing beams at the lower storeys. Re-design of the elements showing DCR values greater than unity leads to increasing longitudinal steel reinforcement in beams but in such a way that it does not compromise other verifications. This case certainly represents the most convenient design solution compared to the other suites.

Fig. 6-30 shows that for UF-S1 (Section 6.2.1.3) the scaling of earthquake #4 and #7, carried out to reduce the effect of the outliers in UF-U suite, leads to a design solution which is now mostly dependent on earthquake #3 and #4 (see Fig. 6-16b), which show the largest flexural DCR values and have $I_{eq,max}$ equal to +0.0492 g and +0.0489 g respectively (see Table 6-2). Even after this scaling, the design of beams and columns of the staircase is still very critical (see Fig. 6-30). On the contrast, UF-S2 suite (Section 6.2.1.3) leads to more convenient results than UF-U and UF-S1 as also shown by the largest $I_{eq,max}$ that is equal to +0.034 g being smaller with respect to the previous cases (see Table 6-3). Even if results of the UF-S2 suite are still not acceptable for design (because the DCR values are greater than one), they are certainly less critical than the previous cases compared to RSA design, as shown by Fig. 6-30 (i.e., the largest DCR value is about 1.70 and it refers to the flight beam at the 2nd storey). The I_{eq} index is used for the UF-S2 suite to target the threshold value of 0.03 g. This value is found to be an optimal value for the design of the benchmark building through LTHA. The optimal value is obtained by fitting the results of a sufficient number of earthquakes as described in Section 6.2.2.

The comparison LTHA versus RSA in terms of design values of IDR at LS-LS shows that if an IDR limit of 2% is chosen as threshold for Life Safety Building Performance Level (FEMA 1997; ATC 1996; FEMA 2000), all the suites satisfy the verification. The largest IDR equal to about 1% is

achieved by UF-U and UF-S1. For spectral-matched GMs (UF-SM) the design IDRs are relatively close to those of RSA, showing underestimations between the 4th and 6th storeys and difference that tends to be larger at the upper storeys where the relative error becomes larger (see Fig. 6-15). No "unacceptable cases" occur when the design is checked in terms of displacement quantities.

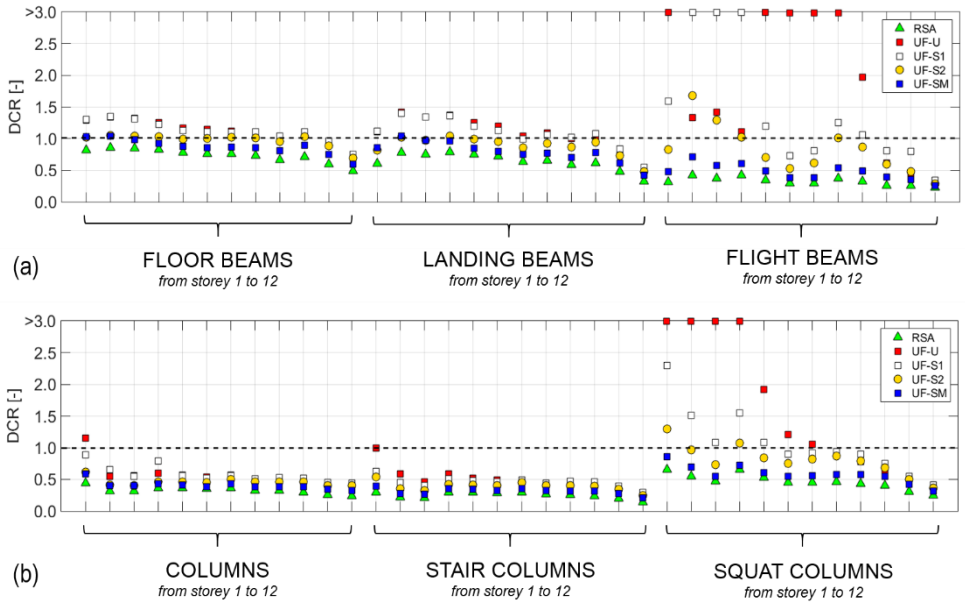

Fig. 6-30 Design DCR values of LTHA and RSA from flexural verifications at LS-LS for (a) beams and (b) columns. For RSA and UF-SM these results refer to the maximum values of the envelopes at each storey while for the other LTHA suites (i.e., spectrum-compatible suites) they refer to the maximum values of the means at each storey for each suite.

6.2.2. I_{eq} for LTHA ground motion selection at Life Safety-Limit State

In this section, a linear regression of the results in the semi-logarithm space of the flexural DCR versus the I_{eq} index of the GM spectrum (i.e., log(*DCR*) vs I_{eq}), together with its confidence bands, is obtained in order to calibrate an optimum value of I_{eq} that can be suggested as a target value for designers approaching GM selection for LTHA at LS-LS. This operation is performed for the different groups of structural members identified within the building (see Fig. 4-3): floor beams, staircase beams, squat columns, and other columns. Different suites of unscaled GMs belonging to specific-field conditions are considered, such as FF-U, NFPL-U, NFNPL-U and PL-U that are described in the following. These GMs are selected from earthquakes that result compatible with the disaggregation at the site in terms of moment magnitude and source-to-site distance (see Fig. 6-31). A total of 84 earthquakes were considered for the fitting (i.e., seven from UF-U, three from UF-SM, seven from UF-S1, seven from UF-S2, twenty-two from FF-U, fourteen from NFPL-U, fourteen from NFNPL-U, and ten from PL-U) plus the results obtained from RSA for I_{eq} equal to zero.

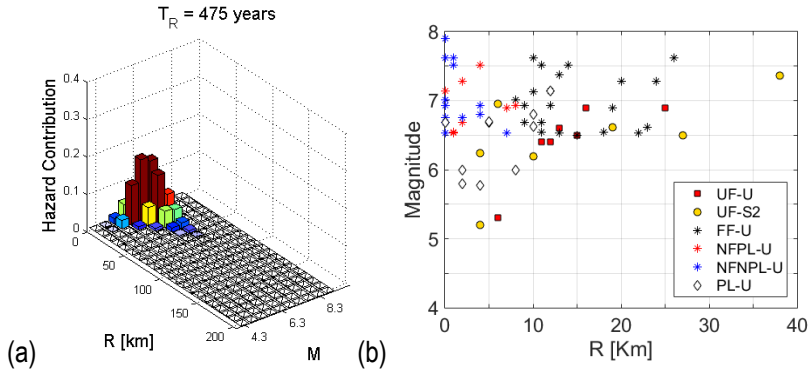

Fig. 6-31 Selection of GMs for fitting of LTHA results: (a) disaggregation for S_a(1 s) of the seismic hazard at Pettino, L'Aquila (Italy) for LS-LS (T_R = 475 years) obtained from REXEL (Iervolino et al. 2010a) and (b) selected earthquakes in terms of Moment Magnitude (M) and Source-to-Site distance (R).

I_{eq} allows designers to estimate the weight in terms of flexural DCR of a specific GM within a suite resulting from the analysis and it is a proxy for "unacceptable cases". In the following the fit is presented using the subscripts "max" for I_{eq} and *DCR* as the first is the maximum among the two GM spectrum horizontal components and the second is the maximum for the structural member category considered. The best fit relationship between the DCR_{max} and $I_{eq,max}$ is presented in the form of Eq. (6.1):

$$\ln(DCR_{max}) = a\, I_{eq,max} + b \qquad 6.1$$

where *a* and *b* are the values reported in Fig. 6-32 for each structural member group. Linear regressions of the results show values of R^2 equal to 0.82, 0.47, 0.52 and 0.76 for floor beams, staircase beams, squat columns and other columns, respectively. While for floor beams and other columns the goodness of the linear regressions can be considered accurate (i.e., R^2 values closer to unity), for staircase beams and squat columns the distribution of the DCR values is particularly affected by their higher values (as confirmed by the low values of R^2, i.e. 0.47 and 0.52). Results show that a value of $I_{eq,max}$ equal to 0.03 g can be suggested as target value for GM selection leading to alternative design options that can be still considered economically-feasible in professional applications (i.e., convenient changes in the dimensions or reinforcements of the elements with respect to the RSA). This threshold is identified as the minimum value resulting from selections of possible real (scaled and unscaled) spectrum-compatible GM suites with the aim of keeping the DCR_{max} values of the benchmark building reasonably low. Even though this optimal value is found specifically for the benchmark building, it can be still considered as a benchmark value for other applications.

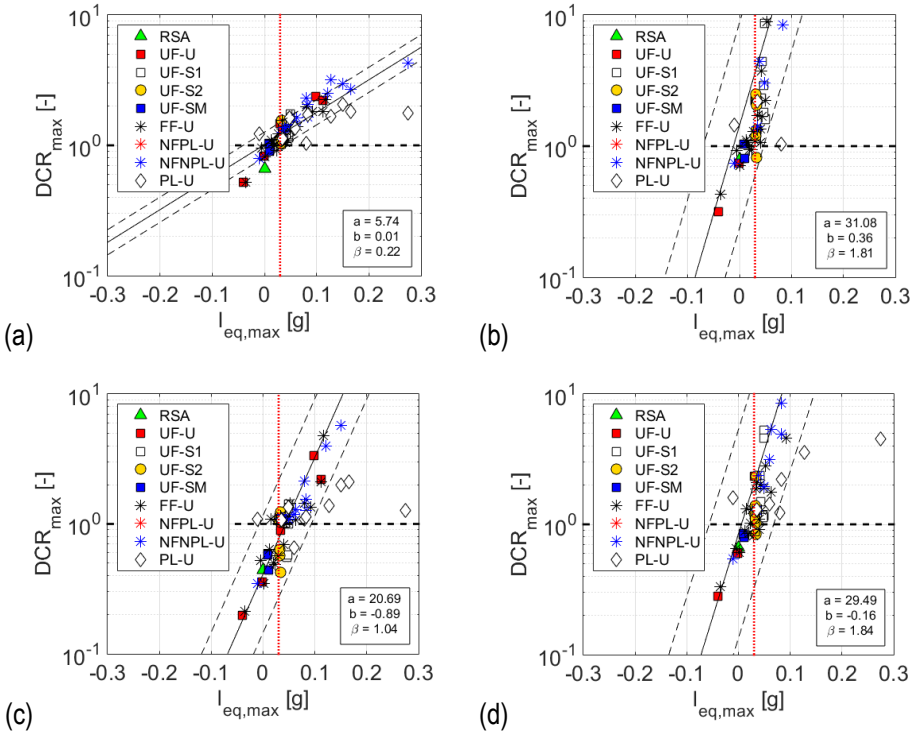

Fig. 6-32 Linear regression (black line) of LTHA results in the plane $I_{eq,max}$ vs DCR_{max} at LS-LS, ±σ confidence bands (black dashed lines) and optimal value of I_{eq} (red dashed line) for different groups of structural members: (a) floor beams, (b) staircase beams, (c) columns, and (d) squat columns.

6.2.2.1. Suite of Far-Field Unscaled (FF-U) and Near-Field Pulse/Not Pulse-Like Unscaled (NFPL-U/NFNPL-U) GMs

In order to consider earthquakes that may experience shaking dependant on directivity (e.g., Somerville et al. 1997; Abrahamson 2000), the far-field and near-field GM suites provided by FEMA P-695 (FEMA 2009) are considered herein. The far-field suite includes 22 earthquakes from sites located at least 10 km from the fault rupture. The near-field suite includes 28 earthquakes from sites located within 10 km from the fault. From the latter suite, 14 earthquakes with strong pulses (called Pulse-Like) and 14 earthquakes without such pulses (called Not Pulse-Like) were judged by wavelet analysis classification (Baker 2007). Three suites are considered in this study: (i) the suite of Far-Field Unscaled (called FF-U) GMs; (ii) the suite of Near-Field Pulse-Like Unscaled (NFPL-U) GMs; (iii) the suite of Near-Field Not Pulse-Like Unscaled (NFNPL-U) GMs. These GMs are downloaded from the latest version of the PEER NGA-West2 ground motion database (PEER 2014). For the near-field conditions rotation of the GMs to the fault-normal (FN) and fault-parallel (FP) directions given the strike angle is adopted (see Section 4.2.3), as recommended by the FEMA P-1050.

6.2.2.2. Suite of Pulse-Like Unscaled (PL-U) GMs

Finally, a last suite of GMs is considered herein to account for Pulse-Like GMs which show relevant effects on the considered benchmark building (called PL-U). Ten pairs of unscaled real GMs are

selected from the Shahi and Baker's classification (Shahi 2013) to present a pulse period (T_P) smaller than the fundamental period of the structure (T_1). These GMs present T_P between the period of the 3rd and the 6th mode of vibrations of the benchmark building and they are expected to excite in a relevant way the higher modes of vibration of the building (see Fig. 6-33). In agreement with the previous section, GMs are rotated to FN and FP directions.

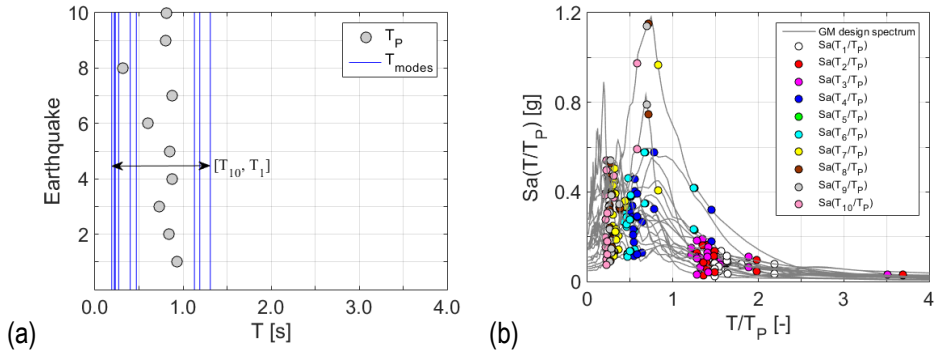

Fig. 6-33 The unscaled pulse-like GMs having T_P<T_1 selected for the PL-U suite at LS-LS: (a) pulse periods of such GMs and (b) their design spectral accelerations in function of T/T_P where the condition T_{modes}/T_P identifies the design spectral acceleration of the GMs corresponding to the periods of vibration of the benchmark building.

6.2.3. I_{eq} versus $I_{eq,SRSS}$

In the following, the proposed I_{eq} index is compared to $I_{eq,SRSS}$, the latter implementing the Square Root of the Sum of Squares (SRSS) of the spectral differences as per Eq. (6.2). The SRSS of the spectral differences is a well-established approach for ground motion selection strategies in literature (e.g., Naeim et al. 2004; Jayaram et al. 2011). For this reason, this section is meant to investigate the suitability of I_{eq} and $I_{eq,SRSS}$ for the purpose of LTHA ground motion selection.

$$I_{eq,SRSS,j} = \sqrt{\sum_{i=1}^{n_p}\left[P_i\left(S_{ae,eq,j}(T_i) - S_{a,target,j}(T_i)\right)^2\right] \Big/ \sum_{i=1}^{n_p} P_i} \qquad j = 1,2 \qquad 6.2$$

I_{eq} and $I_{eq,SRSS}$ are evaluated for each ground motion component of the suites described in Section 6.2.2. The comparison is showed in Fig. 6-34a in terms of I_{eq} versus $I_{eq,SRSS}$ for the same ground motion component. It is possible to observe that $I_{eq,SRSS}$ always provides larger values than I_{eq} as confirmed by the points located above the bisectors. For ground motion spectra characterised by always positive spectral differences (i.e., $S_{ae,eq}(T_i) > S_{a,target}(T_i)$) the two indexes tends to align along the right-hand bisector. In analogy, for ground motion spectra characterised by always negative spectral differences (i.e., $S_{ae,eq}(T_i) < S_{a,target}(T_i)$) the two indexes tends to align along the left-hand bisector. However, when the spectral differences are negative and positive at different periods, $I_{eq,SRSS}$ tends to divert from I_{eq}. In order to quantify the differences between I_{eq} and $I_{eq,SRSS}$, the Pearson's linear correlation coefficient, denoted by ρ is evaluated for each ground motion suite (see Fig. 6-34b). From Fig. 6-34b, it is possible to observe that the correlation between I_{eq} and $I_{eq,SRSS}$ is always positive for the selected suites in this paper and it is small for the optimised ground motion

suite UF-S2 being ρ = 0.14. On the contrast, when ground motions are selected to be higher with respect to the target spectrum, e.g. NFPL-U, the correlation between I_{eq} and $I_{eq,SRSS}$ is large being ρ = 0.85.

The $I_{eq,SRSS}$ implements the SRSS of the spectral differences that has been widely applied for NTHA ground motion selection. It is difficult to state if I_{eq} can provide a better performance in ground motion selection than $I_{eq,SRSS}$. However, I_{eq} having the sign is more informative than $I_{eq,SRSS}$ for potential scaling or changes of single ground motions within a suite.

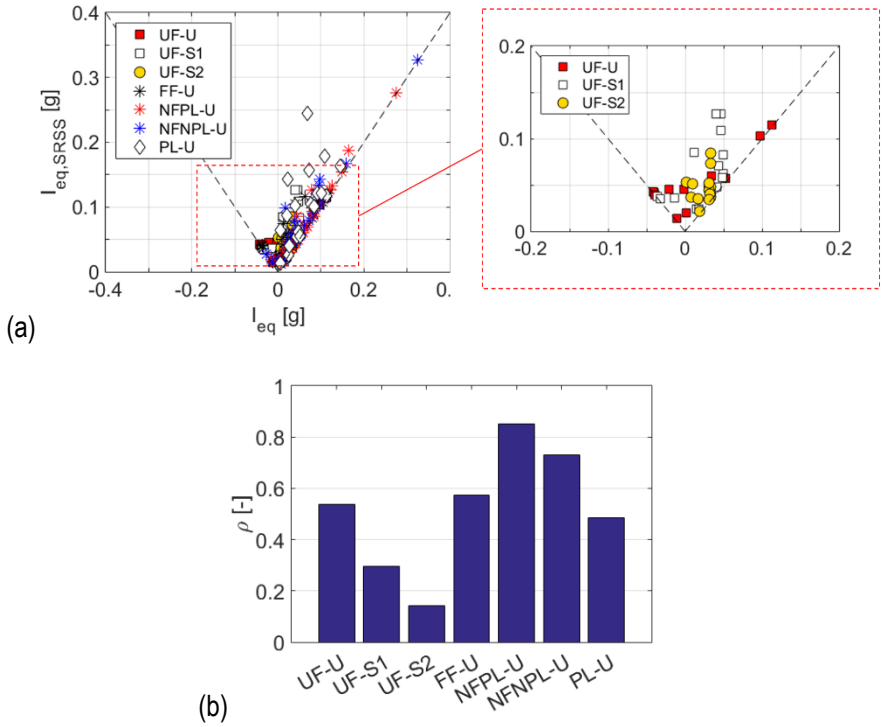

Fig. 6-34 I_{eq} versus $I_{eq,SRSS}$: (a) values of the indexes for each ground motion component of the suites, and (b) Pearson's linear correlation coefficient (ρ) for each ground motion suite.

6.2.4. Design comparison at Damage Limitation-Limit State

At DL-LS conditions, it is expected that there is only slight damage of the structural members (prevented from significant yielding) and some minor non-structural damage (e.g. cracks in infills and partitions), but the damage is economically repairable. In other words, it is expected that the structure has neglectable permanent drifts and it does not need any repair measures (IBC 2018). The reference seismic action for the benchmark building is expressed in terms of elastic target spectrum with 63% probability of exceedance in 50 years (return period of 50 years) (IBC 2018). EC8-1-based design at DL-LS requires a deformability check on the maximum IDR of the building. As explained in Section 3.3, the benchmark building is characterised by infills that are in contact with the frame without any structural connection with it. In this case, the EC8-1 only requires checking that the maximum IDR is lower than 0.5%. This verification, however, was not critical for the benchmark

building designed through RSA since the maximum IDR was equal to 0.2% (see Section 3.3.6). In order to show a comparison between LTHA and RSA at DL-LS, one suite of GMs is considered herein, and results are commented in terms of seismic demand and subsequently in terms of DCR values from IDR verifications at different storeys.

A suite of seven pairs of unscaled real GMs is selected from the European Strong Motion database (ESM 2008) to be spectrum-compatible with the target spectrum for the DL-LS. Such suites are meant to be selected without any distinction in terms of field conditions. The selection of the GMs is performed through the Matlab-based software REXEL (Iervolino et al. 2010a). The spectrum-compatibility is performed so that the average of the selected GMs (μ) matches the target spectrum between 10% lower and 30% upper tolerances over the period range [0, 4] seconds, even if the required period range is [$0.2T_1$, $2T_1$]. It is worth mentioning that the 30% upper tolerance is not indicated by EC8, but it is suggested in Iervolino et al. (2010a). The goodness of the spectrum-compatibility can be observed in Fig. 6-35a. Fig. 6-35b shows the disaggregation of the seismic hazard at the site of interest obtained through REXEL. It results that for spectral acceleration corresponding to one second, the earthquakes contributing to the hazard at the site are in the intervals of moment magnitude and source-to-site distance equal to [4.5, 7.3] M and [0, 70] km, respectively. Notwithstanding the good matching of the average spectrum to the target spectrum, the variability of the selected spectra is high, indicated in Fig. 6-35a by the average ± one standard deviation ($\mu \pm \sigma$). The high variability is due to earthquake #3 that represents the strongest earthquake within the GM suite.

The comparison between RSA and LTHA is shown in Fig. 6-36 in terms of maximum IDR along X and Y directions over time and combinations. It is worth mentioning that according to the EC8, the average of the results obtained from the seven pairs of GMs should be used for design purposes. The Coefficient of Variation (CoV) at each storey and for both the directions ranges within the interval [0.75, 1.16] with maximum values at the intermediate storeys (see Fig. 6-37). The comparison between LTHA and RSA shows relative error ranging between [0.39, 0.86] with maximum values at the upper storeys (see Fig. 6-38).

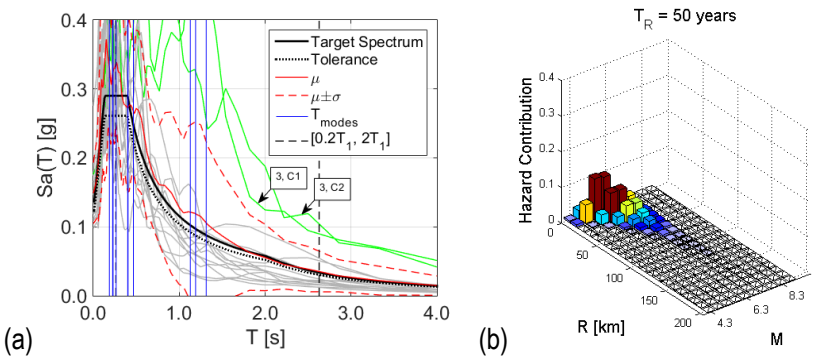

Fig. 6-35 GM selection at DL-LS: (a) elastic spectra and (b) disaggregation for S_a(1 s) of the seismic hazard at Pettino, L'Aquila (Italy) for DL-LS (T_R = 50 years) obtained from REXEL (Iervolino et al. 2010a). In the figure μ denotes the average spectrum and ±σ its one standard deviation.

Results in Fig. 6-39 show that the maximum DCR value is always lower than unity. Indeed, the deformability verification was not restrictive when the benchmark building was designed through RSA (see Section 3.3.6). Contrarily to the average DCR values expressed in terms of local forces, the average DCR values expressed in terms of displacements are not relevantly affected by the strongest earthquake within the GM suite (i.e., earthquake #3 in Fig. 6-39). However, the high variability of the average results still needs to be controlled (see Fig. 6-36). The optimal GM selection for DL-LS is not investigated herein because verifications for this limit state are not critical for the benchmark building (i.e., DCR values much lower than unity and no unacceptable cases occur). When this verification is relevant, the optimisation of the GM selection for DL-LS can be performed, without loss of generality, in the same way as showed for LS-LS by using the proposed I_{eq} index evaluated in terms of elastic response spectra.

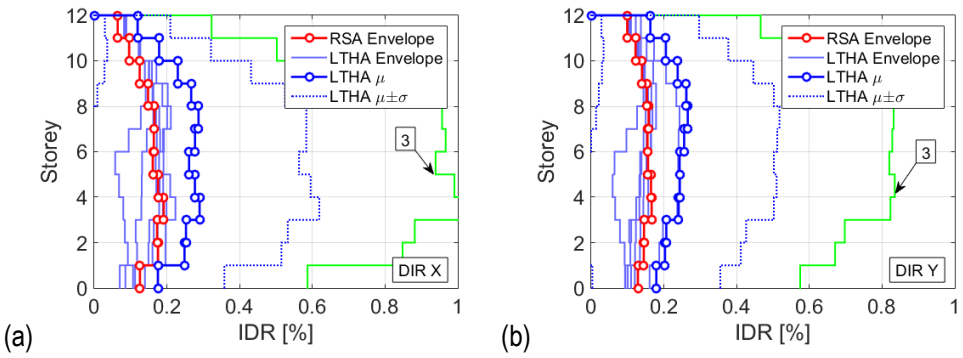

Fig. 6-36 Comparison of the seismic demand between LTHA and RSA in terms of maximum Interstorey Drift Ratio (IDR) along X and Y directions at DL-LS. In the figure μ denotes the average, ±σ its one standard deviation and "envelope" the envelope of the seismic combinations. Plots indicated by the text boxes represent the most critical earthquakes for LTHA design.

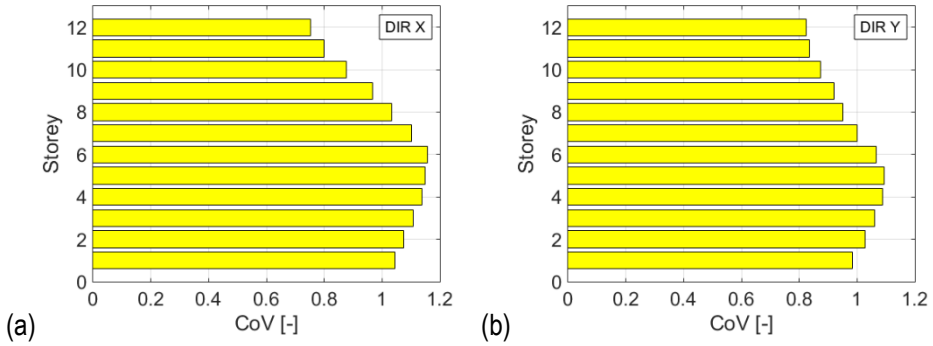

Fig. 6-37 Coefficients of Variation (CoVs) expressed as ratio of the first standard deviation (σ) and average (μ) of the maximum Interstorey Drift Ratio (IDR) along X and Y direction at DL-LS for LTHA.

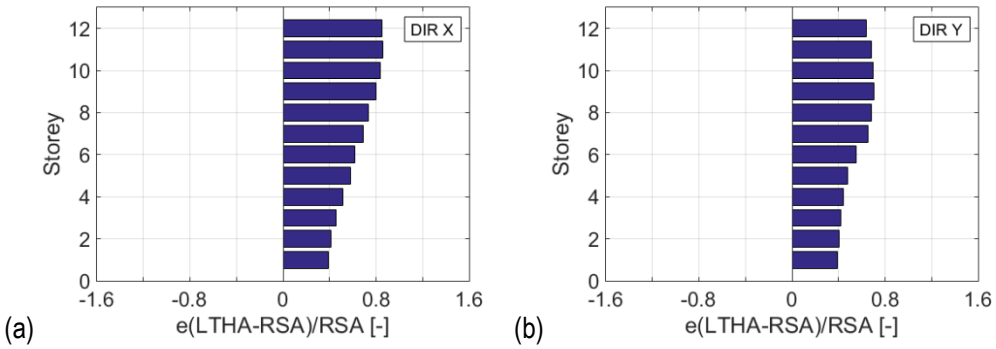

Fig. 6-38 Relative errors between LTHA and RSA in terms of Interstorey Drift Ratio (IDR) along X and Y direction at DL-LS.

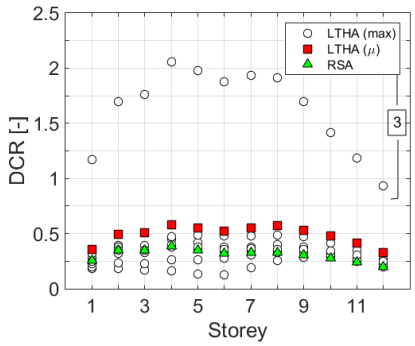

Fig. 6-39 DCR values of LTHA and RSA from deformability verifications at DL-LS. For RSA these results refer to the maximum values of the envelopes at each storey while for LTHA they refer to both the maximum values of the envelopes at each storey for each GM (max) and the maximum values of the means at each storey for the suite (μ).

6.3.LTHA as design method: comparison with NTHA

In this section, results obtained from NTHA are compared to those obtained from LTHA and RSA for the 12-storey RC-MRF benchmark building described in Section 3.3. This comparison is important to provide a better understanding of LTHA results. The code framework for the nonlinear analyses of the benchmark building is described in Section 5.2. For the sake of comparison, the benchmark

building, which is designed through RSA, is assessed through NTHA and comments on LTHA results for some GM suite are presented. The procedure used for LTHA allows a direct comparison between LTHA and NTHA results since the GM selection employed for LTHA is fully compatible with NTHA. In the following, the comparison is presented for two limit states: (i) LS-LS and (ii) DL-LS. The variability of NTHA results is quantified through the Coefficient of Variation (CoV) defined as ratio between the standard deviation and the average. The difference between NTHA and LTHA is expressed in terms of relative error (denoted by e = (LTHA-NTHA)/NTHA) assuming NTHA results as benchmark.

6.3.1. Design comparison at Life Safety-Limit State

Results are compared only for the GM suites UF-U and UF-S2 that represent a case with relevant "unacceptable cases" and one without them, respectively. The UF-U suite is characterised by two "unacceptable cases" represented by earthquake #4 and earthquake #7 having response spectra with $I_{eq,max}$ equal to 0.0976 g and 0.1124 g, respectively (see Fig. 6-2b and Table 6-1). The UF-S2 suite is made of GMs which spectra present $I_{eq,max}$ equal to about 0.03 g, identified in Section 6.2.2 as optimal value for avoiding "unacceptable cases".

The comparison between NTHA and LTHA for UF-U and UF-S2 suites is shown in Fig. 6-40 and Fig. 6-46, respectively, in terms of maximum storey shears along X and Y directions over time and combinations. It is worth mentioning that according to the EC8, the average of the results obtained from the seven pairs of GMs should be used for design purposes. The average of the maximum storey shears evaluated through LTHA are always lower than NTHA. The CoV of NTHA results for UF-U and UF-S2 ranges between [0.14, 0.27] and [0.04, 0.22], respectively (see Fig. 6-41 and Fig. 6-47). The CoVs of LTHA are higher than NTHA, being for LTHA within the ranges of [0.37, 0.66] and [0.07, 0.18], respectively (see Fig. 6-4 and Fig. 6-25). For LTHA, forces are reduced by the behaviour factor q_{LTHA} equal to 4.86 and amplified by the P-Delta amplification factor that ranges between [1, 1.11] for both UF-U and UF-S2 suites. The relative error of LTHA respect to NTHA ranges between [-0.37, -0.67] and [-0.54, -0.69] for UF-U and UF-S2, respectively, with maximum values at the upper storeys (see Fig. 6-42 and Fig. 6-48).

On the contrast, the comparison between LTHA and NTHA at LS-LS in terms of maximum IDR allows different comments. Fig. 6-43 and Fig. 6-49 show the maximum IDR values evaluated through LTHA for UF-U and UF-S2 suite, respectively, compared to those of NTHA. The CoV values of NTHA ranges within the interval of [0.47, 1.02] and [0.15, 0.62] for UF-U and UF-S2, respectively, with the largest values at the lower storeys (see Fig. 6-44 and Fig. 6-50). The CoV values of NTHA are larger than those of LTHA. The relative error of LTHA respect to NTHA ranges between [-0.38, 0.28] and [-0.35 0.24] for UF-U and UF-S2, with overestimations of LTHA at the top storeys (see Fig. 6-45 and Fig. 6-51). NTHA results show that significant plastic deformations occur at the lower storeys where

LTHA underestimates the IDRs. Because of the plastic deformations there is a related reduction of lateral stiffness within the building that LTHA cannot predict.

Fig. 6-52 shows the DCR values in terms of chord rotation at yielding (i.e., DCR_y as per Eq. 5.8a) and chord rotation at LS-LS (i.e., DCR_u as per Eq. 5.8b) obtained from NTHA for UF-U and UF-S2 suites. These results can provide a better understanding of the seismic response of the benchmark building and make some comments about the results of RSA and LTHA. It is possible to observe from NTHA results in Fig. 6-52a that floor beams and landing beams both for UF-U and UF-S2 suite achieved the yielding stage, especially at the intermediate storeys, while flight beams do not yield. On the other hand, columns in Fig. 6-52b, designed through RSA according to capacity design, achieve the yielding stage at the 1st storey while the squat columns show much larger plastic deformations from the 1st to the 8th storey. None of the beams and columns achieves the LS-LS condition for UF-S2, while there is only one case for UF-U that presents DCR equal to 1.02 for the squat columns. For both UF-U and UF-S2, the largest DCR values at LS-LS are shown by the squat columns from the 1st to the 6th storey. RSA results in terms of flexural verifications (see Fig. 6-30) approximately describe a similar condition even though it does not seem to be that critical for the squat columns as much as NTHA shows. LTHA results in Fig. 6-30 describe an excessively conservative condition of the benchmark building compared to NTHA results, especially for the staircase beams and the squat columns. For LTHA, these structural members experience high tensile axial force values that strongly penalise the flexural capacity of their cross-sections. These results show that the "force-based" capacity models typically used for design would lead for LTHA to expensive design solutions that are not necessary as confirmed by NTHA results. In the following a possible solution to this problem is proposed and further results are presented.

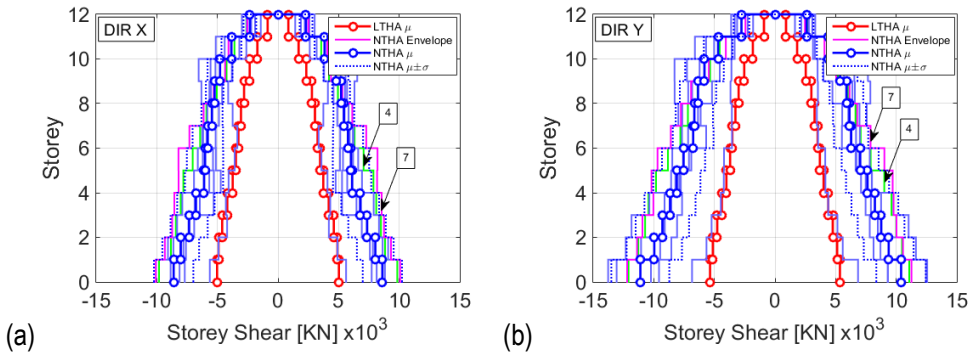

Fig. 6-40 Comparison of the seismic demand between NTHA and LTHA in terms of maximum storey shear along X (a) and Y (b) directions at LS-LS for the suites of UF-U. In the legend μ denotes the average, ±σ its one standard deviation and "envelope" the envelope of the seismic combinations. Plots indicated by the text boxes represent the most critical earthquakes for LTHA design as shown by the corresponding I_{eq} values in Table 6-1.

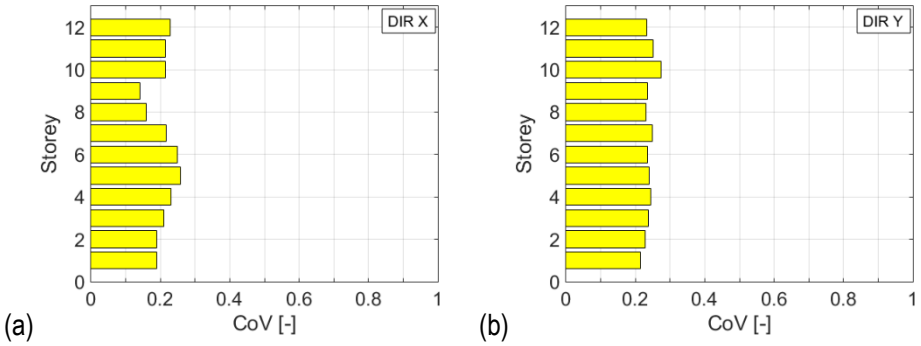

Fig. 6-41 Coefficients of Variation (CoVs) expressed as ratio of the first standard deviation (σ) and average (μ) of the maximum storey shears along (a) X and (b) Y direction at LS-LS for the NTHA suites of UF-U.

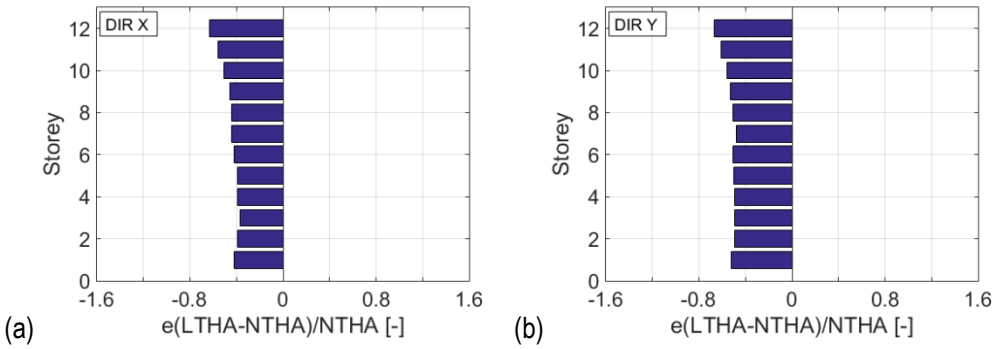

Fig. 6-42 Relative errors between LTHA and NTHA in terms of storey shear along (a) X and (b) Y direction at LS-LS for the suites of UF-U.

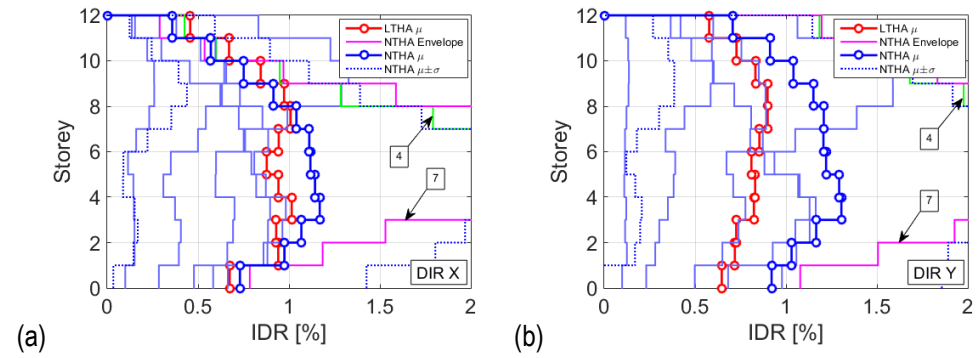

Fig. 6-43 Comparison of the seismic demand at DL-LS between NTHA and LTHA in terms of maximum Interstorey Drift Ratio (IDR) along (a) X and (b) Y direction for UF-U. In the figure μ denotes the average, ±σ its one standard deviation and "envelope" the envelope of the seismic combinations for each earthquake. Plots indicated by the text boxes represent the most critical earthquakes for LTHA design as shown by the corresponding I_{eq} values in Table 6-1.

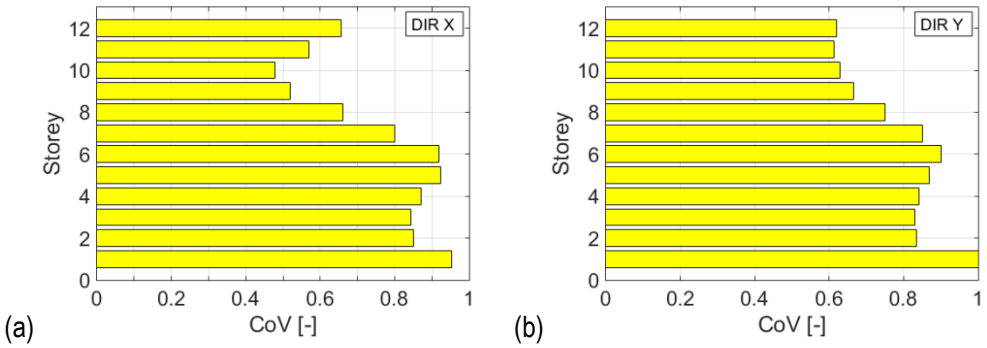

Fig. 6-44 Coefficients of Variation (CoVs) expressed as ratio of the one standard deviation (σ) and average (μ) of the maximum Interstorey Drift Ratio (IDR) along (a) X and (b) Y directions at DL-LS for the NTHA suite of UF-U.

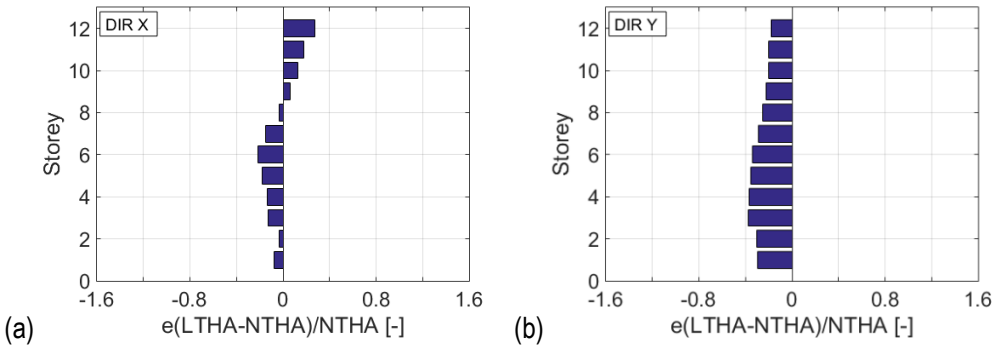

Fig. 6-45 Relative errors between LTHA and NTHA in terms of Interstorey Drift Ratio (IDR) along (a) X and (b) Y direction at DL-LS for UF-U.

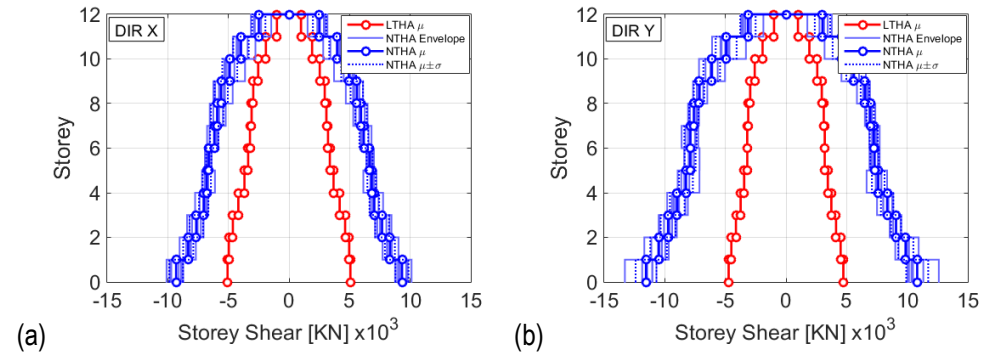

Fig. 6-46 Comparison of the seismic demand between NTHA and LTHA in terms of maximum storey shear along (a) X and (b) Y directions at LS-LS for the suites of UF-S2. In the legend μ denotes the average, ±σ its one standard deviation and "envelope" the envelope of the seismic combinations.

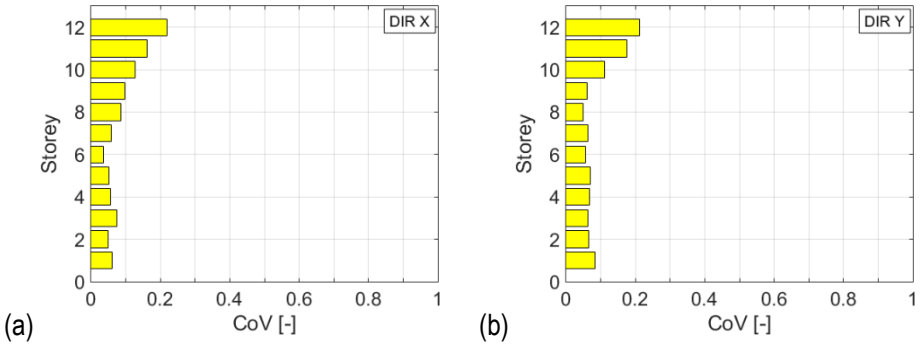

Fig. 6-47 Coefficients of Variation (CoVs) expressed as ratio of the first standard deviation (σ) and average (μ) of the maximum storey shears along (a) X and (b) Y direction at LS-LS for the NTHA suites of UF-S2.

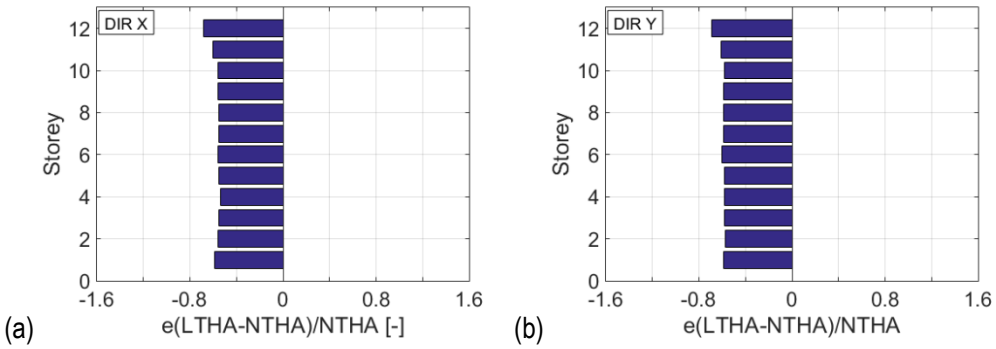

Fig. 6-48 Relative errors between LTHA and NTHA in terms of storey shear along (a) X and (b) Y direction at LS-LS for the suites of UF-S2.

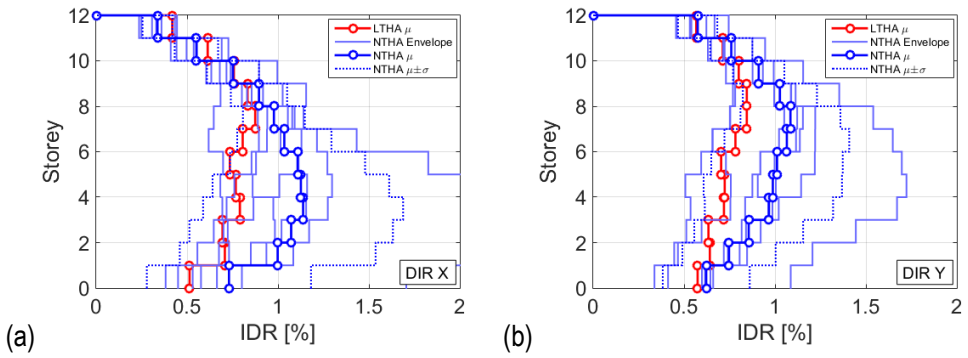

Fig. 6-49 Comparison of the seismic demand at DL-LS between NTHA and LTHA in terms of maximum Interstorey Drift Ratio (IDR) along (a) X and (b) Y direction for UF-S2. In the figure μ denotes the average, ±σ its one standard deviation and "envelope" the envelope of the seismic combinations for each earthquake.

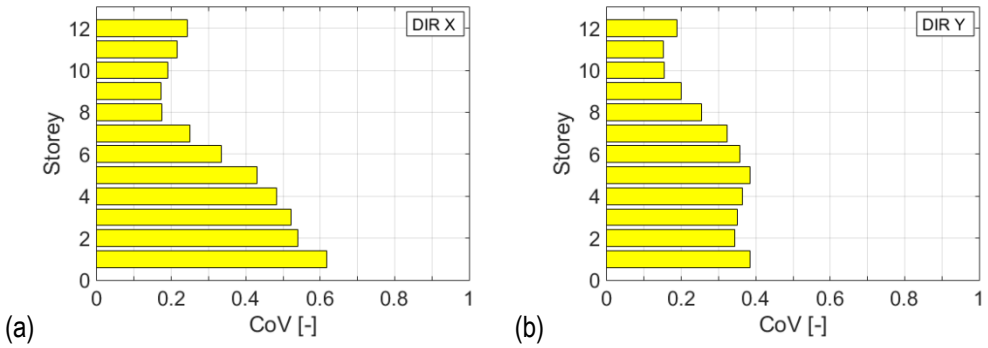

Fig. 6-50 Coefficients of Variation (CoVs) expressed as ratio of the one standard deviation (σ) and average (μ) of the maximum Interstorey Drift Ratio (IDR) along (a) X and (b) Y directions at DL-LS for the NTHA suite of UF-S2.

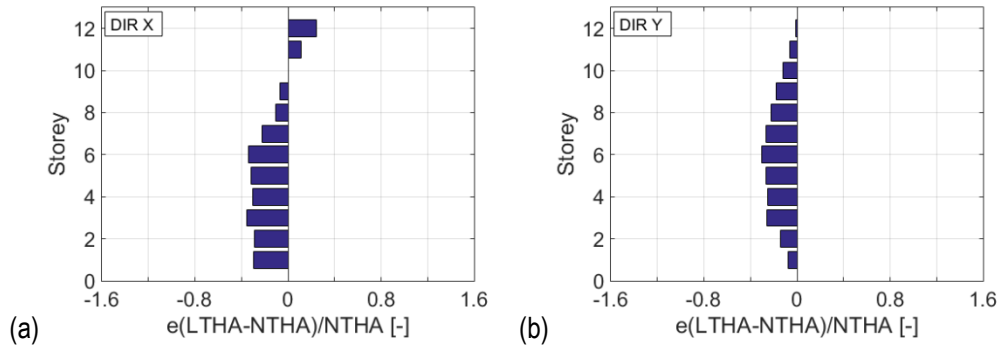

Fig. 6-51 Relative errors between LTHA and NTHA in terms of Interstorey Drift Ratio (IDR) along (a) X and (b) Y direction at DL-LS for UF-S2.

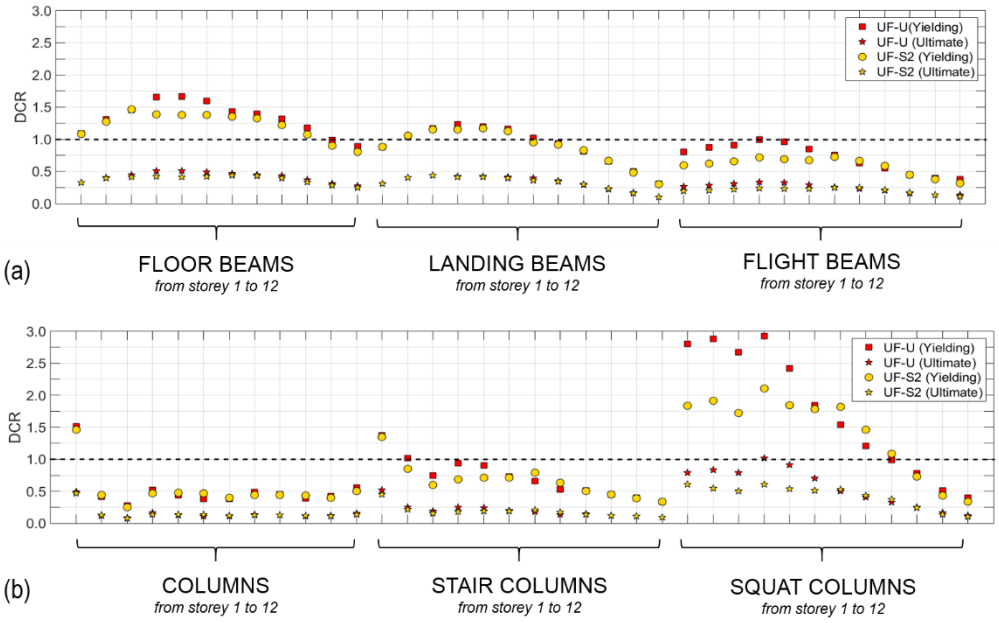

Fig. 6-52 Mean DCR values of NTHA from flexural verifications in terms of chord rotation at yielding and LS-LS for (a) beams and (b) columns. These results refer to the maximum values of the means at each storey for each suite.

6.3.2. Design comparison at Damage Limitation-Limit State

In the case of buildings having infills considered as non-structural elements made of brittle materials without any gap to the structure, the EC8-1 indicates to control the IDR and to assume a limit equal to 0.5% for verifications. The IDR as global structural response parameter is an effective global representation of local element rotations (due to rotations in the columns, beams and panel joints) for moment resisting frames (Fardis 2009). However, the EC8-3 does not give any limit for IDR at DL-LS but it provides a formulation to evaluate the chord rotation capacity at yielding (θ_y). It is also suggested in literature to not verify existing buildings in terms of IDR at DL-LS unless the infills are included in the model (Fardis 2009). In this light, results of LTHA are compared to those of NTHA considering for the latter DCR values expressed both in terms of chord rotation and IDR. It is worth mentioning that the DCR values in terms of chord rotation are assumed as benchmark for the comparisons in the following.

It is expected that LTHA leads to unconservative results with respect to NTHA when the elastic stiffness of the structural members is considered as uncracked for RC and masonry structures (see Section 4.2.1). For these structures, the cross-section flexural stiffness of members should account for an equivalent reduction of stiffness (e.g., from cracking). This can be obtained by reducing the second moment of area (i.e., $I = \alpha I_g$ where I_g is the gross uncracked second moment of area and α is the equivalent stiffness reduction factor). While nonlinear models with fibre-sections can account for the effective stiffness of the structural members during the earthquake, the equivalent reduction of stiffness for linear models is an approximate approach to consider the secant stiffness at yielding (Fardis 2009). For design purposes, the secant stiffness at yielding would rigorously depend on the design of the members itself and analysis iterations should be performed. The benchmark building considered in this research work accounts for α = 50%, according to the EC8-1. In the following different cases for the equivalent stiffness factor are analysed for LTHA, such as: (i) linear model without any reduction (Case 1, α = 100%), (ii) linear model with α adopted according the EC8-1 (Case 2, α = 50%), (iii) linear model with α equal to 40% and 70% for beams and columns, respectively, as suggested in some design codes (SNZ 2004, ACI 2008) for the magnification of moments in compression members and frames due to second-order effects (Case 3, α_b = 40% and α_c = 70%), and (iv) a more simplified assumption based on the previous one where α is equal to 40% for columns considering columns subjected to tensile axial forces and high ductility frames in serviceability limit state conditions (Priestley 2003).

Table 6-4 reports the relevant periods of vibration of the linear model considering different cases for the equivalent stiffness reduction factor α, together with the same periods evaluated for the nonlinear model with initial stiffness, where the difference between the periods of the nonlinear model and the linear one, the latter having uncracked gross-sections (α = 100%), is due to the contribution of the steel longitudinal reinforcement in fibre models.

Table 6-4 Periods of vibration of the benchmark building for LTHA (considering different equivalent stiffness reduction factors α) and NTHA.

Structural model	**Case**	**Periods of vibration T_i [s]**									
		1	***2***	***3***	***4***	***5***	***6***	***7***	***8***	***9***	***10***
Linear α = 100%	1	0.94	0.91	0.82	0.33	0.31	0.29	0.19	0.17	0.17	0.13
Linear α = 50%	2	1.31	1.19	1.13	0.47	0.40	0.40	0.27	0.23	0.22	0.19
Linear α_b = 40%, α_c = 70%	3	1.36	1.20	1.16	0.48	0.41	0.40	0.27	0.23	0.22	0.18
Linear α = 40%	4	1.47	1.30	1.25	0.52	0.44	0.44	0.30	0.26	0.25	0.21
Nonlinear	-	0.93	0.90	0.81	0.33	0.30	0.29	0.19	0.17	0.16	0.13

The difference between Linear model Case 1 (i.e., uncracked cross-sections) and Nonlinear model is attributable to the minor stiffness contribution of steel longitudinal reinforcement modelled in fibre-section models and typically neglected in linear models.

To investigate the differences between LTHA and NTHA at DL-LS, 24 earthquakes are chosen from the latest version of the PEER NGA West2 ground motion database (PEER 2014), having moment magnitudes ranging within the interval of [5.1, 7.4] and source-to-site distance within the interval of [0, 123] km (see Fig. 6-53a). No restrictions are imposed regarding the distances, fault-type, soil type.

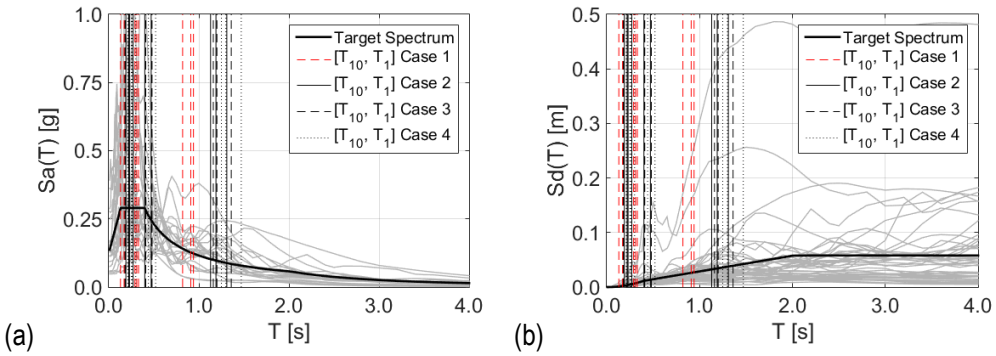

Fig. 6-53 GM for evaluating the influence of the equivalent stiffness factor (α) at DL-LS for LTHA: (a) elastic response spectra in terms of pseudo-acceleration and (b) corresponding spectra in terms of displacement ($Sd = Sa / \omega^2$, $\omega = 2\pi/T$). In the figure [T_{10}, T_1] denotes the period interval of the relevant modes of vibration of the benchmark building for different cases of equivalent stiffness factors (Case 1 to 4 in Table 6-4).

Fig. 6-54 shows the DCR values obtained from analysing the building through NTHA and LTHA, the latter considering different equivalent stiffness reduction factors (Case 1 to 4 in Table 6-4). NTHA results represent the benchmark and results are shown both in terms of IDR and chord rotation (Fig. 6-54b). It is possible to observe that DCR values in terms of IDR obtained through NTHA are, on

average, larger than those in terms of θ, even if very similar being the average of the DCR values (denoted by μ_{DCR}) equal to 0.91 against 0.82. LTHA, regardless of the adopted stiffness reduction, not always leads to larger DCR values (Fig. 6-54a). This aspect mainly depends on the fact that every earthquake has different dynamic properties and the stiffness reduction that would maximise the displacements of the building would rigorously depend on the earthquake itself (see Fig. 6-53b). Moreover, such reduction of stiffness should be consistent with that adopted for LS-LS. The difference between NTHA and LTHA seems to be minimised if the first is compared with DCR evaluated in terms of θ, which is also what EC8-3 recommends for the assessment of existing buildings. Case 2 (i.e., α = 50%, assumed as benchmark in this study), similarly to Case 3, leads to DCR values larger than NTHA with DCR evaluated in terms of θ for 13/24 earthquakes (54%) while Case 4 for 14/24 earthquakes (~58%). However, on average, the difference between them is neglectable. The use of uncracked gross-sections (Case 1) leads to larger DCR values for LTHA for only 6/24 earthquakes (~25%) and it is not recommended.

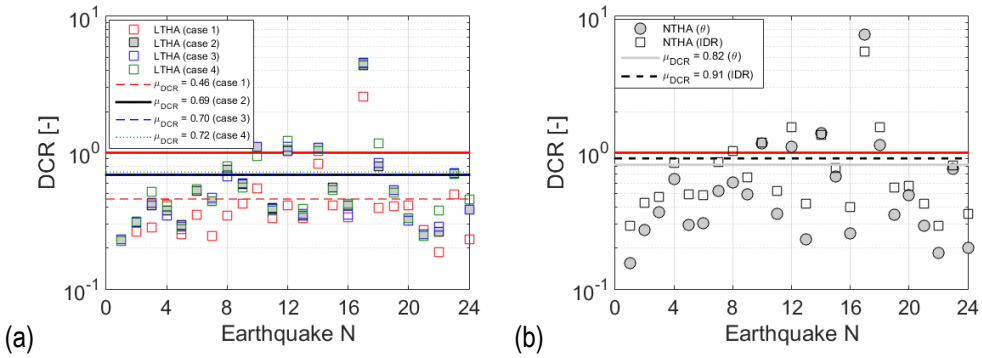

Fig. 6-54 Maximum DCR values at DL-LS of 24 earthquakes for: (a) LTHA in terms of Interstorey Drift Ratio (IDR) considering different stiffness reduction factors (α), and (b) NTHA in terms of both chord rotation (θ) and IDR. The average of these results is denoted by μ_{DCR}.

6.4.LTHA as assessment method

LTHA results for LS-LS presented in Fig. 6-30 are obtained considering capacities of beams and columns with the design strength of concrete and steel reinforcement evaluated according to the EC2 (i.e., f_{cd} = 0.85 f_{ck}/1.5 and f_{syd} = f_{syk}/1.15). This assumption is consistent with "force-based" design approach through linear analyses that is based on verifications in which the design seismic demand in structural members is checked against the design capacity of them. In the following, a further investigation of LTHA as assessment method, without using design material strenghts but considering the mean values in LTHA verifications, is attempted herein to investigate more in detail the above discrepancies. Fig. 6-55 shows the comparison between RSA and LTHA, the latter implementing DCR values with mean capacities. It is possible to observe that unacceptable cases still occur for UF-U as shown by the disproportionately high values of DCR for flight beams and squat columns. However, the condition described by UF-S1 and UF-S2 suite (selected through I_{eq} index) seems much more convenient. NTHA results in Fig. 6-52 showed that flight beams are not the critical

members within the building while squat columns exhibit relevant plastic deformations with the highest DCR values. The assumption of mean capacity for UF-S2 leads to LTHA results that are more consistent with RSA and NTHA results. While RSA can make some approximation in the evaluation of the DCR values of flight beams and columns (because these elements are characterised by interaction of axial force with bending moment that is not accurately evaluated through CQC), LTHA leads to higher DCR values for these elements, especially for the squat columns which are the critical members within the building as shown by NTHA. On the contrast, this assumption seems too convenient for LTHA employing spectral-matched GMs (UF-SM) that leads to DCR values even lower than RSA.

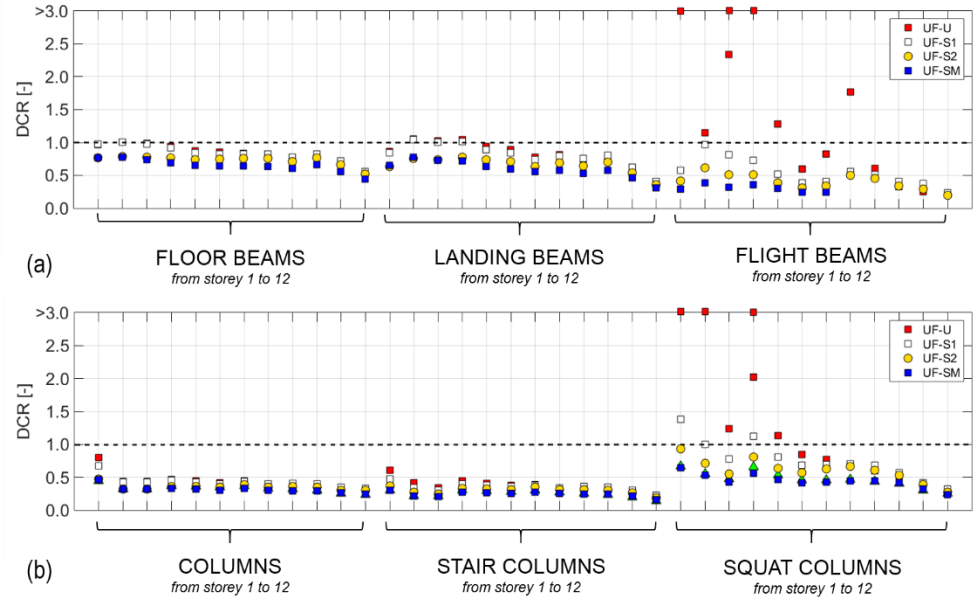

Fig. 6-55 Mean DCR values of LTHA from flexural verifications at LS-LS for (a) beams and (b) columns. For UF-SM these results refer to the maximum values of the envelopes at each storey while for other LTHA suites (i.e., spectrum-compatible suites) they refer to the maximum values of the means at each storey for each suite.

6.5.Conclusion

The scope of this chapter is to investigate on LTHA as a novel seismic design method of analysis. In the previous chapters an EC8-compliant LTHA design framework was proposed that is based on a seismic input selection compatible with that allowed for NTHA for design purposes. Thanks to this aspect, it is possible to compare directly results of LTHA and NTHA and provide some useful comments. Firstly, LTHA results are compared to those obtained from RSA by analysing the 12-storey RC-MRF benchmark building of this research work. Results shows that:

- LTHA, whether the seismic input is characterised by spectrum-compatible or spectral-matched GMs, provides higher seismic demand in terms of local forces with respect to those predicted by RSA for the 12-storey RC-MRF building considered in this thesis;

- The difference between LTHA employing three pairs of spectral-matched GMs (referred as to UF-SM suite) and RSA shows that the largest difference is always found at the upper storeys in terms of both storey shears (+79%) and maximum interstorey drift ratios (+41%). Some lower estimations for LTHA with respect to RSA are found at the intermediate storeys (-4%). The maximum CoV is equal to 0.20;
- LTHA employing seven pairs of spectrum-compatible GMs can show significant variability (i.e., CoVs) of the seismic demand in terms of both storey shears and interstorey drift ratios (e.g., UF-U suite). Moreover, design can be affected by "unacceptable cases" which are related to the outliers within the GM suite. These unacceptable cases are certainly due to the high seismic demand imposed to beams and columns by the strongest earthquakes within the GM suite but are also due to the limits of the capacity models typically employed for "force-based" design of structural members. It is found that the most critical members in the benchmark building are the staircase beams and the squat columns which are subjected to high tensile axial forces that drastically reduce the flexural capacity of these members;
- Unacceptable cases can be controlled when the proposed index I_{eq} is used for selecting GM suites. This index can identify the earthquakes that very likely lead to "unacceptable cases". It is found for the analysed case study that the optimum value of I_{eq} that allows to limit the effect of the "unacceptable cases" is 0.03 g. This value is obtained from fitting the results obtained from 84 earthquakes, considering far-field and near-field pulse/not pulse-like GMs. The comparison between LTHA and RSA for the suite selected considering $I_{eq} \approx 0.03$ g (i.e., UF-S2 suite) shows results certainly more convenient compared to other analysed GM selections, with largest differences at the upper storeys in terms of both storey shears (+119%) and interstorey drift ratios (+74%). The maximum CoV is equal to 0.32.

Subsequently, LTHA results are compared to those obtained through NTHA. It is found that:

- NTHA results allows to get a better understanding of the condition of the benchmark building. According to the expected dissipative mechanism aimed by EC8 design, beams show plastic hinge dissipation together with the columns at the first storey. However, it is found that most of the plastic deformations are localised in the squat columns from the 1st to the 8th storey which show the highest DCR value in terms of chord rotation at LS-LS stage. For suite UF-U such value is equal to 1.02 while for UF-S2 it is equal to 0.61. Floor beams at the intermediate storeys and other columns at the first storey achieve about 1.5 times the chord rotation at yielding stage. These results show that LTHA without control of unacceptable cases is too conservative;
- It is found that the use of mean values of properties for concrete and steel (i.e., f_{cm} and f_{sym}) for evaluating the capacity of beams and columns rather than the design values (i.e., f_{cd} = 0.85 f_{ck}/1.5 and f_{syd} = f_{syk}/1.15) represents an alternative that leads to results more consistent

with NTHA results. While RSA can make some approximations in evaluating the "actual" interaction between axial force and bending moment for staircase beams and columns, LTHA is more accurate than RSA and the results found are better describing the situation of the benchmark building as compared to NTHA results. However, this approach needs further investigations because it seems suitable for assessment but not suitable for design where the material properties should be those required in design, i.e. f_{cd} and f_{syd};

- Results at DL-LS for 24 earthquakes show that LTHA, on average, underestimates the seismic demand in terms of maximum interstorey drift ratios compared to NTHA for the benchmark building. Several procedures for taking into account the equivalent stiffness reduction factor (α) of the reinforced concrete members for LTHA are considered. It is shown that for α = 50%, which is the value recommended by the EC8-1, LTHA underestimates, on average, the maximum interstorey drift ratios of NTHA of about 32%. However, the EC8-3 suggests using the chord rotation at yielding stage for DL-LS. In this case LTHA with α = 50% underestimates, on average, the DCR value of NTHA of about 17%. These results would suggest the in order to make LTHA conservative for design purposes at DL-LS, displacements should be amplified by a coefficient rather than furtherly reduce the elastic stiffness of the members.

Chapter 7: LTHA for Simplified Fragility Assessment

Part of this chapter is based on the following reference:

Lombardi L and De Luca F (2019). Linear Time-History Analysis for Fragility Curves at Design Stage, Earthquake Engineering and Structural Dynamics (under review).

Objectives of this chapter

This chapter introduces Linear Time-History Analysis (LTHA) as simplified method to derive fragilities at design stage within the performance-based seismic design methodology. This novel approach is herein investigated for the 12-storey Reinforced Concrete-Moment Resisting Frame (RC-MRF) benchmark building designed through modal Response Spectrum Analysis (RSA) and assessed through LTHA and Nonlinear Time-History Analysis (NTHA). It is meant to open up new opportunities for professional applications towards a time-efficient simplified performance-based approach to derive fragility curves through LTHA for comparison of different design solutions without the necessity to develop a nonlinear model. The objectives of this chapter are:

- to present the proposed LTHA-based fragility assessment framework at design stage for ultimate and serviceability limit states. This framework is EC8-compliant, it being based on a preliminary design through RSA and subsequent assessment through LTHA assuming an EC8-compliant ground motion selection;
- to demonstrate the suitability of LTHA to derive fragility curves at design stage by comparing results to those obtained through NTHA for the same seismic input. This can be obtained through a direct comparison of the assumptions characterising ground motion selections, modelling choices, and acceptance criteria;
- to assess the sensitivity of the fragilities to ground motion suite size through robust fragility assessment and bootstrap method in order to investigate the possibility of using a limited number of ground motions while considering an acceptable level of accuracy;
- To assess the influence of LTHA "unacceptable cases" at ultimate limit states, providing a simple tool to avoid bias in fragility estimation based on the proposed I_{eq} index which can be easily used by designers and analysts.

7.1.Introduction

Performance-based seismic design is considered as an alternative to current code-based prescriptive design procedures, for its capability to demonstrate that a certain design solution can provide one or more defined levels of performance in order to meet stakeholder's expectations

(FEMA 2018c). As explained in Section 2.4, performance of buildings is typically quantified in probabilistic terms, considering inherent uncertainties, using metrics directly understood by stakeholders, such as repair cost, repair time, casualties, etc. Such performance is expressed in terms of a series of discrete performance levels which are applied to both structural and non-structural components. The probable performance can be evaluated considering different approaches for the seismic hazard level characterisation, such as a specific elastic response spectrum, or an earthquake scenario consisting of specific magnitude and source-to-site distance, or all the earthquakes that may occur in a specific time period for cost-benefit analysis (FEMA 2018c). FEMA P-58 provides guidelines for implementing the performance-based seismic design of buildings methodology which can be applied to assess the performance of a given building, to design a new building for a desired performance, and to design the retrofit of an existing building. The technical basis of the methodology is the framework for Performance-Based Earthquake Engineering (PBEE) developed by the Pacific Earthquake Engineering Research (PEER) center (Moehle and Deierlein 2004) which assumes NTHA as reference method for structural analysis of buildings. Simplified analysis procedures based on equivalent lateral force methods are also allowed but with some restrictions on regularity, height, and usable engineering demand parameters (FEMA 2018a). In this procedure, design is iteratively assessed until the design meets the targeted building performance. The same FEMA P-58 recommend using simplified methods of analysis for preliminary performance assessment as NTHA can be not practical.

In this chapter, LTHA is proposed as novel method of analysis that can be used for simplified performance-based seismic design. LTHA can overcome the complexity of nonlinear modelling allowing a time-efficient approach for performance-based seismic design. LTHA can be a good means to make practitioners familiar with performance-based approaches and ground motion selection that are aspects typically faced for NTHA and by expert users. In the following, the fragility assessment of the benchmark building is carried out through Cloud Analysis (CA) for the two limit states required by the Italian National Annex: Life Safety-Limit State (LS-LS) and Damage Limitation-Limit State, as already analysed in Chapter 6. The proposed LTHA procedure is based on four steps that are conceived for design purposes: (i) selection of ground motions consistent with the hazard at the site (e.g., range of moment magnitude and source-to-site distance), (ii) identification of possible LTHA "unacceptable cases" through the proposed $I_{eq,max}$ index, (iii) accomplishment of EC8 requirements for ground motion selection (i.e., spectrum-compatibility), and (iv) checking of criteria for CA-based assessment in order to avoid errors in the regression (e.g., Miano et al. 2018). Robust fragility assessment according to Jalayer et al. (2015) is also presented, aiming at incorporating the uncertainty in the assessment of the fragility parameters given the selected GM suite. Moreover, this chapter includes a study on the effects of imposing the spectrum-compatibility in GM selection for CA, and the influence of the GM suite size by implementing the bootstrap method. The bootstrap

method, already used in Vamvatsikos and Cornel (2004), is a resampling technique used to estimate statistics on a population by sampling a dataset with replacement (Tibshirani and Efron 1993). The common approach of considering a single fragility curve can bring large uncertainties and bias in loss estimation unless an elevated number of GMs is carefully chosen to be consistent with the seismic hazard of the site (Kohrangi et al. 2017). For this reason, this research work investigates the possibility of using a limited number of ground motions without compromising significantly the accuracy of results. The proposed procedure can be used within EC8 for the evaluation of probabilistic parameters within performance-based methodologies that can be used at design stage by designers and analysts for comparative loss estimations of different design solutions avoiding the development of a nonlinear model.

The probabilistic model for CA can be expressed as per Eq. 6.2a-b (e.g. Jalayer et al. 2015) where DCR_{LS} is the critical Demand over Capacity Ratio (DCR) for a prescribed limit state (for brevity denoted by DCR) which is expressed in terms of Engineering Demand Parameters (EDPs), $\eta_{DCR|Sa}$ is the median DCR_{LS} given $S_a(T_1)$ (herein assumed as Intensity Measure, IM, for brevity denoted by S_a), a and b are parameters of linear regression in the logarithmic plane $\ln S_a$ versus $\ln DCR$ (which is the standard basis for the underlying lognormal distribution model) of i cloud data-points, and $\beta_{DCR|Sa}$ is the (constant) logarithmic standard deviation. The structural fragility curve can be expressed as per Eq. 6.2c where Φ denotes the standardized Gaussian Cumulative Distribution Function (CDF).

$$\ln \eta_{DCR|S_a} = \ln a + b \ln S_a \tag{6.2a}$$

$$\beta_{DCR|S_a} = \sigma_{\ln DCR|S_a} = \sqrt{\sum_{i=1}^{N} \left(\ln DCR_i - \ln \eta_{DCR|S_{a\,i}}\right)^2 / (N-2)} \tag{6.2b}$$

$$P\left[DCR > 1 \mid S_a\right] = P\left[\ln DCR > 0 \mid S_a\right] = 1 - \Phi\left(\frac{-\ln \eta_{DCR|S_a}}{\beta_{DCR|S_a}}\right) = \Phi\left(\frac{\ln \eta_{DCR|S_a}}{\beta_{DCR|S_a}}\right) \tag{6.2c}$$

It is worth mentioning that this research work does not apply the full PBEE methodology but it is limited to the evaluation of fragility curves at design stage which can be subsequently used for loss analysis according to the methodology in Fig. 2-9 and Eq. 2.14. In Eq. 6.2c, $P\,[DCR > 1|S_a]$ replaces $P\,[EDP > edp \mid IM = im]$ in Eq. 2.14 and DCR is adopted as a proxy for the structural performance variable DV that is convoluted directly with IM to estimate the seismic risk (e.g., Miano et al. 2017).

7.1.1. Fragility comparison at Life Safety-Limit State

The target response spectrum at Life Safety-Limit State adopted herein as representative of the seismic hazard at the site of the benchmark building is the elastic code spectrum corresponding to a probability of exceedance of 10% in 50 years (return period of 475 years). GM selection for LTHA at the ultimate limit states requires a specific strategy. In fact, because of the linear-elastic behaviour of the numerical model, structural responses due to strong earthquakes can lead to “unacceptable cases” in terms of DCR values from flexural verifications of structural members, as showed in Chapter

6. The use of the lexical expression “unacceptable cases” (herein denoted by UCs) recalls the meaning of “unacceptable responses” in the context of NTHA in FEMA P-1050 (BSSC 2015). For NTHA these “unacceptable responses” can be due to dynamic instability collapse, non-convergence limits of the deformation or force-controlled models, etc. Treatment of these cases is an open and debated issue even in the case of NTHA (Haselton et al. 2017b, Zimmerman et al. 2017). However, no UCs are found in this research work when the benchmark building is analysed through NTHA. This is due to (i) the building is designed according to the EC8-1 and (ii) the assessment is carried out at LS-LS, therefore collapses should not occur. It is worth mentioning that fragilities at collapse are not investigated in this work. It was showed in the previous chapter that unacceptable cases for LTHA may occur when the building, designed through RSA for the code response spectrum at LS-LS, is analysed under strong earthquakes which GM spectra significantly differ from the smoothed code spectrum. This results in very high seismic demand on structural members which can lead to observe limitations of the capacity models typically employed for “force-based” approaches (i.e., disproportionate and unrealistic high values of DCRs. In this light, the proposed I_{eq} index can be adopted to select possible GMs for LTHA. Compared to the use of I_{eq} index made in the previous section for design purposes only, here the target is selecting GMs for the purpose of fragility assessment but still avoiding “unacceptable cases” that could affect the evaluation of the parameters for the regression through CA. For this reason, when LTHA is to be used to derive fragilities, an optimal value of I_{eq} for GM selection should be be identified to fulfil the scopes of derivation of fragility curves. To achieve this, a suite of GMs is selected for the assessment of the building at LS-LS. It includes some of the earthquake events presented in the FEMA P-695 (FEMA 2009), already used in Chapter 6. In particular, the far-field list includes 22 earthquakes from sites located at least 10 Km from the fault rupture, while the near-field list includes 14 earthquakes non-pulse-like (near-field pulse-like are not investigated in this study). For the near-field GMs, each pair of horizontal components is rotated to the fault-normal (FN) and fault-parallel (FP) directions, as specified in FEMA P-1050. It results in 36 pairs of horizontal GMs which are used in the following for both LTHA and NTHA. These GMs are compatible with the results of the disaggregation of the seismic hazard at the site in terms of moment magnitude and source-to-site distance (see Fig. 6-31), and their number can be considered sufficient to obtain reliable estimates for fragility assessment (e.g., Shome and Cornell 1999, FEMA 2018a).

Fig. 7-1a shows the spectrum-compatibility of this suite with the site-specific target spectrum (grey line), and Fig. 7-1b the corresponding code-design spectrum accounting for the behaviour factor reduction (q = 5.85) and imposed lower bound value of the pseudo-acceleration (i.e., horizontal design spectrum branch from T = 1.1 s) together with the GM spectra scaled by $1/q_{LTHA}$ (= 1/4.86), according to Section 4.2.2.

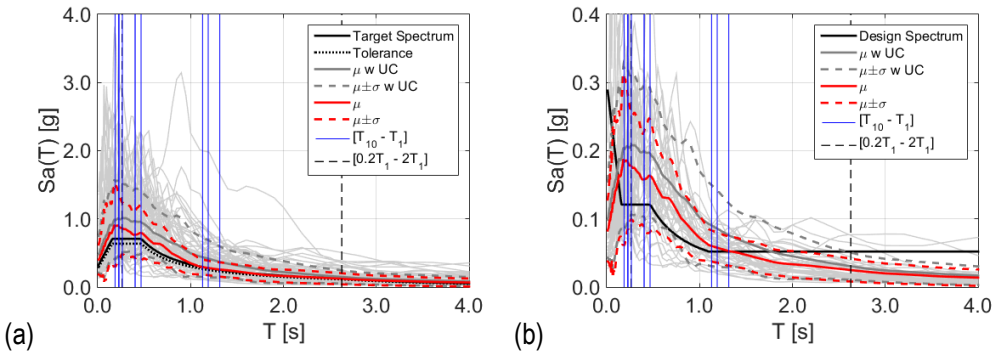

Fig. 7-1 GM selections for fragility assessment at LS-LS for NTHA (grey line) and LTHA (red line that excludes Unacceptable Cases, UC): (a) spectrum-compatibility of the elastic spectra and (b) corresponding design spectra scaled by q_{LTHA}. In the figure μ denotes the average spectrum and $\pm\sigma$ its one standard deviation.

Fig. 7-2a shows the results for each GM in terms of maximum flexural DCR (maximum DCR of the whole structure evaluated from the envelopes among seismic combinations and time) versus the maximum I_{eq} index (maximum between the horizontal GM components). As shown in Fig. 7-2a, UCs occur for values of $I_{eq,max}$ > 0.05 g. This limit is identified through the intersection of two linear regressions: (1) the blue linear regression (having R^2 = 0.71) which fits initial data points showing acceptable values of DCR and (2) the black linear regression (having R^2 = 0.44 if the point having $I_{eq,max}$ = 0.32 g that significantly differs from the others, i.e. outlier, is included otherwise R^2 = 0.75 if it is excluded) which fits data points characterized by high values of DCR. Bilinear regression model was used in past researches to provide more accurate fit of the data instead of using single linear models (e.g., Ramamoorthy et al. 2006). These UCs occur because of the high DCR values of structural members subjected to high axial forces (both tension and compression) and bending moments for the strongest earthquakes. High DCR values occur for both far-field and near-field without any difference. It is worth noting that if UCs are considered, LTHA would lead to the mean values in terms of DCR (μ_{DCR}) strongly dependent on the outliers (e.g., μ_{DCR} = 804 over 36 earthquakes in Fig. 7-2a). Contrarily, if μ_{DCR} is evaluated considering a selection of GMs, excluding the earthquakes with $I_{eq,max}$ > 0.05 g, it would lead to a value reflecting reasonable result for a DCH structure designed according to EC8 through RSA (i.e., μ_{DCR} = 1.36 over 20 earthquakes in Fig. 7-2a). Moreover, the exclusion of these earthquakes would result in 20 earthquakes which lead to a better spectrum-compatible GM suite (red line in Fig. 7-1).

Fig. 7-2b displays the comparison of the DCR values obtained from LTHA in terms of bending moment with NTHA in terms of chord rotation at LS-LS. LTHA leads to higher values of DCR in 94% of cases. It is worth mentioning that since the building is designed according to modern seismic criteria, it is generally expected that its condition is not critic at LS-LS when the structure is analysed through NTHA, even when the strongest earthquakes of the suite are considered. Indeed, for the benchmark building, NTHA results show a significant number of earthquakes that lead to DCR values greater than unity (16/36 earthquakes = 44%) but no UCs are found for NTHA and μ_{DCR} results to be

very similar to that of LTHA when excluding earthquakes with $I_{eq,max}$ > 0.05 g (i.e., μ_{DCR} = 1.36 over 20 earthquakes in Fig. 7-2b). In conclusion, it is shown that the proposed index limit can be a suitable choice to identify UCs for LTHA when selecting GM suites for LTHA. In the following section, $I_{eq,max}$ ≤ 0.05 g is selected as criterion to derive fragility curves at design stage through CA.

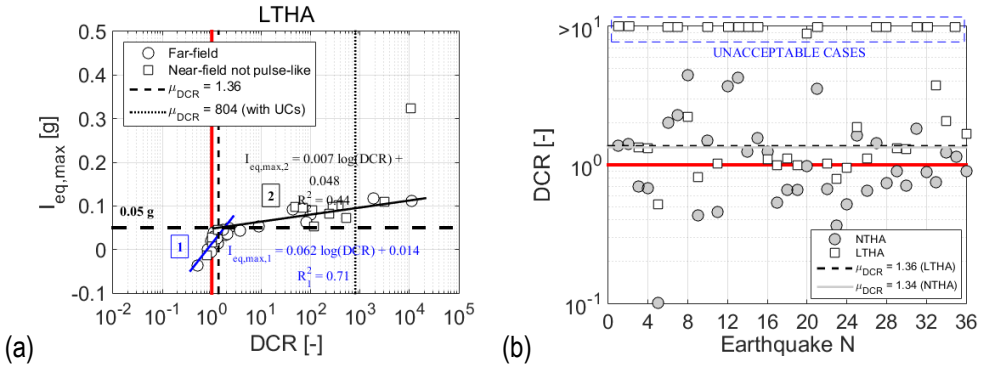

Fig. 7-2 Definition of an optimal value of I_{eq} for LTHA GM selection: (a) plot of the maximum DCR values at LS-LS versus $I_{eq,max}$ with piecewise linear regression and identification of the limit value of acceptable cases (i.e., $I_{eq,max}$ = 0.05 g) for LTHA, and (b) comparison of the DCR values between LTHA and NTHA, the latter in terms of chord rotation at LS-LS. The average of these results is denoted by μ_{DCR}.

The LTHA-based procedure for deriving fragility curves at design stage through CA is schematically represented in Fig. 7-3. The far-field and the near-field non-pulse-like GMs in Fig. 7-1 are firstly considered as suite, subsequently random subsuites are selected from the GM list through the bootstrap method. Generally, 10-20 earthquakes can be considered a sufficient number to provide reasonable accuracy in the estimation of seismic demand when using the spectral acceleration at the fundamental period (in the following denoted by *SaT1*) as intensity measure for mid-rise buildings (Shome and Cornell 1999). FEMA P-58 recommend using 20 or more earthquakes in order to obtain reliable estimates of collapse fragility (FEMA 2018a). For LTHA, it is found that UCs are avoided if $I_{eq,max}$ < 0.05 g which statistically allows to avoid disproportionately high values of DCR in terms of bending moment. Once unacceptable cases are excluded, it is possible to extract suites according to the requirements indicated for code spectrum-compatibility (CEN 2004a) and perform the fragility assessment at design stage. Furthermore, when performing CA fragility assessment, it is important to meet different criteria summarised in the following:

- the selected GMs should cover a wide range of *SaT1* values in order to reduce errors in the estimation of the regression slope (Barbosa 2011; Jalayer et al. 2012);
- a significant portion of earthquakes should lead to DCR > 1 (e.g., more than 30% should have DCR values greater than unity, Miano et al. 2018) in order to provide enough data-points in the region of interest;
- not too many GMs (e.g., more than 10% of total number) should come from the same earthquake event in order to reduce the potential correlation between DCR values evaluated for different GMs (Haselton 2006);

– *SaT1* as intensity measure should be checked to reflect the effects of realistic tectonic settings and site conditions (Barbosa 2011; Jalayer et al. 2012).

When the assessment is carried out considering few earthquakes, as herein investigated for design stage, it is furtherly suggested that:

– 80% of the selected earthquakes should have DCR values ranging within the interval of [0.3, 2] that can be assumed as that area surrounding the unity which significantly affects the estimation of the regression slope;
– at least the 10% of the earthquakes should present DCR < 0.9 in order to consider some earthquakes which allow to anchor the regression slope to data-points far from unity.

These further conditions are provided in this study from the observation of numerous fragility curves obtained from bootstrapped GM suites, as described in the following, and it is stated that if they are satisfied it is possible to obtain results more consistent with those obtained through robust fragiltiy when a limited number of earthquakes are considered.

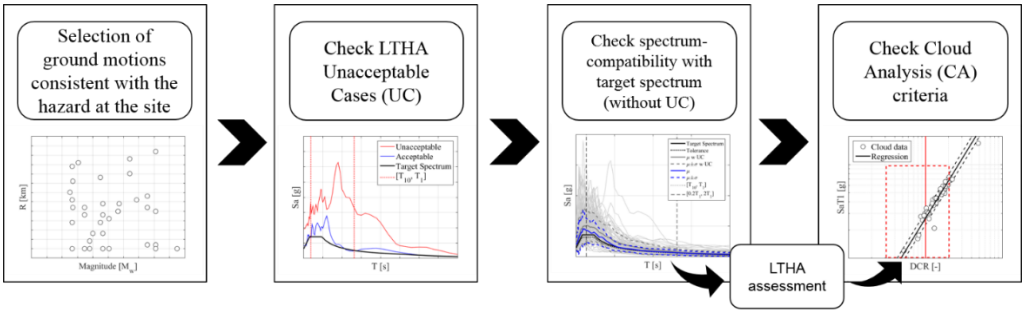

Fig. 7-3 LTHA-based procedure for deriving fragility curves at design stage through Cloud Analysis (CA)

7.1.1.1. Fragility curves at Life Safety-Limit State through NTHA: benchmark

In order to build up fragility curves that can be used as benchmark for LTHA, NTHA results for all the 36 earthquakes are preliminarily presented. It is worth observing that when LTHA and NTHA are compared in terms of fragility curves, the choice of a consistent *SaT1* must be taken. For the sake of comparison, fragility curves obtained for NTHA are evaluated considering the same value of *SaT1* assumed for LTHA, i.e. the value of the spectral acceleration corresponding to the fundamental period of the elastic model accounting for the 50% equivalent reduction of stiffness due to cracks (i.e., spectral acceleration corresponding to T_1 = 1.31 s for the benchmark building). *SaT1* of the elastic GM spectra ranges within [0.12, 1.68] g. The average value of *SaT1* (denoted by μ_{SaT1} in the following) is equal to 0.37 g and its standard deviation is equal to ±0.23 g.

From the analyses,16/36 earthquakes (~44%) lead to DCR values greater than unity (see Fig. 7-4a). The fragility curve obtained from the linear regression in the logarithmic plane in Fig. 7-4b shows that the median of the *SaT1* values leading to LS-LS (denoted by η_{SaT1}) is equal to 0.39 g (having β =

0.48) which is 1.5 times larger than *SaT1* on the target spectrum (= 0.26 g). Fragility curves obtained for each structural member category (i.e., floor beams, staircase beams, columns, and squat columns) can provide more detailed information on the local behaviour of the structure and critical element categories, as shown in Fig. 7-4b. These fragility curves are evaluated considering the DCR values of the different members. The values of η_{SaT1} for each member category is equal to 0.74 g (β = 0.36), 0.82 g (β = 0.41), 0.78 g (β = 0.53) and 0.39 g (β = 0.48) for the floor beams, staircase beams, columns and squat columns, respectively. This assessment shows that the global behaviour of the structure locally depends on the squat columns as also confirmed by the overlap of the global (thick black line) and squat columns fragility curves (thin red line) in Fig. 7-4b.

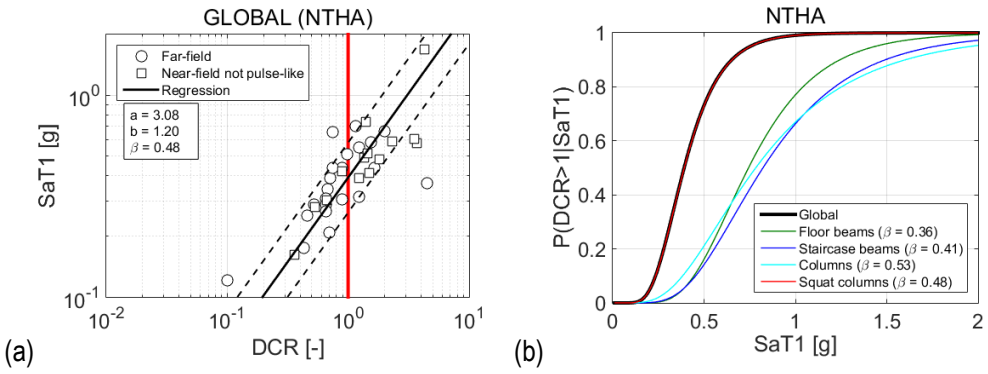

Fig. 7-4 NTHA-based fragility assessment at LS-LS through CA: (a) regression of 36 data-points and (b) corresponding fragility curve (global) compared to the fragility curves obtained for each structural member category. In figure a and b are the regression parameters and β is the logarithmic standard deviation.

7.1.1.2. Fragility curves at Life Safety-Limit State through LTHA

Among the initial suite of 36 GMs, 20 pairs are classified as acceptable according to the procedure in Fig. 7-3. This number of earthquakes can be still considered enough to provide sufficient accuracy in the estimation of seismic demand using *SaT1* as intensity measure for mid-rise buildings (Shome and Cornell 1999). These GMs are considered to build up a suite, that would still result to be spectrum-compatible with the target spectrum and would better match it with respect to the suite made of all the 36 GMs which includes UCs for LTHA (see Fig. 7-1). This confirms that $I_{eq,max}$ allows reducing the record-to-record variability in the GM selection.

The subgroup of 20 earthquakes presents GM spectra with *SaT1* ranging within [0.12, 0.55] g and the value of μ_{SaT1} is equal to 0.26 g (very close to the target spectrum) with standard deviation ±0.10 g. Fig. 7-5a shows the results in terms of linear regression in the logarithmic plane and correspondent fragility curves, including the effect of including UCs which are discussed later. LTHA results show that 14/20 earthquakes (= 70%) lead to DCR values greater than unity (see Fig. 7-5a) against 16/36 (~44%) in the case of NTHA (see Fig. 7-4a). The fragility curves obtained from the linear regression (see Fig. 7-5b) show that the value of η_{SaT1} is equal to 0.23 g (having β = 0.27), against *SaT1* of the target spectrum equal to 0.26 g. For NTHA, η_{SaT1} is equal to 0.39 g (having β = 0.48) (see Fig. 7-4b).

The difference between LTHA and NTHA is equal to 1.70 which is a value of the same order of magnitude of the partial safety factors for material property (i.e., 1.5 for concrete and 1.15 for steel reinforcement), conventionally used to evaluate "force-based" capacities so to convert the nominal value of strength to the design one. Fragility curves obtained for each element category show a more detailed comparison as shown in Fig. 7-5b. The values of η_{SaT1} for each element category is equal to 0.27 g (β = 0.13), 0.25 g (β = 0.13), 0.42 g (β = 0.27) and 0.29 g (β = 0.21) for the floor beams, staircase beams, columns and squat columns, respectively. This assessment shows that the global behaviour of the structure assessed through LTHA essentially depends on the staircase beams which show lower value of η_{SaT1} (= 0.25 g). Considering UCs lead to significant dispersion in linear regression as shown in Fig. 7-5a where β is way larger with respect to the case in which they are excluded (β = 1.90 with UCs against 0.27 without them), even if the difference in terms of η_{SaT1} is not generally large for this case (see Fig. 7-5b in terms of global fragility curves). However, this difference can be significant in local terms, especially for those categories of elements which are particularly penalized by high values of tensile axial forces in the evaluation of their capacities (e.g., staircase beams and squat columns in the case study analysed herein).

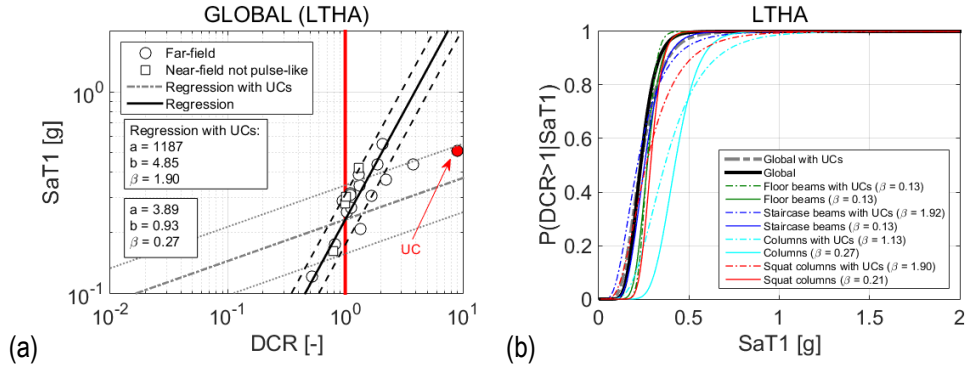

Fig. 7-5 LTHA-based fragility assessment at LS-LS through CA: (a) regression of 20 data-points without Unacceptable Cases (UCs) and (b) corresponding fragility curve (global) compared to the fragility curves obtained for each structural member category. In figure a and b are the regression parameters and β is the logarithmic standard deviation.

7.1.1.3. Sensitivity to the GM suite size through bootstrap method

The possibility to use a reduced number of GMs to build up possible suites is herein investigated. Results of spectrum-compatible GM suites extracted according to the bootstrap method are presented both for LTHA and NTHA in order to show the sensitivity of results to the number of GMs. According to the procedure described in Fig. 7-3, the bootstrap procedure programmed using Matlab (MathWorks 2015) selects LTHA-spectrum-compatible GM suites within the list of 20 earthquakes satisfying the condition $I_{eq,max}$ < 0.05 (i.e., acceptable cases). A total of 200,000 combinations of n earthquakes are randomly generated. Subsequently, unique combinations (duplicated combinations are avoided) are analysed to accomplish criteria for fragility assessment through CA. The number of earthquakes (i.e., size of the suite) varies from 7, which is the minimum number suggested by the EC8-1, to 15. The values η_{SaT1} and β of the fragility curves are evaluated for the possible suites n.

Subsequently, the exponential of the mean of the logarithmic of η_{SaT1} (denoted by $\mu_{\eta SaT1,n}$) and the mean of the β (denoted by $\mu_{\beta,n}$) are evaluated for all the possible combinations found with this procedure and for different GM suite sizes, including their standard deviations. Same procedure is applied for NTHA without considering any check for UCs (i.e., they do not occur). The same procedure is applied for both LTHA and NTHA without imposing the spectrum-compatibility condition as typically assumed for CA. Indeed, the spectrum-compatibility imposes conditioning on a given hazard level given the intensity measure which might lead to unnecessary reduction of the record-to-record variability and hence a potential underestimation in the limit state probability evaluation. For the sake of clarity, results are commented for the case in which the spectrum-compatibility condition is imposed in the first place (referred to as "w S-C") and, subsequently, results are discussed for the case without it (referred to as "w/o S-C"). From the results obtained in Fig. 7-6a it is possible to state that $\mu_{\eta SaT1}$ shows a neglectable increasing trend when the suite size increases from 7 to 15 both for LTHA and NTHA while their standard deviations decrease, indicating the benefits of considering a larger GM suite size. Fig. 7-6b shows that μ_{β} is more sensitive than $\mu_{\eta SaT1}$ and it is almost constant for NTHA while it tends to a slight increase for LTHA for suite size from 7 to 15. For 7 earthquakes, NTHA shows values of $\mu_{\eta SaT1}$ and μ_{β} equal to 0.37 g (±0.04 g) and 0.48 (±0.17), respectively. For LTHA, it results that the values of $\mu_{\eta SaT1}$ and μ_{β} are equal to 0.24 g (±0.02 g) and 0.23 (±0.08), respectively. For a suite of 11 GMs, which is the minimum suggested in ASCE/SEI 7-16, it results that for NTHA the values of $\mu_{\eta SaT1}$ and μ_{β} are equal to 0.38 g (±0.03 g) and 0.49 (±0.12) respectively, while for LTHA they are equal to 0.24 g (±0.01 g) and 0.25 (±0.06) respectively. Table 7-1 reports the values obtained from this sensitivity analysis. It appears obvious that if the intent is to reduce the variability of the results, more earthquakes should be considered. However, it seems evident from these results that 11 earthquakes, as suggested in ASCE/SEI 7-16, represent a good compromise between accuracy of the results and computational time.

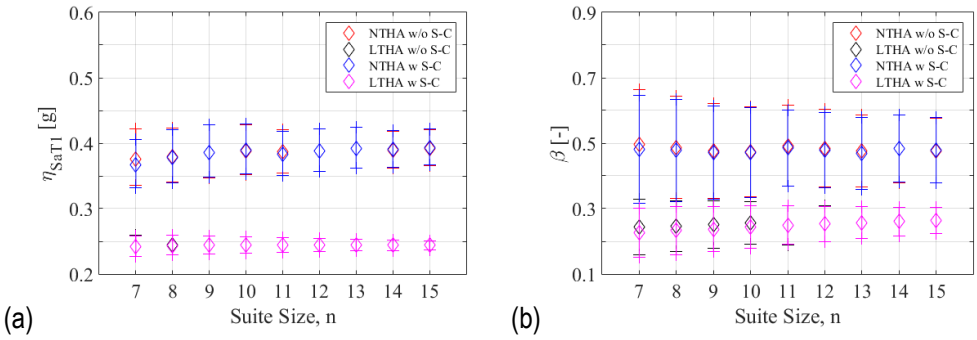

Fig. 7-6 Sensitivity to the GM suite size for LTHA and NTHA-based fragility assessment through CA at LS-LS, in terms of (a) median of the SaT1 values leading to LS-LS (η_{SaT1}) and (b) logarithmic standard deviation (β).

When CA is performed without imposing the spectrum-compatibility with the target spectrum, some differences arise for small suite sizes. Results are reported in Table 7-2 where it is possible to

observe that the bias (±) in imposing the spectrum-compatibility is always less than 8% compared to the rigorous approach without imposing it. For NTHA, that represents the benchmark in this study, the largest bias is found for suite size n = 7, it being equal to -4% and -3% for η_{SaT1} and β, respectively. For LTHA, the largest bias is found for suite size n = 7, it being equal to -8% for β.

Table 7-1 Sensitivity to the GM suite size for LTHA and NTHA-based fragility assessment through CA at LS-LS in terms of median of the SaT1 values leading to LS-LS (η_{SaT1}) and logarithmic standard deviation (β), considering the spectrum-compatibility of the GM spectra with the target spectrum (referred to as "w S-C" in Figure 7-6).

Suite size	Case	η_{SaT1} [g]	β [-]	Case	Suite size	η_{SaT1} [g]	β [-]
7		0.24±0.02	0.23±0.08		7	0.37±0.04	0.48±0.17
8		0.24±0.02	0.23±0.07		8	0.38±0.04	0.47±0.16
9		0.24±0.01	0.24±0.07		9	0.39±0.04	0.47±0.14
10		0.24±0.01	0.24±0.06		10	0.39±0.04	0.47±0.14
11	LTHA	0.24±0.01	0.25±0.06	NTHA	11	0.38±0.03	0.49±0.12
12		0.24±0.01	0.25±0.05		12	0.39±0.03	0.48±0.11
13		0.24±0.01	0.26±0.05		13	0.39±0.03	0.47±0.11
14		0.24±0.01	0.26±0.04		14	0.39±0.03	0.48±0.10
15		0.24±0.01	0.26±0.04		15	0.39±0.03	0.48±0.10

Table 7-2 Sensitivity to the GM suite size for LTHA and NTHA-based fragility assessment through CA at LS-LS in terms of median of the SaT1 values leading to LS-LS (η_{SaT1}) and logarithmic standard deviation (β), without considering the spectrum-compatibility of the GM spectra with the target spectrum (referred to as "w/o S-C" in Figure 7-6).

Suite size	Case	η_{SaT1} [g]	β [-]	Case	Suite size	η_{SaT1} [g]	β [-]
7		0.24±0.02	0.24±0.09		7	0.37±0.05	0.50±0.17
8		0.24±0.02	0.25±0.08		8	0.38±0.04	0.49±0.16
9		0.24±0.01	0.25±0.07		9	0.39±0.04	0.48±0.15
10		0.24±0.01	0.24±0.06		10	0.39±0.04	0.47±0.14
11	LTHA	0.24±0.01	0.25±0.06	NTHA	11	0.38±0.03	0.49±0.12
12		0.24±0.01	0.25±0.05		12	0.39±0.03	0.48±0.11
13		0.24±0.01	0.26±0.05		13	0.39±0.03	0.47±0.11
14		0.24±0.01	0.26±0.04		14	0.39±0.03	0.48±0.10
15		0.24±0.01	0.26±0.04		15	0.39±0.03	0.48±0.10

7.1.1.4. Robust fragility assessment

The robust fragility is employed in this section to define the confidence interval of the fragility curves obtained in the previous sections for LTHA and NTHA. In this section, the robust fragility assessment

developed in Jalayer et al. (2015), which employs the Bayesian Cloud Analysis procedure taking into account the uncertainty in the parameter of regression, is considered. Contrarily to the bootstrap method where the initial sample is used as the population from which to resample, the robust method uses standard Monte Carlo simulations, in this case cloud-data are used to update the joint probability distribution function for the parameters of regression and the logarithmic standard deviation (i.e., a, b, and β), then, the average of the generated curves is used as robust fragility curve and the dispersion is estimated as the variance of the plausible fragility curves generated. The confidence interval is defined as the ± one standard deviation of the robust fragility curve. This is a possible approach to avoid numerous numerical analyses. Herein, the robust fragility curves (together with their confidence intervals) for the suite of 36 (20 for LTHA) and 7 earthquakes (to test a design procedure based on the minimum allowable number of earthquakes according to EC8) are obtained by means of the ROBUST FRAGILITY TOOL, an opensource Matlab-based software (Jalayer et al. 2015). For the sake of simplicity, they are called Suite-36 and Suite-7 for NTHA. For LTHA, the suite accounting for elimination of the UCs is called Suite-20 while Suite-7 is the same as that used for NTHA. Suite-7 is a randomly extracted suite from the simulations in order to show an example of comparison between LTHA and NTHA based on the same GMs (RSN- 1148, 125, 1485, 1633, 721, 767, 900). This suite presents *SaT1* ranging within [0.12 - 0.55] g. Spectrum-compatibility shows value of μ_{SaT1} equal to 0.26 g (very close to the target spectrum) and its standard deviation equal to ±0.14 g. For NTHA, Suite-7 features a = 4.66, b = 1.62, β = 0.45 while for LTHA they are a = 3.42, b = 0.88, β = 0.11.

In Fig. 7-7 all the possible fragility curves evaluated through the bootstrap method for n = 7 are plotted and compared to the robust fragility curves for Suite-36 (Suite-20 for LTHA) and Suite-7 together with their confidence intervals. The bootstrapped fragility curves allow to define an envelope area which presents similar shape compared to the confidence intervals of the robust assessment. For NTHA, the robust fragility curve of Suite-7 results to be very close to the one of Suite-36 as well as for Suite-20 in the case of LTHA. When performing LTHA fragility assessment, a reasonable value for loss estimation can be the upper confidence value of η_{SaT1} (i.e., $\mu_{\eta SaT1}+\sigma$) which allows to minimise the difference between LTHA and NTHA, being this value likely closer to the lower confidence value of η_{SaT1} (i.e., $\mu_{\eta SaT1}-\sigma$) given by NTHA. For Suite-7, the robust fragility assessment shows value of η_{SaT1} equal to 0.38 g with confidence interval [0.34, 0.44] g for NTHA while it is equal to 0.25 g with confidence interval [0.23, 0.26] g for LTHA. The upper confidence value of η_{SaT1} for LTHA is equal to 0.26 g which is closer to the lower confidence value of η_{SaT1} for NTHA equal to 0.34 g (~31% of difference). This allows to minimise the approximations of LTHA.

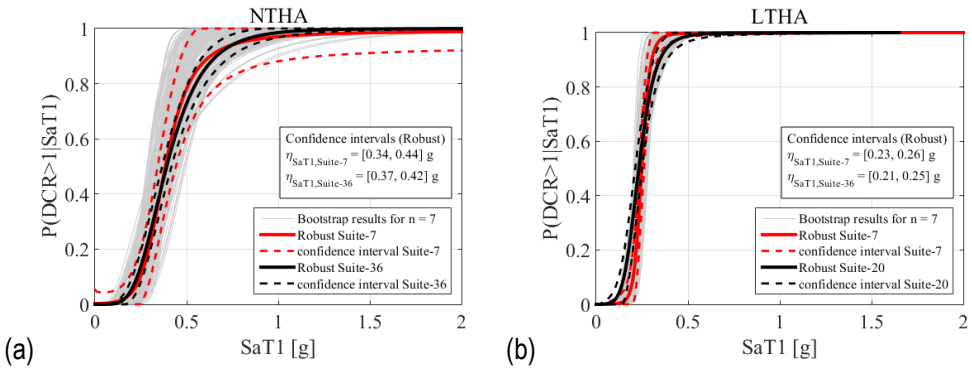

Fig. 7-7 Robust fragility curves at LS-LS through: (a) NTHA for Suite-36 and -7, and (b) LTHA for Suite-20 and -7, together with their confidence intervals and bootstrapped fragility curves for suites of 7 earthquakes.

7.1.2. Fragility comparison at Damage Limitation-Limit State

In the following, the procedure presented in the previous section based on the bootstrap method is applied to define the variability of the fragility assessment parameters at DL-LS. Contrarily to LS-LS, there is no need to identify UCs at DL-LS for LTHA since the assessment is carried out in terms of displacements and DCR does not "explode" for this limit state. The suite of 24 GMs considered in Section 6.3.2 is considered herein and it includes 8 pairs of GMs (RSN- 70, 71, 72, 77, 78, 80, 88, 93) from the same event (M6.61 San Fernando 1971). In order to reduce the potential correlation between DCR values for different GMs, not more than 1 over the 8 pairs of GMs is considered when assembling random suites made of 7 earthquakes. Robust fragility assessment is carried out through LTHA and NTHA for one extracted subgroup of GMs made of 7 earthquakes (RSN- 1, 13, 26, 33, 36, 78, 97). This subgroup is called Suite-7 and it is spectrum-compatible with the target spectrum of the benchmark building at DL-LS. Fig. 7-8 shows the results obtained through NTHA, herein assumed as benchmark for the comparison with LTHA whose results are shown in Fig. 7-9.

The value of *SaT1* corresponds to the spectral-acceleration at the fundamental period of the elastic model with equivalent stiffness reduction factor (α) equal to 50% (Case 2 in Section 6.3.2). The value of *SaT1* ranges between [0.09, 0.24] g and the average value (defined as μ_{SaT1}) is equal to 0.12 g (against 0.09 g of the target spectrum) with standard deviation ±0.06 g. For NTHA, results are shown for DCR evaluated both in terms of *IDR* and θ. For NTHA, the evaluation of DCR in terms of *IDR* leads to more conservative results (red regression and fragility curve in Fig. 7-8a-b), having 4/7 (~57%) earthquakes with DCR values greater than unity. Results obtained from robust assessment show that the value of η_{SaT1} is equal to 0.16 g with confidence interval [0.15, 0.17] g. NTHA in terms of θ shows value of η_{SaT1} equal to 0.19 g (1.19 time larger than the previous one) with confidence interval [0.17, 0.23] g. For LTHA, the equivalent stiffness reduction does not lead to significant differences when the linear regression is carried out (Case 2, 3, and 4 in Section 6.3.2), except for the case without any reduction that it is not realistic and not recommended by any code (Case 1).

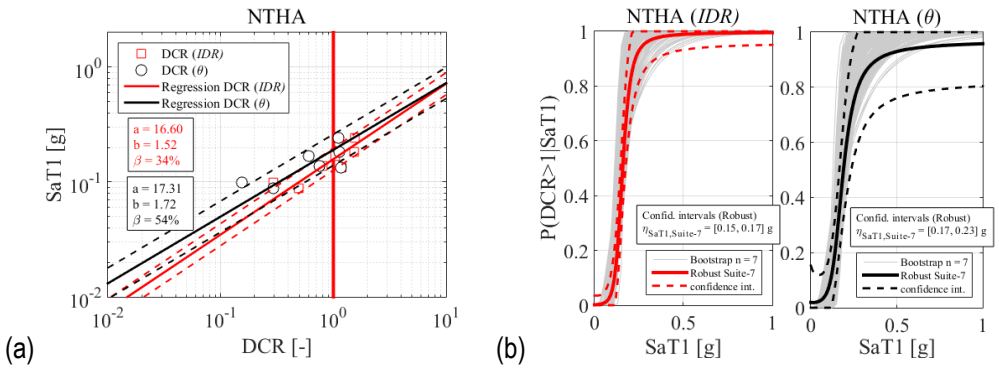

Fig. 7-8 NTHA-based fragility assessment at DL-LS through CA: (a) regression of 7 data-points for DCR values in terms of chord rotation (θ) and maximum Interstorey Drift Ratio (IDR), and (b) corresponding robust fragility curves (global) for Suite-7, together with their confidence intervals and bootstrapped fragility curves for suites of 7 earthquakes extracted from a group of 24. In figure a and b are the regression parameters and β is the logarithmic standard deviation.

Fig. 7-9 shows the results obtained for equivalent stiffness reduction factor equal to 50% (i.e., Case 2). For this case, the number of earthquakes leading to DCR values greater than unity is 2/7 (~29%). The value of η_{SaT1} is equal to 0.20 g (1.25 and 1.05 times larger than NTHA with DCR in terms of *IDR* and θ, respectively) and confidence interval [0.18, 0.25] g. Even if LTHA fragility assessment is non-conservative with respect to NTHA for this suite, the robust assessment shows results very close to NTHA with DCR in terms of θ. This is confirmed, also, by the shape and density of the fragility curves obtained through the bootstrap method for n = 7 earthquakes, not very different from the confidence intervals evaluated through robust assessment. One way to employ LTHA fragility assessment at DL-LS in a conservative way is considering the lower confidence value of η_{SaT1} (i.e., η_{SaT1}-σ) which would very likely be contained within the confidence interval of NTHA in terms of θ. For the example shown, the lower confidence value of η_{SaT1} for LTHA is equal to 0.18 g which is included within the confidence interval of η_{SaT1} for NTHA in terms of θ (i.e., [0.17, 0.23] g). This allows to minimise the approximations of LTHA.

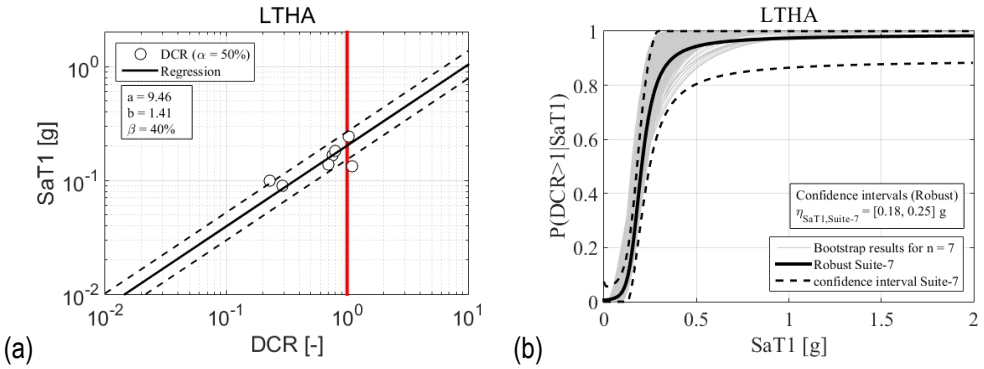

Fig. 7-9 LTHA-based fragility assessment at DL-LS through CA: (a) regression of 7 data-points for DCR values in terms maximum Interstorey Drift Ratio (IDR), and (b) corresponding robust fragility curves (global) for Suite-7, together with their confidence intervals and bootstrapped fragility curves for suites of 7 earthquakes extracted from a group of 24. In figure a and b are the regression parameters and β is the logarithmic standard deviation.

7.2.Further considerations for Life Safety-Limit State

LTHA results for LS-LS presented above are obtained considering capacities of beams and columns with the design strength values of concrete and steel reinforcement evaluated according to the EC2 (i.e., f_{cd} = 0.85 f_{ck}/1.5 and f_{syd} = f_{syk}/1.15). This assumption is consistent with "force-based" design approach through linear analyses that is based on verifications in which the design seismic demand in structural members is checked against the design capacity of them. In the following, a further analysis without using design material strength values but considering the mean values in LTHA verifications is attempted herein to investigate more in detail the above discrepancies for the derivation of fragility curves at LS-LS through LTHA. For this case, LTHA results show that 5/20 earthquakes (= 25%) lead to DCR values greater than unity (see Fig. 7-10a) against 16/36 (~44%) in the case of NTHA (see Fig. 7-4a). The fragility curves obtained from the linear regression (see Fig. 7-10b) show that the value of η_{SaT1} is equal to 0.36 g (having β = 0.15), against *SaT1* of the target spectrum equal to 0.26 g. For NTHA η_{SaT1} is equal to 0.39 g (having β = 0.48) (see Fig. 7-4b). The difference between LTHA and NTHA in terms of η_{SaT1} is equal to 0.92 (i.e., - 8%). Fragility curves obtained for each element category show a more detailed comparison as shown in Fig. 7-10b. The values of η_{SaT1} for each element category is equal to 0.45 g (β = 0.13), 0.42 g (β = 0.12), 0.78 g (β = 0.16) and 0.39 g (β = 0.19) for the floor beams, staircase beams, columns and squat columns, respectively. This assessment shows that the global behaviour of the structure assessed through LTHA essentially depends on the squat columns which show lower value of η_{SaT1} (= 0.39 g). Results are summarised in Table 7-3 which reports a comparison between NTHA and LTHA with design capacities and mean capacities. The comparison in terms of robust (global) fragility curves in Fig. 7-11 between NTHA for Suite-36 and LTHA for Suite-20 shows confidence intervals at η_{SaT1} equal to [0.37, 0.42] g and [0.34, 0.38] g, respectively.

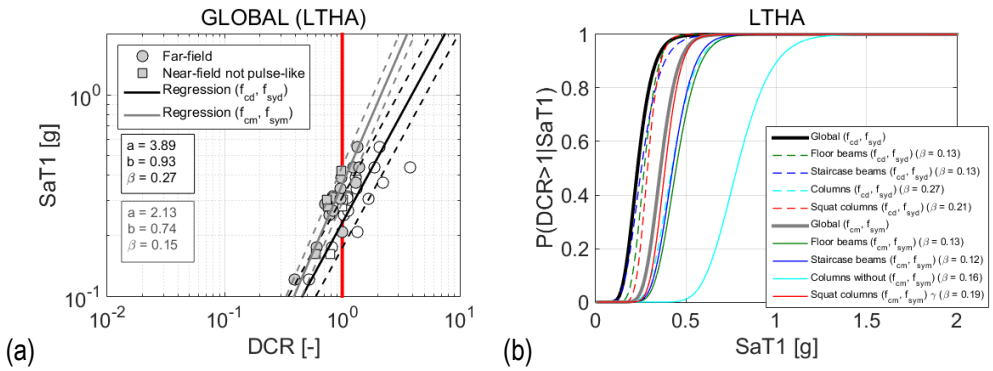

Fig. 7-10 LTHA-based fragility assessment at LS-LS through CA: (a) comparison of the regressions of 20 data-points between LTHA with design capacities (f_{cd} and f_{syd}) and LTHA with mean capacities (f_{cm} and f_{sym}) and (b) corresponding fragility curves (global). In figure a and b are the regression parameters and β is the logarithmic standard deviation.

Table 7-3 Comparison of the fragility assessment results at LS-LS through NTHA and LTHA with design capacities (f_{cd} and f_{syd}) and mean (f_{cm} and f_{sym}).

Case	Global		Floor beams		Staircase beams		Columns		Squat columns	
	η_{SaT1} [g]	β [-]	η_{SaT1} [g]	β [-]	η_{SaT1} [g]	β [-]	η_{SaT1} [g]	β [-]	η_{SaT1} [g]	β [-]
LTHA Suite-20 Design capacities	0.23	0.27	0.27	0.13	0.25	0.13	0.42	0.27	0.29	0.21
LTHA Suite-20 Mean capacities	0.36	0.15	0.45	0.13	0.42	0.12	0.78	0.16	0.39	0.19
NTHA Suite-36	0.39	0.48	0.74	0.82	0.82	0.41	0.78	0.53	0.39	0.48

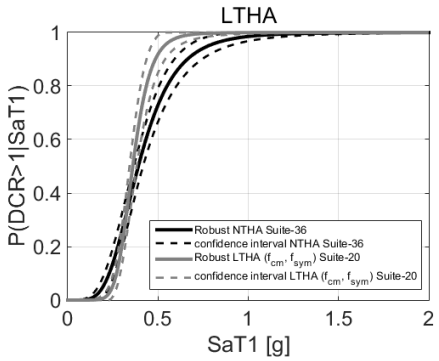

Fig. 7-11 Comparison of the robust fragility curves at LS-LS obtained through NTHA and LTHA with mean capacities (f_{cm} and f_{sym}).

7.3.Conclusion

In the following, the results obtained from the proposed LTHA-based procedure for deriving simplified fragility curves at design stage are commented. It is worth mentioning that in order to make consistent the comparison between LTHA and NTHA results, the *IM* is taken as the spectral acceleration corresponding to the fundamental period of the benchmark building accounting for the 50% equivalent stiffness reduction (denoted by *SaT1*) while the *EDP* is taken as the DCR in terms of flexural verifications, i.e. bending moment for LTHA and chord rotation for NTHA. The following conclusions can be made based on the results of LTHA and NTHA:

- the "unacceptable cases" significantly increase the dispersion in linear regression for LTHA. In the proposed procedure they are avoided through the proposed I_{eq} index by imposing that all the earthquakes showing $I_{eq} \leq 0.05$ g can be considered. This value is larger than the one proposed for design in order to allow a larger record-to-record variability for fragility assessment;
- if "unacceptable cases" in LTHA are avoided, LTHA can underestimate the median of the *SaT1* values leading to LS-LS (η_{SaT1}) of 41% with respect to NTHA. This huge difference is

related to the implicit conservativity in design. However, when the DCR values for LTHA are evaluated in terms of mean values of the material strenghts, the underestimation drops to 8% with respect to NTHA;

- LTHA results show logarithmic standard deviations (denoted by β) lower than NTHA as expected. When the DCR values for LTHA are evaluated in terms of mean values of the material properties, the values of β are reduced further;
- if the spectrum-compatibility is imposed, the increase of the GM suite size tends to increase the accuracy in estimation of η_{SaT1} and β for both LTHA and NTHA. However, LTHA shows less sensitivity to the variation of η_{SaT1} and β for increasing GM suite size than NTHA. It is found that eleven GMs (minimum suggested by ASCE/SEI 7-16) can be a good compromise between accuracy of the results and computational effort. The spectrum-compatibility condition can lead to bias up to 4% and 8% for NTHA and LTHA, respectively;
- robust fragility assessment tends to estimate smaller confidence intervals compared to the ones obtained through bootstrapped GM suites. This result is largely expected given the different nature and scope of the two techniques (the first used to assess the number of necessary GMs for stable estimations, the second used to investigate the uncertainty in the estimation of fragility parameters given the selection of a GM suite);
- using the upper confidence value as estimated from robust fragility (i.e., $\mu_{\eta SaT1}+\sigma$) for LTHA, can minimise the difference between NTHA and LTHA results in terms of fragilities at LS-LS and leads to relatively accurate estimation of the performances. In the same way, the lower confidence value (i.e., $\mu_{\eta SaT1}-\sigma$) for LTHA can minimise the difference between NTHA and LTHA results in terms of fragilities at DL-LS.

Chapter 8: Conclusions & Further Work

8.1.Conclusions

LTHA is proposed as alternative to modal Response Spectrum Analysis (RSA), allowing to overcome limits of RSA and being able to provide more accurate response quantities for verifications. To this purpose, a clear and complete EC8-compliant "force-based" LTHA design framework for buildings is proposed in this research work. This procedure is described in Chapter 4 and it is discussed at each step, such as Ground Motion (GM) selection, modelling, behaviour factor, damping model, P-Delta effects, load combinations, and acceptance criteria. This design framework presents similarities with respect to the one proposed by FEMA P-1050, recently adopted by ASCE/SEI 7-16. However, the main difference between the proposed framework and the one adopted by the US standards consists in the selection of the seismic input. FEMA P-1050 suggests using three pairs of spectral-matched (horizontal) GMs through wavelet adjustment so that LTHA can replicate as closely as possible the typical outcome of RSA. The benefit of using such a procedure is that the record-to-record variability is considerably reduced, and it is possible to obtain a stable estimate of the structural response without making difficult for engineers selecting GMs. However, this approach presents some limitations such as possible alteration of important features of real GMs (i.e., pulse-like GMs), difficulties in matching an entire code spectrum, and unsuitability for assessing inelastic responses In this thesis, LTHA seismic input is investigated adopting seven pairs of spectrum-compatible (horizontal) GMs in the same way as NTHA, which is the minimum number of GMs in EC8 for averaging results of NTHA for a GM suite (in ASCE/SEI 7-16 the minimum is eleven pairs). In this way, it is possible to consider the record-to-record variability as design aspect to account for in LTHA results. To show a practical example, a regular 12-storey Reinforced-Concrete (RC) Moment-Resisting-Frame (MRF) building located in medium-high seismicity area is considered. The benchmark building, described in Chapter 3, is designed through RSA for Ductility Class High (DCH) specifications according to the EC8 and it accounts for critical design aspects, such as quite large number of storeys for frame systems (so that results can be generalised for RC-MRF typology), and the presence of staircase and squat columns. The staircase represents a critical design aspect in buildings and most studies showing new methodological approaches on archetype buildings in literature neglect it. This building is representative of typical modern building practice in Italy and Mediterranean region and it represents a limit for RC-MRF building design as typical 12-storey RC buildings are designed with shear walls in order to control the deformability of medium-rise buildings.

The proposed framework is implemented in a Matlab/OpenSees code developed in this thesis. This code, described in detail in Chapter 5, is designed for performing linear and nonlinear seismic analyses and evaluating the performance of ductile RC-MRF buildings (steel X-CBF and steel MRF are not related to this thesis but the capability of the code was tested for these cases too in Di Cuia

et al. 2017). This code is characterised by a simple and flexible structure which allows improvements and additions in future and it can run, automatically, multiple tasks within the pre-processing, processing, and post-processing stages. The linear modelling framework is tested comparing results with those obtained from SAP2000 for the benchmark building. For the nonlinear modelling, the code implements recently developed numerical models available in literature, and its capability is shown for a RC column experimentally tested in the past and for a three-dimensional portal analysed through NTHA and pushover analysis. This chapter also contains useful recommendation for nonlinear modelling and analysis of buildings in OpenSees.

Chapter 6 shows that when LTHA is conceived as a "force-based" design approach and spectrum-compatible GM suites are selected for the benchmark building, the verifications of staircase beams and squat columns at LS-LS can be particularly critical. These structural members are subjected to high tensile axial forces that significantly reduce the flexural capacity of these members, resulting in disproportionately high Demand over Capacity Ratio (DCR) values. The use of the lexical expression "unacceptable case" recalls the meaning of the expression "unacceptable responses" in the context of NTHA in FEMA P1050 where they can be due to dynamic instability, non-convergent analysis, and responses exceeding valid ranges. For LTHA these unacceptable cases are related to the structural responses induced by the strongest earthquakes within the GM suite that lead to DCR values significantly high from the others (i.e., outliers). Other than significantly increasing the variability of the results, these unacceptable cases can lead to LTHA design solutions much more expensive than NTHA. This issue would never make LTHA design appealing for engineers who would rather prefer using RSA despite of its limitations. To facilitate the identification of potential unacceptable cases in GM selection for LTHA, an index denoted by I_{eq} is presented in this thesis. This index is building-dependent, and it is based on the evaluation of the weighted average of the differences of spectral accelerations between the GM spectra and the target one at each relevant period of the building. The weights at each period of the building are defined in terms of modal participating masses. Such index is compared to its version implementing the well-consolidated square root of the sum of squares of the spectral differences (denoted by $I_{eq,SRSS}$) in order to investigate the suitability of I_{eq} and $I_{eq,SRSS}$ for the purpose of GM selection for LTHA. It is found that LTHA always leads to higher seismic demand in terms of maximum storey shears predicted by RSA for the 12-storey RC-MRF building considered in this thesis, whether the seismic input is based on spectrum-compatible GM or spectral-matched GMs (as per FEMA P1050). LTHA employing three pairs of spectral-matched GMs through wavelet adjustment is more convenient for re-design of structural members initially designed through RSA. LTHA employing seven pairs of spectrum-compatible GMs can show significant variability of the seismic demand. However, such variability can be reduced when the proposed index I_{eq} is used for selecting GMs to be lower than a certain I_{eq} threshold. If unacceptable cases are not controlled in GM selection for LTHA, the conservativity of LTHA can be considered excessive compared to NTHA

results. Results obtained through NTHA showed that the squat columns represent the most critical members within the benchmark building. Moreover, if LTHA results of spectrum-compatible GM suites are used together with capacities of beams and columns evaluated in terms of mean values of strenghts for concrete and steel, LTHA is more accurate than RSA and these results are found being better to describe the condition of the benchmark building assessed through NTHA.

Results at DL-LS showed that LTHA, on average, underestimates the seismic demand in terms of maximum interstorey drift ratios compared to NTHA for the RC-MRF benchmark building. It is suggested that rather than reduce further the elastic stiffness of beams and columns (that would make results inconsistent with those of LS-LS), displacements could be amplified by a properly calibrated coefficient (similar to the deflection amplification factor C_d in ASCE/SEI 7-16) which can implicitly account for aspects typically not considered in linear-elastic analysis (e.g., extension of cracks, nonlinear elastic behaviour of materials, amount of steel reinforcement, etc.).

This thesis also aims to the development of a simplified EC8-compliant performance-based design framework for buildings using LTHA. In particular, this thesis focuses on a simplified fragility assessment procedure based on Cloud Analysis (CA) that allows to obtain fragility curves at design stage through LTHA. Results could be used for comparing design solutions in terms of economic losses due to earthquakes at design stage without needing the definition of a nonlinear model. The PBEE methodology developed by the Pacific Earthquake Engineering Research (PEER) centre is of high interest nowadays and many efforts are currently made to investigate and improve it. NTHA is the reference method of analysis in the PEER's methodology for characterising the probabilistic relationship between Engineering Demand Parameters (EDP) and Intensity Measures (IMs). However, the complexity of NTHA in terms of modelling choices, post-processing data elaboration, solution of the numerical problems, can limit its use in the professional field. In this thesis, LTHA is shown to be a valid compromise between design practice and incoming performance-based methodologies. Moreover, its simplicity of implementation in commercial software packages and velocity of analyses make LTHA an intuitive and effortless tool for practitioners and analysts. In Chapter 7, a new procedure for LTHA-based fragility assessment through CA is presented in detail. This procedure is based on four steps: (i) selection of GMs consistent with the hazard at the site of interest, (ii) check of possible LTHA "unacceptable cases" through the proposed I_{eq} index, (iii) check of the spectrum-compatibility with the target (code) spectrum in order to be consistent with design purposes, and (iv) check of CA criteria to avoid bias. As example, the procedure is presented assuming as case study the 12 storey RC-MRF building described in Chapter 3 and it is presented for two limit states: LS-LS and DL-LS. Chapter 7 also includes a study on the sensitivity to the uncertainties in the parameters of regression related to the GM suite size through the bootstrap method. It is shown, for the benchmark building, that if the "unacceptable cases" in LTHA are avoided and mean capacities are considered, it can overestimate the median of the *SaT1* values leading to

LS-LS (denoted by η_{SaT1}) by only 8% with respect to NTHA. It is suggested that eleven earthquakes can be a reasonable minimum limit for GM suite size for LTHA.

This research work provides recommendations that could be implemented in future guidelines and/or design codes and it can open up to further studies on LTHA. The main aim of this work is contributing in refining the current seismic design practice, providing a useful tool for engineers and analysts that can be easily implemented by any commercial software package.

8.2.Limitations and future research

The work presented in this thesis can be extended in many directions. In the following, a list of possible limitations of this work and relevant topics for future work is provided:

- the results found in this research work are valid for the considered regular 12-storey RC-MRF building. While the proposed LTHA-based design procedure is conceptually applicable to design of non-building structures and irregular buildings (both in plan and in elevation), such systems are not explicitly considered in this work. However, indications on how to carry out LTHA-based design of irregular buildings are provided herein but further research is needed to validate them. Other case studies could be buildings with different configurations (e.g., dimensions, number of storeys) as well as different structural typologies (e.g., RC walls, steel braces, isolated structures). The code framework developed in this thesis is flexible enough for allowing implementation of specific numerical structural models suitable for shear walls, braces, isolators, etc.;
- the staircase modelled in the benchmark building represents a critical element within the structure and it relevantly affects the results found in this work. Many studies in the literature neglected the presence of the staircase. While neglecting the staircase would lead to results closer to the ideal behaviour contemplated by design codes, it represents a realistic design feature that should be considered for the sake of consistency with the construction practice. Future works could be addressed at evaluating, for the benchmark building of this work and/or other case studies, the differences in terms of seismic behaviour between buildings with/without staircase or different design solutions;
- accidental eccentricity is neglected in this research work. Even if it should be considered for regular buildings too, such as the benchmark building considered in this research work. However, its influence for regular buildings is not particularly relevant but its inclusion for future studies can make results more accurate, especially if irregular buildings are analysed. In this light, the code framework developed in this thesis is meant to help with analysing different cases with shift of centre of mass;
- the main type of uncertainty addressed in this research work is that related to the ground motion selection. While this type of uncertainty can be considered as the most critical in

terms of impact on results, other types of uncertainty can be relevant and affect the results found in this work. Other uncertainties can be those related to material properties, geometry, constructional details, modelling aspects, etc. These uncertainties can have relevant impact on results for both LTHA and NTHA. For NTHA, modelling uncertainties can even be larger than LTHA and this can affect the comparison results between LTHA and NTHA presented in this work. Further work could aim at assessing the impact of different uncertainties on the results found in this research work;

Appendix

Table A-1 Summary of earthquake events for the suite of Unspecified-Field Unscaled (UF-U) ground motions selected for Life Safety-Limit State from the European Strong Motion database.

N	*Waveform ID*	*Earthquake Event*	*Station ID*	M_w	R_{epi} [km]	*EC8Soil Class*	*SF*	I_{eq} [g]
1	196	Montenegro (1979)	Petrovac-Hotel Oliva	6.9	25	B	1.00	0.0491; -0.0142
2	239	Dursunbey (1979)	Dursunbey-Kandili	5.3	6	B	1.00	0.0402; -0.0415
3	291	Campano-Lucano (1980)	Calitri	6.9	16	B	1.00	0.0302; 0.0017
4	535	Erzincan (1992)	Erzincan	6.6	13	B	1.00	0.0976; 0.0527
5	4673	South Iceland (2000)	Hella	6.5	15	B	1.00	-0.0390; 0.0339
6	6328	South Iceland (aftershock)	Kaldarholt	6.4	12	B	1.00	-0.0210; -0.0011
7	6334	South Iceland (aftershock)	Solheimar	6.4	11	B	1.00	-0.0107; 0.1124

Table A-2 Summary of earthquake events for the suite of Unspecified-Field Spectral-Matched (UF-SM) ground motions selected for Life Safety-Limit State from the European Strong Motion database.

N	*Waveform ID*	*Earthquake Event*	*Station ID*	M_w	R_{epi} [km]	*EC8Soil Class*	*SF*	I_{eq} [g]
1	196	Montenegro (1979)	Petrovac-Hotel Oliva	6.9	25	B	1.00	0.0093; 0.0077
2	291	Campano-Lucano (1980)	Calitri	6.9	16	B	1.00	0.0091; 0.0101
3	535	Erzincan (1992)	Erzincan	6.6	13	B	1.00	0.0089; 0.0090

Table A-3 Summary of earthquake events for the suite of Unspecified-Field Scaled N1 (UF-S1) ground motions selected for Life Safety-Limit State from the European Strong Motion database.

N	***Waveform ID***	***Earthquake Event***	***Station ID***	M_w	R_{epi} **[km]**	***EC8Soil Class***	***SF***	I_{eq} **[g]**
1	196	Montenegro (1979)	Petrovac-Hotel Oliva	6.9	25	B	1.00	0.0491; -0.0142
2	239	Dursunbey (1979)	Dursunbey-Kandili	5.3	6	B	4.50	0.0461; 0.0402
3	291	Campano-Lucano (1980)	Calitri	6.9	16	B	1.20	0.0492; 0.0151
4	535	Erzincan (1992)	Erzincan	6.6	13	B	0.70	0.0489; 0.0174
5	4673	South Iceland (2000)	Hella	6.5	15	B	1.10	-0.0364; 0.0437
6	6328	South Iceland (aftershock)	Kaldarholt	6.4	12	B	1.75	0.0119; 0.0468
7	6334	South Iceland (aftershock)	Solheimar	6.4	11	B	0.60	-0.0324; 0.0415

Table A-4 Summary of earthquake events for the suite of Unspecified-Field Scaled N2 (UF-S2) ground motions selected for Life Safety-Limit State from the PEER NGA West2 database.

N	RSN ID	Earthquake Event	Station ID	M_w	R_{jb} [km]	EC8Soil Class	T_P [s]	SF	I_{eq} [g]
1	15	Kern County (1952)	Taft Lincoln School	7.36	38	385	-	2.50	0.0333; 0.0331
2	20	Northern Calif-03 (1954)	Ferndale City Hall	6.5	27	219	-	1.40	0.0333; 0.0313
3	30	Parkfield (1966)	Cholame – SA#5	6.19	10	290	-	1.48	0.0334; 0.0015
4	57	San Fernando (1971)	Castaic – Old Ridge Route	6.61	19	450	-	1.57	0.0078; 0.0326
5	6	Imperial Valley-02 (1940)	El Centro Array #9	6.95	6	213	-	1.18	0.0307; 0.0192
6	95	Man. Nicaragua-01 (1972)	Managua ESSO	6.24	4	289	-	1.23	0.0171; 0.0328
7	96	Man. Nicaragua-02 (1972)	Managua ESSO	5.2	4	289	-	1.76	0.0315; 0.0099

Table A-5 Summary of earthquake events for the suite of Far-Field Unscaled (FF-U) ground motions selected for Life Safety-Limit State from the PEER NGA West2 database (source FEMA P-695).

N	RSN ID	Earthquake Event	Station ID	M_w	R_{jb} [km]	$V_{S,30}$ [m/s]	EC8Soil Class	T_P [s]	SF	I_{eq} [g]
1	1111	Kobe (1995)	Nishi-Akashi	6.9	7	609	B	-	1.00	0.0405; 0.0188
2	1116	Kobe (1995)	Shin-Osaka	6.9	19	256	C	-	1.00	0.0148; 0.0087
3	1148	Kocaeli (1999)	Arcelik	7.51	11	523	B	7.791	1.00	-0.0370; -0.0358
4	1158	Kocaeli (1999)	Duzce	7.51	14	282	C	-	1.00	0.0167; 0.0805
5	1244	Chi-Chi (1999)	CHY101	7.62	10	259	C	5.341	1.00	0.0087; 0.0497
6	125	Friuli-01 (1976)	Tolmezzo	6.5	15	505	B	-	1.00	-0.0035; 0.0013
7	1485	Chi-Chi (1999)	TCU045	7.62	26	705	B	9.338	1.00	0.0132; 0.0235
8	1602	Duzce (1999)	Bolu	7.14	12	294	C	0.882	1.00	0.0768; 0.1122
9	1633	Manjil (1990)	Abbar	7.37	13	724	B	-	1.00	0.0099; 0.0401
10	169	Imp. Valley-06 (1979)	Delta	6.53	22	242	C	-	1.00	-0.0107; 0.0128
11	174	Imp. Valley-06 (1979)	El Centro Array #11	6.53	13	196	C	-	1.00	0.0139; 0.0195
12	1787	Hector Mine (1999)	Hector	7.13	10	726	B	-	1.00	0.0224; 0.0525
13	68	San Fernando (1971)	LA – HS FF	6.61	23	316	C	-	1.00	-0.0050; -0.0350
14	721	Superstition Hills-02 (1987)	EC I CC	6.54	18	192	C	-	1.00	0.0338; 0.0082
15	725	Superstition Hills-02 (1987)	Poe Road (temp)	6.54	11	317	C	2.87	1.00	0.0292; 0.0076
16	752	Loma Prieta (1989)	Capitola	6.93	9	289	C	-	1.00	0.0927; 0.0207
17	767	Loma Prieta (1989)	Gilroy Array #3	6.93	12	350	C	2.639	1.00	0.0128; 0.0263
18	829*	Cape Mend. (1992)	Rio Dell Overpass	7.01	8	NA	NA	NA	1.00	0.0632; 0.0426

19	848	Landers (1992)	Coolwater	7.28	20	353	C	-	1.00	-0.0054; 0.0424
20	900	Landers (1992)	Yermo Fire Station	7.28	24	354	C	7.504	1.00	0.0348; 0.0050
21	953	Northridge-01 (1994)	BH- 14145 Mulhol	6.69	9	356	C	-	1.00	0.1058; 0.1167
22	960	Northridge-01 (1994)	CC - WLC	6.69	11	326	C	-	1.00	0.0164; 0.0442

** Selected from PEER NGA West1 since not available in the latest version.*

Table A-6 Summary of earthquake events for the suite of Near-Field Pulse-Like Unscaled (NFPL-U) ground motions selected for Life Safety-Limit State from the PEER NGA West2 database (source FEMA P-695).

N	RSN ID	Earthquake Event	Station ID	M_w	R_{jb} [km]	$V_{S,30}$ [m/s]	EC8Soil Class	Strike [deg]	T_P [s]	SF	I_{eq} [g]
1	1063	Northridge-01 (1994)	RRS	6.69	0	282	C	122	1.246	1.00	0.2742; 0.0666
2	1086	Northridge-01 (1994)	Sylmar - OVM FF	6.69	2	441	B	122	2.436	1.00	0.1497; 0.0781
3	1165	Kocaeli (1999)	Izmit	7.51	4	811	A/E	271	5.369	1.00	-0.0156; -0.0103
4	1503	Chi-Chi (1999)	TCU065	7.62	1	306	C	20	5.74	1.00	0.1650; 0.1075
5	1529	Chi-Chi (1999)	TCU102	7.62	1	714	B	20	9.632	1.00	0.0799; 0.0210
6	1605	Duzce (1999)	Duzce	7.14	0	282	C	270	-	1.00	0.0437; 0.0832
7	181	Imp. Valley-06 (1979)	El Centro Array #6	6.53	0	203	C	323	3.773	1.00	0.0347; 0.0260
8	182	Imp. Valley-06 (1979)	El Centro Array #7	6.53	1	211	C	323	4.375	1.00	0.0591; 0.0402
9	292	Irpinia-01 (1980)	Sturno	6.9	7	382	B	313	3.273	1.00	-0.0144; 0.0486
10	723	Sup. Hills-02 (1987)	Parachute Test Site	6.54	1	349	C	127	2.394	1.00	0.1266; 0.0678
11	802	Loma Prieta (1989)	Saratoga - Aloha Ave	6.93	8	381	B	128	4.571	1.00	0.0387; 0.0158
12	821	Erzican (1992)	Erzican	6.69	0	352	C	122	-	1.00	0.1206; 0.0121
13	828	Cape Mend. (1992)	Petrolia	7.01	0	422	B	350	2.996	1.00	0.0827; 0.0442
14	879	Landers (1992)	Lucerne	7.28	2	1369	A/E	336	5.124	1.00	0.0623; 0.0124

Table A-7 Summary of earthquake events for the suite of Near-Field Not Pulse-Like Unscaled (NFNPL-U) ground motions selected for Life Safety-Limit State from the PEER NGA West2 database (source FEMA P-695).

N	RSN ID	Earthquake Event	Station ID	M_w	R_{jb} [km]	$V_{S,30}$ [m/s]	EC8Soil Class	Strike [deg]	T_P [s]	SF	I_{eq} [g]
1	1004	Northridge-01 (1994)	LA - SVAH	6.69	0	380.06	B	122	0.931	1.00	0.0915; 0.1011
2	1048	Northridge-01 (1994)	N- 17645 SS	6.69	0	280.86	C	122	-	1.00	0.0976; 0.0471
3	1176	Kocaeli (1999)	Yarimca	7.51	1	297	C	271	4.949	1.00	0.0207; 0.0534
4	126	Gazli (1976)	Karakyr	6.8	4	259.59	C	267	-	1.00	0.0821; 0.0407
5	1504	Chi-Chi (1999)	TCU067	7.62	1	433.63	B	20	-	1.00	0.1087; 0.0444
6	1517	Chi-Chi (1999)	TCU084	7.62	0	665.2	B	20	-	1.00	0.3243; 0.1588
7	160	Imp. Valley-06 (1979)	Bonds Corner	6.53	0	223.03	C	323	-	1.00	0.0969; 0.0377
8	165	Imp. Valley-06 (1979)	Chihuahua	6.53	7	242.05	C	323	-	1.00	0.0152; 0.0007
9	2114	Denali (2002)	TAPS PS #10	7.9	0	329.4	C	298	3.157	1.00	0.0731; 0.0620
10	495	Nahanni (1985)	Site 1	6.76	2	605.04	B	160	-	1.00	0.0283; 0.0176
11	496	Nahanni (1985)	Site 2	6.76	0	605.04	B	160	-	1.00	-0.0268; -0.0133
12	741	Loma Prieta (1989)	BRAN	6.93	4	476.54	B	128	-	1.00	0.0890; 0.0206
13	753	Loma Prieta (1989)	BV #10_ WR	6.93	0	462.24	B	128	-	1.00	0.0451; 0.0398
14	825	Cape Mend. (1992)	Cape Mendocino	7.01	0	567.78	B	350	4.84	1.00	0.0313; 0.0950

Table A-8 Summary of earthquake events for the suite of Pulse-Like Unscaled (PL-U) ground motions with $T_P \leq T_1$ selected for Life Safety-Limit State from the PEER NGA West2 database (source Shahi 2013).

N	RSN ID	Earthquake Event	Station ID	M_w	R_{jb} [km]	$V_{S,30}$ [m/s]	EC8Soil Class	Strike [deg]	T_P [s]	SF	I_{eq} [g]
1	1004	Northridge-01 (1994)	LA - S VA Hospital	6.69	0	380	B	122	0.931	1.00	0.0915; 0.1011
2	1051	Northridge-01 (1994)	P D (upper left)	6.69	5	2016	A/E	122	0.84	1.00	0.1454; 0.0727
3	1052	Northridge-01 (1994)	P K C	6.7	5	508	B	122	0.728	1.00	0.0441; 0.0248
4	1602	Duzce (1999)	Bolu	7.14	12	294	C	270	0.882	1.00	0.0768; 0.1118
5	4097	Parkfield-02 (2004)	Slack Canyon	6	2	648	B	141	0.854	1.00	0.0057; 0.0274
6	4116	Parkfield-02 (2004)	P – S C 4E	6	8	246	C	141	0.6	1.00	0.1081; 0.0405
7	415	Coalinga-05 (1983)	Transmitter Hill	5.77	4	477	B	355	0.88	1.00	0.0469; 0.0063
8	4211	Niigata (2004)	NIG021	6.63	10	419	B	212	0.322	1.00	0.0229; 0.0690
9	4874	Chuetsu-oki (2007)	Oguni Nagaoka	6.8	10	562	B	34	0.8	1.00	0.1007; 0.0202
10	568	San Salv. (1986)	G I Center	5.8	2	489	B	32	0.805	1.00	0.0849; 0.0522

Table A-9 Summary of earthquake events for the suite of Unspecified-Field Unscaled (UF-U) ground motions selected for Damage Limitation-Limit State from the European Strong Motion database.

N	***ESM ID***	***Earthquake Event***	***Station ID***	***M_w***	***R_{epi}* [km]**	***EC8Soil Class***	***SF***
1	229	Montenegro (aftershock)	ST75	6.2	17	B	1.00
2	233	Montenegro (aftershock)	ST74	6.2	22	B	1.00
3	291	Campano Lucano (1980)	ST276	6.9	16	B	1.00
4	436	Kyllini (1988)	ST171	5.9	14	B	1.00
5	640	Umbria Marche (aftershock)	ST86	5.6	20	B	1.00
6	1314	Ano Liosia (1999)	ST1101	6	17	B	1.00
7	6330	South Iceland (aftershock)	ST2482	6.4	21	B	1.00

Table A-10 Summary of earthquake events for the suite of 24 ground motions selected for Damage Limitation-Limit State from the PEER NGA West2 database.

N	RSN ID	Earthquake Event	Station ID	M_w	R_{jb} [km]	$V_{S,30}$ [m/s]	EC8Soil Class	SF
1	1	Helena Montana-01 (1935)	Carroll College	6	2	593	B	1.00
2	100	Hollister-03 (1974)	San Juan Bautista 24 Polk St	5.14	9	336	C	1.00
3	11	Northwest Calif-03 (1951)	Ferndale City Hall	5.8	54	219	C	1.00
4	12	Kern County (1952)	LA – Hollywood Stor FF	7.36	115	316	C	1.00
5	13	Kern County (1952)	Pasadena – CIT Athenaeum	7.36	123	415	B	1.00
6	16	Northern Calif-02 (1952)	Ferndale City Hall	5.2	43	219	C	1.00
7	22	El Alamo (1956)	El Centro Array #9	6.8	121	213	C	1.00
8	26	Hollister-01 (1961)	Hollister City Hall	5.6	20	199	C	1.00
9	31	Parkfield (1966)	Cholame – Shandon Array #8	6.19	13	257	C	1.00
10	33	Parkfield (1966)	Temblor pre-1969	6.19	16	528	B	1.00
11	34	Northern Calif-05 (1967)	Ferndale City Hall	5.6	27	219	C	1.00
12	36	Borrego Mtn (1968)	El Centro Array #9	6.63	45	213	C	1.00
13	50	Lytle Creek (1970)	Weightwood – 6074 Park Dr	5.33	11	486	B	1.00
14	70	San Fernando (1971)	Lake Hughes #1	6.61	22	425	B	1.00
15	71	San Fernando (1971)	Lake Hughes #12	6.61	14	602	B	1.00
16	72	San Fernando (1971)	Lake Hughes #4	6.61	19	600	B	1.00
17	77	San Fernando (1971)	Pacoima Dam (upper left abut)	6.61	0	2016	A	1.00
18	78	San Fernando (1971)	Palmdale Fire Station	6.61	24	453	B	1.00

19	8	Northern Calif-01 (1941)	Ferndale City Hall	6.4	45	219	C	1.00
20	80	San Fernando (1971)	Pasadena – Old Seismo Lab	6.61	22	969	A	1.00
21	88	San Fernando (1971)	Santa Felita Dam (Outlet)	6.61	25	389	B	1.00
22	93	San Fernando (1971)	Whittier Narrows Dam	6.61	39	299	C	1.00
23	97	Point Mugu (1973)	Port Hueneme	5.65	15	249	C	1.00
24	99	Hollister-03 (1974)	Hollister City Hall	5.14	9	199	C	1.00

Bibliography

Abrahamson NA (2000). Effects of rupture directivity on probabilistic seismic hazard analysis. Sixth International Conference on Seismic Zonation, Palm Springs, California, November 12-15.

Alam MS and Barbosa AR (2018). Probabilistic seismic demand assessment accounting for finite element model class uncertainty: Application to a code-designed URM infilled reinforced concrete frame building. Earthquake Engineering and Structural Dynamics; 47:2901-2920.

Almufti I, Motamed R, Grant DN, and Willford M (2015). Incorporation of velocity pulses in design ground motions for response history analysis using a probabilistic framework. Earthquake Spectra; 31(3):1647-1666.

American Concrete Institute Committee, and International Organization for Standardization (2008). Building code requirements for structural concrete and commentary, ACI 318-08, MI, USA.

Antoniou S and Pinho R (2004). Development and verification of a displacement-based adaptive pushover procedure. Journal of Earthquake Engineering; 8(5):643-661.

ASCE/SEI 41-13 (2014). Seismic Evaluation and Retrofit of Existing Buildings, American Society of Civil Engineers, Reston, VA.

ASCE/SEI 7-16 (2017). Minimum design loads and associated criteria for buildings and other structures, American Society of Civil Engineers, Reston, VA.

ASDEA Software (2019). Scientific ToolKit for OpenSees, STKO.

ATC (1996). Seismic Evaluation and Retrofit of Concrete Buildings, ATC 40 Report, Volumes 1 and 2, Applied Technology Council, Redwood City, CA.

Aswegan K and Charney FA (2014). A simple linear response history analysis procedure for building codes. Proceedings of the 10th US National Conference in Earthquake Engineering, Anchorage, Alaska, July 21-25.

Bachmann H, Ammann WJ, Deischl F, Eisenmann J, Floegl I, Hirsch GH, Klein GK, Lande GJ, Mahrenholtz O, Natke HG, Nussbaumer H, Pretlove AJ, Rainer JH, Saemann EU, and Steinbeisser L (1995). Vibration Problems in Structures. Practical Guidelines. Birkhauser, Basel.

Baker JW (2007). Quantitative classification of Near-Fault ground motions using wavelet analysis. Bulletin of the Seismological Society of America; 97(5):1486-1501.

Baker JW (2011). Conditional mean spectrum: tool for ground-motion selection. Journal of Structural Engineering, ASCE; 137(3):322-331.

Baker JW (2015). Efficient analytical fragility function fitting using dynamic structural analysis. Earthquake Spectra; 31(1):579-599.

Baker JW and Cornell CA (2005). A vector-valued ground motion intensity measure consisting of spectral acceleration and epsilon. Earthquake Engineering and Structural Dynamics; 34(10):1193-1217.

Barbosa AR (2011). Simplified vector-valued probabilistic seismic hazard analysis and probabilistic seismic demand analysis: application to the 13-storey NEHRP reinforced concrete frame-wall building design example, a dissertation for the degree of PhD, University of California, San Diego, California, USA.

Barbosa AR, Fahnestock LA, Fick DR, Gautam D, Soti R, Wood R, Moaveni B, Stavridis A, Olsen MJ, and Rodrigues H (2017). Performance of Medium-to-High Rise Reinforced Concrete Frame Buildings with Masonry Infill in the 2015 Gorkha, Nepal, Earthquake. Earthquake Spectra; 33(S1):S197-S218.

Basu D, Constantinou MC, and Whittaker A (2014). An equivalent accidental eccentricity to account for the effects of torsional ground motion on structures. Engineering Structures; 69:1-11.

Bazzurro P, Cornell CA, Shome N, and Carballo JE (1998). Three proposals for characterizing MDOF nonlinear seismic response. Journal of Structural Engineering (ASCE); 124(11):1281-1289.

Beck JL and Au SK (2002) Bayesian updating of structural models and reliability using Markov chain Monte Carlo simulation. Journal of Engineering Mechanics; 128(4):380–391

Bernal D (1994). Viscous damping in inelastic structural response. Journal of Structural Engineering (ASCE); 120(4):1240–1254.

Berry M, Parrish M, and Eberhard M (2004). PEER Structural Performance Database. Pacific Earthquake Engineering Research Center, University of California, Berkeley, California. Available at: https://nisee.berkeley.edu/spd/. Last access in January 2017.

Bhatt C and Bento R (2014), The Extended Adaptive Capacity Spectrum Method for the Seismic Assessment of Plan-Asymmetric Buildings. Earthquake Spectra; 3(2): 683-703.

Biskinis D and Fardis MN (2010a). Deformations at flexural yielding of members with continuous or lap-spliced bars. Structural concrete; 11(3):127-138.

Biskinis D and Fardis MN (2010b). Flexure-controlled ultimate deformations of members with continuous or lap-spliced bars. Structural concrete; 11(2):93-108.

Biskinis DE (2007). Resistance and deformation capacity of concrete members with or without retrofitting, a dissertation for the degree of PhD, University of Patras, Patras, Greece.

Bommer JJ and Acevedo AB (2004). The use of real earthquake accelerograms as input to dynamic analysis. Journal of Earthquake Engineering; 8(1):43-91.

Bommer JJ, Scott SG, and Sarma SK (2000). Hazard-consistent earthquake scenario. Soil Dynamics and Earthquake Engineering; 19(4):219-231.

Börgesson L (1996). ABAQUS. Developments in Geotechnical Engineering; 79:656-570.

Bousias SN (1993). Experimental and analytical study of RC columns in cyclic biaxial bending with axial force, a dissertation for the degree of PhD, University of Patras, Patras, Greece.

Bousias SN, Panagiotakos TB, and Fardis MN (2002). Modelling of RC members under cyclic biaxial flexure and axial force. Journal of Earthquake Engineering; 6(2):213-238.

Building Seismic Safety Council (2015). NEHRP Recommended seismic provisions for new buildings and other structures. Vol 1 – Part 1 Provisions, Part 2 Commentary. Technical Report, Washington, DC, FEMA P-1050-1.

Building Seismic Safety Council (2016). 2015 NEHRP Recommended seismic provisions: design examples. Technical Report, Washington, DC, FEMA P-1051.

Cacciola P, Colajanni P, and Muscolino G (2004). Combination of modal responses consistent with seismic input representation. Journal of Structural Engineering, ASCE; 130:47-55.

Calabrese A, Almeida JP, and Pinho R (2010). Numerical Issues in Distributed Inelasticity Modeling of RC Frame Elements for Seismic Analysis. Journal of Earthquake Engineering; 14(S1):38-68.

Calvi GM (2018). Revisiting design earthquake spectra. Earthquake Engineering & Structural Dynamics, https://doi.org/10.1002/eqe.3101

Calvi GM, Pinho Rui, and Crowley H (2006). State-of-the-knowledge on the period elongation of RC buildings during strong ground shaking. 1st European Conference on Earthquake Engineering and Sismology, a joint event of the 13th ECEE & 30th General Assembly of the ESC. Geneva, Switzerland, September 3-8.

Campbell K and Bozorgnia Y (2007). Campbell-Bozorgnia NGA Ground Motion Relations for the Geometric Mean Horizontal Component of Peak and Spectral Ground Motion Parameters. PEER Report No. 2007/02, Pacific Earthquake Engineering Research Center, University of California, Berkeley.

Caughey TK (1960). Classical normal modes in damped linear dynamic systems. Journal of Applied Mechanics (ASME); 27(2):269–271.

Chang GA and Mander JB (1994). Seismic Energy Based Fatigue Damage Analysis of Bridge Columns: Part 1 – Evaluation of Seismic Capacity. Technical Report NCEER-94-0006. National Center for Earthquake Engineering Research, State University of New York, Buffalo, NY.

Charney FA (2015). A new linear response history analysis procedure for the 2015 NEHRP Recommended Provisions and for ASCE 7-16. Structural Congress.

Charney FA (2008). Unintended consequences of modeling damping in structures. Journal of Structural Engineering (ASCE); 134(4):581–592.

Chioccarelli E and Iervolino I (2010). Near-source seismic demand and pulse-like records: a discussion for 888 L'Aquila earthquake. Earthquake Engineering and Structural Dynamics; 39:1039-1062.

Chopra AK (2012). Dynamics of the structures: theory and applications to earthquake engineering. Pearson, 4th Edition, Prentice Hall.

Chopra AK and Goel RK (2002). A modal pushover analysis procedure for estimating seismic demands for buildings. Earthquake Engineering and Structural Dynamics; 31(3):561-582.

Chopra AK and McKenna F (2016). Modelling Viscous Damping in Nonlinear Response History Analysis of Buildings for Earthquake Excitation. Earthquake Engineering and Structural Dynamics; 45:193-211.

Cimellaro GP and Marasco S (2015). A computer-based environment for processing and selection of seismic ground motion records: OPENSIGNAL. Frontiers in Built Environment; 1(17):1-13.

Clough RW and Penzien J (2003). Dynamics of Structures. Computers & Structures, Inc., 3rd Edition.

Computers and Structures Inc. (1976). SAP2000 v18, Berkeley, CA.

Cornell CA, Jalayer F, Hamburger RO, Foutch DA (2002). Probabilistic basis for 2000 SAC federal emergency management agency steel moment frame guidelines. Journal of Structural Engineering, ASCE;128(4):526-533.

D'Ayala D, Meslem A, Vamvatsikos D, Porter K, and Rossetto T (2015). Guidelines for Analytical Vulnerability Assessment of Low/Mid-Rise Buildings, Vulnerability Global Component Project.

De La Llera JC and Chopra AK (1994). Accidental torsion in buildings due to base rotational excitation. Earthquake Engineering and Structural Dynamics; 23:1003-1021.

De Luca F and Galasso C (2015). Influence of RC columns' failure mode on simplified seismic loss estimation. 12th International Conference on Applications of Statistics and Probability in Civil Engineering, Vancouver, Canada, July 12-15.

De Luca F and Verderame GM (2013). The accuracy of CQC and response spectrum analysis in the case of impulsive earthquakes. Proceedings of the 11th International Conference on Structural Safety and Reliability, ICOSSAR.

De Luca F, Verderame GM, and Manfredi G (2014). Eurocode-based seismic assessment of modern heritage RC structures: The case of the Tower of the Nations in Naples (Italy). Engineering Structures; 74:96-110.

Deierlein GC, Reinhorn AM, and Willford MR (2010). Nonlinear structural analysis for seismic design. NEHRP Seismic Design Technical Brief No. 4, produced by the NEHRP Consultants Join Venture, a partnership of the Applied Technology Council and the Consortium of Universities for Research in Earthquake Engineering, for the National Institute of Standards and Technology, Gaithersburg, MD, NIST GCR 10-917-5.

Der Kiureghian A (1981). A response spectrum method for random vibration analysis of MDF systems. Earthquake Engineering and Structural Dynamics; 9:419–435.

Der Kiureghian A. and Nakamura Y (1993). CQC modal combination rule for high-frequency modes. Earthquake Engineering and Structural Dynamics; 22:943–956.

Di Cuia A. Lombardi L, De Luca F, De Risi R, Caprili S, and Salvatore W (2017). Linear Time-History Analysis for EC8 Design of CBF Structures. X International Conference on Structural Dynamics, Rome, Italy, September 10-13.

Elnashai AS and Mwafy AM (2002). Overstrength and force reduction factors of multistorey reinforced-concrete buildings. The Structural Design of Tall Buildings; 11:329-351.

European Committee for Standardization, CEN (2001). Eurocode 1: Actions on structures – Part 1-1: General actions – Densities, self-weight, imposed loads for buildings, EN 1991-1-1:2001, Brussels, BE.

European Committee for Standardization, CEN (2002). Eurocode 0: Basis of structural design, EN 1990:2002, Brussels, BE.

European Committee for Standardization, CEN (2003). Eurocode 1: Actions on structures – Part 1-3: General actions – Snow loads, EN 1991-1-3:2003, Brussels, BE.

European Committee for Standardization, CEN (2004a). Eurocode 8: Design of structures for earthquake resistance – Part 1: General rules, seismic actions and rules for buildings, EN 1998-1:2004, Brussels, BE.

European Committee for Standardization, CEN (2004b). Eurocode 2: Design of concrete structures – Part 1-1: General rules and rules for buildings, EN 1992-1-1:2004, Brussels, BE.

European Committee for Standardization, CEN (2005). Eurocode 8: Design of structures for earthquake resistance – Part 3: Assessment and retrofitting of buildings, EN 1998-3:2005, Brussels, BE.

European Strong-Motion database (2008). EC Commission for Community Research 5th Framework. Available at: http://www.isesd.hi.is/ESD_Local/frameset.htm. Last access in July 2018

Faggella M, Barbosa AR, Conte JP, Spacone E, and Restrepo JI (2013). Probabilistic seismic response analysis of a 3-D reinforced concrete building. Structural Safety; 44:11-27.

Fajfar P (2000). A nonlinear analysis method for performance-based seismic design. Earthquake Spectra; 16(3): 573–593.

Fardis MN (2009). Seismic design, assessment and retrofitting of concrete buildings – based on EN-Eurocode 8. Springer.

FEMA (1996). Performance Based Seismic Design of Buildings, Report No. FEMA-283, Federal Emergency Management Agency, Washington, D.C.

FEMA (1997). NEHRP Guidelines for Seismic Rehabilitation of Buildings, Report No. FEMA-273, Federal Emergency Management Agency, Washington, D.C.

FEMA (2000). Commentary for the seismic rehabilitation of buildings. FEMA-356, Federal Emergency Management Agency, Washington, DC.

FEMA (2009). Quantification of Building Seismic Performance Factors. FEMA P-695, prepared for the Federal Emergency Management Agency by the Applied Technology Council.

FEMA (2018a). Seismic Performance Assessment of Buildings: Vol. 1 – Methodology. FEMA P-58-1, Second Edition.

FEMA (2018b). Seismic Performance Assessment of Buildings: Vol. 2 – Implementation Guide. FEMA P-58-2, Second Edition.

FEMA (2018c). Guidelines for Performance-Based Seismic Design of Buildings: Vol. 6. FEMA P-58-6, Second Edition.

Filippou FC, Popov EP, and Bertero VV (1983). Effects of Bond Deterioration on Hysteretic Behavior of Reinforced Concrete Joints. Report EERC 83-19. Earthquake Engineering Research Center, University of California, Berkeley, California.

Fragiadakis M and Papadrakakis M (2008). Modeling, analysis and reliability of seismically excitet structures: Computational issues. International Journal of Computational Methods; 5(4):483-511/

Fragiadakis M, Ioannidou D, and Papadrakakis M (2007). Assessment of Nonlinear Static Analysis Procedures in the Framework of Performance-Based Design. 8th National Congress on Mechanics (HSTAM2007), June 12-17, 2007, Patras, Greece.

Fragiadakis M, Vamvatsikos D, and Aschheim M (2014). Application of nonlinear static procedures for the seismic assessment of regular RC moment frame buildings. Earthquake Spectra; 30(2):767-794.

Galasso C, Zhong P, Zareian F, Iervolino I, and Graves RW (2013). Validation of ground-motion simulations for historical events using MDoF systems. Earthquake Engineering and Structural Dynamics; 42:1395-1412.

Ghobarah A (2001). Performance-based design in earthquake engineering: state of development. Engineering Structures; 23:878-884.

Giannopoulos D and Vamvatsikos D (2018). Ground motion records for seismic performance assessment: To rotate or not to rotate? Earthquake Engineering & Structural Dynamics; 47(12):2410-2425.

Goda K and Atkinson GM (2011). Seismic performance of wood-frame houses in south-western British Columbia. Earthquake Engineering and Structural Dynamics; 40:903-924.

Goel RK and Chopra AK (2005). Extension of Modal Pushover Analysis to Compute Member Forces, Earthquake Spectra; 21(1):125-139.

Goulet CA, Haselton CB, Mitrani-Reiser J, Beck JL, Deierlein GG, Porter KA, and Stewart JP (2007). Evaluation of the seismic performance of a code-conforming reinforced-concrete frame building – from seismic hazard to collapse safety and economic losses. Earthquake Engineering and Structural Dynamics; 36:1973-1997.

Gupta AK (1992). Response spectrum method in seismic analysis and design of structures. CRC Press.

Hall JF (2006). Problems encountered from the use (or misuse) of Rayleigh damping. Earthquake Engineering and Structural Dynamics; 35:525–545.

Hancock J, Bommer JJ, and Stafford PJ (2008). Numbers of scaled and matched accelerograms required for inelastic dynamic analyses. Earthquake Engineering and Structural Dynamics; 37(14):1585-1607.

Hancock J, Watson-Lamprey J, Abrahamson N, Bommer J, Markatis A, McCoy E, and Mendis R (2006). An improved method of matching response spectra of recorded earthquake ground motion using wavelets. Journal of Earthquake Engineering; 10(1):67-89.

Haselton C, Ghannoum W, Hachem M, Hooper JD, and Pujol S (2017c). Guidelines for Nonlinear Structural Analysis for Design of Buildings - Part IIb – Reinforced Concrete Moment Frames. NEHRP Seismic Design Technical Brief No. 4, produced by the Applied Technology Council for the U.S. Department of Commerce Engineering Laboratory National Institute of Standards and Technology, Gaithersburg, MD, NIST GCR 17-917-46v3.

Haselton CB (2006). Assessing Seismic Collapse Safety of Modern Reinforced Concrete Moment Frame Buildings. A dissertation for the degree of PhD, Stanford University, California.

Haselton CB, Baker JW, Stewart JP, Whittaker AS, Luco N, Fry A, Hamburger RO, Zimmerman RB, Hooper JD, Charney FA, and Pekelnicky RG (2017a). Response history analysis for the design of new buildings in the NEHRP provisions and ASCE/SEI 7 standard: Part I – Overview and specification of ground motions. Earthquake Spectra; 33(2):373-395.

Haselton CB, Fry A, Hamburger RO, Baker JW, Zimmerman RB, Luco N, Elwood KJ, Hooper JD, Charney FA, Pekelnicky RG, and Whittaker AS (2017b). Response-history analysis for the design of new buildings in the NEHRP provisions and ASCE/SEI 7 standards: Part II – Structural analysis procedures and acceptance criteria. Earthquake Spectra; 33(2):397-417.

Haselton CB, Liel AB, Deierlein GG, Dean BS, and Chou JH (2011). Seismic collapse safety of reinforced concrete buildings. I: Assessment of ductile moment frames. Journal of Structural Engineering (ASCE); 137(4):481-491.

Haukass T and Scott MH (2006). Shape Sensitivities in the Reliability Analysis of Nonlinear Frame Structures. Computers and Structures; 84(15):964-977.

Iervolino I and Cornell CA (2005). Record selection for nonlinear seismic analysis of structures. Earthquake Spectra; 21(3):685-713.

Iervolino I, De Luca F, and Cosenza E (2010b). Spectral shape-based assessment of SDOF nonlinear response to real, adjusted and artificial accelerograms. Engineering Structures; 33:2776-2792.

Iervolino I, Galasso C, and Cosenza E (2010a). REXEL: computer aided record selection for code-based seismic structural analysis. Bulletin of Earthquake Engineering; 8:339-362.

Iervolino I, Giorgio M, Galasso C, and Manfredi G (2010c). Conditional Hazard Maps for Secondary Intensity Measures. Bulletin of the Seismological Society of America; 100(6), 3312–3319

Iervolino I, Maddaloni G, and Cosenza E (2008). Eurocode 8 compliant real record sets for seismic analysis of structures. Journal of Earthquake Engineering; 12(1):54–90.

Italian Building Code (2008). Technical recommendations for buildings – D.M. 14/01/2008. G.U. n.29 del 04/02/2008, NTC 2008, Rome, Italy (in Italian).

Italian Building Code (2018). Technical recommendations for buildings – D.M. 17/01/2018. G.U. n.42 del 20/02/2018, NTC 2018, Rome, Italy (in Italian).

Jalayer F (2003). Direct Probabilistic seismic analysis: implementing non-linear dynamic assessments. a dissertation for the degree of PhD, Stanford University, California.

Jalayer F and Cornell CA (2009). Alternative non-linear demand estimation methods for probability-based seismic assessments. Earthquake Engineering & Structural Dynamics; 38(8):951-972

Jalayer F, De Risi R, and Manfredi G (2015). Bayesian cloud analysis: efficient structural fragility assessment using linear regression. Bulletin of Earthquake Engineering; 13:1183-1203.

Jalayer F, Franchin P and Pinto PE (2007). A scalar damage measure for seismic reliability analysis of RC frames. Earthquake Engineering & Structural Dynamics; 36(13):2059-2079.

Jalayer F, Iervolino I, and Manfredi G (2010). Structural modeling uncertainties and their influence on seismic assessment of existing RC structures. Structural Safety; 32(3):220-228.

Jalayer F, Beck JL, and Zareian F (2012) Analyzing the sufficiency of alternative scalar and vector intensity measures of ground shaking based on information theory. Journal of Engineering Mechanics; 138(3):307-316.

Jarrett JA, Zimmerman RB, Charney FA, and Jalalian A (2017). Response-history analysis for the design of new buildings in the NEHRP provisions and ASCE/SEI 7 standards: Part IV – A study of assumptions. Earthquake Spectra; 33(2):449-468.

Jayamon JR and Charney F (2015). Multiple ground motion response spectrum match tool for use in response history analysis. Structural Congress 2015.

Jayaram N, Lin T, and Baker JW (2011). A Computationally Efficient Ground-Motion Selection Algorithm for Matching a Target Response Spectrum Mean and Variance. Earthquake Spectra; 27(3):797-744.

Jehel P, Leger P, and Ibrahibegovic A (2014). Initial versus tangent-stiffness based Rayleigh damping in inelastic time history analysis. Earthquake Engineering and Structural Dynamics; 43:476–484.

Kappos AJ (1999). Evaluation of behaviour factors on the basis of ductility and overstrength studies. Engineering Structures; 21:823-835.

Karsan AI and Jirsa JO (1969). Behavior of Concrete under Compressive Loadings. Journal of the Structural Division (ASCE); 95:2535-2563.

Katsanos EI and Sextos AG (2015). Inelastic spectra to predict period elongation of structures under earthquake loading. Earthquake Engineering and Structural Dynamics; 44:1765-1782.

Kircher CA, Reitherman RK, Whitman RV, and Arnold C (1997). Estimation of Earthquake Losses to Buildings. Earthquake Spectra; 13(4):703-720.

Kohrangi M, Vamvatsikos D, and Bazzurro P (2017). Site dependence and record selection schemes for building fragility and regional loss assessment. Earthquake Engineering and Structural Dynamics; 46(10):1625-1643.

Kohrangi M, Vamvatsikos D, and Bazzurro P (2018). Pulse-like versus non-pulse-like ground motion records: Spectral shape comparisons and record selection strategies. Earthquake Engineering and Structural Dynamics; 1-19.

Kohrangi M, Bazzurro P, and Vamvatsikos D (2016a). Vector and Scalar IMs in Structural Response Estimation, Part I: Hazard Analysis. Earthquake Spectra; 32(3):1507-1524.

Kohrangi M, Bazzurro P, and Vamvatsikos D (2016b). Vector and Scalar IMs in Structural Response Estimation, Part II: Building Demand Assessment. Earthquake Spectra; 32(3):1525-1543.

Kolozvari K, Orakcal K, and Wallace J (2015). Shear-Flexure Interaction Modeling for Reinforced Concrete Structural Walls and Columns under Reversed Cyclic Loading. PEER Report No. 2015/12. Pacific Earthquake Engineering Research Center, University of California, Berkeley, California.

Kottke AR and Rathje EM (2008). A semi-automated procedure for selecting and scaling recorded earthquake motions for dynamic analysis, Earthquake Spectra; 24:911–932.

Krawinkler H and Miranda E (2004). Performance-based earthquake engineering. Earthquake engineering: from engineering seismology to performance-based engineering; 9:1-9.

Kreslin M, Fajfar P (2011). The extended N2 method taking into account higher mode effects in elevation, Earthquake Engineering and Structural Dynamics; 40(14):1571-1589.

Lanzi A and Luco JE (2018). Elastic Velocity Damping Model for Inelastic Structures. Journal of Structural Engineering (ASCE); 144(6):04018065.

Lee HS (1996). Revised Rule for Concept of Strong-Column Weak-Girder Design. Journal of Structural Engineering; 122(4):359-364.

Liel AB, Haselton CB, Deierlein GG, Baker JW (2009) Incorporating modeling uncertainties in the assessment of seismic collapse risk of buildings. Structural Safety; 31(2):197–211

Lin T and Baker JW (2013). Introducing adaptive incremental dynamic analysis: a new tool for linking ground motion selection and structural response assessment. 11th International Conference on Structural Safety and Reliability (ICOSSAR 2013). New York, NY, June 16-20.

Liu PL and Der Kiureghian A (1991). Finite Element Reliability of Geometrically Nonlinear Uncertain Structures. Journal of Engineering Mechanics, ASCE; 117(8):1806-1825.

Luco N and Cornell CA (2007). Structure-specific scalar intensity measures for near-source and ordinary earthquake ground motions. Earthquake Spectra; 23(2):357-392.

Luco N and Bazzurro P (2007). Does amplitude scaling of ground motion records result in biased nonlinear structural drift responses? Earthquake Engineering and Structural Dynamics; 36:1813-1835.

Luco N, Ellingwood BR, Hanburger RO, Hooper JD, Kimball JK, and Kircher CA (2007). Risk-targeted versus current seismic design maps for the conterminous United States. Proceedings of the 76th Annual SEAOC Convention, SEAOC.

Luco JE and Lanzi A (2017). A new inherent damping model for inelastic time-history analyses. Earthquake Engineering and Structural Dynamics; 46:1919-1939.

Luzi L, Pacor F, Puglia R (2017). Italian ACcelerometric Archive v 2.3. Istituto Nazionale di Geofisica e Vulcanologia, Dipartimento della Protezione Civile Nazionale. ITACA. Available at: http://itaca.mi.ingv.it. Last access in Dec 2017.

Mahaney JA, Paret TF, Kehoe BE, Freeman SA, & US Central United States Earthquake Consortium (1993). The capacity spectrum method for evaluating structural response during the Loma Prieta earthquake. National Earthquake Conference: Earthquake Hazard Reduction in the Central and Eastern United States: A Time for Examination and Action. US Central United States Earthquake Consortium (CUSEC).

Mander JB, Priestley MJN, and Park R (1988). Theoretical stress-strain model for confined concrete. Journal of Structural Engineering, ASCE; 114(8):1804-1826.

MathWorks (2015). Matlab. Last download is Matlab R2015a.

Mavroeidis GP and Scotti CM (2013) Finite-fault simulation of strong ground motion from the 2010 Mw 7.0 Haiti earthquake. Bulletin of the Seismological Society of America 103(5):2557–2576.

Mazzoni S, McKenna F, Scott MH, Fenves GL, and Jeremic B (2007). OpenSees command language manual. Pacific Earthquake Engineering Research Center. University of California, Berkeley.

McGuire RK (2004). Seismic hazard and risk analysis (MNO-10), Earthquake Engineering Research Institute (EERI), 1st Edition.

McKenna F (2011). OpenSees: a framework for earthquake engineering simulation. Computing in Science & Engineering; 13(4), 58-66.

Meletti C, Meroni F, Martinelli F, Locati M, Cassera A, and Stucchi M (2007). Ampliamento del sito web per la disseminazione dei dati del progetto S1. Available at: http://esse1.mi.ingv.it/. Last access in July 2018.

Menegotto M and Pinto PE (1972). Method of analysis for cyclically loaded RC frames including changes in geometry and non-elastic behaviour of elements under combined normal force and bending. Report N.32, University of Rome.

Miano A, Jalayer F, Ebrahimian H, and Prota A (2018). Cloud to IDA: Efficient fragility assessment with limited scaling. Earthquake Engineering and Structural Dynamics; 47(5):1124-1147.

Minas S and Galasso C (2019). Accounting for spectral shape in simplified fragility analysis of case-study reinforced concrete frames. Soil Dynamics and Earthquake Engineering; 119: 91-103.

Moehle J and Deierlein GG (2004). A framework methodology for performance-based earthquake engineering. 13th World Conference on Earthquake Engineering, Vancouver, Canada, August 1-6.

Mpampatsikos V, Nascimbene R, and Petrini L. A critical review of the RC frame existing building assessment procedure according to Eurocode 8 and Italian Seismic Code. Journal of Earthquake Engineering; 12(S1):52-82.

Mwafi AM and Elnashai A (2002). Overstrength and force reduction factors of multistorey reinforced-concrete buildings. Structural Design of Tall Buildings; 11(5):329-351.

Naeim F, Alimoradi A, and Pezeshk S (2004). Selection and scaling of ground motion time histories for structural design using genetic algorithms, Earthquake Spectra; 20:413–426.

Newmark NM and Hall WJ (1982). Earthquake Spectra and Design: Engineering Monographs on Earthquake Criteria, Structural Design, and Strong Motion Records. Earthquake Engineering Research Institute Monograph, Berkeley, CA.

NIST (2010). ATC-76-6: Applicability of Nonlinear Multiple-Degree-of-Freedom Modeling for Design, Report No. NIST GCR 10-917-9, prepared for the National Institute of Standards and Technology by the NEHRP Consultants Joint Venture, Gaithersburg, MD.

Nour A, Cherfaoui A, Gocevski V, and Leger P (2012). CANDU 6 nuclear power plant: reactor building floor response spectra considering seismic wave incoherency. 15th World Conference on Earthquake Engineering. Lisbon, Portugal, September 24-28.

Onem G (2008). Evaluation of Practice-Oriented Nonlinear Analysis Methods for Seismic Performance Assessment, a dissertation for the degree of PhD, Bogazici University, Instanbul, Turkey.

Open Systems for Earthquake Engineering Simulation, OpenSees (2006). Pacific Earthquake Engineering Center, University of California, Berkeley, California. Available at: http://opensees.berkeley.edu/. Last download is OpenSees v2.5.0.

Otani S (1997). Development of Performance-based Design Methodology in Japan. Seismic Design Methodologies for the Next Generation of Codes: 59-67.

Pacific Earthquake Engineering Research Center (2014). PEER NGA Ground Motion Database. Available at: https://ngawest2.berkeley.edu/site. Last access in July 2018.

Panagiotakos TB and Fardis MN (2001). Deformations of RC members at yielding and ultimate. ACI

Papadimitriou C, Beck JL, and Katafygiotis LS (2001) Updating robust reliability using structural test data. Probabilistic Engineering Mechanics; 16(2):103–113

Park R and Paulay T (1975). Reinforced Concrete Structures, John Wiley & Sons, New York.

Paulay T and Priestley MJN (1992). Seismic design of reinforced and masonry buildings. John Wiley & Sons, Inc

Pacific Earthquake Engineering Research Center (2010). Modeling and acceptance criteria for seismic design and analysis of tall buildings. Technical Report PEER 2010/111 or PEER/ATC-72, Pacific Earthquake Engineering Research Center, University of California.

Porter KA (2003). An Overview of PEER's Performance-Based Earthquake Engineering Methodology. Conference on Applications of Statistics and Probability in Civil Engineering Risk, Civil Engineering Risk and Reliability Association (CERRA), San Francisco, CA, July 6-9.

Porter KA, Beck JL, and Shaikhutdinov RV (2002). Investigation of sensitivity of building loss estimates to major uncertain variables for the Vab Nuys testbed. PEER Report 2002/03, 2002/0, University of California, Berkeley.

Priestley MJN (2000). Performance based seismic design. Bulletin of the New Zealand society for earthquake engineering; 33(3):325-346.

Priestley MJN (2003). Myths and fallacies in earthquake engineering, revisited, IUSS press.

Ramamoorthy SK, Gardoni P, and Bracci JM (2006). Probabilistic demand models and fragility curves for reinforced concrete frames. Journal of Structural Engineering; 132(10):1563-1572.

Psyrras NK and Sextos AG (2018). Build-X: Expert system for seismic analysis and assessment of 3D buildings using OpenSees. Advances in Engineering Software; 116:23-35

Ramirez CM and Miranda E (2012). Significance of residual drifts in buildings loss estimation. Earthquake Engineering and Structural Dynamics; 41:1477-1493.

Ramirez CM, Liel AB, Mitrani-Reiser J, Haselton CB, Spear AD, Steiner J, Deierlein GG, and Miranda E (2012). Expected earthquake damage and repair costs in reinforced concrete frame buildings. Earthquake Engineering and Structural Dynamics; 41:1455-1475.

Ribeiro FLA, Barbosa AR, Scott MH, and Neves LAC (2015). Deterioration Modeling of Steel Moment Resisting Frames Using Finite-Length Plastic Hinge Force-Based Beam-Column Elements. Journal of Structural Engineering (ASCE); 141(2): 04014112.

Ribeiro FLA, Neves LAC, and Barbosa AR (2017). Implementation and calibration of finite-length plastic hinge elements for use in seismic structural collapse analysis. Journal of Earthquake Engineering; 21(8):1197-1219.

Ricci P, De Luca F, and Verderame GM (2011). 6th April 2009 L'Aquila earthquake, Italy: reinforced concrete building performance. Bulletin of Earthquake Engineering; 9(1):285-305.

Ricci P, Manfredi V, Noto F, Terrenzi M, Petrone P, Celano F, De Risi MT, Camata G, Franchin P, Magliulo G, Masi A, Mollaioli F, Spacone E, and Verderame GM (2018). Modeling and Seismic Response Analysis of Italian Code-Conforming Reinforced Concrete Buildings. Journal of Earthquake Engineering; 22(sup2):105-139.

Rodden WP and Johnson EH (1994). MSC/NASTRAN aeroelastic analysis: user's guide; Version 68. MacNeal-Schwendler Corporation.

Rodrigues LG, Branco JM, Neves LA, and Barbosa AR (2018). Seismic assessment of a heavy-timber frame structure with ring-doweled moment-resisting connections. Bulletin of Earthquake Engineering; 16(3):1341-1371.

Rosenblueth E (1951). A basis for aseismic design. a dissertation for the degree of PhD, University of Illinois, Urbana, Ill

Rossetto T, Gehl P, Minas S, Galasso C, Duffour P, Douglas J, and Cook O (2016). FRACAS: A capacity spectrum approach for seismic fragility assessment including record-to-record variability. Engineering Structures; 125:337-348.

Scott MH and Fenves G (2006). Plastic Hinge Integration Methods for Force-Based Beam-Column Elements. Journal of Structural Engineering (ASCE); 132(2):244-252.

Scott MH (2011). Numerical integration options for force-based beam-column element in OpenSees. Force-based element integration options in OpenSees; 1-7.

Scott MH and Ryan KL (2013). Moment-Rotation Behaviour of Force-Based Plastic Hinge Elements. Earthquake Spectra; 29(2):597-607.

Shahi SK (2013). A probabilistic framework to include the effects of near-fault directivity in seismic hazard assessment. A dissertation for the degree of PhD, Stanford University; 2013.

Shome N and Cornell CA (1999). Probabilistic seismic demand analysis of nonlinear structures. Report RMS-35, RMS Program, Stanford University, Stanford, California.

Shome N, Cornell CA, Bazzurro P, and Carballo JE (1998). Earthquakes, records, and nonlinear responses. Earthquake Spectra; 14(3):469-500.

SINCE (1989). MIDAS Gen 2015, MIDAS Information Technology Co., Ltd.

Somerville PG, Smith NF, Graves RW, and Abrahamson NA (1997). Modification of empirical strong ground motion attenuation relations to include the amplitude and duration effects of rupture directivity. Seismological Research Letters; 68(1):199-222.

Standards New Zealand (2004). Structural design actions – Part 5: Earthquake actions, NZS 1170.5:2004, Wellington, NZ.

Stewart JP, Abrahamson NA, Atkinson GM, Baker JW, Boore DM, Bozorgnia Y, Campbell KW, Comartin CD, Idriss IM, Lew M, Mehrain M, Moehle JP, Naeim F, and Sabol TA (2011). Representation of bidirectional ground motions for design spectra in building codes. Earthquake Spectra; 27(3):927-937.

Structural Engineers Association of California, Structural Engineers Association of California. Vision 2000 Committee, & California. Office of Emergency Services. (1995). Performance Based Seismic Engineering of Buildings: pt. 3. Preliminary Northridge lessons. pt. 4. Moving the blue book toward performance based engineering (Vol. 2). Structural Engineers Association of California.

Structural Journal; 98(2):135-148.

Taghavi S and Miranda E (2003). Response of non-structural building elements, PEER Report 2003/05, Pacific Earthquake Engineering Research Center, University of California, Berkeley, California.

Tanaka H (1990). Effect of lateral confining reinforcement on ductile behavior of reinforced concrete columns. A dissertation for the degree of PhD, University of Canterbury, Christchurch, NZ.

Tanaka H and Park R. Seismic Design and Behaviour of Reinforced Concrete Columns with Interlocking Spirals. Structural Journal; 90(2):192-203.

Tibshirani RJ and Efron B (1993). An introduction to the bootstrap. Monog. on statistics and applied probability; 57:1-436.

Tsai WT (1988). Uniaxial Compressional Stress-Strain Relation of Concrete. Journal of Structural Engineering (ASCE); 114(9): 2133-2136.

Tsioulou A, Taflanidis AA, and Galasso C (2019). Validation of stochastic ground motion model modification by comparison to seismic demand of recorded ground motions. Bulletin of Earthquake Engineering; 1-28.

Vamvatsikos D (2011). Performing incremental dynamic analysis in parallel. Computers and Structures; 89:170-180.

Vamvatsikos D and Cornell CA (2002). Incremental Dynamic Analysis. Earthquake Engineering and Structural Dynamics; 31(3):491-514.

Vamvatsikos D and Cornell CA (2004). Applied Incremental Dynamic Analysis. Earthquake Spectra; 20(2):523-553.

Veletsos AS and Newmark NM (1960). Effect of inelastic behavior on the response of simple systems to earthquake motions. Proceedings of the 2nd World Conference on Earthquake Engineering, Tokyo, Japan.

Verderame GM, De Luca F, Ricci P, and Manfredi G (2011). Preliminary analysis of a soft-storey mechanism after the 2009 L'Aquila earthquake. Earthquake Engineering and Structural Dynamics; 40(8):925-944.

Vidic T, Fajfar P, and Fischinger M (1994). Consistent inelastic design spectra: strength and displacement. Earthquake Engineering and Structural Dynamics; 23: 502–521.

Watson-Lamprey J and Boore DM (2007). Beyond SaGMRotI: Conversion to SaArb, SaSN, and SaMaxRot. Bulletin of the Seimological Society of America 2007; 97(5):1511-1524.

Watson-Lamprey JA and Abrahamson NA (2006). Bias caused by use of spectrum compatible motions. Eighth U.S. National Conference on Earthquake Engineering, San Francisco, California.

Whittaker A, Atkinson G, Baker J, Bray J, Grant DN, Hamburger R, Haselton C, and Somerville P (2011). Selecting and Scaling Earthquake Ground Motions for Performing Response-History Analyses, Report No. NIST GCR 11-917-15, prepared for the National Institute of Standards and Technology by the NEHRP Consultants Joint Venture, Gaithersburg, MD.

Willford M., Whittaker A., and Klemencic R (2008). Recommendations for the seismic design of high-rise buildings, Council on Tall Buildings and Urban Habitat, Illinois Institute of Technology, Chicago, IL.

Wilson EL (2004). Static and Dynamic Analysis of Structures, Computers and Structures, Berkeley, CA.

Wilson EL (2015). Termination of the response spectrum method. Available at: https://ryanrakhmats.wordpress.com/2015/11/27/ed-wilson-termination-of-the-response-spectrum-method/. Last access in July 2018.

Wilson EL and Habibullah A (1987). Static and dynamic analysis of multi-story buildings, including P-delta effects. Earthquake spectra; 3(2):289-298.

Wilson EL, Der Kiureghian A, and Bayo EP (1981). A replacement for the SRSS method in seismic analysis. Earthquake Engineering and Structural Dynamics; 9:187–192.

Woessner J, Laurentiu D, Giardini D, Crowley H, Cotton F, Grunthal G, Valensise G, Arvdsson R, Basili R, Demircioglu MB, Hiemer S, Meletti C, Musson RW, Rovida AN, Sesetyan K, Stucchi M., and the SHARE Consortium (2015). The 2013 European Seismic Hazard Model: key components and results. Bulletin of Earthquake Engineering; 13:3553-3596.

Yamaguchi Y, Hall R, Sasaki T, Matheu E, Kanenawa K, Chudgar A, and Yule D (2004). Seismic performance evaluation of concrete gravity dams. 13th World Conference on Earthquake Engineering. Vancouver, Canada, August 1-6.

Yassin MH (1994). Nonlinear Analysis of Prestressed Concrete Structures under Monotonic and Cycling Loads. A dissertation for the degree of PhD, University of California, Berkeley, California.

Young WC and Budynas RG (2002). Roark's formulas for stress and strain, 7th Edition, McGraw-Hill.

Youngs RR., Power MS, Wang G, Makdisi FI, and Chin CC (2007). Design ground motion library (DGML) - Tool for selecting time history records for specific engineering applications, in SMIP Seminar on Utilization of Strong-Motion Data.

Zimmerman RB, Baker JW, Hooper JD, Bono S, Haselton CB, Engel A, Hamburger RO, Celikbas A, and Jalalian A (2017). Response history analysis for the design of new buildings in the NEHRP provisions and ASCE/SEI 7 standards: Part III – Example applications illustrating the recommended methodology. Earthquake Spectra; 33(2):419-447.